Preventing nano and micro wear-particle induced inflammation

A thesis submitted *in accordance with the conditions governing candidates* for the degree of
Philosophiae Doctor in Cardiff University

by

Melissa Rivera Rodrigues

April 2018

Cardiff School of Pharmacy and Pharmaceutical Sciences

Cardiff University

Abstract

Aseptic loosening, as a consequence of an extended inflammatory reaction induced by wear particles, remains the most common complication of total joint replacement (TJR), representing a major problem for the long-term success and survival of prostheses. Despite it is high incidence, in the last decade any therapeutic approach has been found to treat or avoid aseptic loosening, leaving revision as the only effective treatment for this condition. The local delivery of anti-inflammatory drugs to modulate wear-induced inflammation has been regarded as a potential therapeutic approach to avoid aseptic loosening.

In this work, an anti-inflammatory drug-eluting implant model system was developed and characterised. The model system was obtained by attaching DEX to functionalised-TiO_2 particles, through different synthetic routes: i) by covalently binding DEX to carboxyl-functionalised particles (amino or mercapto routes) or ii) by coating amino-functionalised particles using Layer-by-Layer (LbL) technique. The chemical and physical properties of DEX-loaded functionalised TiO_2 particles have been determined and the release profiles investigated. Depending on the synthetic route, the DEX release period can vary from hours (amino, mercapto routes) to 3 weeks (LbL route). The model system was then tested for its cytotoxic and anti-inflammatory properties in a rapid and reproducible *in vitro* mouse macrophage-like cellular model, by utilizing murine RAW 264.7 cells. In this model lipopolysaccharide (LPS) was utilized to activate the Raw macrophages, resulting in the secretion of pro-inflammatory cytokines, including nitric oxide (NO) and tumour necrosis factor alpha (TNF-α), the suppression of which was utilized to investigate the anti-inflammatory effect of DEX released from functionalised-TiO_2 particles. *In vitro* studies showed that DEX decreased LPS-induced NO and TNF-α production at non-cytotoxic concentrations, where DEX released from LbL particles showed the most effective suppression of inflammation for at least 2 weeks. Collectively, these findings show that the model system developed can be a potential therapeutic approach to avoid wear-debris induced aseptic loosening of TJR.

Acknowledgments

Table of Contents

List of Figures

List of Tables

List of Equations

xxx

List of abbreviations and acronyms

APTS- (3-Aminopropyl) triethoxysilane

ALG- Alginate

COX-2- Cyclooxygenase-2

CH- Chitosan

DEX- Dexamethasone

DAPI- 4',6-diamidino-2-phenylindole

DMEM- Dulbecco's Modified Eagle's Medium

FBS- Fetal Bovine Serum

FITC- Fluorescein Isothiocyanate

FT-IR- Fourier Transformed Infrared Spectroscopy

iNOS- Inducible Nitric Oxide Synthase

LbL- Layer-by-Layer

LDH- Lactase Dehydrogenase

LPS- Lipopolysaccharide

MPTMS- (3-mercaptopropyl) trimethoxysilane

MTT- Methylthiazolyl Tetrazolium

NF-Kβ- Nuclear factor-kappa B

NJR- National Joint Registry

NO- Nitric oxide

PBS- Phosphate Buffer Saline

PG$_2$- Prostaglandin 2

TGA- Thermogravimetric Analysis

TiO$_2$- Titanium Dioxide

TJR- Total Joint Replacement

TNF-α- Tumour Necrosis Factor Alpha

1. Introduction

1.1 Total joint replacement (TJR)

Like other parts of the body, bone becomes damaged or weakened by age, accidents or disease. Bone and joint degenerative and inflammatory diseases, such as arthritis affect millions of people worldwide. In fact, it is estimated that 8 million people in the UK (Hughes et al. 2010) and 27 million people in the US (Van Manen et al. 2012) are currently suffering from osteoarthritis. As can be seen in Figure 1 total joint replacements (TJR) are used as treatment for arthritic or damaged joints, providing pain relief and improving quality of life of patients with end-stage arthritis (Goodman et al. 2013, 2014; Takakubo et al. 2013). Likewise, data recorded between 2009 and 2017 revealed that osteoarthritis was the predominant diagnosis (>40%) for undertaken hip and knee TJR, followed by other diagnosis such as infection, aseptic necrosis of head and neck of femur and mechanical loosening of joint (National Joint Registry 2017, The NJR Editorial Board 2016).
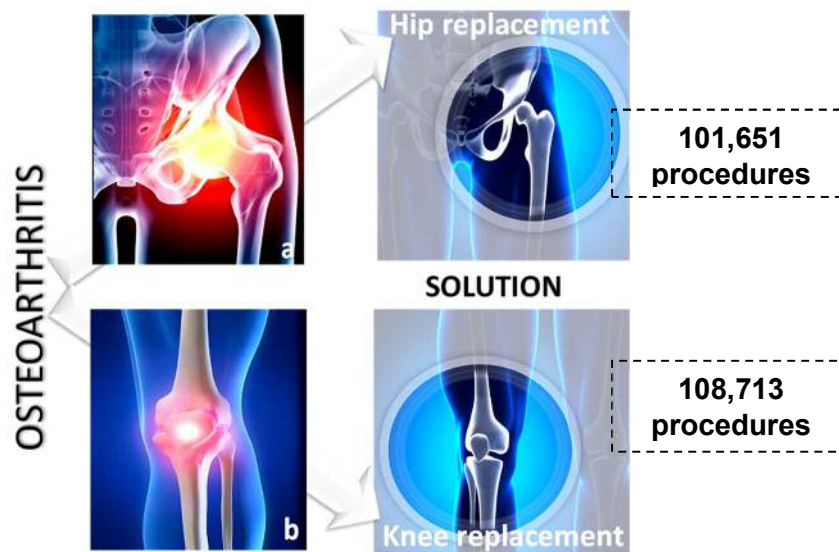
Figure 1. Osteoarthritis and total joint replacement undertaken during 2016: (a) Hip and (b) Knee prosthesis, according to National Joint Registry (National Joint Registry 2017)**.**

Worldwide hip and knee replacement have become popular surgical procedures over the past decades (Cobelli et al. 2011, Hunt et al. 2014, Kurtz et al. 2007). In the United States (USA) more than 200,000 joint replacements are performed each year, where this number is expected to increase dramatically over the next 20 years (Issa & Mont 2013, Ulrich et al. 2008, von Knoch et al. 2010). The same trend was observed in United

Kingdom (UK), according to the last report of the National Joint Registry of England, Wales and Northern Ireland (National Joint Registry 2017), 890,681 and 957,739 primary hip and knee replacement were carried out, respectively between 2003 and 2017 (National Joint Registry 2016). Furthermore, from 2015 to 2016 an increase of 3.5% and 3.8% was recorded respectively for hip and knee procedures in England and Wales (National Joint Registry 2016).

1.2. Revision surgery

Despite regarded as extensively applied and successful orthopaedic medical devices (Bauer et al. 2012, Goodman 2014, Goriainov et al. 2014) TJR are not exempt of complications. TJR have an expected average life span of 10-15 years post-surgery (Labek et al. 2011, Lee & Goodman 2008, Torrecillas et al. 2009). After that period, implants start to experience biocompability problems, causing complications to the patient i.e. long term-pain and functional problems (Goodman et al. 2014) which normally results in revision surgery. The numbers speak from themselves 8% (8417) of the hip and 6% (6194) of knee primary procedures undertaken in UK during 2016, resulted in revision surgery (National Joint Registry 2017). Of those recorded, aseptic loosening (42%, 41%), pain (7%, 10%), adverse soft tissue reaction (13%, 12%) and infection (5%, 23%), were the most common causes, respectively for total hip and knee revision procedures. These statistics are particularly worrisome because due to the aging population, obesity, osteoporosis and increasing frequency of osteoarthritis, the number of revision surgeries is likely to increase (Mihalko et al. 2014, Ulrich et al. 2008). Moreover, the risk of revision surgery after hip or knee replacement has been related to patient age and sex. Last year, an interesting study by Bayliss and co-workers (2017) showed the revision rate older than 70 years is 5% (both men and women). Whilst for patients in their early 50s, a rate of 35% and 15% was reported respectively for men and women groups (Bayliss et al. 2017). In addition, revision results in worse outcome than the primary procedure, thus resulting in more discomfort to the patient (Bhandari et al. 2012, Vallés et al. 2013). All of this involves high healthcare costs, £80 million was the estimated expenditure for UK revision surgeries undertaken in 2015 (Kallala et al. 2015).

1.3. Aseptic Loosening

By observing the above revision surgery statistics (1.2. Revision surgery), it is clear that among all causes, aseptic loosening was the most common indication for replacement surgery, in both hip (MacInnes et al. 2012, Ulrich et al. 2008) and knee replacement (Rozkydal et al. 2007, Schroer et al. 2013), accounting for more than 40% of all revision procedures (Goriainov et al. 2014). Aseptic loosening of the implant occurs as a consequence of an extended inflammatory reaction induced by wear particles, which normally results in severe bone loss i.e. osteolysis around the implant (Landgraeber et al. 2014). This wear particles, which are extremely small sized particles, normally arise from metal-on-metal bearings of TJR after a given period of usage.

As can be seen in Figure 2, after osteolysis the bone around the TJR is not strong enough to fulfil the prosthesis functions leading the implant replacement i.e. revision surgery.

Figure 2. X-ray image of progressive acetabular osteolysis over 1.5 years (a), including 3D computerized tomography reconstruction demonstrating lesion and pelvic discontinuity (b). X-ray taken after surgery, no bone loss observed (c). Figure adapted from (Rajpura & Board 2013)**.**

In general, the degree of osteolysis and inflammatory reactions on bone tissue at the bone–implant interface will depend on the of wear particles features (e.g. morphology, size, material origin) released from the implant surface (Longhofer et al. 2017, Nine et al. 2014). Taking the wear material as an example, previous studies have reported that different levels of osteolysis were observed when animal models were exposed to different wear particles from different materials. Among all metallic particles showed the highest loss of bone density when compared to ceramic ones.

So researchers worldwide have attempted to mitigate release of wear particles and consequent periprosthetic osteolysis by improving of surgical techniques such as the use of medullary plugs, cement guns, lavage of the canal, pressurization, centralization of the stem, and reduction in cement porosity (Holt et al. 2007). Another approach was to modify the bearing materials of implants (Gallo et al. 2013, Ryu & Shrotriya 2013). These

include the utilization of new implant materials such as highly cross-linked polyethylene, titanium and cobalt based alloys, polycarbonate-urethane (Holt et al. 2007, Nine et al. 2014). Also the modification of implant surface with mechanical and chemical methods such as sol-gel, plasma spray, grit-blast, acid-etching, and electrochemical-anodization have been applied to mitigate the risk of osteolytic reaction (Dohan Ehrenfest et al. 2010, Goodman et al. 2014, Singhatanadgit 2009). Although some of them present disadvantages such as non-uniformity in thickness, lack of adherence to implant, and high processing temperature (Koju et al. 2017). In fact, some of them have even resulted in several adverse complications, for example, acid etching method may lead to micro-cracks which affect physical integrity of the implant, or granules used on surface plasma spraying can detach from implant surface, causing damage on surrounding cells and tissues (Ganguly and Shokuhfar, 2013). Despite being considered one of the most common causes of revision surgery, currently there are no drug or effective prevention/treatment for aseptic implant loosening, leaving revision surgery as the only therapeutic option. In this context, a better understanding of the wear-debris induced inflammatory reaction that takes place at implantation site could facilitate the development of more safe and functional improved implants.

1.3.1 Wear-induced inflammation: acute and chronic phase

An innate acute host inflammatory reaction will arise immediately after device implantation, and consists of the response to inevitable tissue injury during device placements and the response to the material itself (Anderson & Cramer 2015, Lucke et al. 2015). This inflammatory response is considered a decisive event because it will help promote the tissue healing/recovery process and eliminate possible infections around implant. Although if prolonged for more time than necessary, inflammation may compromise the integration and biological performance of the implant (Bridges & García 2008). On other hand, there are other factors that can lead to inflammatory response, especially in implants like TJR which are intended to remain *in situ* for the life span of the patient. For example, high levels of activity, and usage of TJR result on release of wear particles from artificial articulating surfaces, which are also thought to induce an inflammatory reaction around the implant (Cobelli et al. 2011, Rao et al. 2012). Regardless the cause i.e. wear-debris or tissue injury, biological events that characterize inflammation will be the same. In this sense, inflammatory response has been described as a complex reaction that comprises different phases (Figure 3), involving recruitment and activation of different cells (e.g. macrophages, fibroblast, osteoclasts), protein adsorption, and secretion of inflammatory mediator, among others (Bridges & García 2008).The initial phase, lasting from minutes to days depending on the tissue injury, is

defined as acute inflammation. Then a later phase takes place i.e. chronic inflammation, where inflammatory reaction continues to develop (1-2weeks) even after tissue deposition occurs (Anderson et al. 2008, Bastian et al. 2011, Lin et al. 2014). In more detail, the initial acute phase is characterized by blood cells influx, such as short-lived neutrophils and monocytes, into the area surrounding the implant (Bridges & García 2008). This response is initiated in response to tissue injury caused by TJR surgery, and aims to recover the tissue homeostasis (Lin et al. 2014). Whereas monocytes will differentiate into macrophages that will play a pivotal role during inflammatory reaction by engulfing foreign bodies i.e. wear particles, eliminating damaged tissue, cell debris, releasing cytokines and other important factors in the transition between inflammation and wound repair events (Lucke et al. 2015).
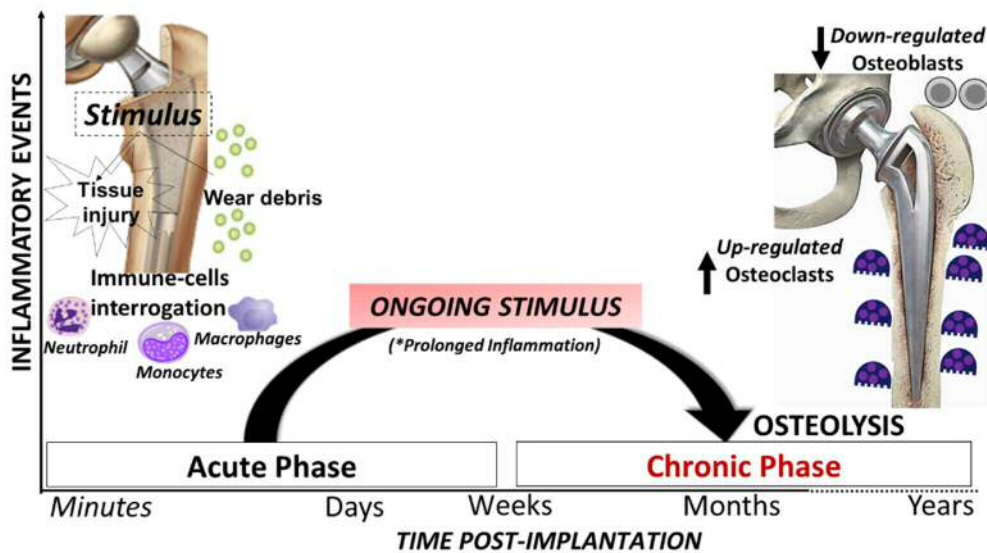
Figure 3. The inflammatory response immediately after implantation, acute and chronic phase: time-scale, cellular interaction with implant surface and related biological events such as osteolysis.

Inflammatory response comprises different phases, acute and chronic, involving recruitment and activation of different cells (e.g. monocytes, macrophages, osteoblasts, osteoclasts). The initial phase, lasting from minutes to days depending on the tissue injury and/or wear debris interaction, is defined as acute inflammation. Then if prolonged, acute phase becomes chronic, in this case inflammatory reaction continues to develop (1-2 weeks) even after tissue deposition occurs. Persistent chronic phase involves the continuous activation of macrophages, which consequently results in the overexpression of osteoclasts and down regulations of osteoblast. This is the main cause for bone erosion and loss around the implant, which is known as osteolysis.
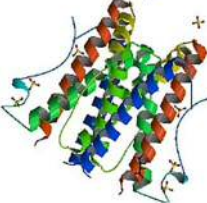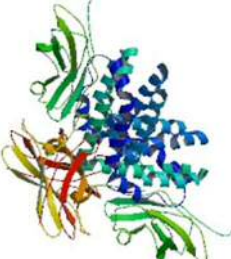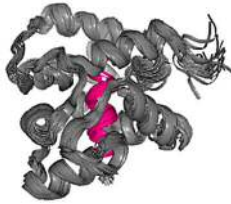
The subsequent chronic phase occurs when the "foreign material" cannot be eliminated by a normal homeostatic mechanism, resulting in a higher incidence and prolonged

activation of lymphocytes, monocytes and macrophages (Anderson et al. 2008, Buckley 2011). In the worst scenario, chronic and dysregulated inflammation can lead to a fibrotic encapsulation of the implant, leading to increased bone resorption and hampered bone formation, thus seriously compromising implant function and even lead to implant aseptic loosening (Bastian et al. 2011, Lin et al. 2014, Ren et al. 2013). In this regard, both processes of acute and chronic inflammation play an important role in tissue healing post-implantation. Among others, the degree and duration of each inflammatory phase, acute or chronic, will depend on several factors, including the damage caused during implantation procedure, implant type e.g. material biocompability (Anderson & Cramer 2015, Anderson et al. 2008) and also the type of wear-particles to be released (e.g. size, morphology) (Nine, *et al.*, 2014). According to previous studies, under favourable i.e. aseptic conditions and when the implanted material is biocompatible, acute and chronic inflammatory phases should not last more than 2 weeks (Anderson et al. 2008). Therefore, the persistence of inflammatory events for more than 3 weeks, acute or chronic, normally indicates an unfavourable outcome, such as infection or osteolysis. It is important to highlight that the major problem out coming from this extended chronic inflammatory reaction, is that the continuous activation of macrophages will consequently trigger the formation of bone reabsorbing cells i.e. osteoclasts, exceeding the number of bone forming cells i.e. osteoblasts. In addition, it may also evoke osteoblasts apoptosis (Rick Sumner 2013). As can be seen in Figure 3., this overexpression of osteoclasts and down regulations of osteoblasts, leads to bone erosion and loss around the implant i.e. osteolysis (Beck et al. 2012, Ren et al. 2011a).

1.3.2 Biological mechanism and inflammatory mediators

Recent studies (Aktan 2004, Lin et al. 2014, Ricciotti & Fitzgerald 2011, Wojdasiewicz et al. 2014, Zhang & An 2007) have demonstrated the presence of the different types of mediators during a wear-debris induced inflammation as summarized in *Table 1*.

Table 1. Summary and description of relevant inflammatory mediators/markers. All crystal structures represented are from human origin molecules, except COX-2 and iNOS which are murine-type and were taken from the Research Collaborator for Structural Bioinformatic (RCSB) Protein data bank (PDB) (www.rcsb.org).

INFLAMMATORY MEDIATORS	DESCRIPTION
Tumor Necrosis Factor alpha (TNF-α)	Earliest and key **pro-inflammatory cytokine**. As the initiator of inflammatory reaction, it amplifies and prolongs the inflammatory reaction by activating a series of inflammatory cells to release interleukins and cytokines. Including NF-kβ pathway activation, and production of iNOS, COX-2, and PG$_2$ synthase.
Interleukin-6 (IL-6)	IL-6 is a pro-inflammatory cytokine that is mainly secreted by activated monocytes and synovial fibroblasts. It Is a potent inducer of the acute phase response, and bone resorption; it is presence is highly correlated to osteoclast formation.
Interleukin-10 (IL-10)	**Anti-inflammatory cytokine**, that act as potent immunoregulatory molecule by controlling the pro-inflammatory cytokine response. Such as by repressing the expression of TNF-α, IL-6 and IL-1 by activated macrophages. It has been proven to be involved in stimulating the synthesis of type II collagen and aggrecan.
Nitric oxide (NO) and iNOS	NO is reactive specie and **important signalling molecule** produced during inflammation, it modulates production of prostaglandins and, also increases the expression of COX-2 protein. It is biosynthesized by inducible nitric oxide synthase (iNOS) **enzyme** from L-arginine. Both NO and iNOS are expressed in activated macrophages.

Prostaglandin 2 (PG₂) and COX-2	PG$_2$, **local mediator** occurred in the inflamed tissues leading to classic signs of inflammation: redness, swelling and pain. It is mainly biosynthesized by the action of cyclooxygenase-2 (COX-2). Both are up-regulated at sites of inflammation. Their biosynthesis is blocked by nonsteroidal anti-inflammatory drugs (NSAISDs).
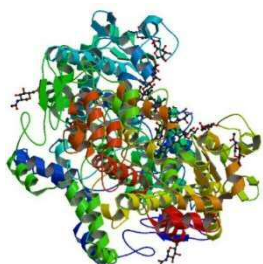
On the other hand, several studies have been done to have further insight about the inflammatory response towards an orthopaedic device (Cherian et al. 2015, Cobelli et al. 2011, Nine et al. 2014). As it can be seen in Figure 4, Immediately after implantation, within seconds, non-specific protein and biomolecules from blood plasma and biological fluids surrounding the implant tend to adsorb onto surface of the implant (Anderson & Cramer 2015, Anderson et al. 2008).This process is known as *Vroman* effect (Slack & Horbett 1995), and, being one of the first events taking place after implantation, it plays a crucial role on the subsequent cascade of inflammatory events (Bixler & Bhushan 2012). The protein adsorption is a dynamic and competitive process, where the type, concentration, and conformation of surface-adsorbed proteins (e.g. fibrinogen, fibronectin) will be influenced by the surface chemistry and morphology of the implant such as surface charge, energy or hydrophobicity (De Jonge et al. 2008), but is also dependent on local surrounding environment i.e. pH, concentration of ions, strength and temperature). For example, several studies (Jäger et al. 2007, Lucke et al. 2015) have reported the influence of surface charge on the protein adsorption. In these studies, the ionic interactions were described as the driving force for protein unfolding and adsorption onto an implant charged surface. Since most of proteins present a negative surface charge, an implant with a positive surface charge would in theory promote protein adsorption.

The adsorbed protein layer act as an interface that will define which cells i.e. bone, white blood cells and their precursors will subsequently approach the implant strongly affecting tissue healing around the implant (Anderson & Cramer 2015). For example, macrophages functions (e.g. phagocytosis, cytokine expression) and phenotype will depend on these layer of proteins adsorbed on implant surface (Bridges & García 2008, Zaveri et al. 2014). Subsequently, within minutes of implantation, the cellular response becomes predominated by immune cells such as neutrophils and macrophages at the host-implant surface. Otherwise, when wear-debris are present, primary immune cells are also recruited to inflammatory sites, so they can engulf these foreign particles.
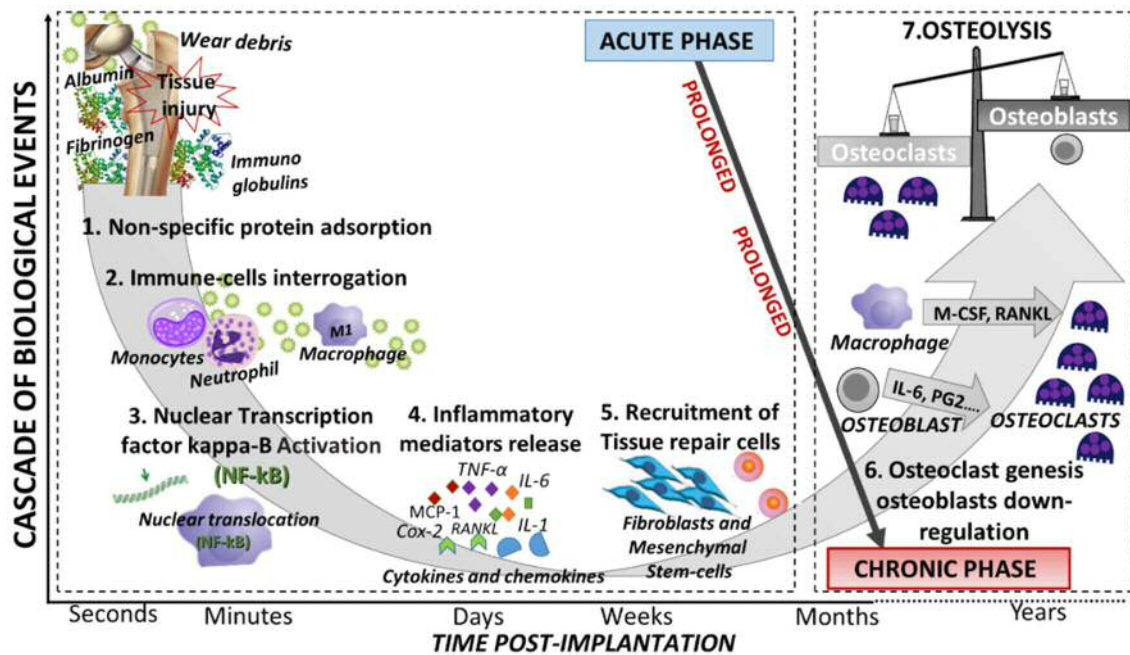
Figure 4. Cascade of molecular and cellular processes that occurs following biologically release of wear particles resulting from the placement of orthopedic implants.

Immediately after implantation starts the acute phase, where non-specific protein and biomolecules (e.g. albumin, fibrinogen) from blood plasma and biological fluids surrounding the implant tend to adsorb onto surface of the implant. Within minutes of implantation, the cellular response becomes predominated by immune-cells such as neutrophils and macrophages at the host-implant surface. Interaction of immune cells and wear particles, particularly macrophages, leads to activation of the factor nuclear-kappa β (NF-κβ) pathway. Hence, resulting in secretion of key immune-regulatory proteins, cytokines and chemokines (e.g. IL-family, TNF-α, NO), which will act as effective messenger molecules by controlling the duration and strength of immune response, including recruitment of tissue repair cells. Although when prolonged this acute phase/stimulus can trigger a chronic inflammation that normally results in bone loss around the implant i.e. osteolytic reaction.

The immune cells response, which takes places within 48-72 hours, is considered to be the hallmark of inflammatory acute phase (Anderson & Cramer 2015). During the first days following implantation, short-lived neutrophils (24h-48h) are the predominant immune cells, then these cells are replaced by long-lived (up to months) macrophages/monocytes. Research studies regarding monocytes/macrophages has been increasing in recent years regarding orthopaedic medical devices implantation, such as TJR (Ingham & Fisher 2005, Linden 2012, Rao et al. 2012). In this context, macrophages are described as key elements in both inflammatory and tissue healing responses, acting as sentinels of body´s reactions that take place after devices implantation (Cobelli et al. 2011, Lucke et al. 2015).

More specifically, after wear particles interaction, macrophages secrete key immune-regulatory proteins resulting from the activation of the factor nuclear-kappa β (NF-κβ) pathway (Figure 4). These immune-regulatory proteins, cytokines and chemokines have different roles (Goodman & Ma 2010): cytokines act as effective messenger molecules by controlling the duration and strength of immune response (e.g. IL-family, TNF-α, *colony-stimulating factor* (CSF). On the other hand, chemokines are a special type of cytokines that are responsible for controlling the immune cell migration i.e. chemotaxis during the inflammatory response (e.g. monocyte chemoattractant protein, MCP-1).

Moreover, upon stimulation with different cytokines and environmental stimulus, macrophages can either recruit more macrophages or change their phenotype (Getts et al. 2014). Macrophages have the ability to differentiate into distinct subpopulations, such as M1 and M2-induced macrophages (Lin et al. 2014, Solary 2012). Each type seems to play a different role during inflammatory response (Anderson et al. 2008, Porcheray et al. 2005), representing two extremes in the spectrum of the macrophages phenotype (Lampiasi et al. 2016). Classically activated M1 macrophages are responsible for phagocytosis and consequent release of pro-inflammatory cytokines. While M2-like macrophages are known for being involved in resolution of inflammation (Italiani & Boraschi 2014, Mills & Ley 2014), more specifically in wound healing and tissue repair, crucial processes to achieve a successful implant integration. Furthermore, it should be noted that although needed to resolve an inflammatory condition, macrophages prolonged and uncontrolled activation can trigger a chronic inflammation. Chronic inflammation, is a state in which acute inflammation, fibrosis and repair occurs simultaneously, and normally results in bone loss around the implant i.e. osteolytic reaction (Ingham & Fisher 2005, Lin et al. 2014). This reaction will mainly depend on wear debris features (e.g. size, morphology, texture), according to previous studies submicron sized (<1µm) particles are considered to be the most reactive (Rao et al. 2012, Revell 2014). When macrophages cannot digest wear particles, more monocytes are recruited to site of inflammation, and according to the level of inflammation they release inflammatory mediators such as pro-inflammatory cytokines (e.g. TNF-α and IL-1β), growth and differentiation factors (e.g. macrophage-colony stimulating factor (M-CSF), receptor activator of nuclear factor kappa β ligand (RANKL). Although the mechanism of macrophages/monocytes linage differentiation into osteoclasts (*Figure 5*) is still not clear, most of the studies (Bedke & Stenzl 2010, Goodman 2014, Kawai et al. 2011, Takashiba et al. 1999) showed that when exposed to a combination of macrophage colony-stimulating factor (M-CSF) and receptor activator of nuclear factor-kappa β ligand (RANKL), macrophages have the ability to differentiate into pre-osteoclasts (Solary 2012).
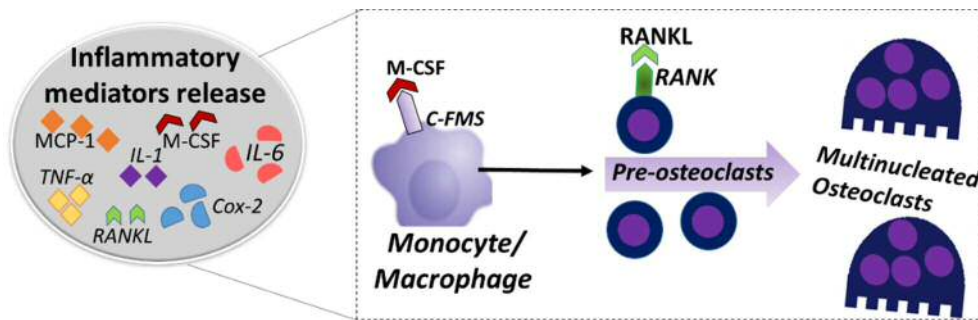
Figure 5. Differentiation of monocytes into osteoclasts and differentiated macrophages (M1 and M2) within exposure to chemokines and cytokines e.g. TNF-α, Interleukins and M-CSF, that are released upon inflammatory stimuli.

These pre-osteoclasts will eventually evolve to mature multinucleated osteoclasts which after cell polarization gain resorptive activity, thus playing central role in osteolysis and, in long term, in aseptic loosening (Lampiasi et al. 2016). In addition, macrophages not only promote osteoclasts formation but they are also capable of directly resorb bone themselves (Tamaki et al. 2008). Konttinen and co-workers (Konttinen et al. 2001) showed that macrophages expressing cathepsin-K, an enzyme involved on bone resorption, were found among the cells collected around loosened hip joint. These data suggest that besides contributing for the pathogenesis of the inflammatory response, macrophages also present an osteolytic potential by directly resorbing periprosthetic bone after being challenged by wear particles. Regarding bone formation, macrophages can also interfere osteoblasts formation; recent study (Ren et al. 2011b) reported that during wear-debris phagocytic process macrophages release high levels of reactive oxygen species that will affect the osteoblast progenitor cells and consequently the process of bone formation. One the reactive oxygen species release is nitric oxide (NO), which is a pro-inflammatory mediator released in high concentrations by activated macrophages (Sharma et al. 2007). It is known that NO impaired production results in undesired effects such vasoconstriction, tissue damage and septic shock (Bogdan 2001). Previous studies have shown that NO is involved in inflammatory joint diseases (Bogdan 2001, Sharma et al. 2007), and its expression reflects the level of inflammation, thus providing a measure of the inflammatory response (Oh et al. 2012, Pinho et al. 2011).

1.3.3 Inflammation models

As described in above sections (1.3.1 Wear-induced inflammation: acute and chronic phase,1.3.2 Biological mechanism and inflammatory mediators) aseptic loosening is caused by an unresolved and extended inflammatory response, which can occur due to

different causes such as tissue injury or wear particles release. Regardless the cause, biological events that characterize inflammation, will be very similar. In this context modulating inflammatory response has been a major focus in the design of novel approaches to avoid aseptic loosening. Following the development of novel anti-inflammatory compounds and systems, it is then important to validate their action in a suitable model of inflammation.

During the last decade different *in vitro* and *in vivo models* (Nine et al. 2014) to mimic wear-debris induced inflammation conditions have been applied to assess the anti-inflammatory potential of novel compounds and systems. Relevant cells such as macrophages, osteoclasts and osteoblast have been utilized as in *vitro* models (Ingham & Fisher 2005). As for *in vivo* models (Langlois & Hamadouche 2011), different species e.g. sheep, rabbits, mice have been used to test biological and mechanical parameters upon wear-debris stimulation. Particularly, monocyte/macrophage *in vitro* based-models, mainly due to key role that macrophages play in inflammatory response. Namely the macrophages ability to i) either recruit more macrophages or change their phenotype (Getts et al. 2014) ii) differentiate into distinct subpopulations, such as M1 (phagocytosis and release of pro-inflammatory cytokines) and M2-induced macrophages linked to the resolution of inflammation (Mills and Ley 2014; Italiani and Boraschi 2014), crucial processes to achieve a successful implant integration.

Among macrophage *in vitro* based-models, inflammation has been studied in robust, rapid and reproducible *in vitro* macrophage-like model with exposure to the bacterial wall component lipopolysaccharide (LPS). Then, at specific time points (post-LPS activation), samples are collected for inflammatory markers analysis such cytokines and chemokines or interleukins; this has been observed for both *in vitro* and *in vivo* models of inflammation (Tweedie et al. 2009a). In this context, LPS-activated murine-like macrophages, Raw 264.7 cell line have been described as a relevant *in vitro* model to investigate study inflammatory process and therefore test the effect of anti-inflammatory compounds and systems. Besides, it is efficacy on screening the potential anti-inflammatory activity of drugs and delivery systems has been already demonstrated in previous studies (Jeon et al. 2000, Yuan et al. 2013). Previous studies have shown the production of inflammatory cytokines such IL-6, tumour necrosis factor- α (TNF-α), prostaglandin (PG) E_2, and reactive oxygen species such as nitric oxide (NO) on LPS-activated Raw 264.7 cells (Kim et al. 2012, Saxena et al. 2003, Sharma et al. 2007). The expression of those cytokines and chemokines on LPS-activated Raw 264.7 reflects the level of inflammation, and therefore provides a measure of the inflammatory response (Oh et al. 2012, Pinho et al. 2011). For assay purposes, some studies (Lee et al. 2013, Petruson et al. 2005, Pinho et al. 2011) have assessed the anti-inflammatory potential by measuring levels of

inflammatory cytokines on LPS-activated cells in presence of materials/compounds to be tested.

From a cellular perspective, the signalling of cytokine metabolic pathway starts immediately after LPS exposition: when exposed to macrophages, LPS binds to the LPS-binding protein (LBP), which delivers LPS to the CD14/TLR4 receptor complex (Sharma et al. 2007).
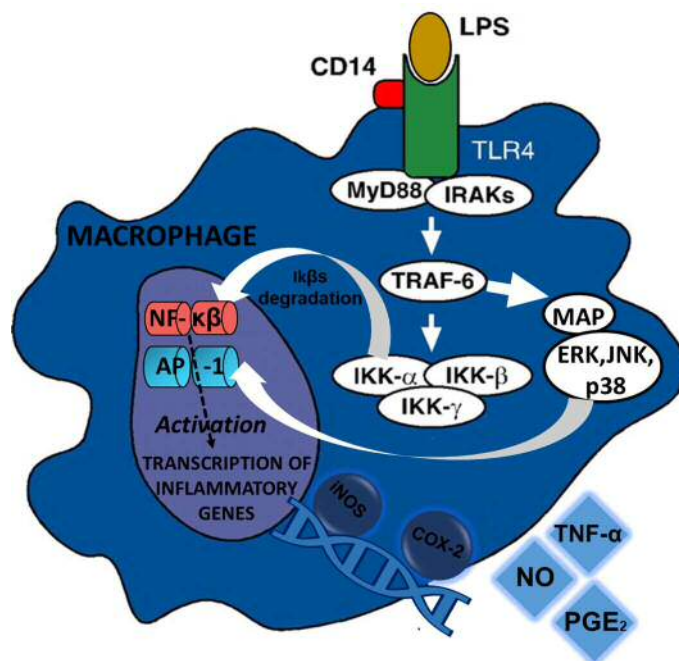
Figure 6. Signalling pathway cascade involved in LPS-induced cytokines production in macrophages. Adapted from (Pedersen & Febbraio 2008)**.**

LPS is recognized by the innate immune system by binding to the TLR4 present on the surface of macrophages. Upon LPS binding, signalling proteins e.g. MyD88-associated kinase are recruited and common upstream activator e.g. IRAK1/4, TRAF6 of NF-κB and MAP kinase (MAPK) are triggered. Specifically, TRAF-6 mediates the activation of inhibitor of κB kinase (IKK) and triggers the phosphorylation-induced proteasomal degradation of IκB, and subsequent NF-κB activation. Activated NF-κB and MAPK translocate to the nucleus and induce the transcription of pro-inflammatory genes (iNOS and COX-2), and respectively the secretion of numerous inflammatory cytokines, such as NO and TNF alpha. (Abbreviations: AP-1: activator protein-1, TLR4: toll-like receptor 4, MyD88: myeloid differentiation primary response gene 88; IRAK: interleukin-1 receptor-associated kinase; TRAF6: TNF receptor associated factor 6; MAPK: mitogen-activated protein kinase, ERK: extracellular signal-regulated kinase: JNK: c-Jun N-terminal kinase; AP-1: activator protein-1).

The signalling pathways are activated by TLR4 engage adaptor molecules such as myeloid differentiation primary response 88 (MyD88). MyD88 is essential through all the signalling process, such as the activation of mitogen-activated protein kinase (MAPK)

and the phosphorylation of inhibitor of kappaβ-kinase (IKK) (Li & Yang 2011). This triggers a complex intracellular signalling cascade, including and nuclear translocation of nuclear factor (NF) kappaβ (NF-κβ) and of the activator protein-1 (AP-1) (Petruson et al. 2005). AP-1 and NF-κB have been classified as the master regulators of inflammation (Li & Yang 2011). Thus, coordinated actions of NF- κB and AP-1 propagate inflammation via promoting the transcription of numerous pro-inflammatory genes (e.g. inducible nitric oxide synthase enzyme (iNOS) and COX-2) and respectively of inflammatory mediators e.g. NO, and cytokines e.g. PGE_2 and TNF alpha (Figure 6).

Regarding NO production, the metabolic L-arginine: NO pathway is the central source for NO production in macrophages (Zamora et al. 2000). This metabolic pathway is triggered by the inducible nitric oxide synthase enzyme (iNOS). The catalytic activity of iNOS is mainly regulated by co-factors (e.g. NADPH) and by the availability of substrates such as calmodulin (Calm) and L-arginine. Then, iNOS utilizes the oxygen and electrons from NADPH to oxidize L-arginine into OH- L-arginine, which will be oxidized into NO (Bogdan 2001). As for TNF-α production, it has been reported in several studies (Bouwmeester et al. 2004, Sabio & Davis 2014, van der Bruggen et al. 1999) that it involves the activation of multiple groups of mitogen-activated protein (MAP) kinases family, such as: extracellular-signal-regulated kinases (ERKs); the cJun NH2-terminal kinases (JNKs); and the p38 MAP kinases (Figure 6). It is worth to note that the utilization of *in vitro* inflammation models, such as LPS-activated Raw 264-7 cells, are less-expensive, simpler and provide faster results, when compared to *in vivo* models; making them ideal models to provide an initial pharmacological screening. Although it is important to recognize that these models have limitations. And in this sense the studies determined by *in vitro* cellular models should be further translated to *in vivo* models, which are more clinically relevant due to their similarity with human in terms of physiology, anatomy and biomechanics (Langlois & Hamadouche 2011).

1.4 Approaches to improve longevity/success rates of total joint replacement procedures

Taking into account the dramatic increase of TJR revision surgeries, in both younger and more active patients (Kurtz et al. 2009), different approaches are being applied to avoid adverse post-operative outcomes such as pain, periprosthetic inflammation and consequent osteolysis around the implant. One of the most common clinical practices is the drug-regimen that usually takes place after orthopaedic surgeries (Bhusal et al. 2016). Normally patients go through, antibiotics and/or anti-inflammatory prophylaxis, in order to manage pain, prevent infectious and inflammatory conditions (Ganguly, *et al*., 2013; Popat, Eltgroth and Desai, 2007). As well as to promote integration of the implant with the natural tissue (Waldron et al. 2013). Particularly, the administration of anti-inflammatory drugs in the post-operative period, and their beneficial effect on patients recovery are well described in other studies (De Oliveira GS Jr.; Almeida MD; Benzon HT;McCarthy RJ 2011, Holte & Kehlet 2002, Salerno & Hermann 2006). The main benefit of administrating anti-inflammatory drugs, is not the treatment of the osteolytic condition itself, but an attempt to avoid it by modulating periprosthetic acute inflammation (Hickey et al. 2002a,b). In theory, the administration of anti-inflammatory drugs, which can be classified as steroidal/corticosteroids and non-steroidal, will control the pain and the overproduction proteins, enzymes, and cells involved in the chronic inflammatory response (Dawes et al. 2011). Since in this study, the model drug (DEX) utilised is a corticosteroid this section will be focused on their anti-inflammatory mechanism of action. The benefits of corticosteroids administration have been extensively reviewed and their clinical efficacy demonstrated over the last decades (Barnes 2006, Baschant et al. 2013, Coutinho & Chapman 2011, Vandevyver et al. 2013). As reported by a previous study regarding knee replacement (Smith et al. 2006) a small single dose (16mg) of a synthetic glucocorticoid, DEX, was sufficient to reduce the C-reactive protein (CRP) levels by 50%, three days following the surgery. Recent studies (Huebner et al. 2014, Urbanska et al. 2014) have reported that DEX has been locally released aiming to modulate the inflammatory reaction. These studies have demonstrated that DEX was able to suppress the activity of inflammatory genes and respective inflammatory cytokines and chemokines, including nitric oxide. As can be seen in Figure 7, corticosteroids, such as DEX, suppress the multiple inflammatory genes that are activated in inflammation, mainly by reversing histone acetylation of activated inflammatory genes through binding of liganded glucocorticoid receptors (GR) to co-activators, and recruitment of histone deacetylase-2 (HDAC2) to the activated transcription complex. Alternatively corticosteroids can also interact with DNA recognition sites to active transcription of anti-

inflammatory genes and then inhibit transcription of several genes linked to corticosteroid side effects (Barnes 2006, Vandevyver et al. 2013).
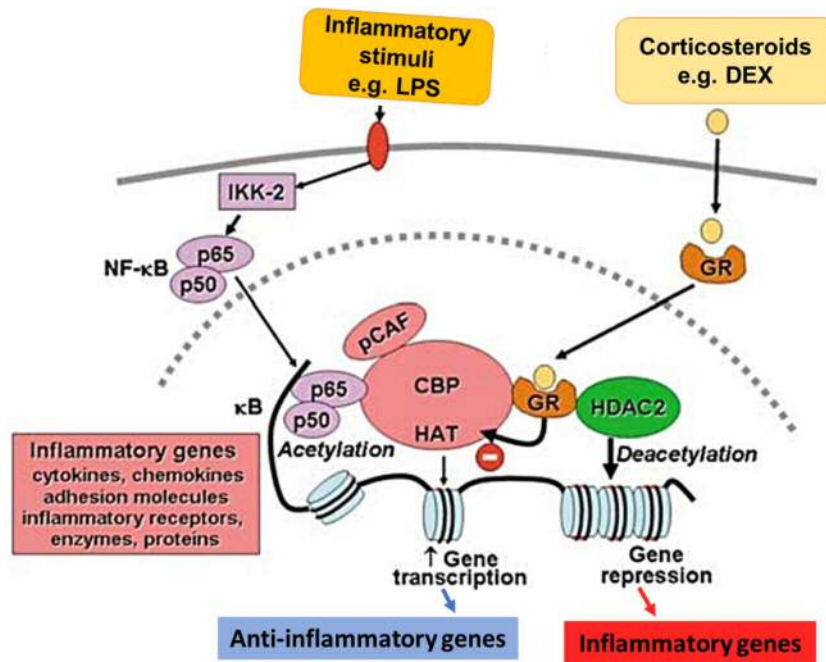
Figure 7. Anti-inflammatory mechanism of action of corticosteroids, by suppression of activated inflammatory genes through signal transduction by their steroid receptor, the glucocorticoid receptor (GR). Adapted from (Barnes 2006)
Inflammatory genes are activated by inflammatory stimuli (e.g. LPS), resulting in activation of IKK2 (inhibitor of I-kB kinase-2), which activates the transcription factor NF-Κβ. A dimer of p50 and p65 NF-κB proteins translocate to the nucleus and binds to specific κB recognition sites, as well as to co-activators, such as cyclic binding protein (CBP) or p300-CBP associated factor (pCAF), which have intrinsic histone acetyltransferase (HAT) activity. This results in acetylation of core histone H4, resulting in increased expression of genes encoding multiple inflammatory proteins. Glucorticoid receptor (GR) after activation by corticosteroids translocate to the nucleus and bind to coactivators to inhibit HAT activity directly and recruiting histone deacetylase-2 (HDAC2), which reverses histone acetylation leading in suppression of these activated inflammatory genes. Besides corticosteroids, GR homodimers can also interact with DNA recognition sites to active transcription of anti-inflammatory genes and thus inhibit transcription of several genes linked to corticosteroid side effects. (Abbreviations: CBP: cyclic binding protein; LPS: Lipopolysaccharide; IKK2: inhibitor of I-kB kinase-2, NF-Κβ: nuclear transcription factor Κβ; pCAF:p300-CBP associated factor; HAT: histone acetyltransferase; GR: glucocorticoid receptor; HDAC2: histone deacetylase-2; DEX: dexamethasone.)

Moreover other studies have shown that DEX has also the ability of promoting osteoblasts differentiation (Tavakoli-Darestani et al. 2014) and down-regulating the

macrophages functions (Bridges & García 2008). Despite all the advantages of anti-inflammatory drugs administration, normal doses of drugs are not effective delivered via conventional administration routes, leading to the administration of high doses which may cause several side effects in other tissues (Oray et al. 2016, Saag et al. 2008) including gastrointestinal bleeding and perforation, osteoporosis (Baschant et al. 2013) and even heart failure or myopathy (Sun et al. 2010, Zhang et al. 2015).

In other words, anti-inflammatory drugs are efficient candidates from a molecular point of view, although when administrated via conventional routes, the cell-type specificity is lacking, thus demanding the utilization of high doses to achieve an *in vivo* therapeutic effect. From the clinical point of view, there are already some drug delivery strategies to locally target joint inflammation in development (Evans et al. 2014), although intraarticular injection remains the method of choice for local therapeutic delivery (Allen et al. 2010, Wernecke et al. 2015). A recent study by Wernecke et al. (2015) showed that DEX intra-articular injection after an injury may prevent later cartilage damage and joint degeneration (Wernecke et al. 2015). For example, the standard approximate dose for intraarticular injection of a corticosteroid, such as dexamethasone sodium phosphate, is between 0.8-4 mg, depending on the joint size (MacMahon et al. 2009). Despite the clear advantages, there are several known contraindications to the corticosteroids injections, including intraarticular sepsis, intraarticular fracture, and joint instability (MacMahon et al. 2009). Other approaches, such as bone grafts and bone grafts substitutes have been applied to restore bone loss during osteolytic reaction (Dattani 2007), however these can only be applied when bone defect is moderated. A revision study regarding hip replacements (Pierson & Harris 1994), reported that the utilization of new cemented femoral components helped to reduce periprosthetic osteolysis, where only 7% of the patients showed osteolysis 8.5 years later. Moreover, gender-specific sizing of implants and utilization of more effective bearing surface have also been employed (Mihalko et al. 2014). Recent studies to treat osteolysis have been dedicated administration of bisphosphonates and anti-cytokines, or gene therapy (Landgraeber et al. 2014, Ren et al. 2013, Talmo et al. 2006). Results obtained are promising however the *in vivo* efficacy of most of these approaches has yet to be proven (Goodman et al. 2013, 2014).

Altogether, the approaches described in this section have shown some significant improvements, although at the same time they produce high incidence of early and late complications, leading to the conclusion that no effective solutions for osteolysis has yet been found in the last decade. Therefore better approaches to modulate inflammatory response developed post-device implantation are needed to maintaining a balance between inflammatory response and effective recovering and tissue healing process (Li

et al. 2015). With this aim, improvements in materials and implants designs are being developed to improve the current limitations (e.g. periprosthetic infection, wear-debris induced inflammation, poor osteointegration) affecting the longevity of TJR. Thus, maximizing the *in vivo* performance of the implant, and of course avoid aseptic loosening. These includes the utilization of passive (e.g. non-biofouling coatings) or more active approaches such as the local delivery of anti-inflammatory agents, which are going to be addressed on the next chapter.

1.4.1 Anti-fouling coatings

Over the past years, the design of orthopaedic devices has primarily focused on the improvements of mechanical properties and function of the implant (De Jonge et al. 2008, Goodman et al. 2013). The goal relies in achieving device stabilization by promoting a more robust tissue healing response and osteointegration i.e. direct bond with adjacent bone at the implant site (Koju et al. 2017). Consequently, the patient will have an earlier rehabilitation and faster functional recovery.

For instance, biocompatible coatings, known for evoking a reduced host response, are currently an option to improve the bio-integration of medical devices after implantation. Ideally an implant coating besides being non-toxic, mechanical and chemical stable (Bridges & García 2008). It should also avoid additional tissue injury and ensure effective device-tissue communication; and preferably present a surface to minimize non-specific protein adsorption i.e. biofouling and inflammatory/immune cell adhesion that would exacerbate the foreign body response (Zhang et al. 2014a). Among the foreign body response events, protein and leukocyte adsorption process i.e. bio-fouling is one of the first events taking place soon after implantation, thus playing a crucial role on the subsequent cascade of inflammatory events (Bixler & Bhushan 2012). For this reason, the utilization of the so-called anti-fouling coating, which are know for minimizing the adsorption of non-specific protein, cell have been the subject of much interest and extensive research within the last few years. In terms of TJR, the aim is to diminish the extension of an inflammatory response or at least avoid the adverse fibrotic encapsulation of the implant, that is known for impairing the implant function (Bixler & Bhushan 2012, Bridges & García 2008).

Among all, polyethylene glycol (PEG) has been one of the most studied anti-fouling coatings (Banerjee et al. 2011); when grafted to a surface this hydrophilic polymer has demonstrated to be a impair specific proteins and bacteria adhesion, mainly due to its ability of retaining interfacial water molecules. More details regarding PEG utilization as anti-fouling strategy can be found in the excellent review published by Banerjee *et al.* (Banerjee et al. 2011). Other studies (Zhang et al. 2014a,b) have also demonstrated that other polymers such as heparin, chitosan and hyaluronic acid can be utilized as anti-fouling coating in orthopedic field to improve the performance (e.g. implant surface osteointegration, bone regeneration) of orthopedic devices (Singhatanadgit 2009, Tejero et al. 2014). The reactive groups (e.g. amino and hydroxyl) present in the polymeric chain have been used to bind these biopolymers to orthopedic metal implants surface (Chiang et al. 2012). For example, chitosan coatings, due to its cationic nature are reported to attract negative charged cytokines and growth factors, promoting cellular attachment and support the formation of natural extracellular matrix (EM), which are crucial factors for

bone healing (Bosco et al. 2012, von Wilmowsky et al. 2014). Also fibronectin, a non-collagen and natural occurring protein that contains in its structure the peptide sequence arginine-glycine aspartic-acid (RGD), has been widely used to facilitate adhesion and spreading of osteogenic cells (Lieder et al. 2012) to a variety of implant surfaces, including titanium (Middleton et al. 2007). Additionally, other studies reported the utilization combination of different bioactive compounds to form a coating with anti-inflammatory properties. Li *et al* (2014) assessed the co-immobilization of heparin and fibronectin in order to improve biocompatibility and anti-inflammatory properties of titanium surface (Li et al. 2014). Results obtained from *in vitro* macrophage culture, including TNF-α (pro-inflammatory cytokine) production, suggested that the co-immobilization of heparin and fibronectin complex improves the anti-inflammatory properties of untreated titanium surfaces.

More recent review (Koju et al. 2017), highlights the utilization of orthopedic implant coatings using the " old biomimetic technique" with some interesting modifications. The main advantage of this technique is that coating is applied onto the implant surface under biomimetic conditions under favorable physiological conditions by using different compositions of simulated body fluid (SBF) (medium pH of 7.4 at 37ºC). As a result, a bone-like calcium deficient carbonated hydroxyapatite coating is formed on the implant surface, which is especial beneficial to form a direct bond with the adjacent implant bone. Regarding the approaches utilised to coat the implants surface it should be noted that despite extensive research efforts only a few techniques have made it to clinical trials and respective commercialization (Bosco et al. 2012). In fact, most of the techniques are still in the early-clinical phase. Determining factors such as coating adhesion, cost-effectiveness and high costs related to upscaling limited the utilization of various novel surface engineering techniques

1.4.2 Anti-inflammatory drug-eluting implants

The systemic drug delivery approaches i.e. drug is administrated via the circulatory system to accomplish anti-inflammatory effect have been shown in the above chapter (1.4 Approaches to improve longevity/success rates of total joint replacement).

In this chapter, the local delivery strategies reported in the last decades and their numerous recognized advantages are reviewed (Figure 8). Local drug delivery is a more direct and site-specific manner to modulate inflammatory response, and in general it implicates the utilization of active surface containing anti-inflammatory agents such as drugs or biomolecules (Luo et al. 2011, Ma et al. 2016, Urbanska et al. 2014). Mainly this approach instigates more efficient therapies with significantly reduced side effects for patients.
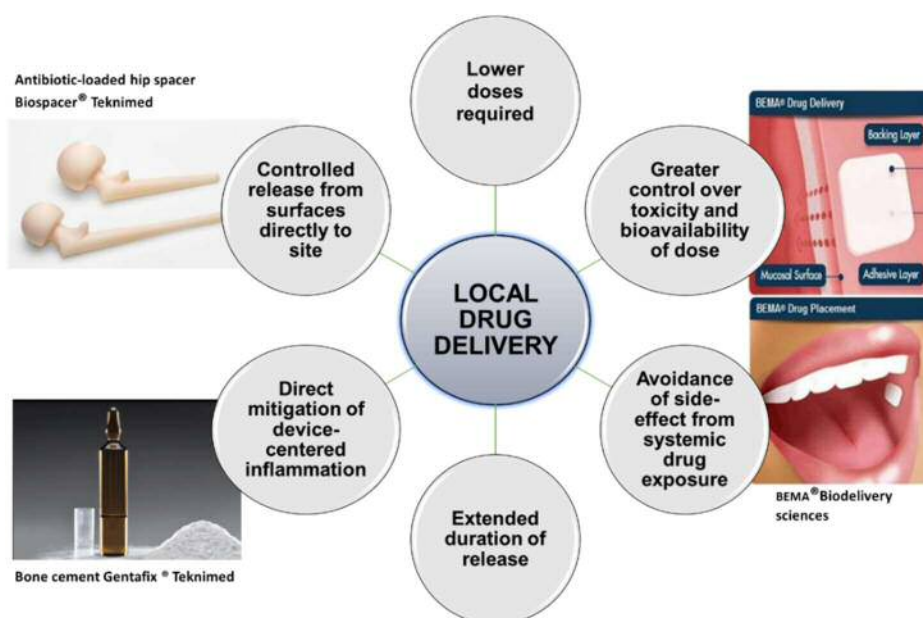
Figure 8. Summary of the advantages of local drug delivery strategies over systemic drug delivery, and examples of some approved local-drug delivery products. Adapted from (Wu & Grainger 2006)**.**

In the last few decades, drug-eluting implants have emerged as an advantageous alternative to traditional systemic drug administration for a broad range of clinical fields (Santos et al. 2014). This concept relies on the utilization of drug delivery systems incorporated on the implant, i.e. drug-eluting implants, capable of locally delivering the different drugs, including anti-inflammatory ones (Bhusal et al. 2016, Chung et al. 2015, Wang et al. 2013, Zhang et al. 2014a). The first drug eluting system to be developed was hormone pellets, which were implanted under the skin of livestock, aiming to improve their growth and make production more efficient (Santos et al. 2014). Regarding

periprosthetic inflammation treatment, the developed drug delivery system should modulate the inflammatory response in way that, a balance between inflammation and repair must be achieved to ensure successful tissue healing around the implant. Mainly, an ideal system will initially modulate acute inflammation, avoiding this way chronic inflammation and thus successfully starting a reparative wound healing phase (Goodman et al. 2013). The utilization of drug delivery systems provides several advantages apart for the drug entrapped *per se* (Dawes et al. 2011, Erdemli et al. 2014, Pioletti 2008)*,* such as; (a) the drug is rapidly and effectively available at peri-implant bone overcoming limitations of systemic delivery; (b) reduction of the amount of drug needed to achieve therapeutic effects, decreasing the potential side-effects of the drug (Lopes et al. 2013, Sun et al. 2010), among others (Anselmo & Mitragotri 2014).

In medical field, the utilization of drug/device combination products has been growing, products such as drug eluting-cardiovascular stents (Zhang et al. 2015), ocular implants (Feng et al. 2014), scaffolds and insulin pumps (Vallejo-Heligon et al. 2016) More detailed reviews regarding drug-eluting devices for orthopedic applications can be find in the literature (Goodman et al. 2013, Koju et al. 2017, Lyndon et al. 2014). From all these, cardiovascular eluting drug-stents to prevent restenosis, and drug-eluting implants to prevent infection in orthopedic and dental application are the ones which have been showing more approved products (Dangas et al. 2010, Gutowski et al. 2014). Recently, FDA approved a DEX intra-vitreal eye-implant, OZURDEX ® that is able to provide an extended 3 months drug release, avoiding the frequent need of DEX injections (Haller et al. 2011). Although, corresponding to the orthopedic applications, most of the studies on drug delivery systems have been performed for targeting infection (Moskowitz et al. 2010, Taha et al. 2013), such as bone cements associated with antibiotics or by simply immobilizing antibiotics onto implant metallic surfaces (Hickok & Shapiro 2012, Lyndon et al. 2014). Other biomaterials such as phosphate cements, hydroxyapatite, chitosan and poly (lactic-co-glycolic acid) have been prepared into different forms e.g. granules, matrices, coatings, foams, hydrogels, membranes, sponges) to be used to develop drug-eluting implants for bone related applications (Lyndon et al. 2014, Santos et al. 2014). For instance, Mendez and co-workers (Mendez *et al*., 2004) reported the study of an injectable bone cement formulation as a potential carrier of anti-inflammatory drug model, fosfosal 2-(Phosphonooxy) benzoic. Results demonstrated a local release of fosfosal from PMMA-Bioactive glass cement that could eliminate the need of anti-inflammatory drugs systemic administration, although further *in vitro* and *in vivo* studies are needed to prove this theory. Likewise application of nanotubes as anti-inflammatory delivery systems have been extensively reported in literature (Doadrio et al. 2015, Minagar et al. 2012). These systems have clearly shown

several advantages in orthopaedic applications such as *in vivo* and *in vitro* biological activity in terms of osteoblasts attachment, proliferation and differentiation (Das et al. 2009, Sobieszczyk & Klotzke 2011) and anti-inflammatory activity *per se* (Luo et al. 2011). Also the utilization of dendrimer-conjugates stand out as particularly promising system to modulate inflammation, mainly due to the possibility of achieving a high drug–loading and a controlled release profile into the site of periprosthetic inflammation (Caminade & Turrin 2014, Gillies & Fréchet 2005, Wu et al. 2015). Some examples regarding utilization of anti-inflammatory delivery systems with potential application in the orthopedic field are summarized in Table 2.

Table 2. Anti-inflammatory delivery systems with potential application to orthopedic field*.*

Anti-Inflammatory Agent	Delivery System	*In Vitro/In Vivo* Assay	Anti-Inflammatory Effect	Reference
Curcumin	Exosomes	Raw 264.7 macrophage cell line	Inhibition of IL-6 and TNF-α when compared to curcumin alone	(Sun et al. 2010)
Dexamethasone (Dex)	Polylactic-co-glycolic acid (PLGA) microspheres	Simian Virus-immortalized Human Fetal Osteoblast (SV-HFO) cells	Promoted osteoblast differentiation and matrix mineralization, when compared to free drug.	(Dawes et al. 2011)
Erythromycin (em)	Poly(amidoamine) dendrimer (PAMAM)	LPS-activated Raw 264.7 macrophages cell line	Inhibition of inflammatory marker i.e. nitric oxide concentration (NO) (~65mM) when compared with cells	(Bosnjakovic et al. 2011)

			treated with free EM (~85mM).	
Dex	N-(2-hydroxypropyl) methacrylamide (HPMA) co-polymer	Murine calvaria model	Single injection of Dex-conjugated-HPMA had the same therapeutic effect i.e.osteolysis attenuation as a daily Dex administration	(Wang et al. 2007)
Fluvastatin	Polylactic-co-glycolic acid (PLGA) microspheres	Rat tibia model	Transdermal injection enhanced formation and mechanical properties of the bone around titanium implants when compared to free drug.	(Masuzaki et al. 2010)
Dex	Rosette nanotubes	Osteoblast cell line	DEX released from nanotubes increased osteoblasts density (3400 cells/cm^2) when compared to free DEX (2800 cells/cm^2).	(Chen et al. 2011)

One of the requirements for these systems is that the drug release should be controlled and reproducible in order to avoid a toxic level or an inefficient level of therapeutic concentration (Ginebra et al. 2012). Moreover anti-inflammatory drug delivery systems must be able to modulate inflammatory reaction, but at the same time allow the bone growing/tissue regeneration in order to promote the implant osteointegration (Bridges &

García 2008). A recent study reported that diclofenac sodium-incorporated in PEF scaffold successfully inhibited PGE_2 production and therefore COX-2 pathway. Although efficient in the treatment of acute inflammation, the inhibition of COX-2 also hampered the processes involved in bone regeneration and fracture healing (Sidney et al. 2015). In this case the anti-inflammatory delivery system does not respect the balance between inflammatory response and bone growth around the implant (osteointegration), making it unappropriated for orthopaedic application.

A potential approach to improve the design of these anti-inflammatory drug-delivery systems might be based on the physiological environment of inflammatory events. Recently it was reported (Chung et al. 2015, Rajamaki et al. 2013) that during inflammation, the pH in joints may reach 6.6. This so called "local acidosis" during inflammation, is a result of infiltration and activation of inflammatory cells in the tissue, leading to increased oxygen and energy demand, enhanced glucose consumption and thus increased secretion of lactic acid. In patients with arthritis the synovial fluid pH was reported to had average pH range of 6.8-7.1, compared with a pH range of 7.4-7.8 observed in healthy synovial fluid (Cummings & Nordby 1966, Fan et al. 2012, Jebens & Monk-Jones 1959). This information suggests that acidic environment (i.e. decrease of pH) may be an important stimulus to trigger the release of anti-inflammatory drugs from total joint replacement surface.

Despite the lack of success of the systems reported above (Table 2), it as to be considered that anti-inflammatory drug delivery systems for orthopaedic applications is still a very recent research topic. In this sense, some optimization of this systems is needed, mainly critical parameters such as the drug releasing kinetics needed to keep concentration within the therapeutic dose, and how to personalize the drug dosage for different clinical applications/therapies. Specifically, to target inflammation, more research is needed to increase the probability of developing a successful system, where the appropriate release and concentration of anti-inflammatory drug would be able modulate the inflammatory response after device implantation, and consequently to reduce the need for revision surgery due to aseptic loosening.

1.5 Aim of the project

Over the past decades, the utilization of TJR has expanded dramatically owing to increased life-expectancy, changing lifestyles and improved implant technology (Losina et al. 2012, Revell 2014). This has extensively improved quality of life of patients worldwide. However, early implant failure and problems during healing have been reported for certain patient groups such diabetic and elder people where bone regeneration is compromised. Besides, with the increasing age of the population, the number of patients with poor bone quality is constantly rising. Also, the increasing lifespan after primary surgery increases the probability for the exigency of revision. These present and upcoming challenges require a better TJR implant device technology. One of the major problems associated with TJR are the exacerbated inflammatory events caused either by tissue injury or wear debris (Gallo et al. 2013), that might end-up as osteolytic events and when not treated in aseptic loosening. Over last decades, although much research has been focused to overcome the TJR aseptic loosening (Ren et al. 2011a, 2013), still this condition cannot yet be prevented or treated by existing nonsurgical methods. It is therefore apparent that localized acute inflammation must be modulated to ensure TJR long lifetime and functionality. This can be achieved using anti-inflammatory agents, such as DEX. Nevertheless, undesired side effects of DEX systemic delivery had been extensively reviewed last decades (Oray et al. 2016, Saag et al. 2008, Schäcke et al. 2002). Hence, strategies have been applied in clinical practice to minimize the undesired side effects of anti-inflammatory drugs, including the local administration/injection of anti-inflammatory drugs into the articular cavity (Petit et al. 2014). Although in terms of clinical outcome, being a soluble drug, a rapid clearance of DEX (e.g. DEX sodium phosphate) is observed, requiring the frequent administration of the therapeutic drug such daily administration for 3−6 weeks (Chung et al. 2015, Elron-Gross et al. 2009). An ideal solution could be the functionalisation of implant surface with an anti-inflammatory agent, where a controlled, and continuous local delivery of DEX therapeutic concentration at the implantation site would be achieved. In this context, hypothetically the model system developed in this study, which consists on the functionalisation of implant surface with an anti-inflammatory drug (DEX) was suggested as a potential approach to avoid aseptic loosening. The DEX eluting model system was prepared through the surface functionalization of TiO_2 particles using different approaches, amino, mercapto and LbL routes. Respectively DEX was either attached by covalent bounding (amino and mercapto routes), or by electrostatic interaction (LbL route), where DEX was attached to (amino)-functionalised TiO_2 particles, with subsequent deposition of CH and ALG layers. The benefits of using functionalised TiO_2 particles as device surface model for drug eluting implants has been extensively

reviewed in literature (Bagherifard 2017, Lyndon et al. 2014, Popat et al. 2007, Wu et al. 2014). The main advantage of this system is that the surface modification performed on TiO_2 particles can be applied on clinically used TJR, made of titanium and titanium alloys. Besides, DEX will be directly release from implant surface rather than systemically, reducing unnecessary side effects. The utilization of different synthetic routes to attach DEX to functionalised- TiO_2 particles, was investigated to assess if the utilization of different linkers i.e. functional groups between DEX and TiO_2 particles will affect the loading efficiency of DEX, drug release profile, and the cellular behaviour e.g. toxicity, bioactivity of the model system.

Regarding model system characterisation, zeta potential measurements, TGA analysis, FT-IR, were performed, thus respectively providing evidence of the different organic group attached i.e. $-NH_2$, -SH on the surface of TiO_2 particles. DEX attachment was also investigated by assessing drug loading and encapsulation efficiency. Moreover, average size and morphology of model system was evaluated by means of transmission electron microscopy (TEM) and scanning electron microscopy (SEM). In addition, *in vitro* release studies were performed to investigate DEX release profile for each route and under different joint conditions, healthy joint (pH=~7) (Goldie & Nachemson, 1970), and inflamed joints, which are associated with local acidosis (pH between 6-6.5) (de Nadai, *et al*., 2013). On the other hand, *in vitro* studies, using a murine macrophages cell line, Raw 264.7, were conducted to investigate parameters such as toxicity or anti-inflammatory properties of the model system herein developed. For that an *in vitro* inflammation model, LPS-activated cells, was previous optimized and validated to investigate the anti-inflammatory activity of DEX released from TiO_2 particles under biological conditions.

The present PhD project aims to develop an anti-inflammatory drug eluting model implant to target one of the major causes for joint revision surgery, aseptic loosening secondary to periprosthetic osteolysis. We hypothesize that local release of an anti-inflammatory drug at bone-implant interface will modulate the inflammatory response induced by wear debris, avoiding this way an uncontrolled and prolonged chronic inflammation, and the following bone loss i.e. osteolysis around the implant (*Figure 9*).
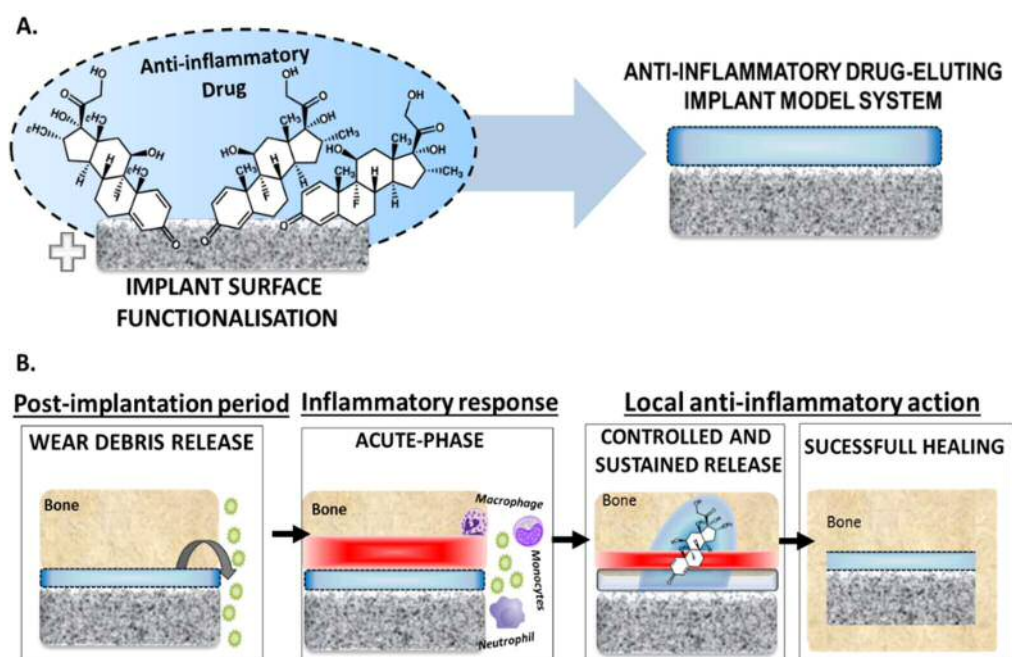
Figure 9. Schematics of (a) an anti-inflammatory drug-eluting surface model system and (b) potential effect when incorporated at implant surface.

To achieve the mentioned goals, an experimental research plan was defined:

(i)   Anti-inflammatory drug delivery model system development by different synthetic routes (amino, mercapto and Layer-by-Layer routes):

In an initial stage, the goal was to develop a model system capable of locally delivering an anti-inflammatory drug. With this aim TiO_2 particles, widely applied in biomedical field for its biocompability, easy scale-up and cost-effective characteristics, were selected as drug delivery model system. It is expected that surface modification performed on TiO_2 particles can be applied on clinically used total joint replacements, made of titanium and titanium alloys. We hypothesize that by preparing TiO_2 particles loaded with DEX through different synthetic routes, it will result in different level of drug loading, different release kinetics and subsequently different anti-inflammatory efficacy. With this aim, TiO_2 particles containing DEX were prepared by modifying the surface of TiO_2 particles through different synthetic routes: **Amino, mercapto and**

Layer-by-Layer (LbL), were targeted to introduce surface functionality on TiO₂ surface for subsequent attachment of an anti-inflammatory drug model. For this purpose, DEX, a synthetic glucocorticoid has been employed as a drug model, since it is already clinically used to modulate the inflammatory reaction after prosthesis implantation.

a)   **Amino and Mercapto routes**, the model system was prepared by covalently binding DEX to carboxyl functionalised TiO₂ particles. In this case, the carboxyl-functionalized surface will interact with hydroxyl group of DEX, thus forming an ester bond between the anti-inflammatory drug and surface of TiO₂ particles.

b)   **Layer-by-Layer (LbL) route** the aim was to test an alternative synthetic route to covalent bonding, where the anti-inflammatory drug will be adsorbed into amino-functionalised TiO₂ particles (template) using electrostatic interactions, and it will be surrounded by multilayer of positively and negatively charged polymers, chitosan and alginate.

(ii) Surface and chemical/material analysis:

In a second stage, aiming to gain further insight on functionalization of TiO₂ particles and attachment of DEX, the whole synthetic process of TiO₂ particles surface modification in different routes (before and after DEX loading) was investigated by means of thermogravimetric analysis (TGA), Fourier Transformed infra-spectroscopy (FT-IR) and zeta potential measurements. Also, other parameters such as the average size and morphology of DEX loaded-functionalised TiO₂ particles were evaluated by Transmission electron microscopy (TEM), as well as DEX release profile under different pH conditions.

(iii) *In vitro* cell studies:

Macrophages are the first immune cells to act towards invading organisms or tissue injury, and they play a key role in inflammatory response (Goodman et al. 2014, Hallab 2016). Thus, making them the *in vivo* targets in the orthopaedic applications envisaged for model system here in studied. For this purpose, *in vitro* Raw 264.7 macrophage cell line, was used to assess the biological behavior i.e. cytotoxicity and anti-inflammatory activity of DEX released from functionalised-TiO₂ particles. Besides, it is efficacy on screening the potential anti-inflammatory activity of drugs and delivery systems has been already demonstrated in previous studies (Jeon et al. 2000, Yuan et al. 2013).

(a) Cytotoxicity assessment

Before assessing the bioactivity of drug delivery model system on the cells, preliminary studies were done to investigate the individual effect of LPS and DEX on the RAW 264.7 cells viability. This way is possible to assess if the concentration of DEX that is released from the functionalised-TiO_2 particles, and the LPS concentration used to induce inflammation, will cause any adverse reaction to the cells. To assess cell cytotoxicity Methylthiazolyl Tetrazolium (MTT) and Lactase dehydrogenase (LDH) release assay were performed.

(b) Characterization and optimization of *in vitro* inflammation model

Murine macrophage cell line (Raw 264.7) is known for exhibiting features in common with monocyte macrophages, although it does not mimic macrophages behaviour under inflammatory conditions. For this purpose, RAW 264.7 cells were treated with lipopolysaccharide (LPS), a component of bacterial wall, known to induce a variety of inflammatory cytokines production in macrophages. Different Raw 264.7 cell seeding densities upon different LPS concentrations were tested to optimize the *in vitro* model. For this purpose, after exposing the cells to LPS, nitric oxide (NO) and tumor necrosis factor-alpha (TNF-α) production was measured to investigate the RAW 264.7 cells LPS-activation and consequently the reliability of the *in vitro* inflammation model. Being respectively a pro-inflammatory mediator and a pro-inflammatory cytokine, NO and TNF-α expression was simultaneous assessed to get further insight about the inflammation level. Moreover, cellular morphological changes after LPS addition were observed using fluorescence microscopy.

(c) Anti-inflammatory activity assessment

Once the preliminary *in vitro* studies (iii, a and b) were performed, the biological activity of DEX-loaded functionalised-TiO_2 particles was investigated to assess the anti-inflammatory activity. For this purpose, the LPS-stimulated RAW 264.7 cells were exposed to the broths collected from drug release studies. This way the cytotoxicity and anti-inflammatory activity of DEX released from drug delivery model system were investigated. As reported in previous studies (Joo et al. 2014, Soromou et al. 2012, van der Bruggen et al. 1999) LPS-activated macrophages secrete several inflammatory cytokines. Particularly, high production of NO and TNF-α has been associated with chronic inflammation (Parameswaran & Patial 2010, Zamora et al. 2000). On the other hand, DEX is known to block transcription if nuclear factor-kappa B (NF-Kβ), and consequently suppress the expression of inflammatory cytokines including nitric oxide (NO) and tumor necrosis factor-alpha (TNF-α) (Huebner, Shrive, & Frank, 2014).

Therefore, inhibition of NO and TNF-α production in LPS-stimulated cells was simultaneous assessed to get further insight about inflammatory effect of DEX released from functionalised-TiO$_2$ particles. Aiming to analyse the levels pro-inflammatory cytokines, Enzyme Linked Immunosorbent Assay (ELISA) (TNF-α,), and Griess reagent (Nitric oxide) assay were performed. As shown in Figure 9.b, we speculate that release of DEX from functionalised-TiO$_2$ particles will modulate the inflammation in LPS-activated macrophages. Moreover, cellular morphological changes after LPS addition were observed using inverted microscopy.

2. Materials & Methods

2.1 Chemicals

Dex-Loaded TiO$_2$ Particles synthesis

Titanium (IV) oxide (Anatase, <25nm, 99.7%), (3-mercaptopropyl) trimethoxysilane (MPTMS, 95%), (3-Aminopropyl)triethoxysilane (APTS, 99%), succinic anhydride (≥99%), Dexamethasone (Dex, >97%), 4-Pentenoic acid (≥98%, FG), 1-(3-Dimethylaminopropyl)-3-ethyl-carbodiimide hydrochloride (EDC, 98+%), N-hydroxysulfosuccinimide (Sulfo-NHS, 98%), N-morpholino) ethanesulfonic acid (MES) hydrate (>99.5%), Chitosan, Sodium Alginate, Phosphate buffer solution (PBS, pH=7.4) tablets, Sodium acetate trihydrate (≥99%), sodium chloride (ACS reagent, ≥99%), citric acid monohydrate (ACS reagent, ≥99%), disodium phosphate (ACS reagent, ≥99%) were purchased from Sigma-Aldrich, UK. HPLC grade acetonitrile, Glacial Acetic Acid, Methanol, Dichloromethane (DCM) and Toluene were all purchased from Fisher, UK. All other chemicals were reagent grade, stored according to manufacturer's guidelines and used as received.

2.2. Buffers preparation

2.2.1 2-(N-morpholino) ethanesulfonic acid (MES) buffer

MES buffer (10^{-2} M, pH 6) was prepared by dissolving 1,95g of MES hydrate in 100 mL of deionized water. The pH was achieved by dissolving one pellet of sodium hydroxide into MES buffer solution.

2.2.2 Acetate buffer

Acetate buffer (10^{-3} M, pH 4 and 5) was prepared by combining different volumes of sodium acetate hydrate (CH$_3$COONa·3H$_2$O) and acetic acid (CH$_3$CO$_2$H) solutions, according to the following table (Table 3).

Table 3. Acetic Acid-Sodium acetate buffer preparation.

pH	Acetic Acid (0.1 M) mL	Sodium acetate (0.1 M) mL
4	82	18
5	30	70
6	7	93

2.2.3 Sodium Chloride (NaCl) buffer

NaCl buffer (10^{-3} M, pH 7) was prepared by dissolving 0.058 g of NaCl in 100 mL of deionized water

2.2.4. Citric acid-disodium phosphate buffer

Citric acid-disodium phosphate buffer was used to obtain pH values between 4 and 7. The buffer was prepared by combining different volumes of citric acid ($C_6H_8O_7$) and disodium phosphate dodecahydrate ($H_{25}\,Na_2O_{16}P$) solutions, according to the following table (*Table* 4):

Table 4.Citric acid-disodium phosphate buffer preparation.

pH	Citric acid (10^{-3} M) mL	Disodium phosphate (10^{-3} M) mL
4	61.45	38.55
5	48.50	51.50
6	36.85	63.15
7	17.65	82.35

2.2.5. Phosphate buffer saline (PBS)

PBS buffer was obtained by dissolving 1 Tablet of PBS (pH=7.4) in 100 mL of deionized water.

2.3 DEX-loaded functionalised TiO$_2$ particles synthesis

2.3.1 Amino-route

1 g of TiO$_2$ particles were dispersed in 15 mL of anhydrous toluene. The TiO$_2$ particles surface was functionalized with amine groups by adding 100μl of APTS under stirring and incubation for 24 hours. Subsequently, the amine-functionalized particles (NH$_2$-TiO$_2$) were isolated by centrifugation at 14000 rpm for 5 minutes (LE-80K Ultracentrifuge, Beckman Coulter, UK) at 20°C followed by washing for at least three cycles with toluene to remove unreacted APTS. To re-disperse the centrifuged particles in the fresh toluene, they were vortex mixed (WhirliMixer^{TM}, Fisherbrand, UK) to make sure a visually well-dispersed suspension was regained before centrifuging again. The resulting particles were dried under the fume hood for 24 hours. Then amine-functionalized particles (NH$_2$-TiO$_2$) (250 mg) were dispersed in 100mL of DCM and purged with nitrogen. Succinic anhydride (25 mg) was dissolved in 2.5 mL of DCM and added to the reaction mixture to obtain carboxylic acid functionalized surface. This solution/suspension was kept under nitrogen for 18 hours. Subsequently, the succinilated-particles (COOH- NH$_2$-TiO$_2$) suspension was isolated by centrifugation at 14000 rpm for 5 minutes at 20°C followed by washing for at least three cycles with methanol to remove unreacted materials,

including re-dispersion/stirring step. The resulting particles were dried under the fume hood for 24 hours. The DEX was loaded into particles following two different methods: DEX adsorption and DEX conjugation.

DEX conjugation

To obtain DEX loading (covalent attachment), 50mg of DEX was dissolved in 100 mL MES buffer (0.1 M, pH 6.0). This solution was used to disperse 250mg of functionalized particles (Amino, Mercapto or Dendron), 10 mg EDC and 10 mg Sulfo-NHS. The suspension was kept under vigorous mixing for 24 hours. The Dex loaded particles were recovered by centrifuging at 14000 rpm for 5 minutes at 20°C by washing for at least three cycles with methanol to remove unattached DEX. To re-disperse the centrifuged particles in the fresh solution, they were vortex mixed for 5 minutes to make sure a visually well-dispersed suspension was regained before proceeding to a new centrifuging/washing cycle again. Then DEX loaded particles were left to dry under the fume hood for 24 hours.

DEX adsorption

For comparison purposes, the physical adsorption of DEX was also assessed. 50mg of DEX was dissolved in 100 mL MES buffer (0.1 M, pH 6.0). This solution was used to disperse 250mg of functionalized particles (Amino, Mercapto or Dendron). The suspension was kept under vigorous mixing for 24 hours. The Dex-loaded particles were recovered by centrifuging at 14000 rpm for 5 minutes at 20°C by washing for at least three cycles with methanol to remove unattached DEX. To re-disperse the centrifuged particles in the fresh solution, they were vortex mixed for 5 minutes to make sure a visually well-dispersed suspension was regained before proceeding to a new centrifuging/washing cycle again. Then DEX loaded particles were left to dry under the fume hood for 24 hours.

2.3.2 Mercapto-route

A similar protocol to the one utilized on the amino route (*2.3.1 Amino-route*) was adopted, with some modifications. Instead of using APTS, the TiO_2 particles surface was functionalized with thiol groups by adding 100μl of MPTMS under stirring and incubation for 24 hours. Similarly, the carboxyl functionalization step was different, where functionalization was achieved through dispersion of thiol-functionalized (Ti-SH) particles (250 mg) in 100 mL of methanol: water (2:1) solution, and then addition of 4-Pentenoic acid (25mg). This suspension was kept under ultraviolet using a hand-held UV lamp (UVGL-58, Cambridge, UK) set at λ = 254 nm for approximately 3 hours. Furthermore, the protocol applied to load DEX was also the same, where DEX conjugation and

adsorption were assessed.

2.3.3 Layer-by-Layer (LbL) Route

2.3.3.1 Preparation of polyelectrolyte solutions

The polyelectrolyte solutions were prepared dissolving sodium alginate (ALG) (2mg/mL), chitosan (CH) (2mg/mL), and DEX sodium phosphate (10mg/mL) in acetate buffer (0.1M, pH 5) with agitation using a magnetic stirrer (at 600 rpm), during 2 h at room temperature (20 ºC).

2.3.3.2 Assessment of polyelectrolytes solution charge

In layer by layer deposition the charge of polyelectrolyte solutions (CH, ALG, and DEX) must be measured to guarantee a correct electrostatic interaction, between the layers i.e. between NH_2-TiO_2 nanoparticles, DEX, ALG and CH layers. So, before starting LbL assembly the charge of each polyelectrolyte solution was evaluated by means of zeta potential measurements.

2.3.3.3 Synthesis of multilayer DEX-loaded-TiO_2 particles

Multilayer capsules were prepared by alternating deposition of alginate, chitosan and DEX layers onto a positively charged template i.e. amino functionalised particles (NH_2-TiO_2 particles). To prepare the template (NH_2-TiO_2 particles), the same method described in *2.3.1 Amino-route* was utilized. After that, the alginate, chitosan, and DEX layers were deposited onto NH_2-TiO_2 particles, by adopting the following protocol: Briefly 250mg of NH_2-TiO_2 particles were exposed to 20mL of ALG (2 mg/mL) solution. The mixture was incubated at room temperature, for 10-15 min under gentle stirring. The excess of polyelectrolyte was removed by two repeated circles of centrifugation at 4000 rpm for 5 minutes (LE-80K Ultracentrifuge, Beckman Coulter, UK) at 20°C with consequently removal of supernatant and re-dispersion in fresh acetate buffer (0.1 M, pH 5), discarding the unabsorbed ALG. The suspension was vortex mixed (WhirliMixer^{TM}, Fisherbrand, UK) to make sure a visually well-dispersed suspension was regained before centrifuging again. After the second cycle of centrifugation, the supernatant was removed, and particles were re-suspended in 20 mL of CH solution (2 mg/mL). The mixture was incubated at room temperature, for 10-15 min under gentle shaking, thus assembling the 2nd layer of the capsule (CH layer). The excess of polyelectrolyte was removed by centrifugation/ re-dispersion cycle in fresh acetate buffer (0.1 M, pH 5), discarding the unabsorbed CH.
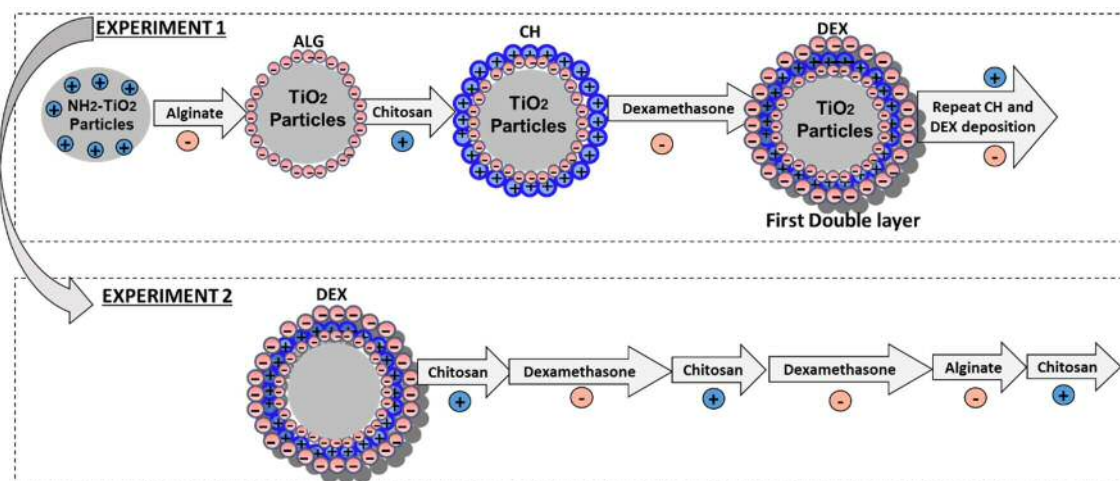
Figure 10. Schematics regarding the preparation of DEX-loaded particles, using amino-functionalised (NH$_2$-TiO$_2$) particles as template.

The following DEX layer was deposited using a similar procedure to the one described before, with the exception that LbL particles were re-suspended in 10 mL of DEX solution (10 mg/mL). To optimize this methodology after depositing the first DEX layer, different approaches i.e. experiment 1 and 2 were tested (Figure 10) by varying the type and combination of layers deposited onto template. Therefore, after the first DEX layer deposition, alternating CH, ALG or DEX layers were deposited according to the approach (Experiment 1 or 2) utilized, until the desired number of layers was achieved.

2.4 Particle characterization

2.4.1 Size measurements and surface morphology

Transmission electron microscopy (TEM)

Images of particles were obtained using a Zeiss 902 transmission electron microscope (TEM) operating at a voltage of 80 kV. The aqueous dispersion of the particles was drop-cast onto a carbon-coated copper grids, and grid was dried at room temperature (20ºC) before loading into the microscope (direct deposition). The average particle size, size-distribution and morphology analysis of the samples was carried out from transmission electron micrographs, where average size was estimated using the software Image J for Windows (Version 1.50i).

Scanning electron microscopy (TEM)

The surfaces of the TiO_2 particles and functionalised ones, were gold coated using a sputter compact coater (Shimadzu model CC-50), and imaged using a scanning electron microscope (SEM, VEGA3, TESCAN) at 15 KeV, with an integrated microanalysis X-ray system (EDS -energy dispersive spectrometer).

2.4.2 Zeta potential measurements

The electrophoretic mobility was determined by Dynamic Light Scattering (DLS) with a Malvern Zetasizer, ZS particle characterization system (Malvern Instruments Limited, UK), using a He–Ne laser (wavelength of 633 nm) at an angle of 17° which is combined with the reference beam to analyse the samples. Zeta potential values were determined by applying the Henry equation to convert electrophoretic mobility) to zeta potential ($ζ$) values Equation 1):

Equation 1: Henry Equation ⎯⎯⎯

Where, $ζ$ describes the zeta potential, $ε$ is the dielectric constant, describes the viscosity, and $f(κa)$ is Henry's function. As electrophoretic determinations of zeta potential are most commonly made in aqueous media and using moderate electrolyte concentration, the $f(Ka)$ is equal to 1.5, and is referred to as the Smoluchowski´s approximation (Nita, Chiriac, Bercea, & Wolf, 2013). The electrophoretic mobility is obtained by performing an electrophoresis experiment on the sample and measuring the velocity of the particles using Laser Doppler Velocimetry (LDV). For measuring zeta potential, 1mg of particles was dispersed in 1mL of buffer solution using the vortex and the ultrasonic bath (~30min). Then suspension was immediately transferred into the capillary cell. For pH 4 and 5, an acetic acid/sodium acetate buffer (0.01 M or 10^{-3} M) was prepared. As for pH 7, Sodium Chloride (NaCl) buffer (0.01 M) was utilized. Results were given as the average ± standard deviation of three measurements.

2.4.3 Fourier Transformed infrared spectroscopy (FT-IR)

FT-IR was used to identify the functional group in the samples before and after functionalization steps. Spectra were recorded on a Shimadzu IRAffinity-1S apparatus equipped with ATR diamond accessory, at room temperature between 4000 and 300 cm^{-1} with 4 cm^{-1} resolution running 16 scans.

2.4.4 Thermogravimetric analysis (TGA)

Thermogravimetric analysis (TGA) was performed using a Perkin-Elmer TGA 4000 instrument. The samples were heated from 50 to 800 °C with a constant heating rate of 10 °C per minute. Weight loss percentage of each sample was calculated relative to initial weight of sample, prior to heating. As for organic and inorganic material percentage, it was calculated by subtracting the point at initial weight loss (%) up to when the line plateaus (approximately around 800°C).

2.4.5 DEX loading and entrapment efficiency estimation

Drug loading was calculated using the High-Performance Liquid Chromatography (HPLC) standard calibration curve of DEX and DEX sodium phosphate, which were plotted to define the quantitative relationship between observed absorbance and concentration of the drug (Figure 81,
I. Appendix). The mass of DEX loaded into functionalised-TiO_2-particles was estimated by analysing the supernatants obtained during the centrifugation/washing cycles, which was part of DEX loading step. Briefly, for amino and mercapto routes, the supernatants were collected from each centrifugation step (3 cycles). As for LbL route, supernatants were collected from each centrifugation step (2 cycles) after loading of each DEX, CH, and ALG layers.

Then, the collected supernatants were analysed using HPLC to quantify the amount of DEX which was lost during centrifugation/washing cycles, and therefore was not loaded into the particles, as previously described (Pu et al. 2014). The DEX loading (%) and entrapment efficiency (%) were estimated based on the following equations (2 and 3) (Papadimitriou & Bikiaris 2009):

Equation 2 Drug loading (%):

Equation 3 Entrapment Efficiency (%):

All experiments were performed in triplicate. results are presented as the average and standard deviation of three samples.

2.5 DEX release profile

DEX loaded-functionalised TiO_2 particles prepared as described above (*2.3 DEX-loaded functionalised TiO2 particles* synthesis), were dispersed in citric acid-disodium phosphate buffer (10 mg ml^{-1}) within a pH range from 4-5, and in sodium acetate buffer (10 mg ml^{-1}) within a pH range from 6-7 at 37°C. The solution was replaced daily with fresh buffer and analysed to quantify the amount of DEX release using reverse-phase High Performance Liquid Chromatography (HPLC). An Agilent series 1100 HPLC system was equipped with analytical column (Waters Spherisorb®, Sigma-Aldrich, St Louis, MO, USA), with Pore size- 80Å, 5 μm, and width x length- 4.6 mm X 150 mm), thermostated at 25°C. The method was adapted from Martín-Sabroso *et al*. (Martín-Sabroso, *et al*. 2013); briefly, the injection volume was 10 μL, the mobile phase was PBS: acetonitrile: acetic acid (70:26:4), with a flow rate of 1 mL/min, and the detector was a UV spectrophotometer at 244 nm. An example of a chromatogram for a 1 mg/mL solution of DEX in DMSO is shown in Figure 81.B (

I. Appendix); the calibration curve of the HPLC detection of DEX is presented in Figure 81.A (

I. Appendix). The renovation of the release medium volume (1 mL) was guaranteed after each sample withdraw. All experiments were performed in triplicate. Results obtained from HPLC analysis are presented as the average and standard deviation of three samples.

2.6. Cell culture and treatments

Cell studies were performed using a commercially available murine macrophage-like cell line, Raw 264.7 cells. We decide to utilize macrophage cell line because, as seen in the introductory chapter (*1.3.2 Biological mechanism and inflammatory mediators*), macrophages are the one the most important immune cells to act towards invading organisms or tissue injury. Consequently macrophages play a key role in inflammatory response (Goodman et al. 2014, Hallab 2016) by producing different inflammatory mediators (e.g. cytokines, NO) in response to pathogens such as bacterial LPS (Oh et al. 2012). For that reason, Raw 264.7 macrophages have been widely used in other studies to investigate the toxicity and bioactivity of different anti-inflammatory compounds(Kim & Ha 2009, Pinho et al. 2011, Vairappan et al. 2013), and potential anti-inflammatory delivery systems (Bosnjakovic et al. 2011, Joo et al. 2014, Yuan et al.

2013).Regarding the treatments, the choice of treating the cells with different concentrations of DEX (3.9- 100 µg/mL) was based on the results obtained on drug release assay studies previously performed *(4.2. DEX release profile).* In addition, the DEX concentration of 100 µg/mL was tested to assess if a higher concentration will induce cell toxicity. As for LPS (LPS; E. coli serotype 026: B6; Sigma Cat. No. L2762) concentrations (0.1-1 µg/mL), it was chosen according to previous studies (Lee et al. 2013, Oh et al. 2012, Pinho et al. 2011). Moreover, aiming to test the effect of DEX released from functionalised-TiO$_2$ particles, Raw 264.7 cells were treated with broths collected from drug release studies previously performed as described above *(2.5 DEX release profile).*

2.6.1 Raw 264.7 macrophages cell line

RAW 264.7 cells (Figure 11) were obtained from European Collection of Cell Cultures (ECACC). Cells were grown in Dulbecco's modified Eagle's Medium (DMEM) containing 10% fetal bovine serum and 100 U/mL of penicillin/streptomycin, under 5% CO$_2$ at 37°C, in humidified air, and 70% of ethanol was used for disinfection of all stages throughout the experiments. The culture media was changed every 3 days, except when cells were thawed, in this case culture media was changed after 1 day to remove debris and unattached cells.
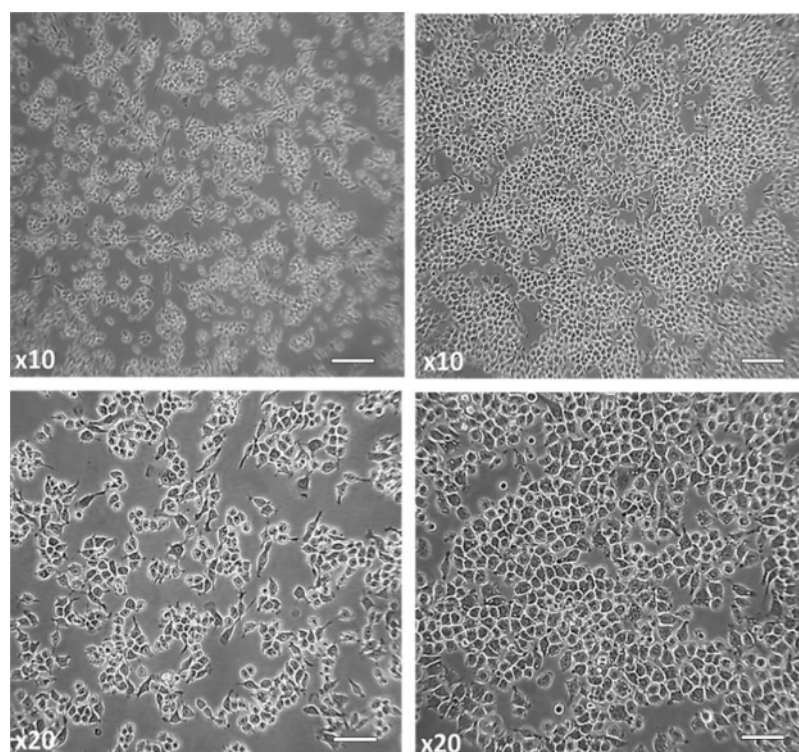
The adherent cells were split once a week before reaching confluence. For splitting the culture medium was removed, 10 mL of fresh medium was added, and cells were scraped off the flask bottom and transferred to universal tube to be centrifuged (5000 RPM, 5 minutes). The obtained pellet of cells was re-suspended in 1mL of fresh media, and 10 μL aliquot of cell suspension was taken to perform cell counting. The cell number and viability in the cell suspension was determined as cells/mL, by using a cell counting chamber. Dead cells were stained with a trypan blue solution and were excluded from counting. Then, after cell counting, the cell suspension obtained after centrifugation was diluted and transferred to a new flask. For all experiments, the cells were subjected to no more than 10 cell passages.
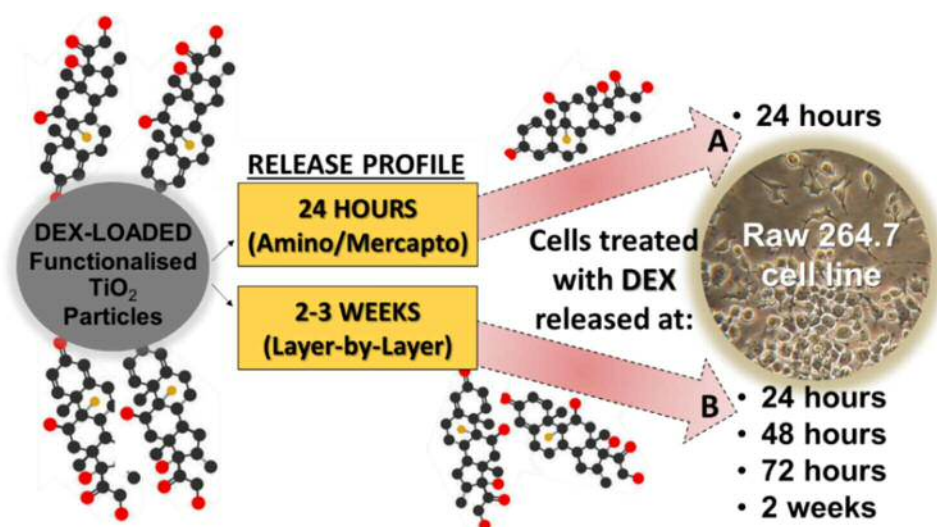
Figure 12. Schematic of the experimental plan adopted to assess the cellular viability and anti-inflammatory activity of DEX-loaded functionalised-TiO₂ particles obtained by different synthetic routes. Cells were exposed to broths (i.e. DEX release from functionalised-TiO₂ particles) according to release profile obtained for each synthetic route. 24h broths for amino/mercapto route (A) and at 24h, 48h, 72h and 2 weeks broths for LbL route (B) studies.

For all assays, cells were seeded at a density of $2x10^5$ cells/mL and permitted to adhere over 4-5-hour period, before treatments were added, as previously described (Pinho et al. 2011). Preliminary studies to optimize cell density (cells/well) were performed, as can be seen in the appendix section (

I. Appendix. Preliminary *in vitro* studies)*. All treatments were freshly prepared by diluting the stock solution in culture DMEM medium. In all experiments, a control was performed where cells were incubated only with culture medium. Raw 264.7 cells were cultured for 7 days, (culture media changed every 3 days), and the cellular behaviour (e.g. viability, NO/TNF-α production) was assessed at different time points. Although all experiments were performed for 7 days, only results up to 3 days were showed in this thesis, mainly because after 3 days, MTT assay and cells observation under inverted microscope, revealed that macrophages were over confluent (

I. Appendix. *Figure 87*) Moreover, as can be seen from drug release studies (3.4 DEX release profile), the route utilized to synthesize DEX-functionalised-TiO$_2$ particles significantly affected the drug release profile. Not only the DEX concentration, but also the release duration were different for particles obtained by amino/mercapto (24 hours), (Figure 40 and Figure 41), and LbL route (2-3 weeks) (Figure 42 and Figure 43). For this reason, cellular behavior of RAW 264.7 macrophages was investigated according to release profile obtained for each synthetic route. Briefly, cells were exposed to broths (i.e. DEX release from functionalised-TiO$_2$ particles) collected at different time points: 24h for amino/mercapto route (Figure 12.A), and 24h,48h, 72h and 2 weeks for LbL route studies (Figure 12.B). The aim of this experimental set up was to assess the potential anti-inflammatory effect during the total period that is DEX released: 24h for amino/mercapto and 2 weeks for LbL routes.

2.6.2 LPS-activated Raw 264.7 cell line: inflammation model

Murine macrophage cell line, Raw 264.7 is known for exhibiting features in common with monocyte macrophages, although it does not mimic macrophages behaviour under inflammatory conditions. For this purpose, in several studies RAW 264.7 cells were treated with lipopolysaccharide (LPS), an endotoxin, known to induce a variety of inflammatory modulators production in macrophages (Pinho et al. 2011, Sharma et al. 2007). This is entirely applicable, since LPS-activated Raw 264.7 cells have been utilized in previous studies to evaluate the anti-inflammatory effect of potential anti-inflammatory drugs and delivery systems (Bosnjakovic et al. 2011, Joo et al. 2014, Lee et al. 2013, Terra et al. 2007, Yuan et al. 2013). LPS concentrations to be tested were chosen according to previous studies (Lee et al. 2013, Pinho et al. 2011), which also aimed to investigate anti-inflammatory activity.

In an initial stage, preliminary studies were performed to assess the more effective LPS concentration to activate the cells, and the optimal seeding density which will produce measurable amounts of NO. Briefly, during preliminary studies, 2.5 x10^4 cells/well were stimulated with LPS concentrations ranging from 0.01-1 µg/ml and NO was measured at

18, 24, 48 and 72 hours to optimize LPS concentration. Then different cell densities were stimulated with 1 µg/ml of LPS, and NO and TNF-α were measured at 18, 24, 48 and 72 hours to optimize cell seeding density, and evaluate the temporal pattern of inflammatory markers production.

Raw 264.7 cells were seeded at a density of $2x10^5$ cells/mL in a 96 well-plate and permitted to adhere over a period of 4-5 hours. Cell were then treated with DEX or broths collected from drug release studies for one hour, followed by incubation with LPS (1µg/mL), to stimulate/activate the macrophages. After the addition of LPS the cells were cultured for 3 days. Then cellular behavior (e.g. viability, NO production) was then assessed at different time points. The effect of treatments (DEX and broths collected from drug release studies performed at pH 4, 6 and 7) in the absence of LPS were also assessed, to observe if they induced changes in basal levels of the assays performed.

2.7 Cellular viability

2.7.1 Methylthiazolyl Tetrazolium (MTT) assay

Cellular viability/proliferation of cells after being exposed to tested compounds was assessed using the mitochondria dependent reduction of Methylthiazolyl Tetrazolium (MTT) to formazan (Figure 13), according to Oh and collaborators (Oh *et al*., 2012) with some modifications.
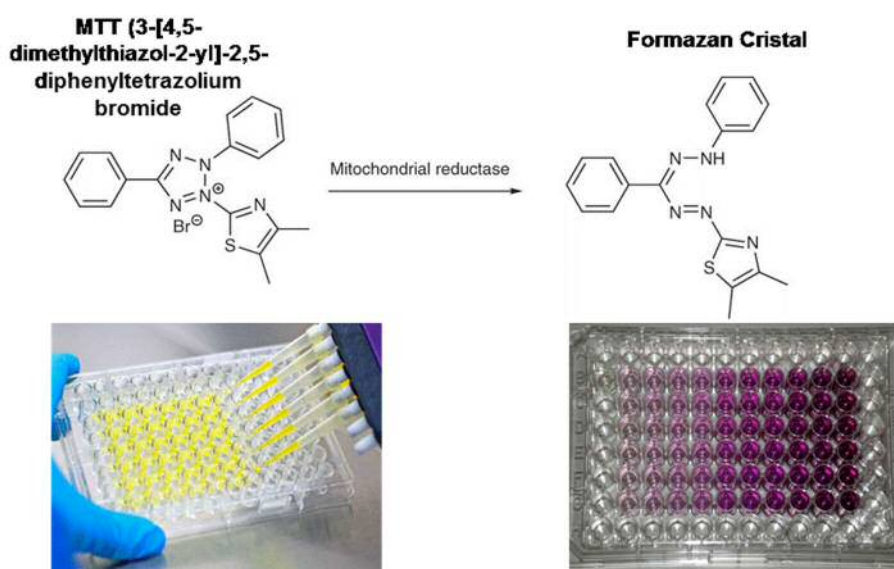
Figure 13. The reduction reaction of the tetrazolium salt MTT to a formazan dye, is catalyzed by mitochondrial reductases only in living cells and is therefore used to assess cell viability.

After described above incubation (2.6. Cell culture and treatments), the culture medium was removed and 20µL of the MTT solution (5mg/mL) was added to each well and incubated at 37°C in a humidified 5% CO2 atmosphere, for another 4 hours. Then supernatant was carefully discarded and 100µL of Dimethyl sulfoxide (DMSO) was added to each well to solubilize formazan. The absorbance at 540 nm was measured using ELISA reader. The absorbance (MTT values) by untreated cells (control) was chosen as the 100% value. Although, for LPS-activated Raw 264.7 cells the absorbance of treatment groups was normalized to the LPS-treated control and expressed as a percentage

2.7.2 Lactase dehydrogenase (LDH) release assay

Quantification of lactate dehydrogenase (LDH) is a method to investigate the cytotoxicity of a substance. This assay is based on the release of LDH, cytosolic enzyme, upon cell lysis. Therefore, LDH released into culture media assay was used to evaluate cell damage after treatment with test compounds. Briefly an aliquot of cell culture medium was carefully taken from each well, and the LDH activity in the medium was determined using an LDH cytotoxicity detection kit (Sigma). A 150 µl of reaction mixture was added to 75 µl aliquot of each well, and the reaction was incubated for 30 min at 37°C in a humidified 5% CO_2 atmosphere. The absorbance of each well was measured at 490 nm using a microplate reader. Results are expressed as a percentage of the respective control (with or without LPS).

2.8 Inflammatory markers measurement

2.8.1 Measurement of Nitric oxide (NO) levels (Griess reagent)

Previous studies have shown the production of inflammatory reactive oxygen species such as nitric oxide (NO) on LPS-activated Raw 264.7 cells (I.-T. Kim et al. 2012; Saxena, Vallyathan, and Lewis 2003; Sharma, Al-Omran, and Parvathy 2007). The expression of those cytokines and chemokines on LPS-activated Raw 264.7 reflects the level of inflammation, and therefore provides a measure of the inflammatory response (Pinho et al. 2011; Oh et al. 2012). NO is a very short-lived and reactive molecule, and easily degrades into more stable end products, such as nitrate and nitrite (Lundberg et al. 2008). Therefore, NO formation has to be quantified by measuring its stable decomposition products, nitrite (NO_2^-) and nitrate (NO_3^-) in the cell culture media (Bryan & Grisham 2007). This method requires that NO_3^- first be reduced to NO_2^-, and then NO_2^- is determined by the Griess reagent, a spectrophotometric technique based in an enzymatic reaction(Sun et al. 2003), as shown in Figure 14.

The Griess reagent system (Thermo Fisher Scientific ®) was utilized to measure nitrite (NO_2^-), which is the stable metabolite of nitric oxide (NO), in the supernatants of Raw

264.7 macrophages, as previously described by (Pinho et al. 2011). After incubation (as described in 2.6. Cell culture and treatments), 100 µL of cell culture supernatant was mixed with the same volume of Griess reagent for 30 min at room temperature. Samples of fresh culture media were used as blanks for all experiments. Then nitrite produced was determined by measuring optical density of the mixture at 540 nm in a microplate reader. Nitrite was quantified by an external standard, using sodium nitrite ($NaNO_2$) to generate a standard calibration curve (Figure 82, supplementary information).
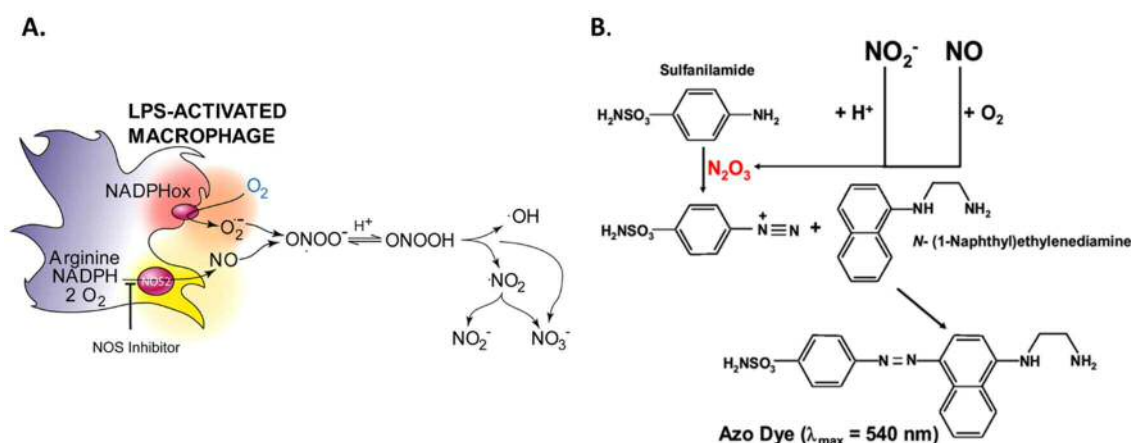
Figure 14. A. Nitric oxide production in LPS activated macrophages (A.). In the Griess Reaction (B.), the nitrosating agent dintrogen trioxide (N_2O_3) generated from acidified nitrite (or from the autoxidation of NO) reacts with sulfanilamide to yield a diazonium derivative. This reactive intermediate will interact with N-1-naphthylethelene diamine to yield a coloured diazo product that absorbs strongly at 540 nm. Image adapted from (Bryan & Grisham 2007)**.**

Results are expressed as the nitrite production percentage compared with the respective control (with or without LPS). The NO concentration was calculated by comparison with a $NaNO_2$ (0–100 µM) standard curve. The results were expressed as inhibition of NO production compared to the control (LPS) using:

Equation 4 NO production (%to LPS):

$$NO \text{ production (\%to LPS)} = ([nitrite]_t * 100)/[nitrite]_c$$

where $[nitrite]_c$ and $[nitrite]_t$ is the nitrite concentration in the LPS control group and test sample, respectively. Under the same experimental conditions, cell viability was evaluated by conducting MTT assay. MTT assays were performed to simultaneous evaluate the cytotoxic effect of tested compounds toward RAW 264.7 cells with and without LPS. Briefly, after transferring 100 µL of media to 96-well plate to measure NO

production, MTT solution was added to each well, and cells were further incubated at 37°C for 3-4 h as described above (2.6. Cell culture and treatments).

2.8.2 Assessment of TNF-α expression

Tumor necrosis factor alpha (TNF-α) expression was assessed using the murine TNF-α enzyme-linked immunoabsorbent assay (ELISA) development kit (Peprotech, US). For this study, 3.5×10^4 macrophages/well were cultured in 48-well plates, then treatments were added with or without LPS (1µg/mL).
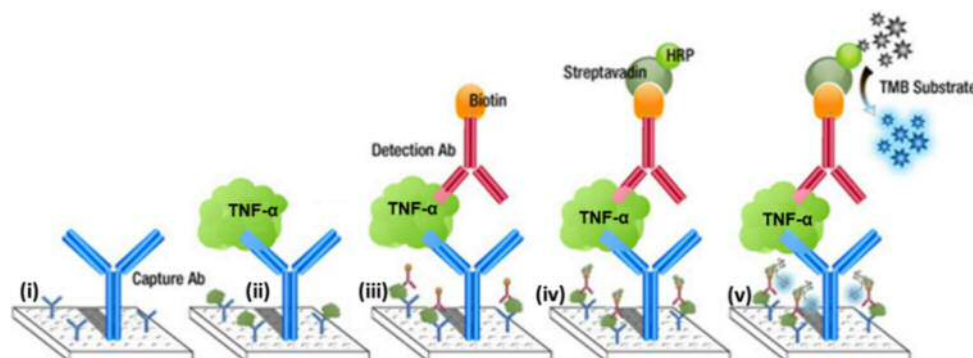
Figure 15. Schematic diagram of Sandwich ELISA assay utilized to detect TNF-α.
(i) Capture antibody specific affinity for murine TNF- α was attached to 96-well plate. (ii) Sample is added to the well and the target protein (TNF-α) is captured by the ligand. (iii) A detection ligand that also binds to the target protein (TNF-α) is added to the well and creates a "sandwich" with two ligands surrounding the target protein. (iv) Streptavidin protein with a horse radish peroxidase (HRP) is added to the well. The streptavidin binds to the biotin end of the detection ligand. (v) then, the TMB (HRP substrate) is added to the well and a blue coloured product is produced that can be detected with a spectrophotometer.

Briefly, TNF-α concentration was quantified according to the folowing protocol (Figure 15) :

(i)   **Plate preparation**: 100µL of the capture antibody (Polyclonal Rabbit Anti-Murine TNF-α, 0.50µg/ml in PBS) were added to each ELISA plate well, the plate was sealed and incubated overnight at room temperature. Then, the wells were washed (0.05% Tween-20 in PBS) three times and incubated with 300 µL of blocking buffer (1%BSA in PBS) for at least 1 hour at room temperature.

(ii)   **Sample incubation :** 100µL of sample were added to each well in triplicate, and incubated at room temperature for at least 2 hours.

(iii)   **Detection :** the wells were aspirated and washed at least four times. Then 100µL of detection antibody (Biotinylated Rabbit Anti-Murine TNF-α, 0.25µg/ml in diluent) were incubated at room temperature for 2 hours.

(iv)   **Streptavidin-HRP Conjugate:** the wells were aspirated and washed at least four times. Then 100µl of Streptavidin-Horseradish Peroxidase (HRP) (0.025ug/ml in diluent) were added to each well and incubated for 30 minutes at room temperature.

(v)   **TMB (3,3',5,5'-tetramethylbenzidine) Liquid Substrate:** the wells were aspirated and washed at least four times. Then 100µl of substrate solution (room temperature) was added to each well and Incubated at room temperature for color development for 20 minutes. Colour development was measured with an ELISA plate reader at 410nm, and with wavelength correction set at 650nm.

2.9 Fluorescent staining of actin

Previous studies have described an important role that cytoskeleton f-actin reorganization/remodelling plays in mediating inflammatory markers production in response to LPS stimulation (Ion et al. 2015, Isowa et al. 1999).

Briefly, RAW 264.7 macrophages grown on glass coverslips were stimulated with LPS for 24h to induce inflammation. The cells were fixed in buffered 4% formaldehyde for 10 min, permeabilized with Tris buffered saline (TBS) containing 0.5% Triton X-100 for 30 minutes, and then blocked in TBS containing 10% of horse serum (NHS) for 1 h. The cells were incubated for 40min with phalloidin-FITC (fluorescein isothiocyanate) (10 µg/ml; Sigma-Aldrich Co.) diluted 1:50 in TBS. After incubation, the coverslips were washed three times in TBS and transferred to glass slides. Cells were mounted using Vectashield mounting medium containing 4',6-diamidino-2-phenylindole (DAPI). The cells were then imaged using an Olympus IX70 fluorescence microscope. Samples were excited at 496 nm and 350 nm wavelength respectively for FITC and DAPI channels.

2.10 Statistical analysis

The statistical significance of differences between means was determined by first testing for global differences by one- or two-way analysis of variance (ANOVA). Experimental results were considered statistical significant at 95 % confidence level (*$p<0.05$). When a P value of <0.05 was found, multiple comparisons post-test was performed to compare treatment groups with control group. All analyses were run using the Graph Pad Prism® software (Version 6.0; GraphPad Software, Inc., San Diego, CA). According the software, statistical difference was very significant (**$p<0.05$), and extremely significant (***$p=0.001$ to 0.01) or (****$p<0.001$). Data are the mean± standard deviation (SD) of three replicate cultures, and at least two independent experiment (n≥2).

3. Results

In this study, an anti-inflammatory eluting implant model system was developed and characterised: TiO$_2$ particles were chosen as model system to mimic the implant titanium surface. DEX, a synthetic glucocorticoid approved by FDA and clinically used to modulate the inflammatory reaction (Holte & Kehlet 2002), was chosen as a model drug because of its potential use to modulate inflammatory events in TJR. The main advantage of this model system is that can be easy translated to clinical application; since all the surface modification performed on TiO$_2$ particles can be applied on clinically used TJR, made of titanium and titanium alloys. Besides, DEX will be directly release from implant surface rather than systemically, reducing unnecessary side effects. For this purpose, the surface of TiO$_2$ particles was functionalised to attach DEX by using different synthetic routes, amino, mercapto and Layer-by-Layer (LbL) routes. In this chapter, the results regarding the synthesis and characterization of the model system, DEX-loaded functionalised TiO$_2$ particles, were described (Figure 16).   Including chemical reactions scheme for each synthetic route, surface charge, fourier transform infrared-spectroscopy (FT-IR), thermogravimetric analysis (TGA), drug loading and entrapment efficiency, DEX release profile, and charge/size/morphology of the functionalized and DEX-loaded particles.
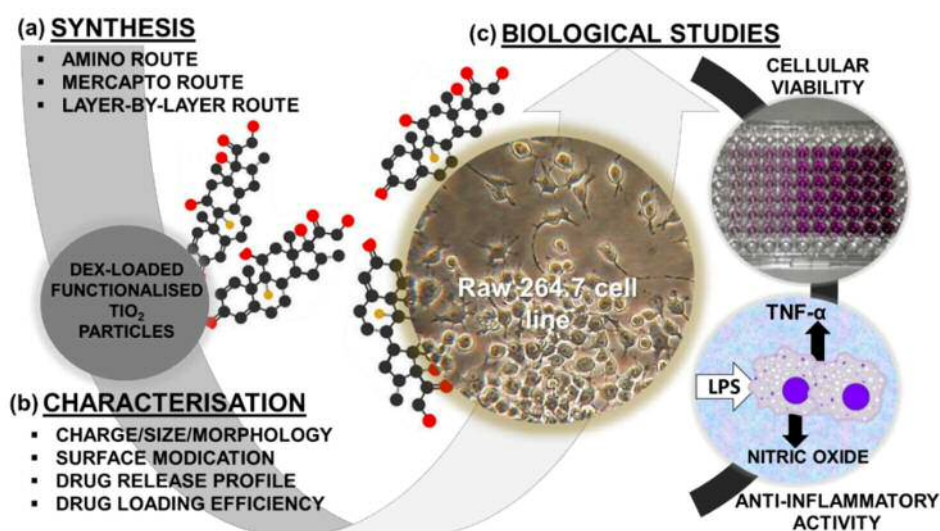
Figure 16. Summarised scheme of (a) synthetic routes, (b) characterization methods and (c) biological studies performed to study the anti-inflammatory-drug eluting model system, DEX-loaded functionalised TiO$_2$ particles.

Moreover, further biological studies were performed to test the cytotoxic and anti-inflammatory efficacy of the model system. A robust, rapid and reproducible *in vitro* mouse macrophage-like cellular model, utilizing RAW 264.7 cells was hence employed. In this model a component of bacteria wall, LPS, was used to activate the Raw 264.7 macrophages, resulting in the secretion of inflammatory mediators including nitric oxide (NO) and tumour necrosis factor alpha (TNF-α). The suppression of which was utilized to investigate anti-inflammatory effect of DEX released from functionalised-TiO$_2$ particles. Being respectively a pro-inflammatory mediator and a pro-inflammatory cytokine, NO and TNF-α, which high production has been associated with chronic inflammation (Parameswaran & Patial 2010, Zamora et al. 2000), their expression provide noteworthy information about the level of inflammation   Therefore, by simultaneously assessing NO and TNF-α expression in LPS-activated macrophages, it was possible to get further insight about DEX anti-inflammatory mechanism of action. This was combined with assessment of cell viability to exclude the decrease of inflammatory mediators due to drug-induced toxicity.

3.1 DEX amino-functionalized particles

3.1.1 Chemical reactions

When amino route was utilized, TiO$_2$ particles were first functionalized with amine groups (-NH$_2$) and then with carboxylic groups (-COOH). Initially the TiO$_2$ inorganic surface was modified with silane agent, APTS, to give terminal amines (-NH$_2$) (Schematic Reaction 1. Figure 17). After that, succinic anhydride was added to the reaction (Schematic Reaction 2. Figure 17), to obtain particles with carboxylic-functionalized surface (-COOH-TiO$_2$). As previously described, (Wu et al. 2011), the carboxylic acid group arises from the ring opening of succinic anhydride through a reaction with the amine group (-NH$_2$) on the surface of the TiO$_2$ particles, creating an amide bond, as previously described (Hermanson 2013, Zhao et al. 2014). The attachment of this –COOH is of outmost importance to obtain successful drug loading, since it will act as a binding site to DEX.
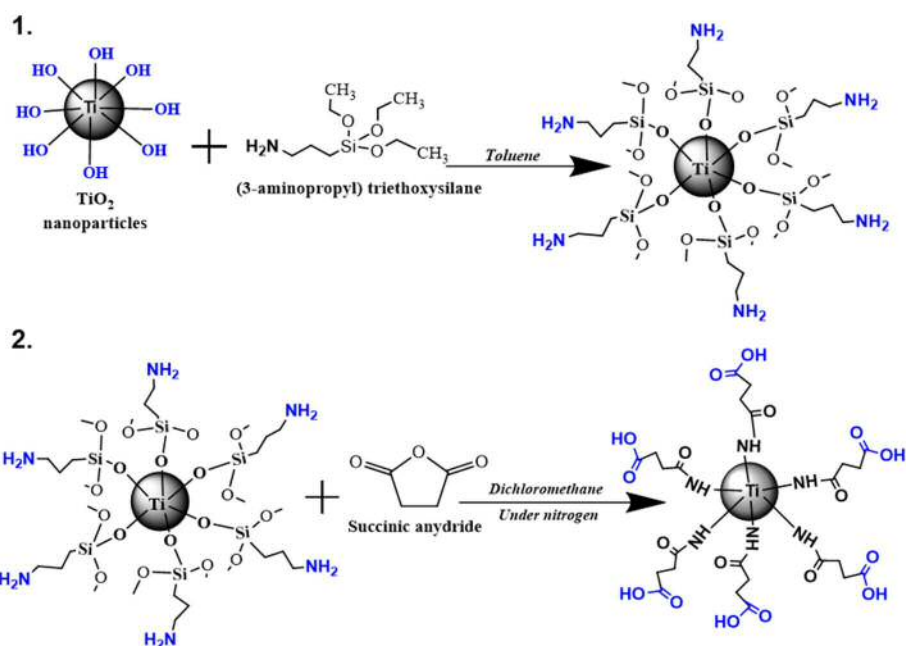
Figure 17. Schematic of reaction regarding carboxyl-TiO₂ particles functionalization, using amino route. Functional groups on TiO₂ particles are highlighted with blue colour.

Finally, DEX was then added to the succinilated-TiO₂ particles, to obtain Dex-loaded TiO₂ particles, with (conjugated) or without adding EDC/Sulfo-NHS (adsorbed) (Figure 18).
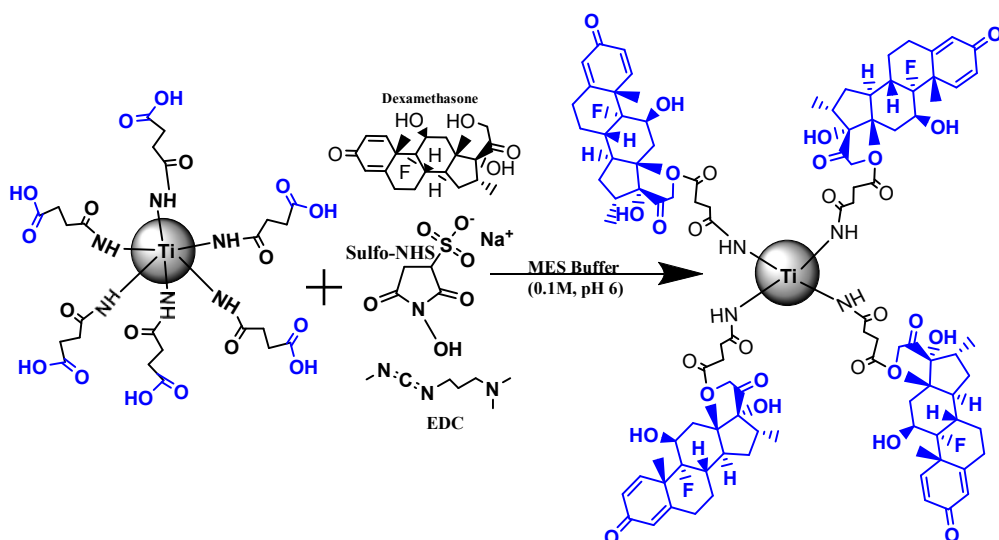
Figure 18. Schematic of reaction regarding DEX loading into carboxyl-functionalized TiO₂ particles using amino route. Functional groups on TiO₂ particles are highlighted with blue color.

NHS/ EDC cross-linking agent was added as an attempt to improve the reaction efficiency, and stability of the bond formed between DEX and –COOH-TiO$_2$ surface (Hermanson, 2013b). Several reports describe the successful attachment of biomolecules, such as peptides (Bartczak & Kanaras 2011), collagen (Cao & Xu 2008) and heparin (Wissink et al. 2001) to delivery systems. Mainly due to EDC/Sulfo-NHS superior properties i.e. biocompability and non-cytotoxicity *in vivo* and *in vitro* when compared to other to cross-linking agents such as glutaraldehyde. As can be seen in Figure 19, EDC and sulfo-NHS have different roles during DEX attachment. EDC is responsible for the activation of carboxyl groups, from EDC and carboxyl acid interaction arises the reactive *o*-acylisourea intermediate that when attacked by a hydroxyl nucleophile it will form an ester bond. Although o-acylisourea is very labile/unstable, so it can be attacked by other nucleophiles such as the oxygen atoms from H$_2$O, thus cleaving-off this intermediate and inactivating EDC.
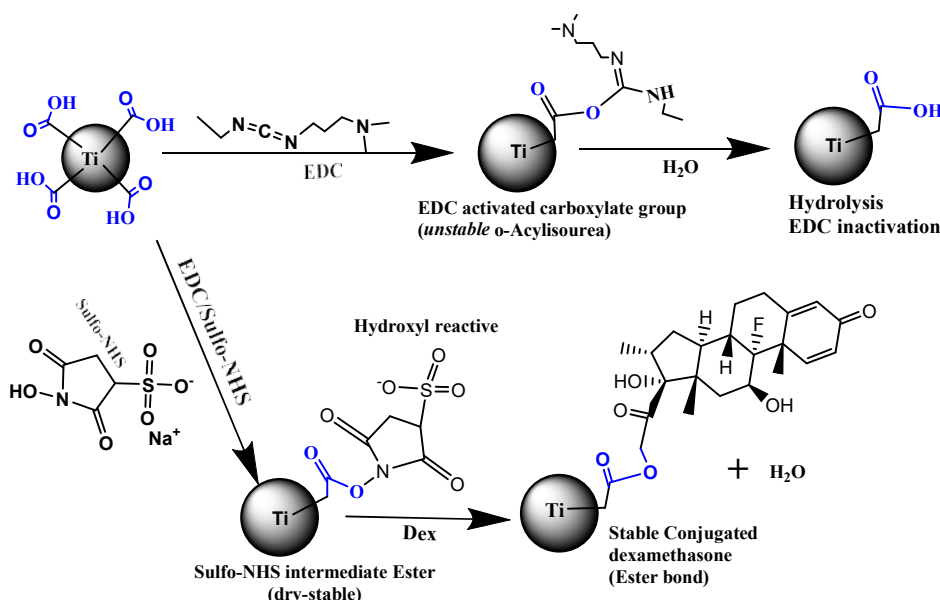
Figure 19. EDC and Sulfo-NHS role during DEX attachment. EDC activates the carboxyl groups, from EDC and carboxyl acid interaction arises the reactive o-acylisourea ester intermediate. Then, when added to the reaction Sulfo-NHS increases water solubility due to the presence of the charged sulfonate group, and thus a more stable intermediate ester is created.

Due this reason sulfo-NHS is added to the reaction, to improve EDC efficiency and reaction stability (Conde et al. 2014) by forming a very hydrophilic and stable intermediate ester with –COOH on surface of TiO$_2$ particles. Then in presence of hydroxyl nucleophiles from DEX, this intermediate ester is easily hydrolyzed allowing the formation of ester bond (Bartczak & Kanaras 2011, Hermanson & Hermanson 2013)

between DEX and activated carboxyl groups on TiO_2 particles surface. Moreover due to the ease removal of the reaction by-products, coupling of DEX is obtained under physiologic conditions and without adding extra chemical entities or organic solvents to the TiO_2 particles (Everaerts et al. 2008).

3.1.2 Determination of morphology and average size

A detailed examination of the morphology of the DEX-loaded TiO_2 particles and the distribution of their size were investigated by transmission electron microscopy (TEM). TEM images of the bare functionalised-TiO_2 particles and functionalized ones with and without DEX (Figure 20) were taken to determine the shape/structure and size of the particles after each step of functionalization.
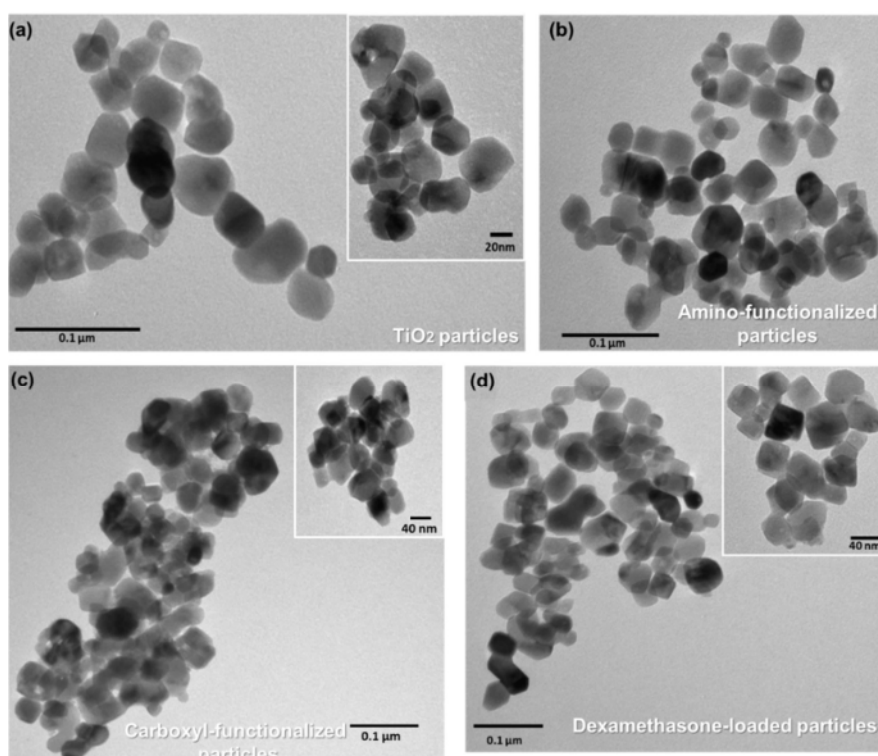
Figure 20. Transmission electron microscopy (TEM) different surface-modified TiO_2 particles: (a) TiO_2 particles, (b) amino-functionalized, (c) carboxyl-functionalized and (d) DEX conjugated-loaded TiO_2 particles for amino route.

The TEM image of uncoated TiO_2 particles show that these particles have a very small size of around 20-25nm diameter with a narrow size distribution. Moreover, they show a cubical and spherical-like shape with dense core (Figure 20.a) which is characteristic of TiO_2 particles. We then observed the morphology and size of the particles after each step of functionalization (amino, carboxyl and DEX loading). As shown in Figure 20 (b. c. and d.) the particles did not present obvious morphological changes, after different steps of surface modification, including DEX loading.

Table 5. Average size values of particles after each functionalization step, for amino route. Data are the mean ± standard deviation (SD) of two independent experiments (n=2).

Sample	Average size (nm) ± SD
TiO_2-particles	32.7±5.6
Amino-functionalised particles	31.0±5.2
Carboxyl-functionalised particles	36.4±6.4
DEX-loaded particles	41.5±3.5

The average size of TiO_2 particles after each step of functionalisation (e.g. amino-functionalised vs TiO_2 particles, or DEX-loaded vs carboxyl-functionalised particles) was also investigated (Table 5). Results showed that minor differences were observed when comparing the size of bare TiO_2-particles with that of functionalised-ones. The most significant ($p<0.05$) difference in size was observed when comparing TiO_2-particles (32.7±5.6nm) with DEX-loaded ones (41.5±3.5nm), where increase of ~9nm was observed. Moreover, aiming to complement the study of particles morphology and dispersion/aggregation (Pereira-da-silva & Ferri 2017, Singh 2016) after each step of functionalisation, scanning electron microscopy was also utilised (Figure 21).
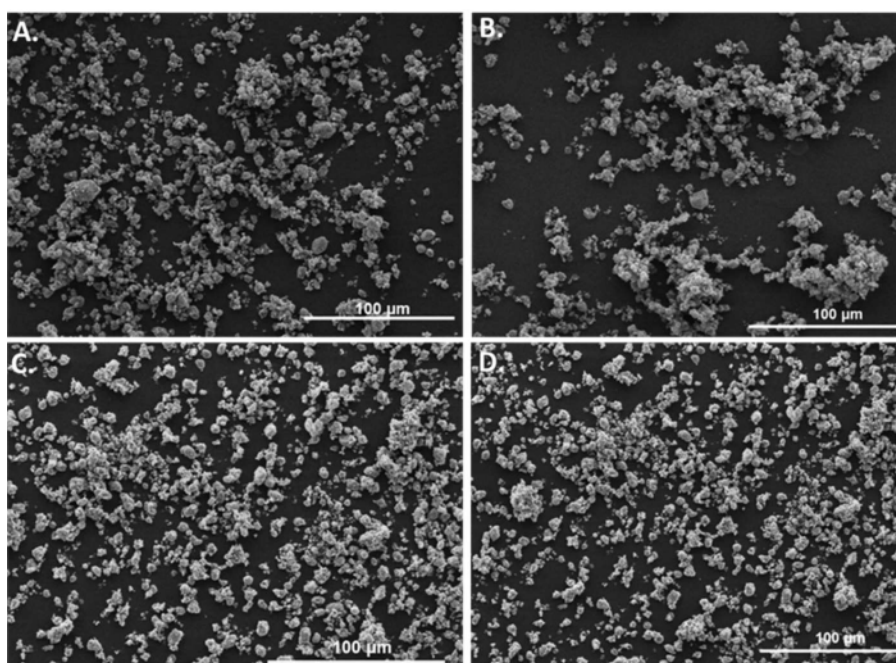
Figure 21. Scanning electron microscopy (TEM) different surface-modified TiO_2 particles: (a) TiO_2 particles, (b) amino-functionalized, (c) carboxyl-functionalized and (d) DEX conjugated-loaded TiO_2 particles for amino route.

SEM images showed that after each step of functionalisation, the TiO$_2$ particles maintained the spherical morphology, where no visible aggregation was observed, when compared to the bare-TiO$_2$ particles.

3.1.3 Zeta Potential measurements

Zeta potential measurements were utilized to assess the attachment of organic groups i.e.–NH$_2$, -SH, -COOH, after each step of TiO$_2$ particles functionalization, including DEX loading.
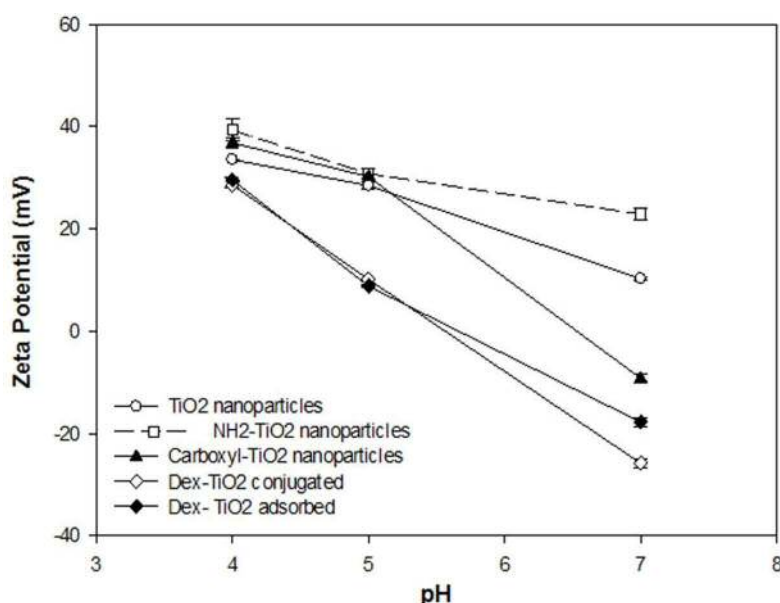
Figure 22. Zeta potentials of different surface-modified TiO$_2$ particle suspensions at different pH values. Data are the mean ± standard deviation (SD) of two independent experiments (n=2). Standard deviation is less than 5% of mean value.

Figure 22 shows that surface potential of TiO$_2$ particles differ after each step of functionalization. Additionally, it can be observed that for all functionalized particles, zeta potential versus pH conditions is consistent, following the same trend: as pH becomes more basic, decrease on surface potential is observed, on the other hand the highest surface potentials are observed under more acidic pH conditions. Moreover, after amino-functionalization, the surface charge of the modified-TiO$_2$ particles was more positive when compared with bare TiO$_2$ particles, for all pH values tested (4-6 pH range). As for succinic anhydride-TiO$_2$ particles and DEX loaded particles, lowest surface potentials were observed especially for more alkaline pH values (Figure 22). Particularly, Dex-functionalised-TiO$_2$ particles conjugated present a more negative zeta potential (-25.8±0.8 mV) when compared to Dex-TiO$_2$ particles adsorbed (-17.8±0.9 mV)

3.1.4 Fourier Transformed infrared spectroscopy (FT-IR)

FT-IR was used to assess the chemical groups present on the surface of TiO_2 particles after each functionalization step. The spectra of bare-TiO_2 particles and functionalized ones (i.e. with APTS, succinic anhydride and DEX) are shown in Figure 23. Firstly, it can be observed that all the peaks between 400 and 700 cm^{-1} (Figure 101,

I. Appendix) are to bending and stretching mode of Ti–O–Ti in TiO_2 particles. Particularly, the intense peak which appears in the vicinity of 500 cm^{-1} is attributed to the stretching vibration of Ti–O–Ti in anatase morphology (Bagheri et al. 2013, Zhao et al. 2012). In addition, the spectrum of bare-TiO_2 particles showed a broad band appearing at 3100–3600 cm^{-1} which is assigned to vibrations of hydroxyl groups (O-H) on TiO_2 surface (Bach et al. 2013, Gao et al. 2004, Vuk et al. 2005).

As for spectrum of functionalised-TiO_2 particles, new bands which could not be observed in the spectrum of bare-TiO_2 particles were detected. For example, the presence of bands at ~3000 and 2857 cm^{-1} which can be respectively assigned to the methyl (C–H vibration) of methoxy (OCH_3) and methylene (CH_2) groups.
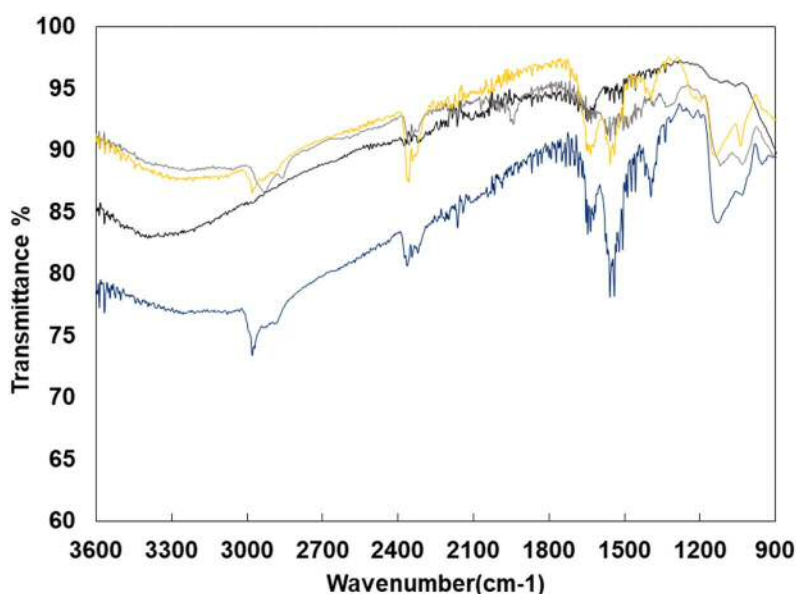
Figure 23. FT-IR spectra for different steps of TiO_2 nanoparticles functionalisation: bare-TiO_2 particles (---), amino-functionalised TiO_2 particles (---), carboxyl-functionalised TiO_2 particles (---), and DEX-loaded TiO_2 particles (---).

Moreover, for amino and carboxyl functionalised TiO_2-particles (Figure 24) a new peak was observed at ~950cm^{-1} which is characteristic of Si-O chemical bonds. Also, the broad band appearing at 3100–3600 cm^{-1} which is assigned to vibrations of hydroxyl groups (OH) on TiO_2 surface is less visible for particles functionalised with APTS.
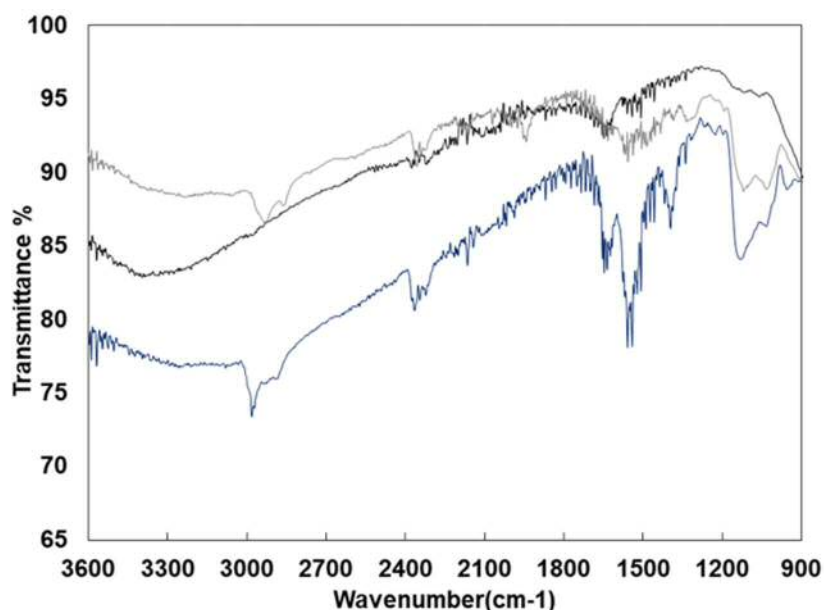
*Figure 24. FT-IR spectra for different steps of TiO$_2$-particles functionalisation using amino route: bare-TiO$_2$ particles (---), amino-functionalised TiO$_2$ particles (---), carboxyl-functionalised TiO$_2$ particles (---). *Amino-functionalization was obtained using APTS ** Carboxyl functionalization was obtained using succinic-anhydride.*

Particularly after APTS-functionalisation, when compared to bare-TiO$_2$ particles new peaks can be observed at ~3000 cm^{-1}, ~1800 cm^{-1} and ~1350 cm^{-1}, which can be assigned to N-H and C-N bending and stretching bonds. Similarly, in the spectra of functionalised-TiO$_2$ particles with succinic anhydride, new visible peaks which can be assigned to the carboxyl group were observed. For example, the presence of a broad band around ~3100–3600 cm^{-1} for (hydroxyl groups) (OH) on TiO$_2$ surface. And the two new strong peaks between 1600-1800 cm^{-1}, which are characteristic of C=O stretching vibration. Moreover, it is worth to note that the peak at ~1350 cm^{-1} was not observed for carboxyl-functionalised TiO$_2$ particles. Although the FT-IR equipment was not sensitive enough to detect the characteristic peaks/bands observed for DEX (as observed in pure DEX, Figure 103), it was clear that a different FT-IR spectra was observed for DEX-loaded particles; such as the presence of strong band around 3100–3600 cm^{1} and at ~1600-1800 cm$^{-1,}$ respectively suggests the presence of C=O stretching vibration band and of hydroxyl groups (OH) on TiO$_2$ surface. Furthermore, the two sharp peaks observed in the region of 1050-1160 cm^{-1} and 1185 cm^{-1}, 1277cm^{-1} for both carboxyl and DEX-loaded functionalised particles can be attributed to the symmetrical and asymmetrical stretching frequencies of the C-O ester groups.

3.1.5 Thermogravimetric analysis (TGA)

Thermogravimetric analysis (TGA) was performed assess the organic functionalization (e.g. amine, carboxyl and DEX attachment) of TiO_2 particles surface. The TGA analysis of the different functionalization steps of TiO_2 particles are shown in Figure 25. TGA studies were only performed for the conjugated DEX-loaded TiO_2 particles surface, mainly because these particles showed better results in terms of drug attachment (3.1.3 Zeta Potential measurements).
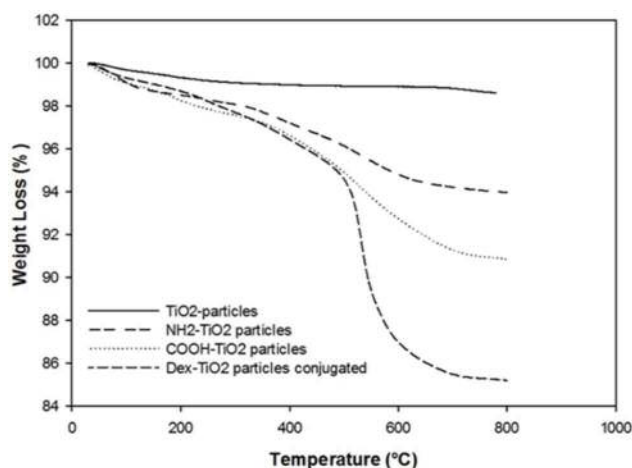
Figure 25. Thermogravimetric curves for the different surface-modified TiO_2 particles: TiO_2 particles, amino (NH_2)-TiO_2, carboxyl-(COOH) TiO_2 particles, and Dex-TiO_2 particles conjugated. Data are the mean ± standard deviation (SD) of two independent experiments (n=2).

The TGA profile of TiO_2 particles after each functionalization step revealed an initial weight loss (~1%) at about 100°C, which is normally attributed to the evaporation of adsorbed water from the samples (Ganesh & Lee 2013). Due to this reason, the organic content of each sample (Table 6) was calculated based on the weight loss beyond 100°C, that truly corresponds to the combustion of organic species (Yodyingyong et al. 2011).

Table 6. Percentage of organic material in functionalized-TiO$_2$ particles at each step of the amino-route synthesis. Data are the mean ± standard deviation (SD) of two independent experiments (n=2). *Amino-functionalization was obtained using APTS ** Carboxyl functionalization was obtained using succinic-anhydride.

Samples	Organic content (%)
TiO$_2$ particles	1.5±0.1
Amino-TiO$_2$ particles	6.1±0.3
**Carboxyl-TiO$_2$ particles	9.2±2.6
Dex-TiO$_2$ particles conjugated	14.8±0.1

Results obtained from TGA analysis (Table 6) show an increase of organic content after amino and carboxyl functionalization when compared with organic content of TiO$_2$ particles (1.54%): 6.05% for amino-TiO$_2$ particles and 9.16% for carboxyl-functionalized TiO$_2$ particles. Moreover, the same behaviour was observed for DEX loaded particles, where an increase of organic content of approximately 6% was detected when compared to carboxyl-functionalized TiO$_2$ particles.

3.2 DEX mercapto-functionalized particles

3.2.1 Chemical reactions

Mercapto route, was another strategy to obtain DEX loaded-functionalised-TiO$_2$ particles. When this route was used, instead of an amine group, a thiol group (-SH) was initially immobilized onto the surface of TiO$_2$ particles (Figure 26). In more detail, the synthesis of DEX functionalised-TiO$_2$ particles was achieved using a two-step surface functionalization process. Firstly, TiO$_2$ particles were mixed with MPTMS to immobilize the thiol groups (-SH) on the surface of TiO$_2$ (Schematic Reaction 1. Figure 26). As previous reported (Bach et al. 2013) this reaction results from the interaction between the hydroxyl (-OH) group present on the TiO$_2$ surface and triethoxysilane group of MPTMS. Consequently, to obtain carboxylic-functionalized TiO$_2$ particles (-COOH-TiO$_2$), pentanoic-acid was added to the reaction (Schematic Reaction 2. Figure 26). This reaction is the same described for amino route (*3.1.1. Chemical reactions*), but in this case the carboxylic acid group arises from the addition of pentanoic-acid to the reaction. Once more, carboxyl (–COOH group) will act as a binding site to attach DEX.
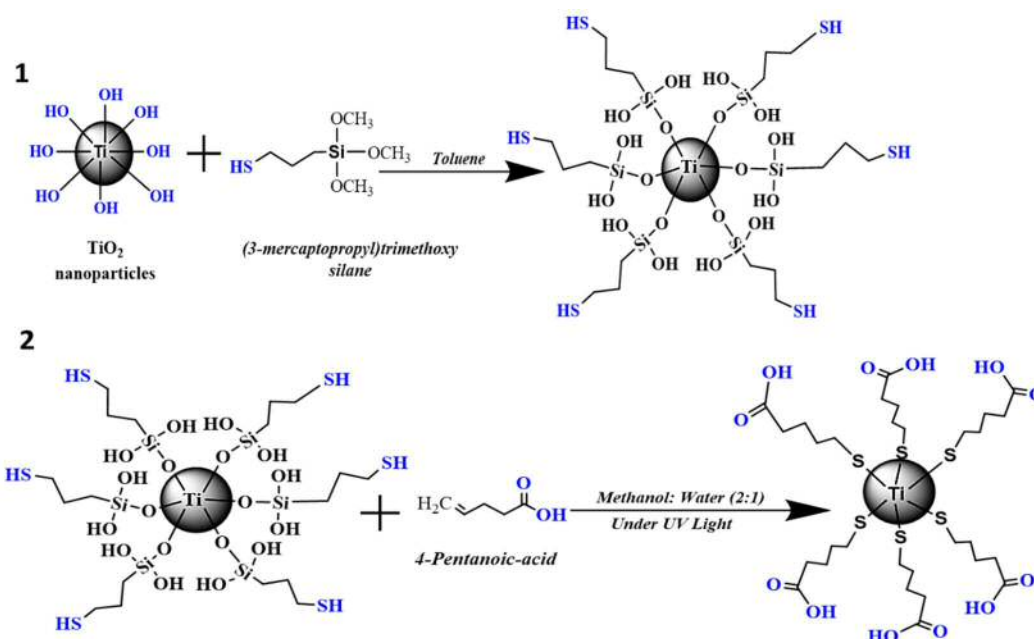
Figure 26. Schematic of reaction regarding carboxyl-TiO₂ particles functionalization, using mercapto route. Functional groups on TiO₂ Particles are highlighted with blue colour.

Finally, DEX was then added to the carboxyl-functionalized TiO₂ particles, to obtain DEX-loaded Functionalised-TiO₂ particles, with (conjugated) or without adding EDC/Sulfo-NHS (adsorbed) (Figure 27).
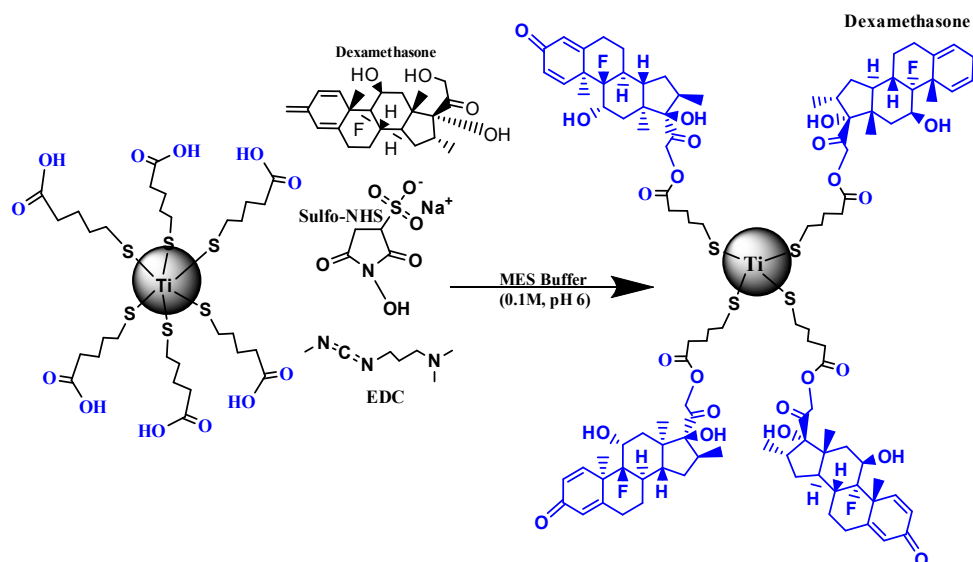
Figure 27. Schematic of reaction regarding DEX loading into carboxyl-functionalized TiO₂ particles using mercapto route. Functional groups on TiO₂ particles are highlighted with blue colour.

3.2.2 Determination of morphology and average size

A detailed examination of the morphology of the DEX-loaded functionalised-TiO$_2$ particles obtained via mercapto route, and the average size of the particles was investigated by TEM. With this aim, TEM images of the uncoated TiO$_2$ particles and functionalized ones (Figure 28), were taken after each step of functionalization.
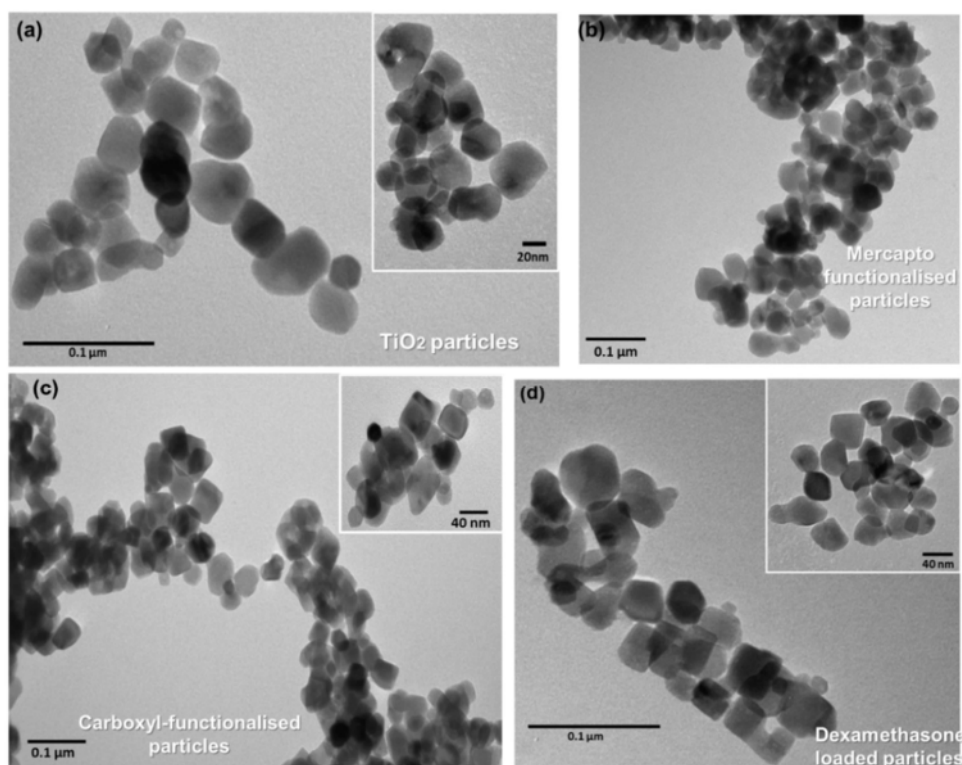
Figure 28. Transmission electron microscopy (TEM) different surface-modified TiO$_2$ particles: (a) TiO$_2$ particles, (b) mercapto-functionalized, (c) carboxyl-functionalized and (d) DEX conjugated-loaded TiO$_2$ particles for mercapto route.

TEM picture of uncoated TiO$_2$ particles show that these particles have a spherical like-shape, and very small size of around 30-35nm diameter with a narrow size distribution. Then the morphology and size of the particles after each step of functionalization (amino, carboxyl and DEX loading) was observed. As shown in Figure 28 (b. c. and d.) the particles did not present obvious morphological changes after different steps of surface modification, including DEX loading

Table 7. Average size values of particles after each functionalization step, for mercapto route. Data are the mean ± standard deviation (SD) of two independent measurement (n=2).

Sample	Average size (nm) ± SD
Tio$_2$ particles	32.7±5.6
Mercapto-functionalised particles	38.9±9.7
Carboxyl-functionalised particles	44.2±7.5
DEX-loaded particles	44.9±10.4

Moreover, the average size of particles after each functionalization step was estimated (Table 7).
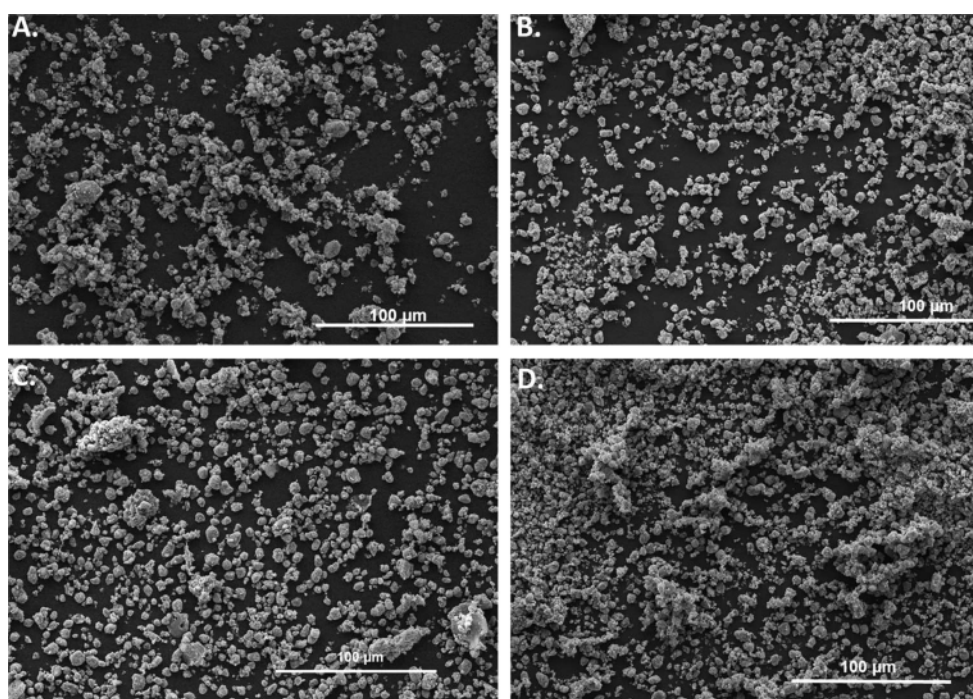
Figure 29. Scanning electron microscopy (TEM) different surface-modified TiO$_2$ particles: (a) TiO$_2$ particles, (b) amino-functionalized, (c) carboxyl-functionalized and (d) DEX conjugated-loaded TiO$_2$ particles for mercapto route.

It can be observed that when comparing the average size after each step of functionalisation (e.g. mercapto-functionalised vs TiO$_2$ particles, or DEX-loaded vs carboxyl-functionalised particles), the average size does not show significant differences (p<0.05), except after carboxyl-functionalisation and DEX loading steps where the average size shows a significant increase (p<0.05) of ~12nm was observed when compared with bare-TiO$_2$ particles. Moreover, aiming to complement the study of particles morphology and dispersion/aggregation (Pereira-da-silva & Ferri 2017, Singh

2016) after each step of functionalisation, scanning electron microscopy was also utilised (Figure 21). SEM pictures showed that after each step of functionalisation, the TiO_2 particles maintained the spherical morphology, where no visible aggregation was observed when compared to the bare-TiO_2 particles.

3.2.3 Zeta potential measurements

Zeta potential after each step of TiO_2 particles functionalization, including DEX loading, was measured to assess the changes in surface charge after the attachment of new organic groups i.e.–NH_2, -SH, -COOH. As depicted in Figure 30 a consistent behavior was observed for all functionalized-TiO_2 particles, where zeta potential measurements are pH-dependent: the highest surface potentials are verified at low pH conditions, whereas when pH increases the zeta potentials are lower.
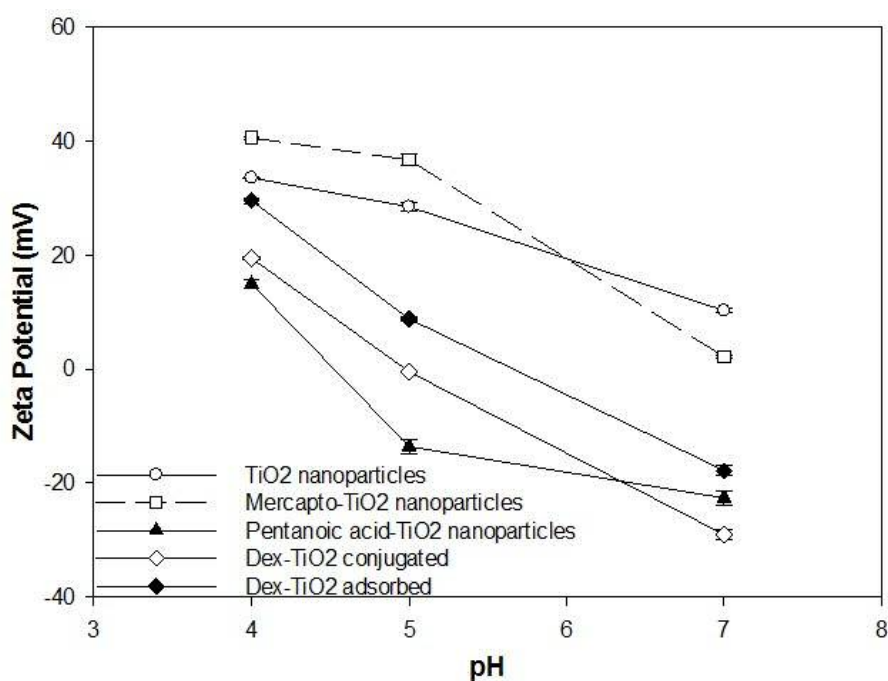
Figure 30. Zeta potentials of different surface-modified TiO₂ particle suspensions at different pH values. Data are the mean ± standard deviation (SD) of three independent measurement (n=3). Standard deviation is less than 5% of mean value.

After thiol-functionalization, the surface charge of the modified-TiO_2 particles was more positive when compared with bare TiO_2 particles. Furthermore, after pentanoic-acid conjugation, an unexpected result was observed, where COOH-TiO_2 particles show a negative zeta potential, higher than the one observed at DEX-loaded particles (Figure 30). Although this behavior was not observed at pH=7, where the DEX-conjugated loaded particles presented a more negative surface charge (-27.8±0.6) than the

functionalised COOH-TiO$_2$ particles (-21.6±1). Regarding Dex-Functionalised-TiO$_2$ particles, conjugated (-27.8±0.6) exhibit a more negative zeta potential when compared to Dex-adsorbed ones (-17.8±0.9) mV for all pH values.

3.2.4 Fourier Transformed infrared spectroscopy (FT-IR)

Figure 31 shows the FT-IR spectrum of bare TiO$_2$ particles and functionalised-particles ones (i.e. with MPTES, pentanoic-acid and DEX) using mercapto route. Firstly, it can be observed that all the peaks bellow 700 cm^{-1} (Figure 102, appendix section) are characteristic from TiO$_2$ particles. Particularly, the intense peak which appears around 500 cm^{-1} is attributed to the stretching vibration of Ti–O–Ti in anatase morphology. In addition, spectrum of bare-TiO$_2$ particles shows a broad band appearing between 3100 and 3600 cm^{-1} which is assigned to vibrations of hydroxyl groups (-OH) which are present on the surface of TiO$_2$ particles.
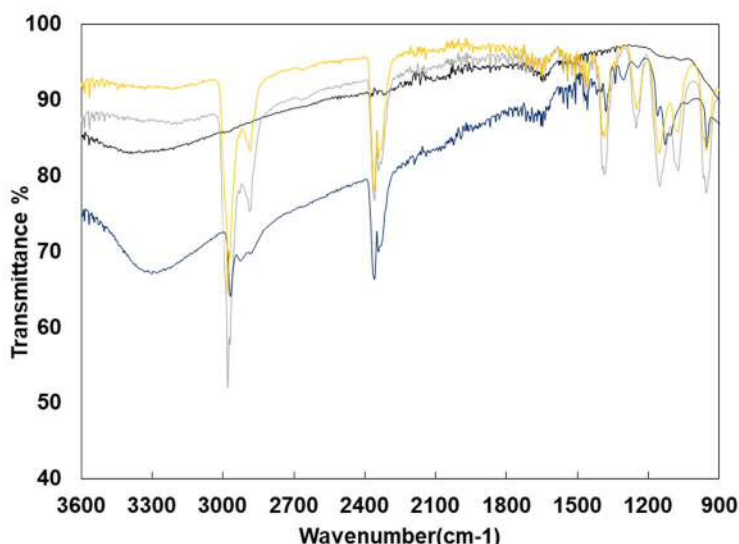
*Figure 31. FT-IR spectra for different steps of TiO$_2$-particles functionalisation using mercapto route: bare-TiO$_2$ particles (---), mercapto-functionalised TiO$_2$ particles (---), carboxyl-functionalised TiO$_2$ particles (---). and DEX-loaded TiO$_2$ particles (---). * Mercapto-functionalization was obtained using MPTES ** Carboxyl functionalization was obtained using 4-pentanoic-acid.*

When comparing bare-TiO$_2$ particles with the ones functionalised with mercapto-silane (MPTES), the band corresponding to thiol (SH) group could not be clearly observed (Figure 32) due to relative low content of thiol and poor sensitivity of IR to this functional group. However, other new bands were observed at ~3000 cm^{-1} and 2800 cm^{-1}, which are attributed to the C–H stretch of methylene of the alkyl chain.
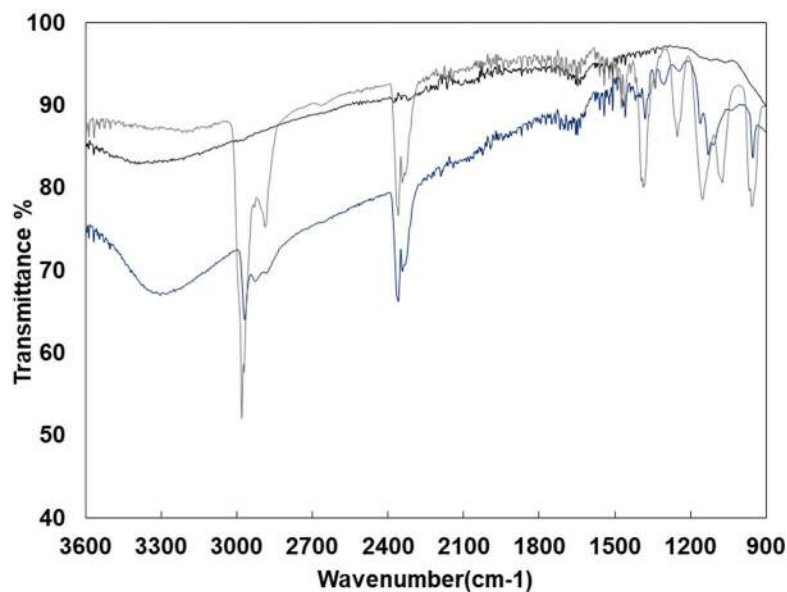
*Figure 32. FT-IR spectra for different steps of TiO₂-particles functionalisation using mercapto route: bare-TiO₂ particles (---), mercapto-functionalised TiO₂ particles (---), carboxyl-functionalised TiO₂ particles (---). * Mercapto-functionalization was obtained using MPTES ** Carboxyl functionalization was obtained using 4-pentanoic-acid.*

The other visible peaks between 900 and 1100 cm^{-1} are due to Si–O–Si and Si–O stretching vibrations, Additionally, the O–H broad peak (3100–3600 cm^{-1}) which appeared in the spectrum of bare-TiO₂ particles, is less visible, which coincides with a decrease in the hydroxyl groups due to the attachment of the MPTES. As for carboxyl and DEX functionalisation, the FT-IR equipment was not sensitive enough to detect the characteristic peaks/bands. Although different FT-IR spectra was observed, particularly a broad peak between 3100–3600 cm^{-1} is visible, which coincides with the increased presence the hydroxyl groups (O–H) due to the attachment of COOH functional and OH groups on surface of functionalised-TiO₂ particles.

3.2.5 Thermogravimetric analysis (TGA)

The TGA analysis of the different functionalization steps of TiO_2 particles are shown in Figure 33.
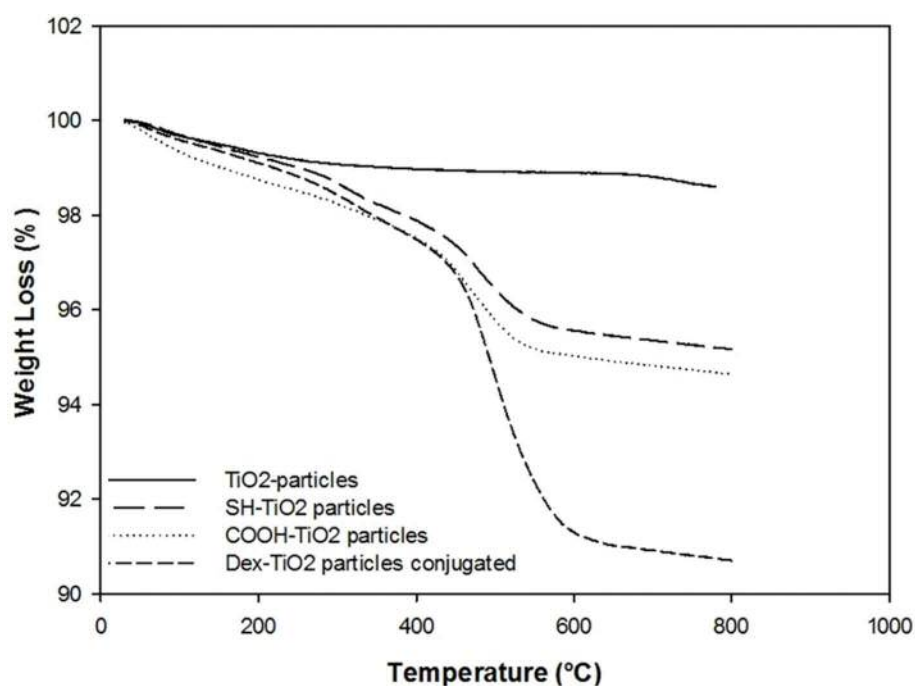
Figure 33. Thermogravimetric curves for the different surface-modified TiO_2 particles: Bare TiO_2 particles, mercapto-TiO_2 and succinilated-TiO_2 particles, and Dex-loaded-TiO_2 conjugated particles. Data are the mean ± standard deviation (SD) of two independent experiments (n=2).

Based on TGA results (Figure 33) the % of organic content present on the surface of TiO_2 particles after each step of functionalization was calculated (Table 8). It can be observed that after each functionalization step there is an increased amount of organic content on the surface of TiO_2 particles. Results show an increase of organic content after mercapto and carboxyl functionalization when compared with organic content of TiO_2 particles (1.53%), 4.84% for mercapto-TiO_2 particles and 5.37% for carboxyl-functionalized TiO_2 particles.

*Table 8. Percentage of inorganic and organic material in functionalized-TiO₂ particles at each step of the mercapto-route synthesis. Data are the mean ± standard deviation (SD) of two independent experiments (n=2). *Mercapto-functionalization was obtained using MPTMS ** Carboxyl functionalization was obtained using succinic-anydride.** Carboxyl functionalization was obtained using 4-pentanoic acid.*

Samples	Organic content (%)
TiO₂ Particles	1.6±0.1
Mercapto-TiO₂ Particles	4.8±0.2
****Carboxyl-TiO₂ Particles**	5.4±0.3
Dex-TiO₂ Particles conjugated	9.2±0.4

Moreover, the same behavior was observed for DEX loaded particles, where an increase of organic content to approximately 9.23% was detected when compared to carboxyl-functionalized TiO$_2$ particles (5.37% of organic content).

3.3 LbL DEX-loaded particles

3.3.1 Zeta Potential measurements

Firstly, it is important to assess the charge density of the CH, ALG and DEX polyelectrolyte solutions that are going to be used during the different set of experiments (Table 9). This initial procedure is crucial to guarantee a successful LbL assembly.

Table 9. Zeta potential values of polyelectrolyte solutions. Data are the mean ± standard deviation (SD) of three independent measurements (n=3).

Polyelectrolyte solution	Zeta Potential (mV) ± SD
Alginate (ALG) solution (2mg/mL)	-24.8±1.1
Chitosan (CH) solution (2mg/mL)	19.3±1.5
DEX solution (10mg/mL)	-9.2±1.2

As can be seen in Table 9, CH and ALG/DEX solutions present opposite surface charge as required to begin the LbL assembly, which means that they can interact by electrostatic forces. Amino-functionalised-TiO$_2$ particles (NH$_2$-TiO$_2$ particles), used as LbL template, presented a positive surface charge of +25.30 mV, as confirmed by zeta potential measurements (Figure 34). The positive value was due to ionized amino-groups that are on the surface of TiO$_2$ particles. After ensuring all the necessary conditions, the

preparation of multilayer DEX-loaded-functionalised-TiO_2 particles was assessed by the measurement of zeta potential values after the addition of each new polyelectrolyte layer. Zeta potential was measured for the different LbL approaches tested, experiment 1 (Figure 34), and experiment 2.
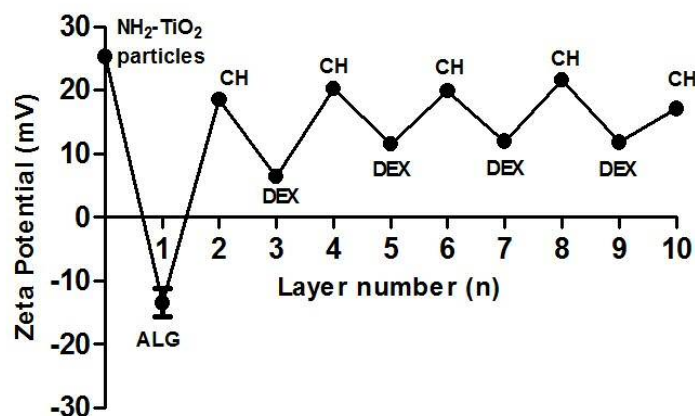
Figure 34. Zeta potential values during LBL assembly of ALG/CH layers and DEX onto amino-functionalised-TiO_2 particles (NH_2-TiO_2 particles), using approach described in experiment 1. Data are the mean ± standard deviation (SD) of three independent measurements (n=3).
The layer 0 represents the template used (NH_2-TiO_2 particles). Standard deviation is less than 5% of mean value.
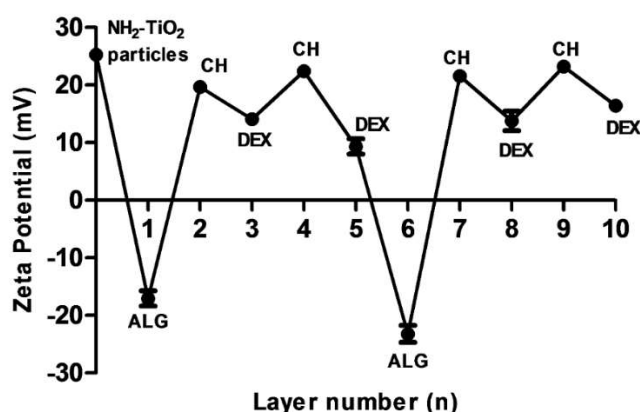
Figure 35. Zeta potential values during LBL assembly of ALG/CH layers and DEX onto amino-functionalised-TiO_2 particles (NH_2-TiO_2 particles), using approach described in experiment 2. Data are the mean ± standard deviation (SD) of three independent measurements (n=3).
The layer 0 represents the template used (NH_2-TiO_2 particles). Standard deviation is less than 5% of mean value.

It was observed that in experiment 1 (Figure 34) and experiment 2 (Figure 35) , the zeta potential measured followed the same trend. In general, the values alternate depending on the last adsorbed outer layer (*n)* on amino-functionalised TiO_2 particles: starting from a positive potential of the template, the charge turned to positive after deposition of the positively charged CH and more negative value after deposition of the negatively charged ALG. Overall, for all approaches testes, upon adsorption of the 1st layer (ALG) the surface charge changed to a negative value (-20 to -30 mV). Subsequently, when the cationic polyelectrolyte (CH) was added the zeta potential turned to a positive value (+30 to +40 mV). Then, when the DEX layer (anionic polyelectrolyte) was added, the surface charge of particles remained positively charged (+5 to +10 mV). This lack of symmetric inversion in zeta potential, observed after DEX deposition, could be attributed to an incomplete coverage by DEX of the surface of functionalised NH_2-TiO_2 particles. On the other hand, it should be noted that when the ALG layer was added after the DEX layer (experiment 2, Figure 35) a more negative charge surface value was observed (-23 mV), when compared to the ones observed for DEX deposition.

3.3.2 Thermogravimetric analysis (TGA)

The amount of organic content (%) on the surface of multilayer DEX-loaded-TiO_2 particles, after the deposition of each new layer of alginate (ALG), chitosan (CH) and DEX was evaluated by thermogravimetric analysis (TGA) for experiment 1 (Figure 36, Table 10) and experiment 2 (Figure 37,Table 11).

Overall, an increase of organic content (%) was observed after the addition of new layers. For example, for experiment 1 (Table 10), the organic content present on the particles surface after deposition of 10th layer was higher than the one observed for 9th,8th,7th,6th and 5th layer. Although this increase on organic content was not constant or gradual, since the organic content (%) observed after 3rd and 4th layers deposition was higher than the one observed after the deposition of 10th layer (Table 10). Regarding the deposition of DEX layers, it can be observed that an increase on organic content of 2.33%, 2.09% and 1.60% was, respectively, observed after the deposition of 3rd, 7th, and 9th layers of DEX.
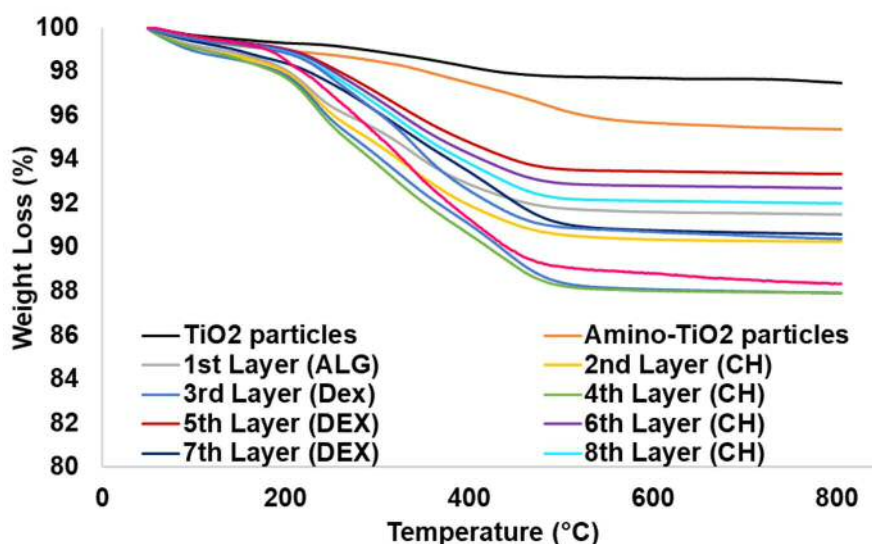
Figure 36. Thermogravimetric curves in multilayer DEX-loaded TiO$_2$ particles after addition of a new layer of alginate (ALG), chitosan (CH) and dexamethasone (DEX) (experiment 1). Data are the mean ± standard deviation (SD) of two independent experiments (n=2).

Table 10. Percentage of organic material in multilayer DEX-loaded TiO$_2$ particles after addition of a new layer of alginate (ALG), chitosan (CH) and dexamethasone (DEX) (experiment 1). Data are the mean ± standard deviation (SD) of two independent experiments (n=2).

Sample	Organic content (%)
TiO$_2$ particles	2.5±0.1
NH$_2$-TiO$_2$ particles	4.6±0.1
1st Layer (ALG)	8.5±0.1
2nd Layer (CH)	9.7±0.1
3rd Layer (DEX)	12.1±0.2
4th Layer (CH)	12.1±0.2
5th Layer (DEX)	6.7±0.1
6th Layer (CH)	7.3±0.2
7th Layer (DEX)	9.4±0.3
8th Layer (CH)	8.0±0.4
9th Layer (DEX)	9.6±0.1
10th Layer (CH)	11.7±0.1
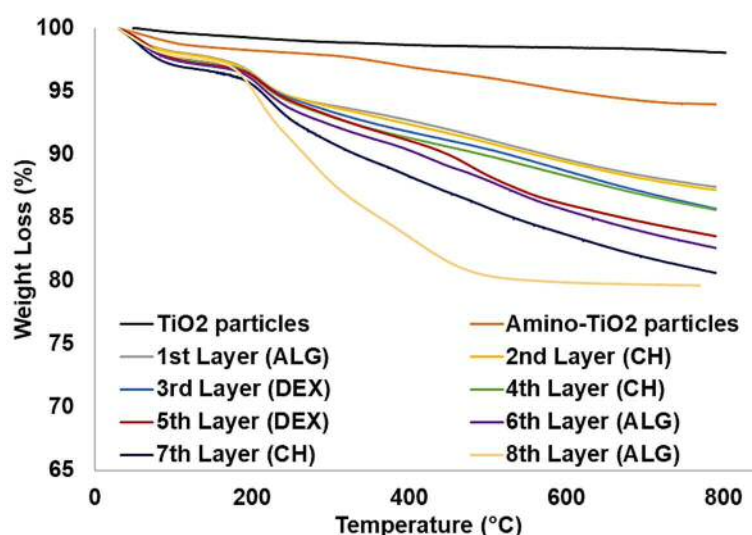
Figure 37.Thermogravimetric curves in multilayer DEX-loaded TiO$_2$ particles after addition of a new layer of alginate (ALG), chitosan (CH) and dexamethasone (DEX) (experiment 2). Data are the mean ± standard deviation (SD) of two independent experiments (n=2).

Similar results were observed for experiment 2 (Table 11), where an increase of organic content was observed after deposition of 3rd (1.36%), 5th (1.52%) and 8th layer (0.67%) of DEX.

Table 11. Percentage of organic material in multilayer DEX-loaded TiO$_2$ particles after addition of a new layer of alginate (ALG), chitosan (CH) and dexamethasone (DEX) (experiment 2). Data are the mean ± standard deviation (SD) of two independent experiments (n=2).

Samples	Organic content (%)
TiO$_2$ particles	1.9±0.0
NH$_2$-TiO$_2$ particles	6.0±0.0
1st Layer (ALG)	12.5±0.1
2nd Layer (CH)	12.7±0.3
3rd Layer (DEX)	14.0±0.3
4th Layer (CH)	14.8±0.4
5th Layer (DEX)	16.3±0.1
6th Layer (ALG)	17.1±0.3
7th Layer (CH)	19.7±0.3
8th Layer (DEX)	20.4±0.0

When comparing experiment 1 and 2, it can be seen that only for experiment 2 (Table 10, Table 11) a gradual increase of organic content (%) after the addition of each new layer was observed, where after the addition of 10 layers it was observed a weigh loss of approximately 20%, when compared to the TiO_2 bare nanoparticles.

Overall results showed that for approach utilized in experiment 2, particularly the increase of organic content (%) observed after each DEX layer deposition, together with zeta potential measurements (i.e. high surface charge values after each layer deposition), strongly suggests that this approach could be the most suitable to obtain reproducible and stable LbL-DEX loaded particles. Therefore, the subsequent studies (e.g. Size and morphology, FTIR, drug release profile and biological studies) was assessed with LbL particles prepared by approach described in experiment 2

3.3.3 Fourier Transformed infrared spectroscopy (FT-IR)

FTIR was used to investigate the deposition of CH, ALG and DEX layers in DEX-loaded functionalised TiO_2 particles.
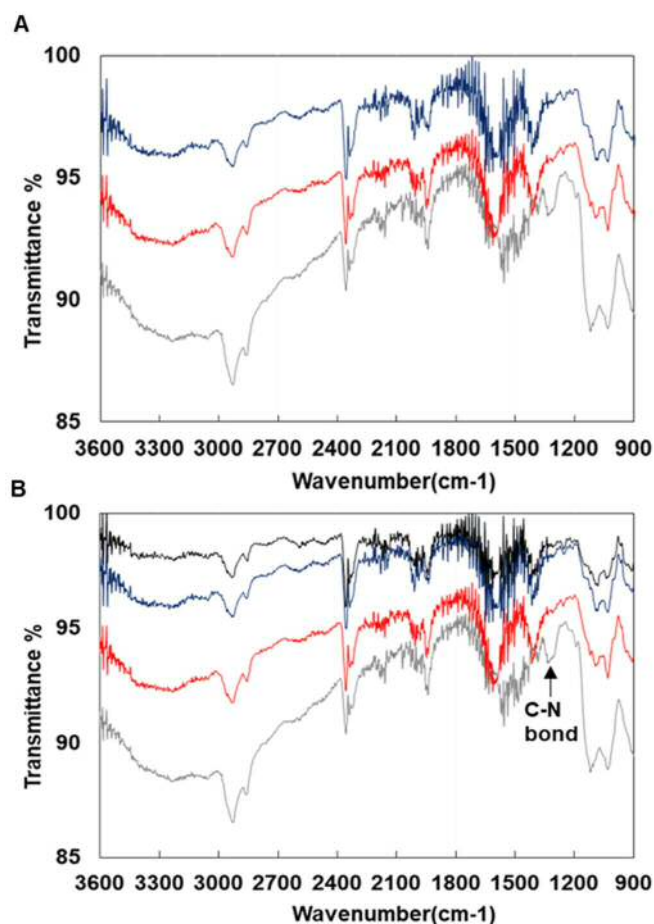
Figure 38. FTIR spectra for CH/ALG multilayer DEX-loaded functionalised TiO₂ particles after each addition of (A) ALG/CH layers and (B) DEX layer. Amino-functionalised TiO₂ particles (---), ALG (1st Layer) (---), CH (2nd Layer) (---) and DEX (3rd layer) (---). The black arrow indicates the peak corresponding to the C-N bond on amino-functionalised TiO₂ particles (---).

Overall, FT-IR results showed that similar spectra were observed for CH/ALG multilayer DEX-loaded functionalised TiO_2 particles after the addition of CH, ALG and DEX layers (Figure 38). As shown in Figure 38 the same peaks were detected for all LbL particles, including the broad band between ~3400-3200 cm^{-1}, which is assigned to hydroxyl groups (O-H). As well as the double peak at ~2800 cm^{-1} which corresponds to the C=H stretching. It is worth to note that though a similar spectrum was observed after deposition of CH, ALG and DEX layer, the band at ~1350 which can be assigned to the C-N bond and was observed for amino functionalised particle was absent on the spectra

of DEX-loaded CH/ALG functionalised-TiO$_2$ particles (Figure 38.B). Also, some new peaks were also observed when comparing the spectra of amino functionalised TiO$_2$ particles with the one of CH/ALG multilayer DEX-loaded functionalised TiO$_2$ particles; such as the strong peak observed at ~1650 cm^{-1} which belongs to the carbonyl group (C-O) stretching groups which are attributed to ALG and CH saccharide structure or characteristic group of DEX. Similar peaks were observed in the spectrum of pure (powder form) of CH, ALG (Figure 105, Figure 104), and DEX (Figure 103)

3.3.4 Determination of morphology and average size

A detailed examination of the morphology of the DEX-loaded functionalised-TiO$_2$ particles obtained via LBL route (experiment 2), and their average size were investigated by TEM. With this aim, TEM images of amino-functionalized TiO$_2$ particles with alginate (ALG), chitosan (CH) and DEX layers (Figure 39) were taken after deposition of each new layer.
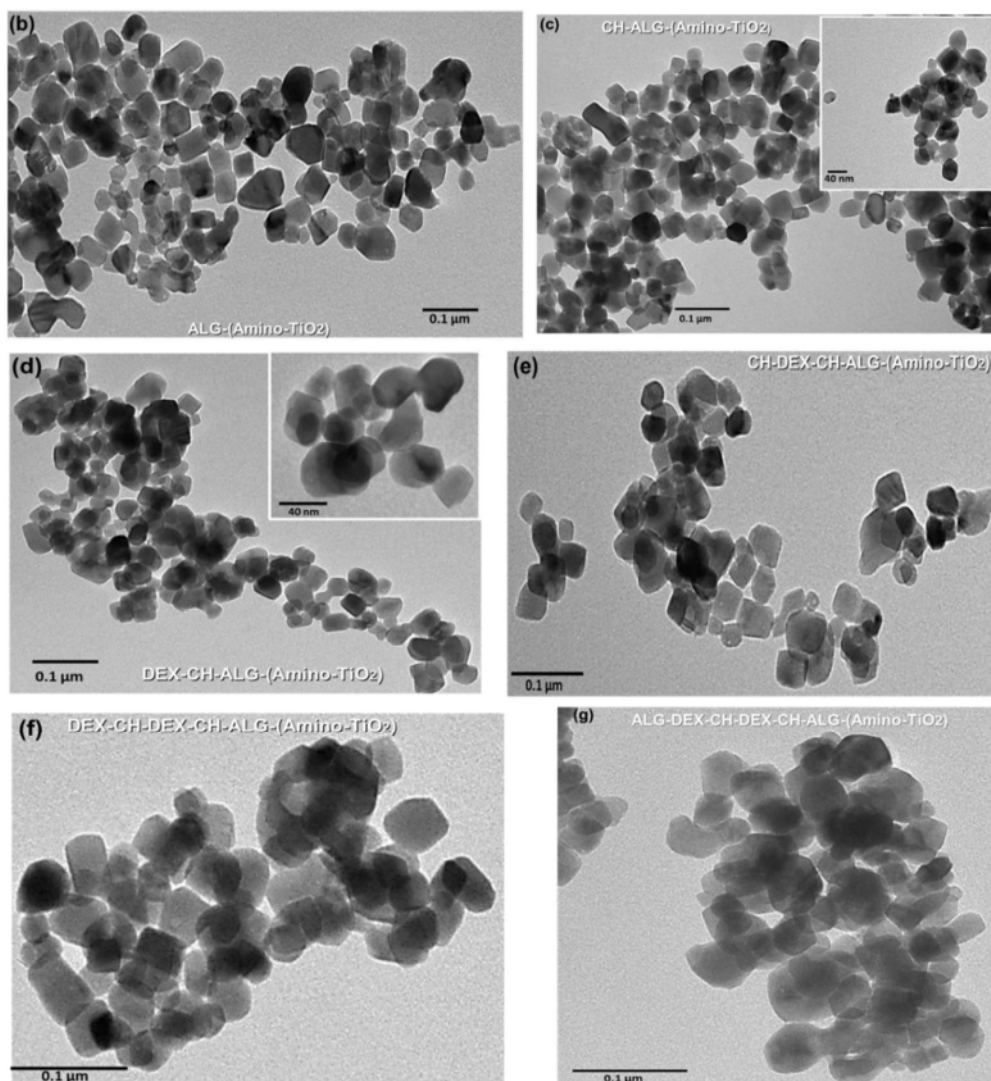
Figure 39.Transmission electron microscopy (TEM) of amino-functionalised-TiO$_2$ particles with 2 multilayers of CH/DEX/ALG. Images are shown after addition of alginate (b,g), chitosan (c,e), and DEX (d,f) layers, for LbL route. All images scale bar is 0.1 µm and 40nm for insets scale bar.

It should be noted that, TEM image of amino-functionalised TiO$_2$ particles was not included on Figure 39, because it was already showed in TEM results for amino route (Figure 20).

Table 12. Average size values of particles obtained via amino route after each new layer deposition on the template, amino-functionalized particles (NH$_2$-TiO$_2$ particles). Data are the mean ± standard deviation (SD) of two independent measurements (n=2).

Sample	Average size (nm) ± SD
Tio$_2$ bare particles	32.7±5.6
Amino-functionalized-Tio$_2$ particles (NH$_2$-TiO$_2$ particles)	31.7±4.4
(NH$_2$-TiO$_2$ particles) -ALG-	40.4±9.3
(NH$_2$-TiO$_2$ particles) -ALG-CH	48.8±6.2
(NH$_2$-TiO$_2$ particles) -ALG-CH-DEX	41.6±3.7
(NH$_2$-TiO$_2$ particles) -ALG-CH-DEX-CH	38.6±5.3
(NH$_2$-TiO$_2$ particles) -ALG-CH-DEX-CH-DEX	44.7±5.8
(NH$_2$-TiO$_2$ particles) -ALG-CH-DEX-CH-DEX-ALG	38.3±4.4

Additionally, the average size of particles obtained via LBL route was estimated (Table 12). It can be observed that when comparing the average size of particles after the deposition of new layer (e.g. NH$_2$-TiO$_2$ particles vs (NH$_2$-TiO$_2$ particles)-ALG), the average showed significant differences ($p<0.05$). Although this increase on particles size was not constant or gradual, since the particles with more layers (~39nm for NH$_2$-TiO$_2$ particles-ALG-DEX-CH-DEX-CH-ALG) showed a smaller average size than that of particles with less layers (~48nm NH$_2$-TiO$_2$ particles-CH-ALG).

3.4 DEX release profile

The drug release profile of the DEX from functionalised-TiO$_2$ particles obtained via different routes (amino, mercapto and LbL) was carried out at different pH values (5-7), and the presence of DEX on samples was quantified using HPLC.

3.4.1 Amino-route

Results revealed that, for most part of the conditions tested, pH=5, 6 and 7, the DEX was released within the first 24 hours (Figure 40). Moreover, the DEX released from amino-functionalised TiO$_2$ particles was pH-dependent: the highest concentrations of DEX were released at higher pH values, pH=7 (13.1 ±0.2 µg/mL) and pH=6 (13.8±0.3 µg/mL). While at more acidic conditions (pH=5) minor concentrations of DEX (2.8±0.1 µg/mL) were released.
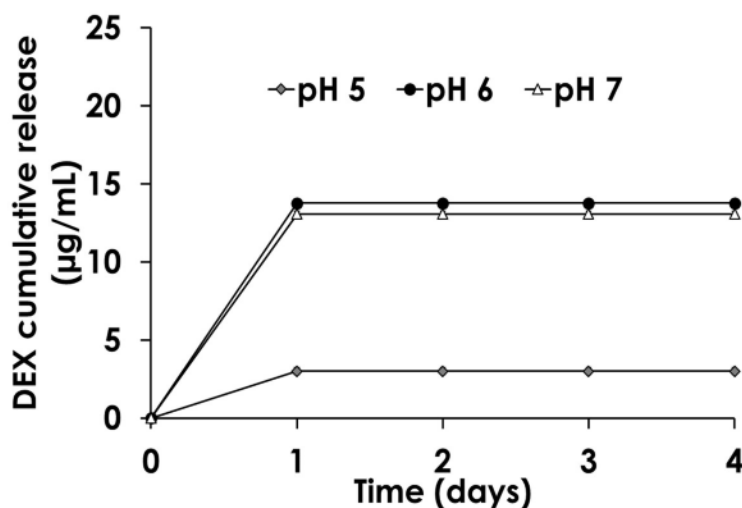
Figure 40. Cumulative release of conjugated DEX from functionalised-TiO$_2$ particles obtained via amino route at different pH values (pH=5,6 and 7). Data are the mean ± standard deviation (SD) of two independent experiments (n=2). Standard deviation is less than 5% of mean value.

3.4.2 Mercapto-route

In Figure 41 is shown the drug release profiles for functionalised-TiO_2 particles obtained by mercapto route. For all the conditions tested (pH=5, 6 and 7) DEX was released from functionalised-TiO_2 particles, within the first 24 hours.
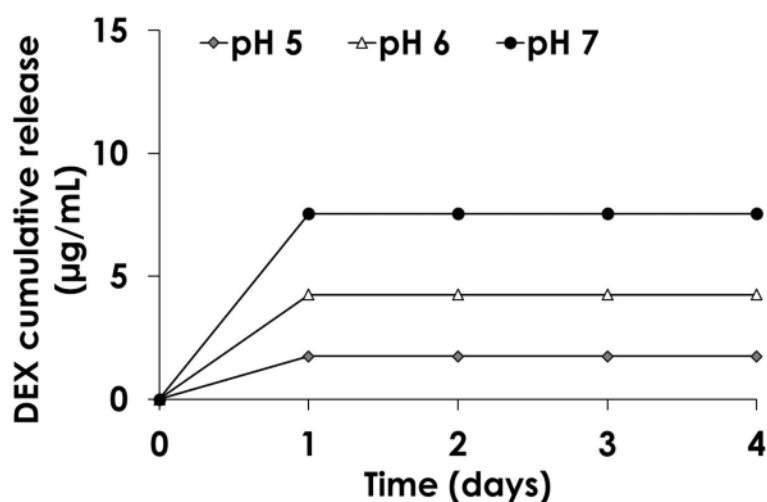
Figure 41. Cumulative release of conjugated DEX from functionalised-TiO_2 particles obtained via mercapto route at different pH values (pH=5,6 and 7). Data are the mean ± standard deviation (SD) of two independent experiments (n=2). Standard deviation is less than 5% of mean value.

Moreover, the release of DEX is pH-dependent, where the highest amount of DEX, 7.5±0.1 µg/mL and 4.3±0.0 µg/mL, was respectively released at higher pH values, pH=7 and pH=6. On the other hand, at more acidic conditions (pH=5) minor concentrations of DEX (1.8±0.0 µg/mL) were released.

3.4.3 Layer-by-Layer route

The DEX release from functionalised-TiO_2 particles obtained via LbL route was also investigated, and release profile at pH=6 and pH=7 (Figure 42, Figure 43) was plotted. Experimentally the release profile of DEX from the LbL-functionalised TiO_2 particles portrays an initial release phase during the first 24 hours, followed by a constant release of DEX for at least 20 days; where a gradual decrease in the rate release was observed for both pH=6 (Figure 42), and pH=7 (Figure 43). Although constant, the pH conditions and number of layers deposited on the surface of TiO_2 particles, particularly around DEX layer, significantly ($p<0.05$) affected DEX release profile. For instance, at pH=6 the total amount of drug released when DEX is the outer layer (DEX sample) was higher (1.1-1.3 mg/mL), than the one released at pH=7 (0.6-0.8 mg/mL).
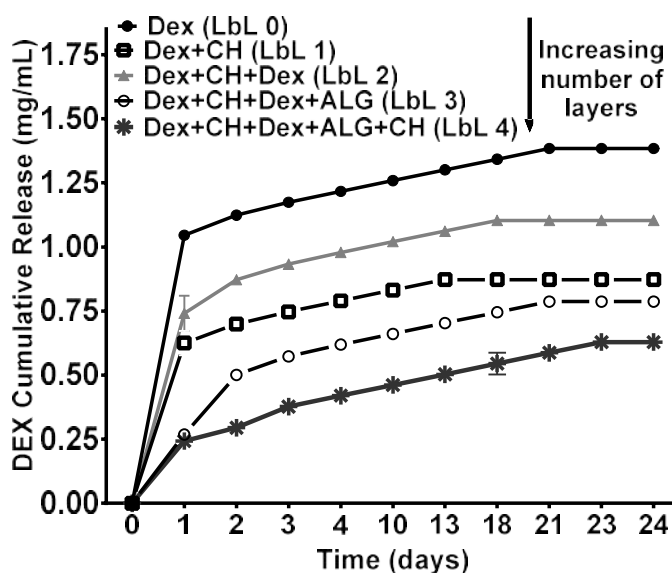
Figure 42. **Cumulative release of DEX from LbL-functionalised TiO_2 particles at pH=6. The DEX release profile for functionalised TiO_2 particles with different number and type of outer layers was investigated: for LbL particles where DEX was the outer layer (*DEX (LbL 0)* and *DEX*+CH+*DEX (LbL 2)* samples). And for particles where CH or ALG were the outer layers: *DEX*+CH (LbL 1), *DEX*+CH+*DEX*+ALG (LbL 3) and *DEX*+CH+*DEX*+ALG+CH (LbL 4). Data are the mean ± standard deviation (SD) of two independent experiments (n=2). Standard deviation is less than 5% of mean value.**

Furthermore, for both pH=6 and pH=7, DEX released from functionalised-TiO_2 particles where DEX was the outer layer, LbL 0 and LbL 2, was higher than the one released from particles where DEX layer was surrounded by CH/ALG layers, LbL 1, LbL 3 and LbL 4.

For example, at pH=7 (Figure 43), results showed the highest concentrations of DEX were released from LbL 0 (~1 mg/mL) and LbL 2 (~0.9 mg/mL). On the other hand, the smallest concentrations were released from LbL 1 (~0.85 mg/mL), LbL 3 (~0.56mg/mL) and LbL 4 (~0.53mg/mL). Similar trend was observed for DEX release at pH=6 (Figure 42), where the higher concentrations of DEX were released for functionalised-TiO_2 particles where DEX was the outer layer (LbL 0 and LbL 2 samples).
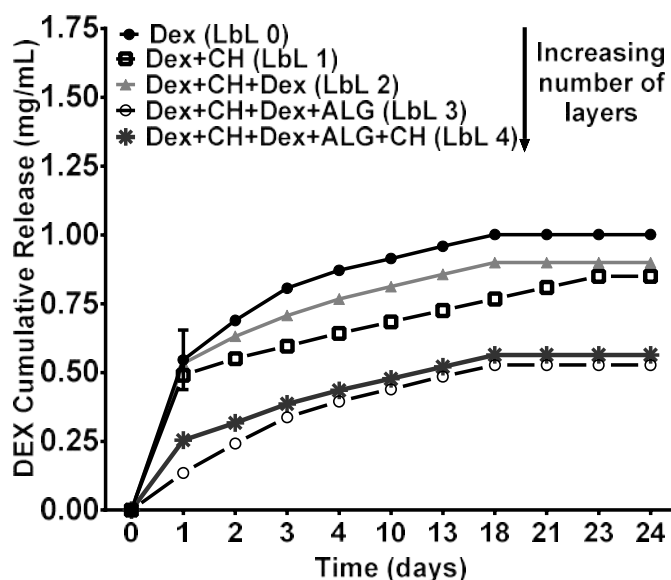
Figure 43. Cumulative release of DEX from LbL-functionalised TiO_2 particles at pH=7. The DEX release profile for functionalised TiO_2 particles with different number and type of outer layers was investigated: for LbL particles where DEX was the outer layer (DEX (LbL 0) and DEX+CH+DEX (LbL 2) samples). And for particles where CH or ALG were the outer layers: DEX+CH (LbL 1), DEX+CH+DEX+ALG (LbL 3) and DEX+CH+DEX+ALG+CH (LbL 4). Data are the mean ± standard deviation (SD) of two independent experiments (n=2).

Moreover, independently of the pH conditions and for all LbL particles (LbL 0, LbL 1, LbL 2 and LbL 4) it was observed that the concentration of DEX release from LbL particles decreased over time. Likewise, the highest concentrations of DEX were released during the initial 24h, whilst smaller concentrations were released in the following days (~20 days). Taking as example LbL 0 and LbL 4, the following concentrations of DEX were released at pH=6 (Figure 42) for LbL 0 (1.05, 0.8, 0.05 and 0.04 mg/mL), and for LbL 4 (0.24,0.07, 0.06 and 0.04 mg/mL) respectively at 24h, 48h, 72h and 2 weeks. Similarly, at pH=7 (Figure 43) the following concentrations of DEX were released from LbL 0 (0.55, 0.14, 0.12 and 0.05 mg/mL), and for LbL 4 (0.25, 0.06, 0.07 and 0.05 mg/mL), respectively at 24h, 48h, 72h and 2 weeks.

3.5 DEX Loading (%) and Entrapment Efficiency (%)

The amount of DEX loaded onto functionalised-TiO$_2$ particles, and respective encapsulation efficiency (EE%) were calculated for the different synthetic routes (Table 13). Functionalised-TiO$_2$ particles obtained by amino and mercapto presented very similar values for both drug content (~0.13mg of DEX/mg of functionalised-TiO$_2$ particles) and encapsulation efficiency (~68%).

Table 13. Drug loading and entrapment efficiency of DEX-loaded functionalised TiO$_2$ particles prepared by amino, mercapto and LbL routes. Data are the mean ± standard deviation (SD) of two independent experiments (n=2).

DEX-loaded TiO$_2$ particles (Synthetic route)	Loading (%)	Entrapment efficiency (%)
Amino route	13.6±0.2	68.1±0.1
Mercapto route	13.6±0.0	67.9±0.2
LbL route: Sample LbL 0	27.2±0.1	42.9±0.2
LbL route: Sample LbL 4	40.5±0.1	50.6±0.2

For LbL route, drug loading and entrapment efficiency were calculated for samples 0 (DEX was the outer layer) and sample 4 (DEX was surrounded by 4 CH/DEX/ALG layers). This was performed because drug release studies (**3.4.3 Layer-by-Layer route**) have shown that the number of layers surrounding DEX-loaded functionalised TiO$_2$ particles significantly affected the DEX release profile. Accordingly, results (Table 13) showed that when compared to sample 0, both encapsulation efficiency and drug loading were higher for sample 4. This difference was more evident for drug loading calculations (%), where an 0.35-fold increase of drug loading was observed for sample 4.

3.6 Cellular viability studies

The assessment of cytotoxicity of drug delivery systems is a central factor in the evaluation of novel systems for future *in vivo* applications. Although, before assessing the cytotoxicity of the model system, a preliminary study was performed to determine if the broths collected from drug release experiments and concentrations of DEX released from functionalised-TiO$_2$ particles were potentially toxic to the Raw 264.7 macrophages. For this purpose, a range of DEX concentrations (3.9-100µg/mL), and the broths collected from drug release assay performed at pH=6 and pH=7 were exposed to Raw 264.7 macrophages with and without LPS. The broths collected from drug release studies performed at pH=4 and pH=5 were not tested, due to the low cellular viability they caused when exposed to the cells (

I. Appendix Figure 77).

3.6.1. Preliminary studies on Raw 264.7 cells

<u>DEX</u>

The effect of DEX concentrations (3.9–100 µg/mL) effect on cellular viability was also assessed, with and without LPS (Figure 44). After 18h, 24h and 48h, DEX alone caused a significant ($p<0.001$) 264.7 Raw macrophages death of approximately 20-30%, as evaluated by MTT assay (Figure 44.A). This decrease on cellular viability was more evident when cells were exposed to a higher DEX concentration such as 40 and 100 µg/mL. However, for the same concentrations of DEX (3.9–100 µg/mL), and in the presence of LPS after 18h, 24h and 48h, cell viability of RAW 264.7 macrophages were significantly (*p<0.05*) equal or higher than 100% relative to control (Figure 44.B). After 72 hours, the DEX affected cellular viability in a dose-dependent manner for both cells treated with or without LPS (Figure 44). Accordingly, the cells treated with minor concentrations of DEX (3.9 and 10 µg/mL) showed the lowest (10-15% relative to control) or any decrease on cellular viability, respectively for Raw 264.7 macrophages without (Figure 44.A) or with LPS (Figure 44.B).On the other hand, Raw 264.7 cells treated with higher DEX concentrations (≥20 µg/mL), caused a higher cell death, 25-40% and 5-15%, respectively for cells without or with LPS.

<u>Drug release buffers</u>

Before exposing the cells to the DEX released from functionalised TiO_2 particles (i.e. broths collected from drug release studies), preliminary studies were done to assess if the buffers utilized to perform the drug release studies, acetate buffer (pH=6) and PBS (pH=7), were potentially toxic to the macrophages. Therefore, Raw 264.7 cells were exposed to different concentrations (0-100%) of PBS (Figure 45). In this study, the 100% PBS means that cells were only treated with buffer, and 50% means the buffer was diluted (1:2) in DMEM media.

For cells without LPS (Figure 45.A), results show that all concentrations of PBS tested, except 10%, caused a significant (p<0.05) decrease on the cellular viability, in a concentration-dependant manner, where the higher concentration of buffer tested (100% of PBS) caused a cell death of about 90%, relative to control. However, for the same concentrations of PBS (10–100%), and in the presence of LPS (Figure 45.B), the cell viability of RAW 264.7 macrophages was overall higher than for cells without LPS. Particularly, when cells were exposed to higher PBS concentrations such as 100% and 75%. Despite this fact, the same behaviour was observed for cell treated with or without LPS, where among all concentrations tested only 10% of PBS did not cause a significant

decrease (p<0.05) on cellular viability, showing almost the same behaviour as the LPS control group. The same trend was observed when LPS-activated Raw 264.7 cells were exposed to different concentrations (0-100%) of acetate buffer (pH=6), except after 72h exposure, where 10% acetate buffer caused a significant (p<0.05) but minor decrease of cellular viability when compared to control group (

I. Appendix, Figure 89,).
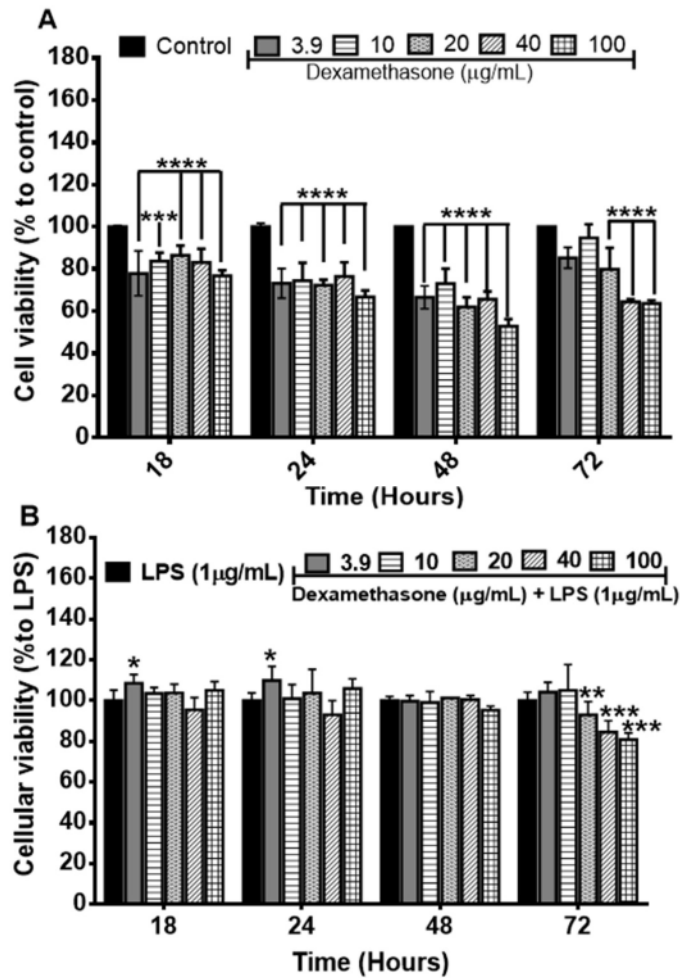
Figure 44. Effect of DEX without (A) and with LPS (B) in cell viability. RAW 264.7 macrophages were exposed to range of concentrations between 3.9 and 100 µg/mL during 18h, 1day, 2 days and 3 days. Cell viability was assessed by MTT study done with 2 x10^4 cells /well. Data are the mean ± standard deviation (SD) of two independent experiments (n=2).
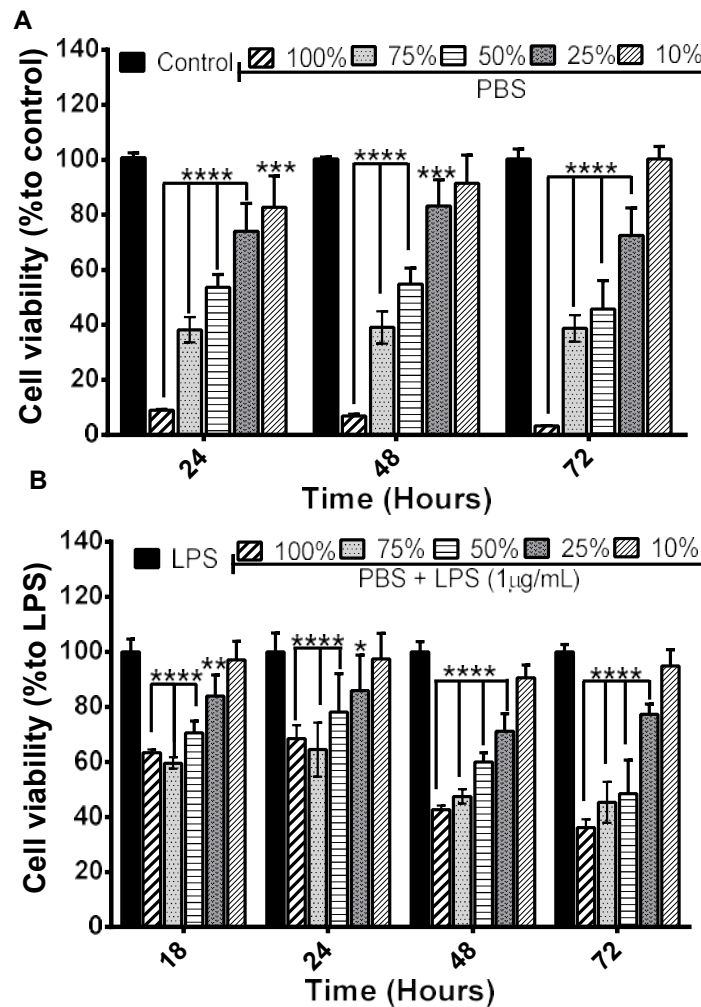
Figure 45. Effect of different concentrations of PBS, buffer utilized for drug release studies (pH=7), (A) with and (B) without LPS in cell viability. RAW 264.7 macrophages were exposed to range of PBS concentrations (10-100%) diluted in DMEM media, for 18, 24, 48 and 72 hours. In the control group cells were only treated with DMEM. Data are the mean ± standard deviation (SD) of two independent experiments (n=2).

<u>Filtered versus non-filtered broths</u>

Results from preliminary studies with drug release buffers have shown that broths should be diluted on DMEM media up to a concentration of 10% before being added to the cells. This way, it can be guaranteed that anti-inflammatory effect of DEX released from functionalised-TiO$_2$ particles will not be due to a decrease of cellular viability. Although, when the cells were exposed to the broths, it was observed that after 18h exposure some black spots were surrounding the cells (Figure 46.A).
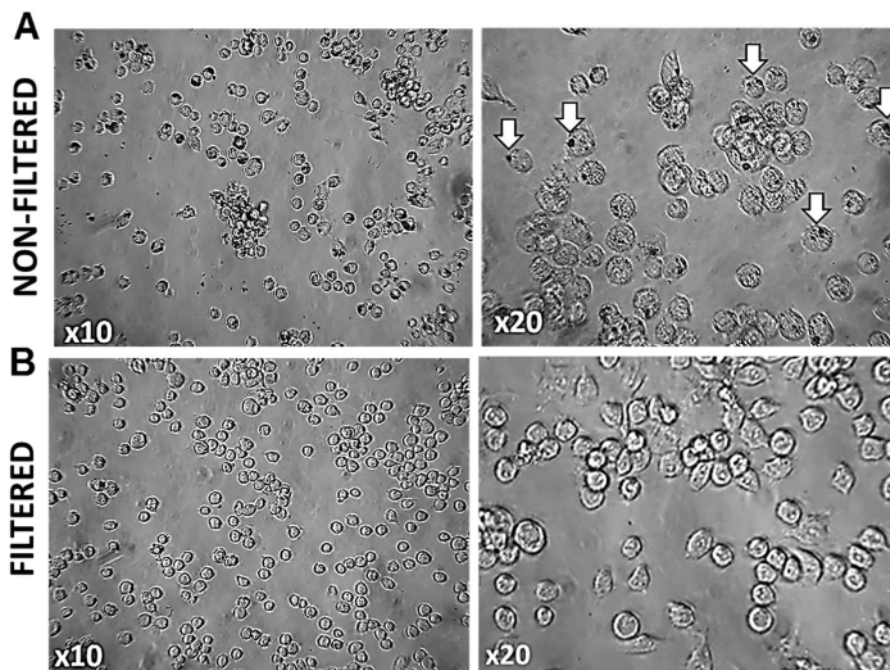
Figure 46. **The effect of A. non-filtered and B. filtered broths on the Raw 264.7 macrophages after 18h-exposure was assessed by inverted microscopy. Dark spots are indicated by the white arrows.**

To assess the effect of these black spots (Figure 46.A), the cellular viability of cells exposed to non-filtered and filtered broths was investigated (Figure 47, Figure 48). Results obtained from MTT assay, showed that for most of the broths tested the cellular viability was significantly ($p < 0.05$) higher when cells were exposed to filtered samples for both pH=6 and pH=7 (amino and mercapto routes). Overall ~ a 2-fold increase on cell viability was observed when comparing cells exposed to filtered broths over the unfiltered ones   (Figure 47, Figure 48). Even after 72 hours-exposure, the cells treated with the filtered broths presented a higher % of cellular viability. Particularly, the broths collected from drug release studies performed pH=7, where cellular viability was very similar (~85% cellular viability) to the one observed for the control group.
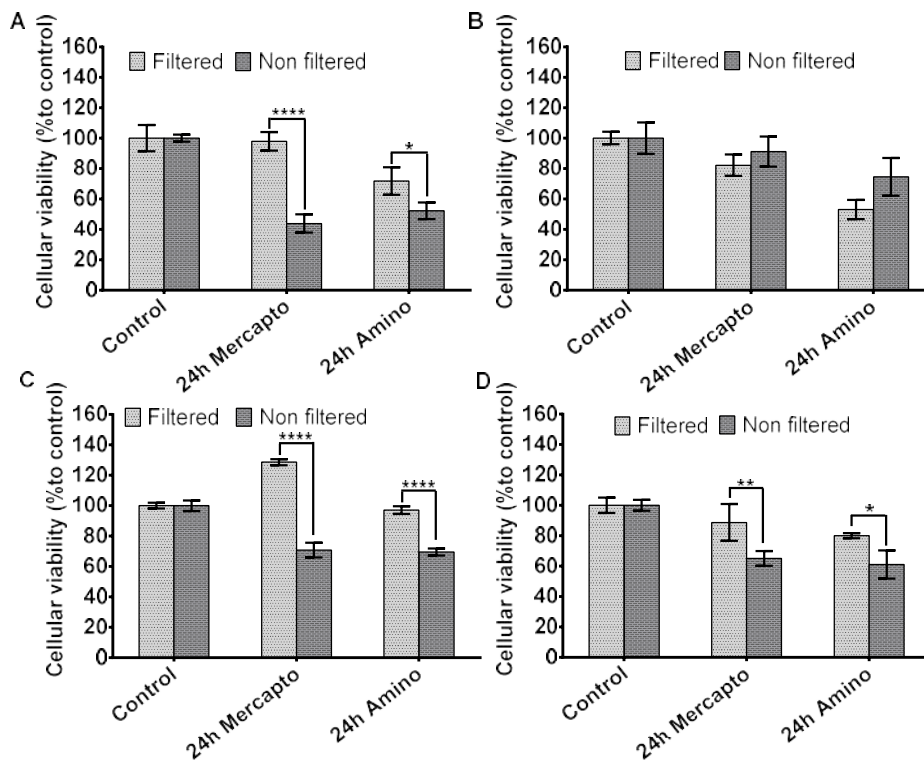
Figure 47. Effect of filtered and non-filtered broths, collected from drug release studies (Amino Route) performed at pH 6, in cell viability. RAW 264.7 macrophages were exposed to broths during (A) 18h, (B) 24h, (C) 48h and (D) 72 hours. Cell viability was assessed by MTT assay. In the control group cells were only treated with DMEM. Data are the mean ± standard deviation (SD) of two independent experiments (n=2).

The same experiment was performed for LPS-activated cells (Figure 49). Similar results were found, overall the LPS-activated Raw 264.7 cells exposed to filtered samples showed significant (p<0.05) and higher cellular viability when compared to non-filtered ones. This behaviour was mostly observed after 72 hours, where the cells treated with filtered broths less than 25% of cell death relative to control. Particularly for cells exposed to filtered broth collected from pH=7 (Figure 50), in this case less than 10% of cell death was observed, when compared to the control.
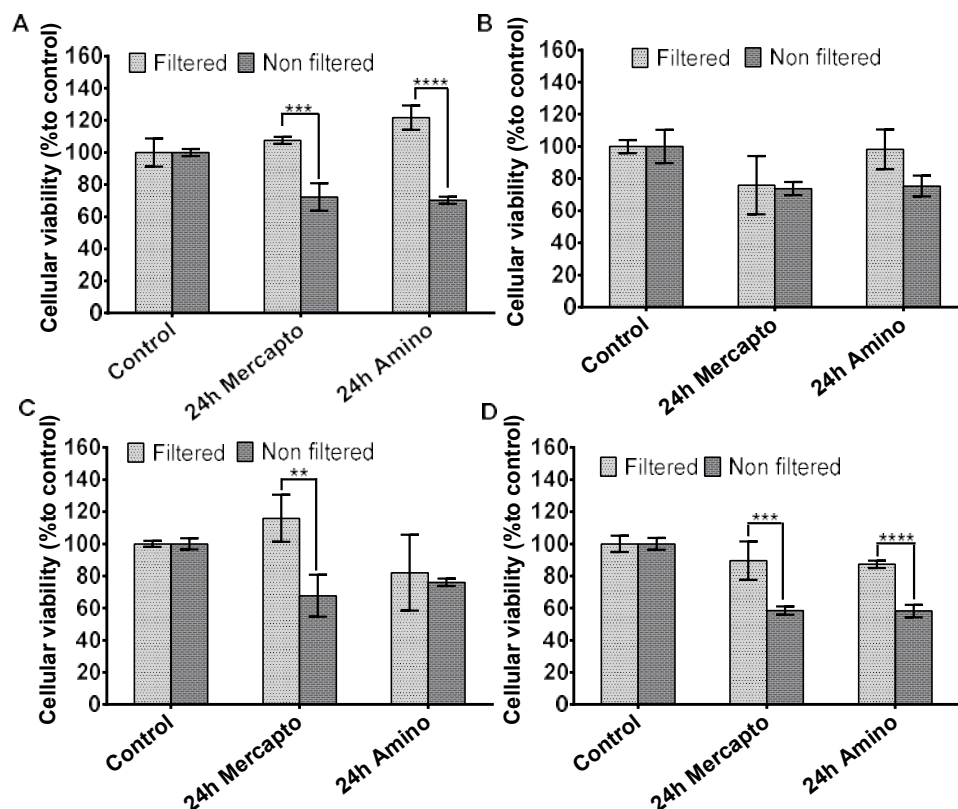
Figure 48. Effect of filtered and non-filtered broths, collected from drug release studies (Amino Route) performed at pH 7, in cell viability. RAW 264.7 macrophages were exposed to broths during (A) 18h, (B) 24h, (C) 48h and (D) 72 hours. Cell viability was assessed by MTT assay. In the control group cells were only treated with DMEM. Data are the mean ± standard deviation (SD) of two independent experiments (n=2).

Furthermore, as shown in Figure 46.B, filtered broths did not induce the black spots previously observed for cells treated with unfiltered samples. Hence, due to the significant higher cellular viability, all subsequent Raw 264.7 cells studies were performed using filtered samples and 1:10 media dilution (concentration of 10% in release buffer).
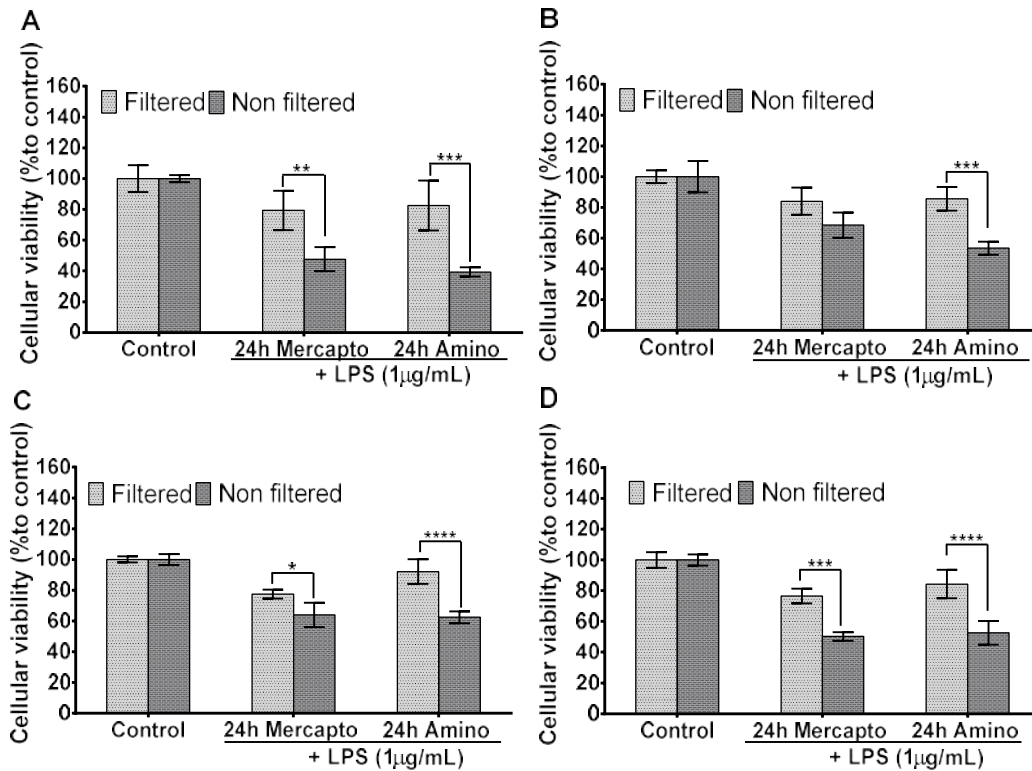
Figure 49. Effect of filtered and non-filtered broths, collected from drug release studies (Amino and mercapto route) performed at pH 6, in cell viability. LPS-activated-RAW 264.7 macrophages were exposed to (A) 18h, (B) 24h, (C) 48h and (D) 72 hours. Cell viability was assessed by MTT assay. In the control group cells were only treated with DMEM. Data are the mean ± standard deviation (SD) of two independent experiments (n=2).
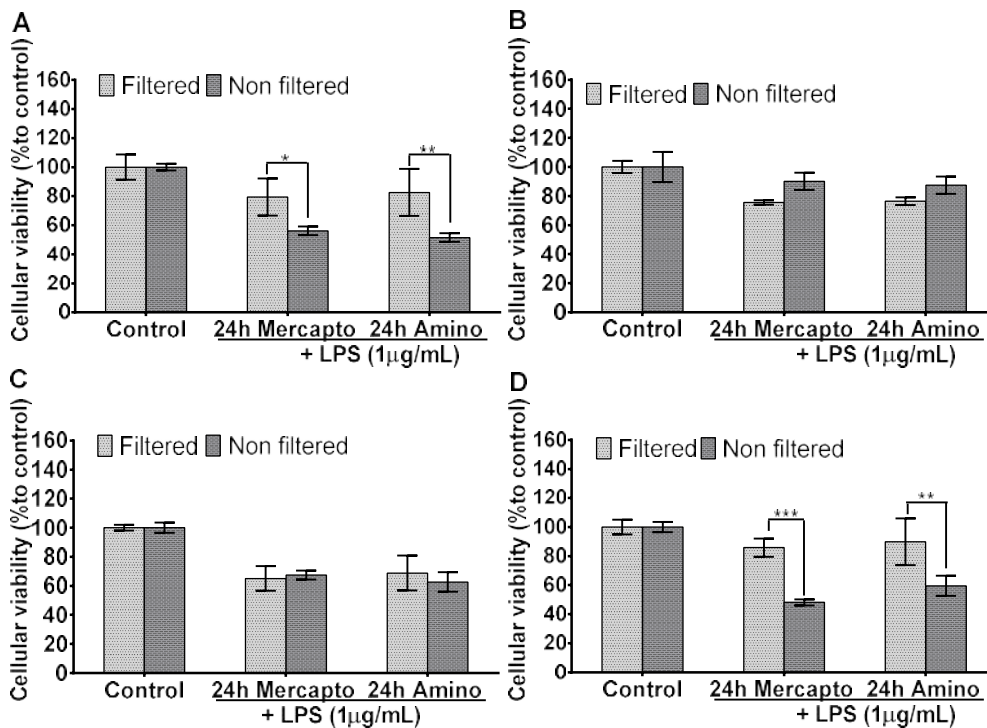
Figure 50. Effect of filtered and non-filtered broths, collected from drug release studies (Amino and Mercapto route) performed at pH 7, in cell viability. LPS-activated-RAW 264.7 macrophages were exposed to (A) 18h, (B) 24h, (C) 48h and (D) 72 hours. Cell viability was assessed by MTT assay. In the control group cells were only treated with DMEM. Data are the mean ± standard deviation (SD) of two independent experiments (n=2).

The same preliminary toxicity studies, for filtered and non-filtered samples, were performed for the broths collected from DEX-loaded functionalised-TiO$_2$ particles obtained by LbL route (

I. Appendix, Figure 84, Figure 85).

3.6.2 Dexamethasone loaded functionalised-TiO₂ particles

The viability of cells exposed to DEX released from functionalised-TiO₂ particles was investigated to exclude the decrease of inflammatory mediators i.e. TNF-α and NO, due to drug-induced toxicity. The broths collected from drug release studies at pH=6 and pH=7 performed for functionalised-particles obtained via amino/mercapto (Figure 51) and LbL routes were exposed to LPS-activated Raw 264.7 macrophages, and cellular viability was assessed.
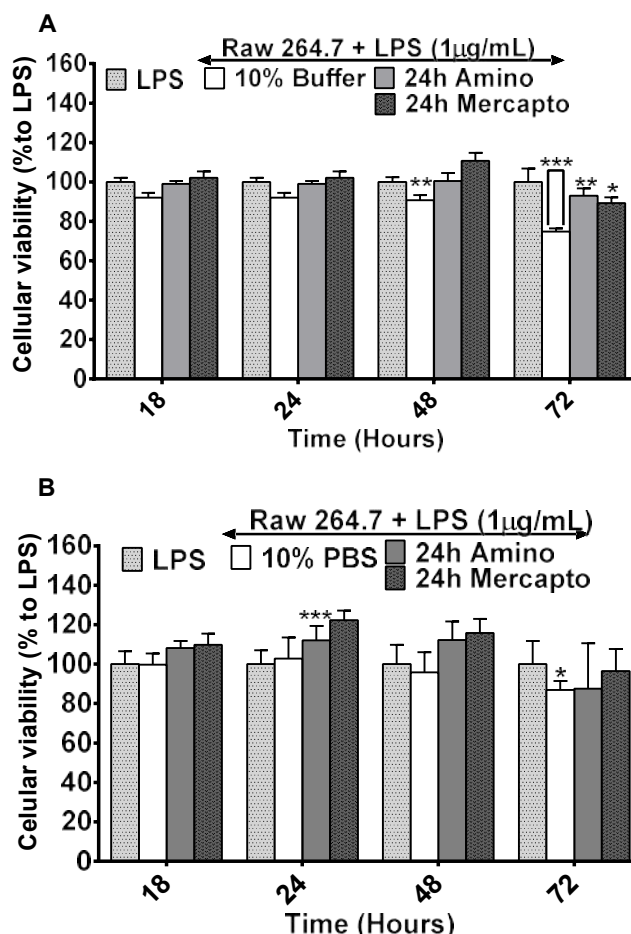
Figure 51. Effect of DEX, released from functionalised-TiO₂ particles, in LPS-activated RAW 264.7 cell viability. Cells were exposed to filtered broths collected at 24h time point (i.e. DEX released after 24h) during 18, 24, 48 and 72 hours. Broths were collected from drug release studies performed at (A) pH=6 and (B) pH= 7 for amino (24h amino) and mercapto (24h mercapto) routes. Cellular viability was assessed by MTT assay. 10%acetate buffer and 10%PBS buffer were respectively used as positive control for broths collected from release studies performed at (A) pH=6 and (B) pH= 7. Data are the mean ± standard deviation (SD) of two independent experiments (n=2).

Results obtained from MTT assay showed that the viability of cells exposed to DEX released from functionalised-particles was very similar (>90% cellular viability) to the one observed for the LPS control group (Figure 51) for both amino and mercapto routes. Except at 72h, where a higher decrease on viability, 7-11% relative to control group, was observed, for cell treated with DEX released at pH=6 (Figure 51.A). Although significant ($p < 0.05$), when compared to control group, this decrease on cellular viability for 24h amino (~7%) and for 24h mercapto (~11%) was not as significant ($p < 0.05$) as the one induced on Raw macrophages (~20%) treated with release buffer alone.

LbL route

The same preliminary cellular viability studies were performed for DEX released from functionalised TiO_2 particles obtained by LbL route (experiment 2). For this study samples were collected from release studies at pH=6 (Figure 52.A) and pH=7 (Figure 52.B). As drug release studies have shown that the concentrations of DEX released varied according to the number of layers surrounding functionalised TiO_2 particles. Accordingly, the cells were exposed to DEX released from LbL-functionalised particles where DEX was the outer layer (LbL 0) or where DEX was surrounded by 4 CH/DEX/ALG layers (LbL 4). For clarity, different names were attributed to DEX-loaded functionalised TiO2 particles obtained by LbL route (experiment 2), where the names varied according to different CH ALG or DEX layers deposited around functionalised-TiO_2 particles (Table 14).

Table 14. Sample names for DEX-loaded functionalised TiO_2 particles obtained by LbL route. CH, ALG and DEX in bold correspond to layers surrounding DEX-loaded functionalised TiO_2 particles.

DEX-loaded functionalised TiO_2 particles	Sample name
(NH_2-TiO_2 particles) -ALG-CH-DEX	LbL 0
(NH_2-TiO_2 particles) -ALG-CH-DEX-CH	LbL 1
(NH_2-TiO_2 particles) -ALG-CH-DEX-CH-DEX	LbL 2
(NH_2-TiO_2 particles) -ALG-CH-DEX-CH-DEX-ALG	LbL 3
NH_2-TiO_2 particles) -ALG-CH-DEX-CH-DEX-ALG-CH	LbL 4

For this set of experiments (Figure 52), cellular viability was assessed for broths collected from LbL-functionalised particles with 0 layers (DEX sample, LbL 0) and 4 layers (DEX+CH+DEX+CH+ALG samples, LbL 4), and collected at different time points (DEX

released at 24h and 48h). Mainly because drug release studies performed for LbL particles (pH=6 *Figure 42*, and pH=7 *Figure 43*) have shown that number of layers (CH, ALG and DEX) surrounding functionalised-TiO_2 particles, significantly affected the DEX release profile (i.e. different release of DEX concentration for same time points).
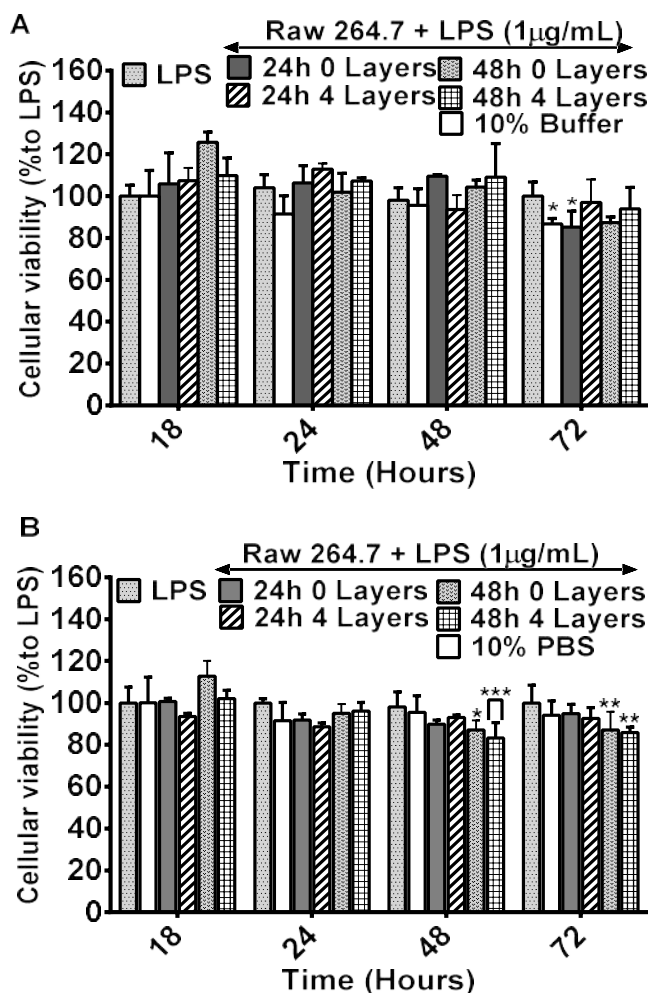
Figure 52. **Effect of DEX released from functionalised-TiO_2 particles, obtained via LbL route in LPS-activated RAW 264.7 cell viability. Cells were exposed to filtered broths collected at 24h and 48h time point *(i.e. DEX released after 24 and 48h)* during 18, 24, 48 and 72 hours. Broths were collected from drug release studies performed at (A) pH=6 and (B) pH= 7 for DEX-loaded particles surrounded by 0 layers or 4 layers. Cellular viability was assessed by MTT assay. 10% acetate buffer and 10% PBS buffer were respectively used as positive control for broths collected from release studies performed at (A) pH=6 and (B) pH= 7. Data are the mean ± standard deviation (SD) of two independent experiments (n=2).**

Therefore, we decided to investigate if the DEX released from functionalised-TiO_2 particles surrounded by 0 (LbL 0) or 4 layers (LbL 4) at different time points, will have a different effect in viability of Raw 264.7 cells.

It can be seen in *Figure 52*, that after 18h and 24h exposure, DEX released from functionalised-TiO_2 particles surrounded by 0 and 4 layers from both studies at pH=6 and pH=7 had minor effect on LPS-activated cells, with insignificant changes on cellular viability (>90%, relative to control). On the other hand, it was observed that after 48h and 72h-exposure, the 48h-collected broths caused a small, but significant decrease on cells viability. Specifically, DEX released from functionalised-TiO_2 particles surrounded by 0 (48h 0 layer) and 4 layers (48h 4 layers) (pH=7 studies, *Figure 52*.B), respectively caused a minor decrease on cellular viability of 10 and 15% relative to LPS control group. Although significant ($p < 0.05$), when compared to control group, this decrease on cellular viability was not as significant ($p < 0.05$) as the one induced on Raw macrophages (~20%) treated with release buffer alone.

3.7. LPS-activated 264.7 Raw macrophages: inflammation model

Another important factor when assessing the anti-inflammatory activity of DEX-loaded functionalised-TiO_2 particles, it is to obtain a reliable *in vitro* inflammatory model. In which LPS exposure will be able to induce inflammation i.e. allow measurable production of inflammatory markers such as nitric oxide (NO) and tumour necrosis factor alpha (TNF-α). To obtain a reliable *in vitro* inflammation model, an appropriate cell density and an optimal LPS concentration should be utilized to assay NO and TNF-α production in culture. Mainly because if the cell density is not appropriated, the NO and TNF-α production might not be detectable in the cell media. As for LPS concentration, high dose could cause cell toxicity, and low concentration might not be enough to activate the macrophages. For this reason, cell density and LPS concentration were optimised to measure the production of inflammatory mediators in LPS-activated macrophages. Due to rapidity and simplicity, the measurement of NO production by Griess reagent was utilized as screening tool for this optimisation study. Likewise, NO production was assessed when different cell densities and LPS concentrations were utilized to find out which experimental conditions would generate the more reliable results. The cellular viability of LPS-activated cells under different parameters (e.g. cell density and LPS concentration) was also investigated to complement the optimization of *in vitro* inflammation model.

3.7.1 Optimal LPS concentration

Aiming to optimize the LPS concentration to activate the macrophages, the cells were treated with different concentrations of LPS (ranging from 0.01 to 1µg/mL) to identify the optimal concentration of the stimulant. Particularly for this experiment, cells were seeded at a density of 1.5×10^4 cells/well on a 96-well plate, stimulated with LPS and then level of NO and TNF-α were analysed at different time points (18, 24, 48 and 72 hours). Overall, results showed (Figure 53) that LPS exposure caused a marked and significant increase in NO and TNF-α protein levels when compared to the unstimulated macrophages, which produced only very low amounts of TNF- α (<35 pg/mL) and NO (<20 µM/mL). As can be seen in Figure 53 both NO and TNF-α production follow a dose-dependent and temporal pattern; where LPS concentration of 1µg/mL was the most powerful for Raw 264.7 macrophages activation.
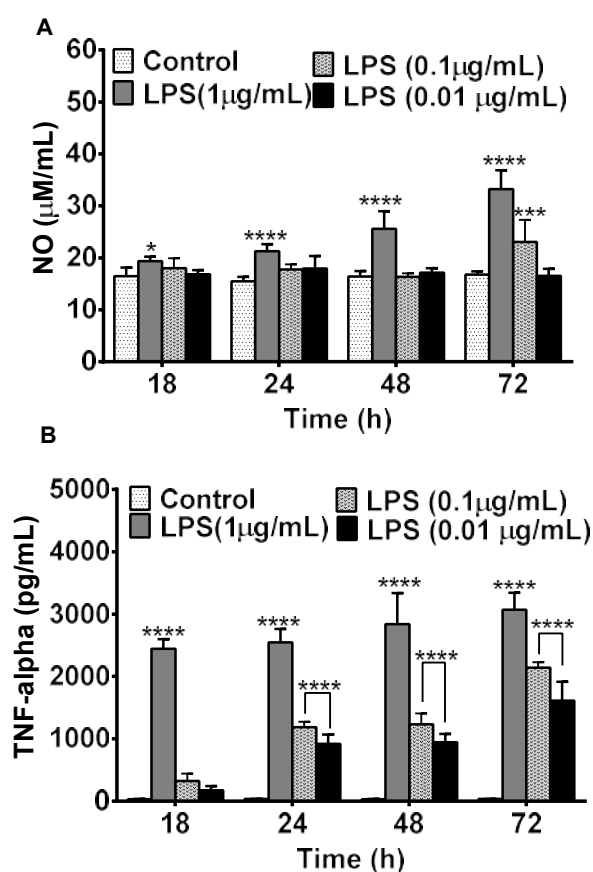
Figure 53. A) Nitric oxide (NO) and TNF- α production upon exposure to different LPS concentrations (0.01-1µg/mL range) during 18, 24, 48 and 72 hours. In the control group cells were only treated with DMEM. For control group, standard deviation is less than 5% of mean value. Data are the mean ± standard deviation (SD) of two independent experiments (n=2).

These results were confirmed after visualising the cells morphology under the inverted microscope, where cells exposed to a higher LPS concentration (1µg/mL) showed a more dendritic-like morphology, typical of activated macrophages (Saxena et al. 2003) (Figure 54).For example (Figure 53), after 18h exposure only macrophages which were stimulated with the highest concentration of LPS (1 μg/ml) have shown to secrete a significant level of inflammatory NO and TNF-α proteins, respectively with an approximate~0.18 and ~68-fold increase when compared to control group. On the other hand, after long LPS-time exposure (72h), inflammatory protein levels were maximally elevated; LPS stimulated-cells secreted approximately 3000 pg/ml of TNF-α, and ~34 µM/mL of NO, respectively a ~100 and 1.1-fold increase when compared protein levels of the unstimulated control group.
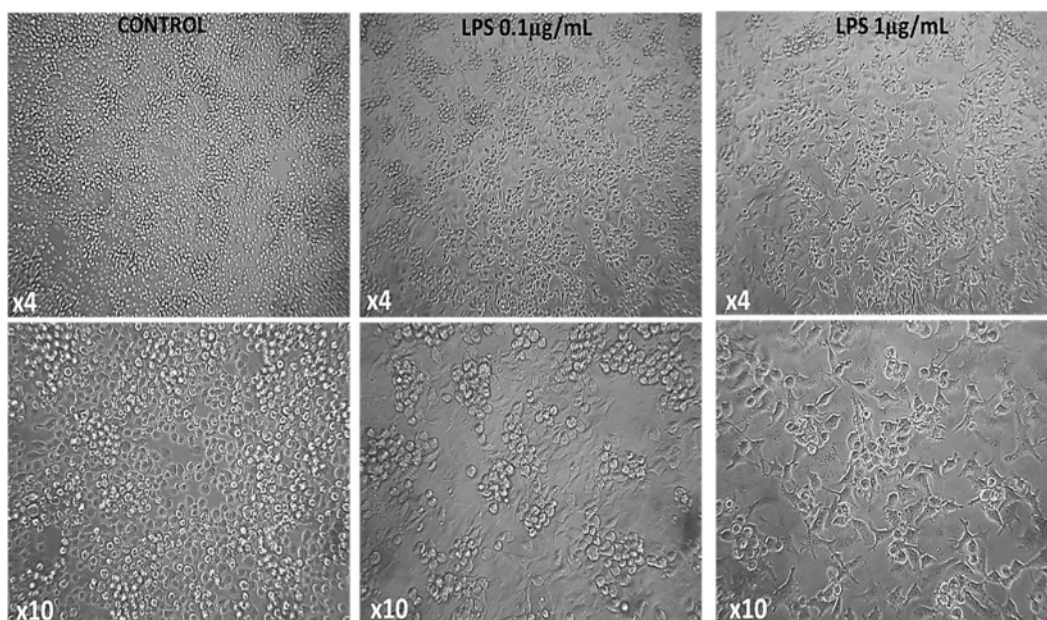
Figure 54. The effect of LPS (0.1 and 1 µg/mL) on the morphology of Raw 264.7 macrophages after 24h exposure was assessed by inverted microscopy. Photographs were taken at magnification of x4 and x10 magnification.

Moreover, results showed that LPS prepared from fresh stock solution instead of frozen one (Figure 86), was more effective i.e. higher NO production for Raw 264.7 macrophages activation.

3.7.2 Optimal cell density

Macrophage density is also an important parameter to regulate the magnitude of inflammatory markers production (Hosseini et al. 2014, Jacobs & Ignarro 2003). Therefore, aiming to optimize the seeding density of Raw 264.7 cells to be used for measuring inflammatory markers production, cells were seeded at different cell densities: 0.5×10^4 cells/well, 1.5×10^4 cells/well, 2×10^4, and 2.5×10^4 cells/well in a 96-well plate. The cells were treated with LPS concentration of 1 µg/ml, which according to our previous results (Figure 53, Figure 54), was the most effective concentration for optimal NO and TNF-α production, and then cell culture supernatant was analysed for NO levels using Griess assay. The data obtained (*Figure 55*) depicts the relationship between cell density and NO production on Raw 264.7 macrophages with and without LPS. As expected, the unstimulated Raw 264.7 cells produced minimal amount of NO, with the levels remaining lower than 20 µM/mL at all time points tested. On the other hand, LPS-stimulated cells showed a higher NO production at 24, 48 and 72 hours when compared to unstimulated ones.
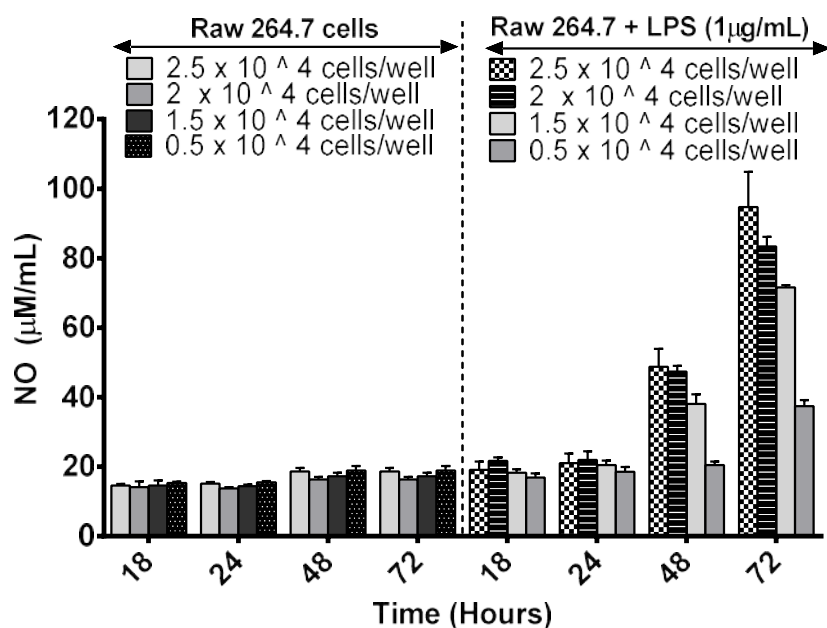
Figure 55. Optimisation of Raw 264.7 cell in culture. Comparison of nitric oxide (NO) production (µM/mL) in cells without (left side of the graph) and with LPS (1 µg/mL) (right side of the graph) during 18, 24, 48 and 72 hours, when different cell densities were utilized (0.5 to 2.5×10^4 cells/well). Data are the mean ± standard deviation (SD) of two independent experiments (n=2).

This trend was particularly observed for high cell densities (2.5 and 2×10^4 cells/well), where the LPS-induced NO production was significantly (p<0.05) enhanced, when

compared to the one observed for lower cell densities. In addition, the results showed that although the Griess reagent assay was not sensitive enough to detect the amounts of NO produced, a minor alteration on cell morphology (Figure 56) was observed for LPS-activated cells when lower cell densities were utilized (0.5 and 1.5 x 10^4cells/well), especially in the first 24 hours.
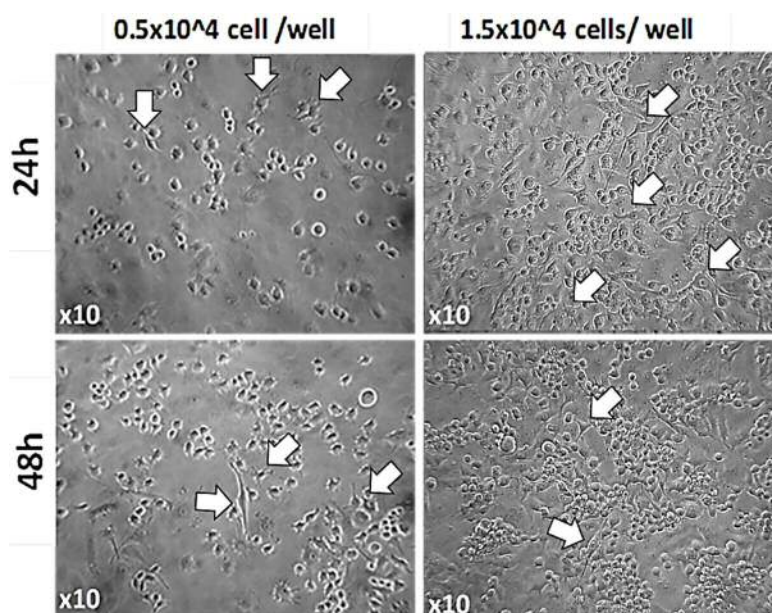
Figure 56. The effect of LPS (1 µg/mL) on the morphology of Raw 264.7 macrophages during 24, 48 and 72 hours-exposure was assessed by inverted microscopy, when different cell densities were utilized. White arrows indicate the dendritic-like cells, a distinctive feature of LPS-activated macrophages.

The viability of cells treated with and without LPS for different cell densities, was also investigated, to evaluate if NO was being released due to LPS cytotoxicity (Figure 57). The viability of cells seeded at low density (0.5 x 10^4cells/well) was not assessed due to lower amount of NO detected (*Figure 55*), when compared to the others cell densities investigated (1.5 x 10^4, 2.0 x 10^4 and 2.5 x 10^4cells/well). Individual and more detailed graphs showing the viability of different cell density with and without LPS are shown in the appendix section (

I. Appendix. *Figure 87*). Results (Figure 57) showed that at 48h, the LPS-stimulated cells showed a higher cellular viability i.e. more metabolic active, when compared to the control. Except for the high cellular density utilized, 2.5 x 10^4cells/well, where microscope images showed that at 48h the cells start to be overconfluent. Only at 72 hours, a decrease on cellular viability was detected for all cell densities, although cellular viability was still high, where ~80% of cellular viability was observed for LPS-activated cells when compared to control group.
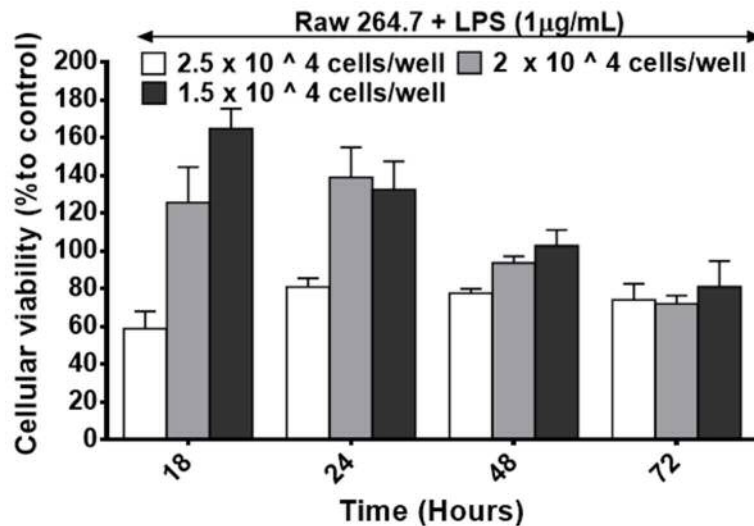
Figure 57. The effect of LPS (1 µg/mL) on the cell viability of Raw 264.7 macrophages during 18, 24, 48 and 72 hours-exposure was assessed by MTT assay, when different cell densities were utilized. Results were plotted against cells seeded at same cell density but without LPS stimulation (control). In the control group cells were only treated with DMEM. Data are the mean ± standard deviation (SD) of two independent experiments (n=2).

Overall results showed that NO production and cellular viability of LPS-stimulated macrophages followed a pattern, which was affected by cell seeding density. Likewise, overtime NO levels showed an increase proportional to cell-density, whereas the higher cell density (>0.5 x 10^4cells/well) was associated with higher production of NO (~100µM/mL). Although, cell viability studies showed that over time the highest cell density 2.5 x 10^4cells/well was associated with the smaller cell viability, which may be caused by the high toxic levels of NO. Accordingly, 2.0 x 10^4cells/well was the seeding density chosen for the following studies. Mainly to assess the anti-inflammatory activity i.e. level of inflammatory markers of DEX released from functionalised TiO_2 particles in LPS-activated Raw 264.7 macrophages.

3.7.3. Optimised model: Cellular morphology, TNF-α and NO production

After establishing the appropriate cell density (2x10^4 cells/well) and LPS concentration (1µg/mL), we further evaluated the morphology of LPS-activated cells (Figure 58) by staining actin rings using fluorescent microscopy.
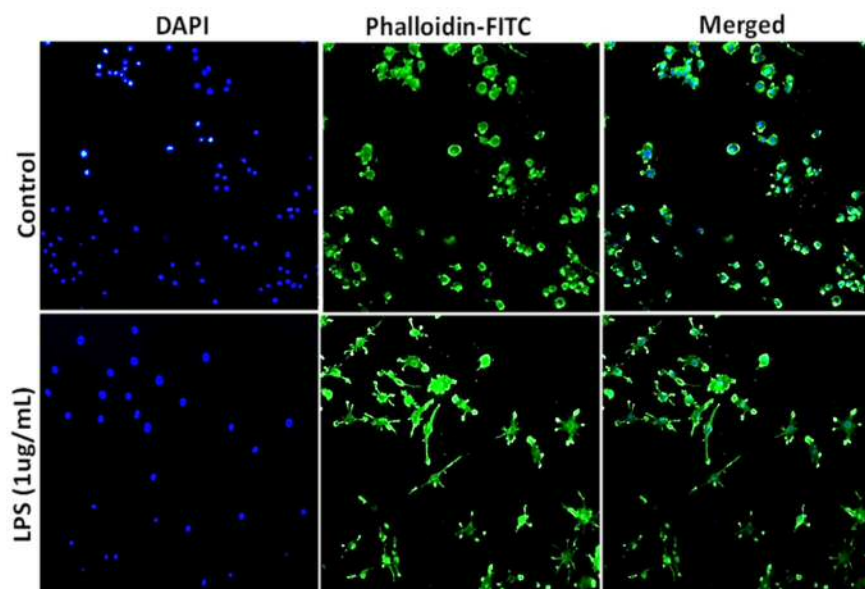
Figure 58. **The effect of LPS (1 µg/mL) on the cellular morphology of Raw 264.7 macrophages after 24h-exposure was assessed by fluorescence microscopy (A). F-Actin rings and nuclei of cells were respectively stained with phalloidin-FITC and DAPI. Photographs were taken at fluorescence microscope at magnification of ×20.**

Results revealed that after 24h exposure, the untreated Raw 264.7 cells showed a regular rounded morphology and did not spread over the surface. On the other hand, LPS exposure (1µg/mL), induced a reorganization in actin distribution of the macrophages resulting in evident difference in cell morphology: cells showed an oval-shaped configuration and visible size increase. Along with this experiment (Figure 58), the cellular viability (Figure 59), TNF-α and NO production (Figure 60) were also measured to get further insight on the behaviour of LPS activated-macrophages.
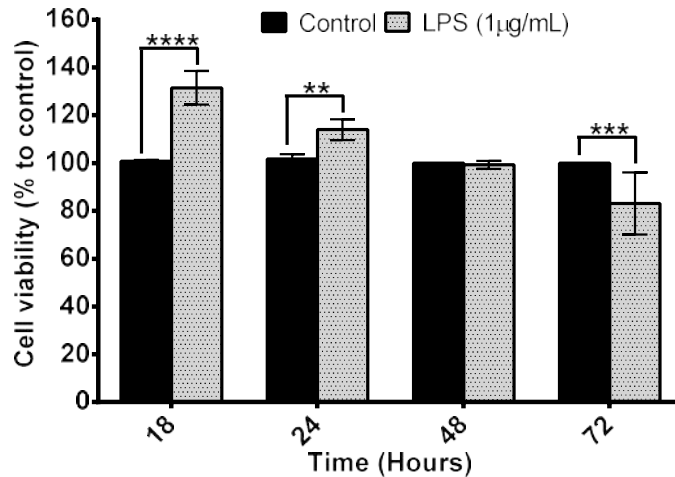
Figure 59. Cellular viability of Raw 264.7 macrophages under optimized LPS concentration (1 µg/mL) and cell density (2x10⁴ cells/well) was measured. Cells were exposed to LPS during 18, 24, 48 and 72 hours. Cellular viability was assessed by MTT assay and NO production by Griess reagent assay. In the control group cells were only treated with DMEM. Data are the mean ± standard deviation (SD) of two independent experiments (n=2).

The LPS cytotoxicity was assessed by preliminary experiment (Figure 57). Results showed that the exposure to LPS (1 µg/mL) for 48 hours did not induce a decrease on cellular viability, when compared to control (Figure 59). On the contrary, after 18 and 24 hours of LPS-exposure, an increase on cellular viability (31.5% and 14.0%, relative to control) was observed with statistical significance (p<0.001). Only after 72 hours-exposure, a decrease on cellular viability was detected, although cellular viability was still high, where ~80% of cellular viability was observed when compared to control. Moreover, cellular viability over time was confirmed by microscope evaluation (

I. Appendix, Figure 88). Regarding inflammatory cytokines production (Figure 60), results showed that a minimal baseline of NO (DMEM, <16 µM/mL) and TNF-α (DMEM, <35 pg/mL) production was observed at non-LPS stimulated macrophages. On the other hand, stimulation of Raw 264.7 cells with LPS resulted in a significant increase (p<0.05) of NO and TNF-α production, which followed a time and concentration-dependent pattern. At 18h, 24h, 48h, 72h activated cells respectively produce 18.7, 19.7, 39.8, 97.3 µM/mL of NO and 1101.2, 2618.6 2923.8, 3164.4 pg/mL of TNF-α. Particularly after 72 hours' exposure, where the LPS-activated Raw-macrophages respectively released 5 and 10^3 times more NO and TNF-α, when compared to untreated control cells.
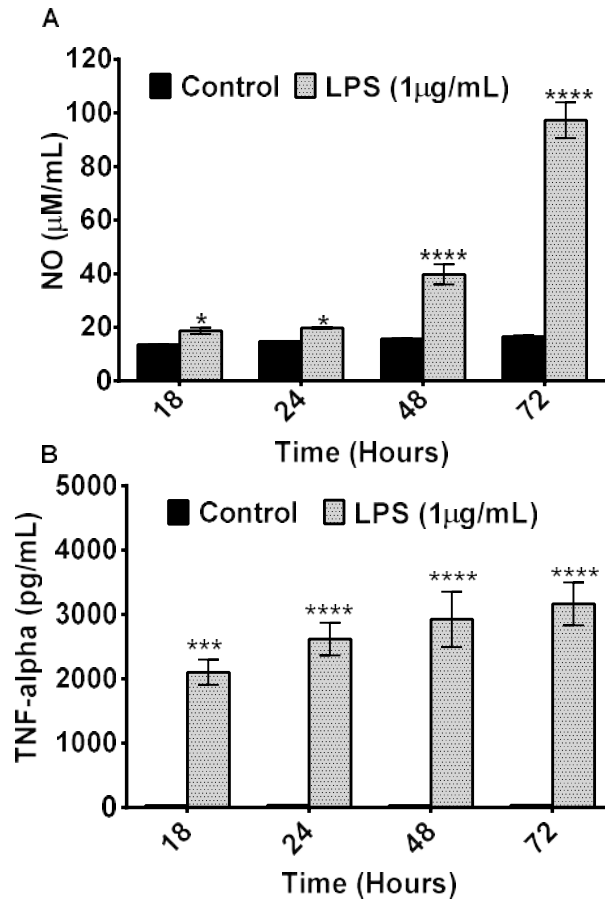
Figure 60. Nitric Oxide (A) and TNF-alpha production (B) of Raw 264.7 macrophages under optimized LPS concentration (1 µg/mL) and cell density (2x10^4 cells/well) were measured. Cells were exposed to LPS during 18, 24, 48 and 72 hours. In the control group cells were only treated with DMEM. Data are the mean ± standard deviation (SD) of two independent experiments (n=2).

3.8 Anti-inflammatory activity studies

As observed in the previous section *(3.7. LPS-activated 264.7 Raw macrophages: inflammation model)*, the LPS stimulation (1µg/mL) has shown to activate Raw 264.7 macrophages, resulting in significant changes on the shape/size of cells (Figure 58), and increased NO and TNF-α production (Figure 60) when compared to the untreated cells (control group). Accordingly, these results reflect the aptitude of LPS-activated Raw 264.7 cells to be utilized as an *in vitro* inflammation model.

In this section, the experiments described were performed to investigate the anti-inflammatory effect of DEX released from the functionalised-TiO_2 particles, obtained via different synthetic routes, amino, (Figure 40), mercapto, (Figure 41) and LbL route (Figure 42 and Figure 43). The anti-inflammatory effect was assessed by measuring both NO and TNF-α production on LPS-stimulated RAW 264.7 macrophages. In principle, the inhibition of NO and TNF-α production on LPS-activated cell will reveal the anti-inflammatory effect of the model system herein developed.

Preliminary studies were performed to investigate the effect of different concentrations (3.9-100µg/mL) of pure DEX on NO production of Raw 264.7 cells, with and without LPS (Figure 61). Although in this section, only the effect of DEX concentrations up to 20 µg/mL were shown, mainly because the cellular viability studies (*Figure 44*.B) showed that DEX concentrations higher than 20 µg/mL induced a significant ($p < 0.05$) cell death at 72 hours.

3.8.1 Preliminary studies: basal levels

Preliminary study was undertaken to investigate the effect of different pure DEX concentrations (3.9-20µg/mL) on the time course of NO production by Raw 264.7 cells, with and without LPS stimulation (Figure 61). Results showed that when cells were incubated without LPS (Figure 61.B) none of the tested concentrations of DEX (3.9-20µg/mL) induced changes in NO basal levels. In fact, the NO production (µM/mL) observed for cells without LPS activation was very similar the one observed for DMEM media alone (<20 µM/mL). On the other hand, for LPS-activated cells (Figure 61.A), results showed that all DEX concentrations tested have significantly ($p < 0.05$) reduced NO production on LPS-activated cell, when compared to (LPS) control group.
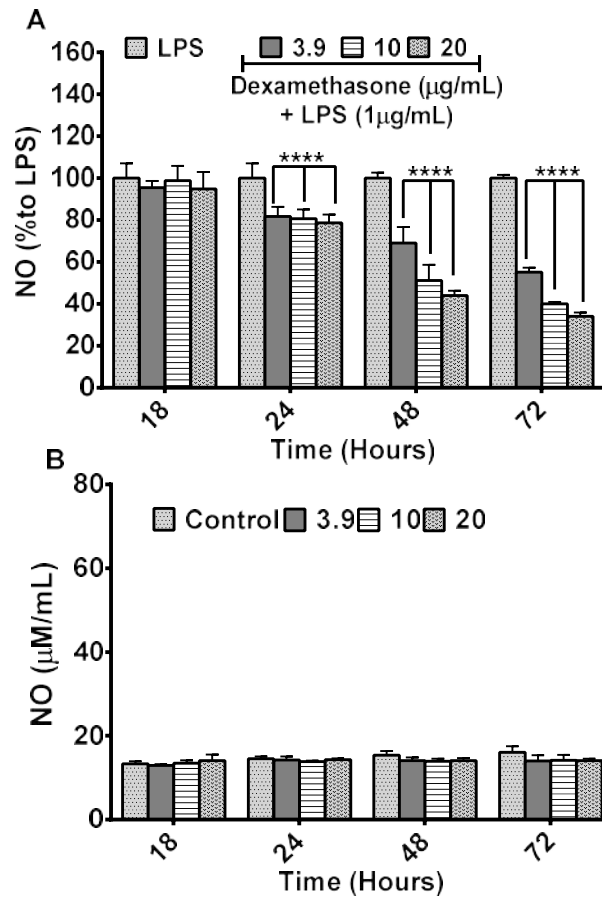
Figure 61. Effect of DEX in nitric oxide (NO) production (µM/mL, or NO% to LPS control) in RAW 264.7 macrophages with (A) and without LPS (B). Cells were exposed to range of DEX (3.9-20 µg/mL) diluted in DMEM media, during 18, 24, 48 and 72 hours. In the control group cells were only treated with DMEM. Data are the mean ± standard deviation (SD) of two independent experiments (n=2).

In general, the inhibition of NO production followed a time and concentration-dependent pattern (Figure 61.A): the highest anti-inflammatory effect (~70-75% reduction of NO production relatively to LPS control) was observed at 72h and when cells were treated with the highest DEX concentrations (10 and 20 μg/mL).

Moreover, the effect of pure DEX (3.9 and 10µg/mL) on TNF-α production of Raw 264.7 cells with and without LPS was also assessed (*Figure 62*). Results showed that when cells were incubated without LPS (*Figure 62*.B) none of the tested concentrations of DEX induced changes on TNF-α basal levels, which were very close to the ones observed for cell treated with DMEM media alone.
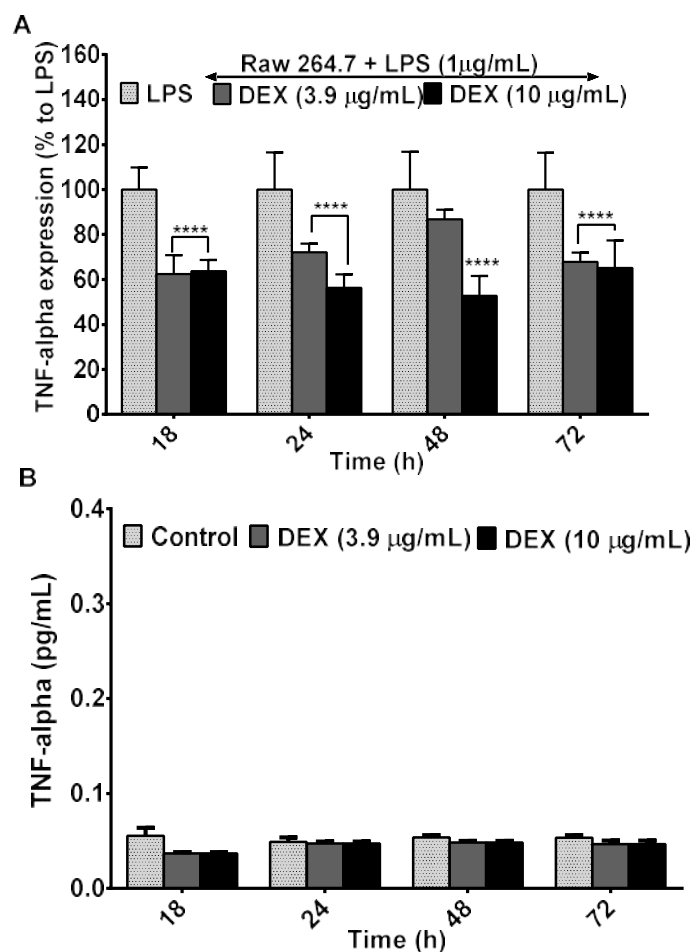
Figure 62. Effect of DEX in TNF-α production (TNF-α % to LPS control) in RAW 264.7 macrophages with (A) and without LPS (B). Cells were exposed to range of DEX (3.9 and 10 µg/mL) diluted in DMEM media, during 18, 24, 48 and 72 hours. In the control group cells were only treated with DMEM. Data are the mean ± standard deviation (SD) of two independent experiments (n=2).

For LPS-activated cells (Figure 62.A), DEX significantly (p<0.05) decreased TNF-α production, in a concentration-dependent pattern: for most of the time points (except 18h), the cells treated with the DEX concentration of 10 µg/mL showed a higher decrease (% relative to LPS) on TNF-α production (~50-45%) when compared to DEX 3.9 µg/mL (~35-25%). In addition, the effect of PBS and acetate buffers, drug release buffers (mainly component of the broths) on NO productions was also investigated in Raw 264.7 cells with and without LPS (Figure 63,Figure 64). When Raw 264.7 cells were exposed to different PBS and acetate buffer concentrations (Figure 63.B,Figure 64.B), the NO production was nearly the same for all treatments, where NO production was very similar to the one observed for control group (NO production >20 µM/mL).
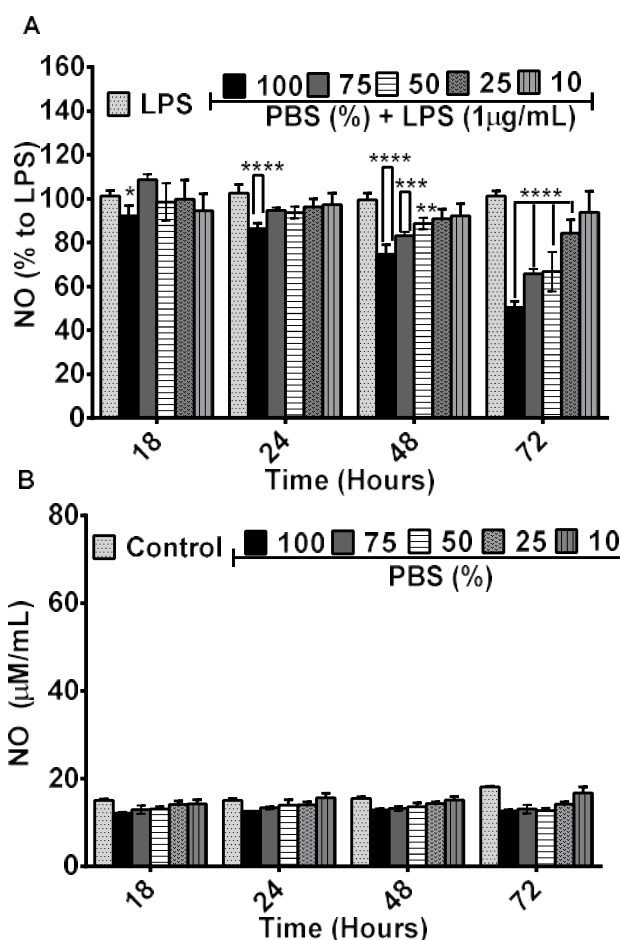
Figure 63. Effect of different concentrations of PBS, in nitric oxide (NO) production (μM/mL, or NO% to LPS control) in Raw 264.7 macrophages (A) with and (B) without LPS. Cells were exposed to range of PBS concentrations (10-100%) diluted in DMEM media, during 18, 24, 48 and 72 hours. In the control group cells were only treated with DMEM. Data are the mean ± standard deviation (SD) of two independent experiments (n=2).

On the other hand, in the LPS-activated cells (Figure 63.A, Figure 64.A) the NO production was significantly ($p<0.05$) affected by the PBS and acetate buffers concentration in a dose-dependent manner. When compared to LPS control group the cells treated with highest buffer concentrations (>25%) have shown the highest decrease of NO production, whereas the only cells treated with lowest buffer concentration (10%) showed a NO production equivalent to the LPS control group. Particularly, after 72h the higher concentration tested (100%) caused a decrease on NO production of about 50% (PBS) and 70% (acetate buffer), relative to LPS control group. Although more pronounced, in general, this decrease follows the effect caused on cellular viability (PBS,

Figure 45, and acetate buffer (I. Appendix, Figure 89), where among all concentrations tested only 10% did not cause a significant decrease (p<0.05) on cellular viability.
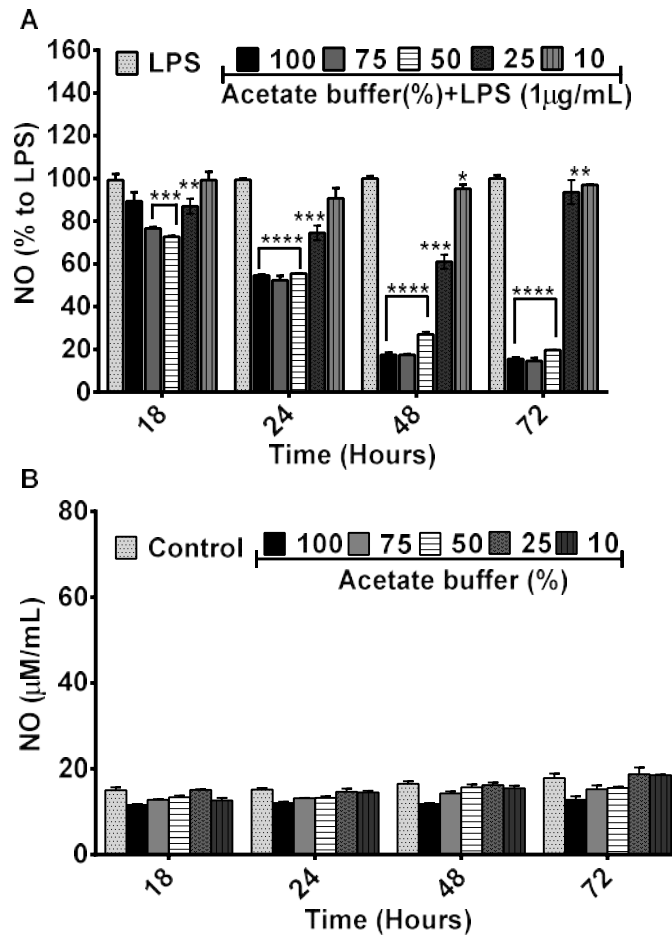
Figure 64. Effect of different concentrations of acetate buffer, in nitric oxide (NO) production (µM/mL, or NO% to LPS control) in Raw 264.7 macrophages (A) with and (B) without LPS. Cells were exposed to range of acetate buffer concentrations (10-100%) diluted in DMEM media, during 18, 24, 48 and 72 hours. In the control group cells were only treated with DMEM. Data are the mean ± standard deviation (SD) of two independent experiments (n=2).

3.8.2 Dexamethasone loaded-functionalised TiO$_2$ particles

The anti-inflammatory activity of DEX released from model system (DEX-loaded functionalised TiO$_2$ particles) obtain by different synthetic routes was assessed by comparing the anti-inflammatory activity of the eluted drug to the respective control (cells only treated with LPS). Drug release studies (3.4 DEX release profile) have shown that the synthetic route utilized to prepare DEX-loaded functionalised TiO$_2$ particles significantly affected the DEX release profile. Not only the DEX concentration released, but also the release duration have shown to differ for functionalied-TiO$_2$ particles obtained by amino/mercapto (24 hours) (Figure 40, Figure 41), and LbL route (2-3 weeks) (Figure 42 and Figure 43). For this reason, the anti-inflammatory effect of DEX released from functionalised-TiO$_2$ particles was investigated according to release profile obtained for each synthetic route, as described in materials and methods section (2.6.1 Raw 264.7 macrophages cell line, Figure 12). For instance, for amino and mercapto route, DEX was released within 24 hours, hence Raw 264.7 macrophages (with and without LPS) were only exposed to DEX released at 24h. On the other hand, for LbL route, DEX release was more prolonged (24h to ~3 weeks), and the concentrations released varied according to the number of layers surrounding DEX-loaded particles. Accordingly, the cells were exposed to DEX released at 24h, 48h, 72h and 2 weeks from LbL-functionalised particles where DEX was the outer layer (LbL 0) or where DEX was surrounded by 4 CH/DEX/ALG layers (LbL 4). The anti-inflammatory activity of DEX released from functionalised-TiO$_2$ particles, was investigated by measuring NO and TNF-α production of LPS-activated macrophages. Furthermore, considering that during inflammation, a local acidosis (pH<7) will be observed, it was decided that TNF-α production would only be assessed for DEX released at pH=6. Priority was given to this pH because it mimics the extracellular environment under inflammatory conditions. Anti-inflammatory activity of DEX released from functionalised-TiO$_2$ particles at more acidic pH values (pH<6); was also measured, although preliminary studies revealed that these treatments caused high % of cell death (>80% relative to control (

I. Appendix, Figure 77). Therefore, only results from pH=6 and pH=7 where presented in this thesis.

The anti-inflammatory activity of DEX released from functionalised-TiO$_2$ particles obtained by amino and mercapto routes was assessed.
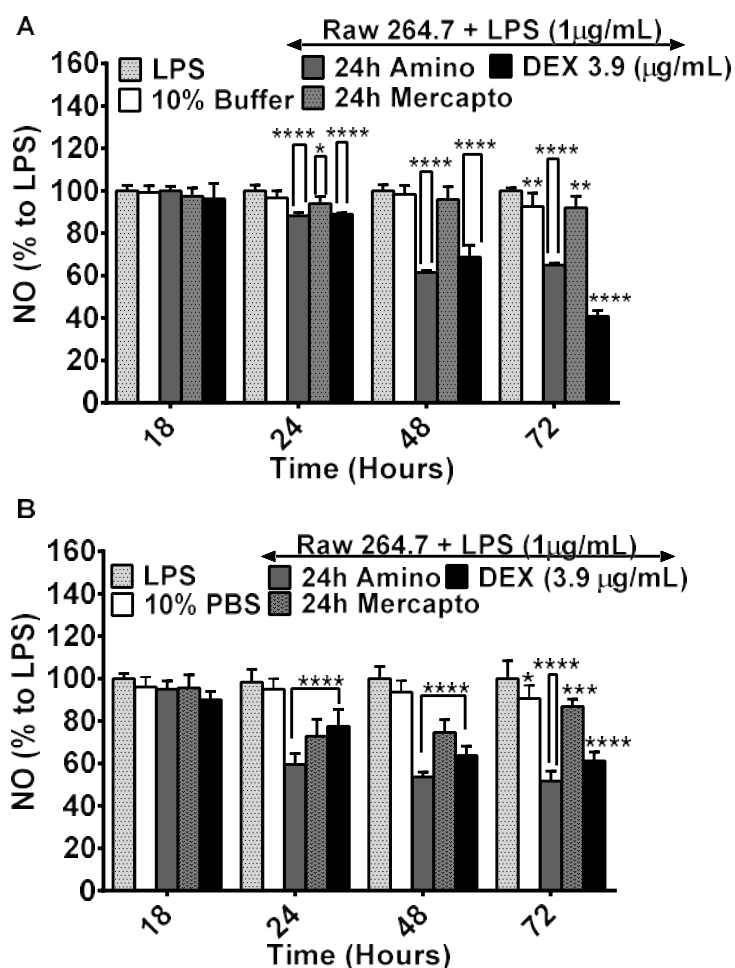
Figure 65. Effect of DEX released from functionalised-TiO$_2$ particles, obtained by amino route (24h amino) and mercapto (24h mercapto) route, *in nitric oxide (NO) production (NO% to LPS control) for LPS-activated RAW 264.7 macrophages.* Cells were exposed 24h amino and 24h mercapto collected from release studies performed at pH=6 (A) and pH=7 (B). Culture supernatants were collected at 18, 24, 48 and 72h then analysed by Griess reagent for NO. RAW 264.7 cells treated with 10% buffer and DEX (3.9 µg/mL) were utilized respectively as negative and positive controls. In the control group cells were only treated with DMEM. Data are the mean ± standard deviation (SD) of two independent experiments (n=2).

For this purpose, Raw 264.7 macrophages (with and without LPS) were exposed to DEX released from functionalised-particles obtained by amino (24h amino) and mercapto (24h mercapto) routes, and NO and TNF-α production was measured. For unstimulated Raw

264.7 macrophages (I. Appendix, Figure 91), results showed that NO production was not significant when exposed to DEX released at pH=6 and pH=7. In fact, NO production for 24h amino and 24h mercapto treatments was very similar to the one observed for control group (NO production >20 µM/mL). Simultaneously, the effect of DEX released from amino and mercapto-functionalised particles in TNF-α production of Raw 264.7 macrophages was investigated. Results showed that DEX released at pH=6 had a different effect on TNF-α production of non-stimulated Raw 264.7 macrophages. At 18h, when compared to control, an alteration on TNF-α baseline was observed for cells treated with 24h amino (I. Appendix, Figure 92). Although significant (p<0.05), this alteration in TNF-α baseline was minor when compared to TNF-α production observed for LPS-stimulated cells (~10 fold more). Simultaneous, the effect of DEX released at pH=6 and pH=7 on NO production of LPS-activated Raw 264.7 macrophages was investigated (Figure 65). With few exceptions, results showed that DEX released from both amino and mercapto-functionalised particles significantly reduced (p<0.05) the NO production (% to LPS) for most of the time points (Figure 65).
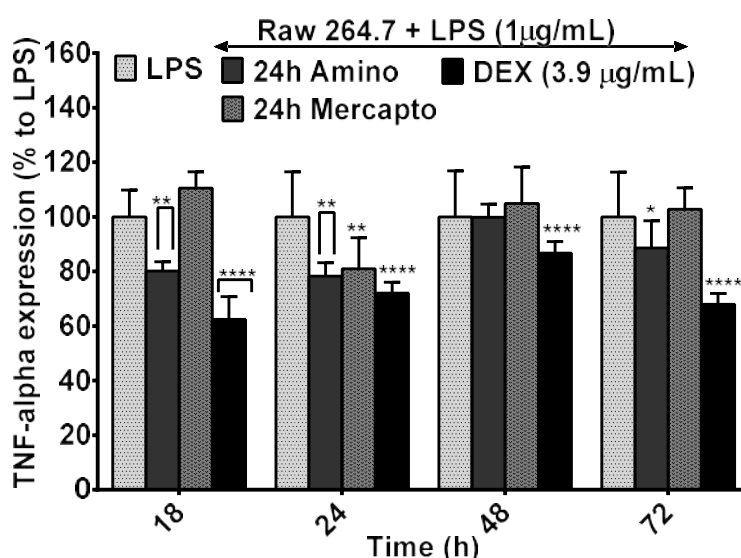
Figure 66. Effect of DEX released at 24h from functionalised-TiO₂ particles, obtained by amino route (24h amino) and mercapto route (24h mercapto), on TNF-α production (TNF-α expression %to LPS control) of LPS-activated RAW 264.7 macrophages. Cells were exposed 24h amino and 24h mercapto collected from release studies performed at pH=6. Culture supernatants were collected at 18, 24, 48 and 72h then analysed by ELISA for TNF-α. Data are the mean ± standard deviation (SD) of two independent experiments (n=2).

Overall, the decrease of NO production was affected by the extracellular environment which DEX was released (pH= 6 vs pH=7) and by the type of route utilised to synthesise DEX-loaded functionalised-TiO_2 particles (amino or mercapto).For instance, 24h amino have showed to exert a higher anti-inflammatory effect i.e. higher decrease of NO production (% to LPS) than 24h mercapto (Figure 65.A). In fact, results showed that when compared to 24h mercapto, 24h amino caused an increase of 0.5, 0.9 and 0.8-fold on NO inhibition, respectively at 24h, 48h and 72h. moreover, when comparing the effect of DEX released at pH=6 and pH=7, NO data showed that for both 24h amino and 24h mercapto, a higher anti-inflammatory effect was observed for pH=7 (Figure 65.B): for 24h amino the following decrease on NO production was observed at 24h (12%, 40%), 48h (39%, 46%) and 72h (35% and 48%), respectively for pH=6 and pH=7 studies. The same trend was observed for 24h mercapto although the differences observed between pH=6 and pH=7 studies were more evident for this treatment. In fact, at pH=6, 24h mercapto showed a minor decrease of NO production (<10% relative to LPS group) for all time points. Considering that during inflammation, a local acidosis (pH<7) will be observed, it was decided that TNF-α production would only be assessed for DEX released at pH=6 (Figure 66). Priority was given to this pH because it mimics the extracellular environment under inflammatory conditions. When comparing the anti-inflammatory effect exerted by 24h amino and 24h mercapto at pH=6, TNF-α data showed a similar inhibitory trend to that observed for NO production (Figure 65): where 24h amino treatment induced a more significant inhibition of TNF-α production than 24h mercapto. For instance, 24h mercapto only showed to significant decrease TNF-α expression at 24 hours (16% relative to LPS group). In contrast, 24h amino significantly decreased ($p<0.05$) TNF-α production at most of the time points: a decrease of 20%, 22%, and 11 (% to LPS control) was respectively observed at 18h, 24h and at 72 hours (Figure 66). Furthermore, for both NO and TNF-α production, when significant, the decrease induced by 24h amino and 24h mercapto was very closely matched the level of suppression observed for DEX (3.9 μg/mL) treatments.

The effect of DEX released from functionalised-TiO₂ particles obtained by LbL route on NO and TNF-α production was investigated. For this purpose, Raw 264.7 macrophages (with and without LPS) were exposed to DEX released from LbL functionalised-particles.
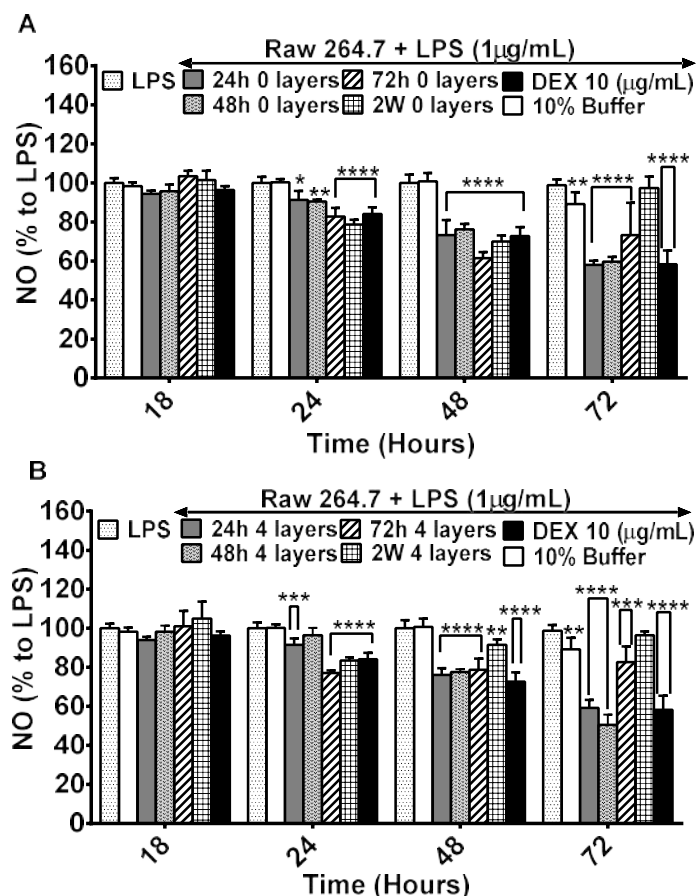
Figure 67. Effect of DEX released from functionalised-TiO₂ particles (LbL route) in nitric oxide (NO) production (NO% to LPS control) of LPS-activated RAW 264.7 macrophages. Cells were exposed to broths collected from drug release studies performed at pH=6, from particles surrounded by 0 layers (LbL 0) (A) and 4 layers (LbL 4) (B) during 18, 24, 48 and 72 hours. Broths used to treat the cells were collected at different time points to assess the effect of DEX released after 24h (24h 0 and 4 layers), 48h (48h 0 and 4 layers), 72h (72h LbL 0 and LbL 4) and 2 weeks (2W 0 and 4 layers). RAW 264.7 cells treated with 10%acetate buffer and DEX (10 μg/mL) were utilized respectively as negative and positive controls. Data are the mean ± standard deviation (SD) of two independent experiments (n=2).

When exposed to Raw 264.7 cells, results showed that DEX released at 24h, 48h, 72h and 2W collected from LbL functionalised-particles surrounded by 0 (LbL 0) or 4 (LbL 4) layers induced a NO and TNF-α production (>20 μM/mL) similar to the control group (

I. Appendix, Figure 93 and Figure 94). As for LPS-activated cells, with few exceptions, results showed that DEX released from LbL particles at all time points (24h,48h,72h and 2W), with both 0 and 4 layers, exerted an anti-inflammatory effect i.e. decreased NO and TNF-α production for most of the time points (Figure 67,Figure 68, and *Figure 69*).
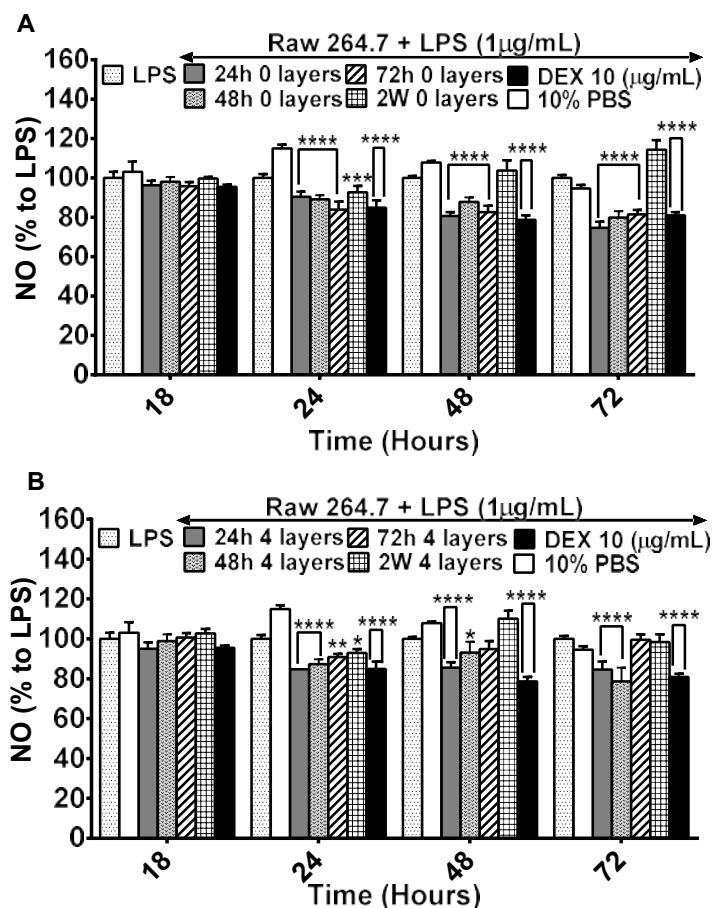
Figure 68. Effect of DEX released from functionalised-TiO₂ particles (LbL route) in nitric oxide (NO) production (NO% to LPS control) of LPS-activated RAW 264.7 macrophages. Cells were exposed to broths collected from drug release studies performed at pH=7, from particles surrounded by 0 layers (LbL 0) (A) and 4 layers (LbL 4) (B) during 18, 24, 48 and 72 hours. Broths used to treat the cells were collected at different time points to assess the effect of DEX released after 24h (24h 0 and 4 layers), 48h (48h LbL 0 and LbL 4), 72h (72h LbL 0 and LbL 4) and 2 weeks (2W 0 and 4 layers). RAW 264.7 cells treated with 10%PBS buffer and DEX (10 µg/mL) were utilized respectively as negative and positive controls. Data are the mean ± standard deviation (SD) of two independent experiments (n=2).

Although significant (p<0.05) for most of the treatments, the production of NO and TNF-α production showed different inhibitory trends depending on i) the extracellular environment which DEX was released (pH= 6 vs pH=7) (*Table 15*), ii) the number of layers surrounding DEX (0 vs 4 layers), as well as the iii) time-point at which DEX was released (24h, 48h, 72h or 2 weeks).

i)   <u>**Effect extracellular environment which DEX was released (pH=6 vs pH=7)**</u>

When the effect of the extracellular environment (i) was investigated (*Table 15*), results showed that for most of the time points, DEX released at pH=6 caused a higher decrease of NO production (% to LPS) when compared to DEX released at pH=7, being this effect more evident at 48h and 72h.

Table 15. Comparison of the effect of DEX released from functionalised-TiO$_2$ particles (LbL route), at pH=6 and pH=7, on NO decrease (%LPS control). Results were only presented for 24, 48h and 72h, because at 18h NO decrease (%LPS) was not significant (ns). Data are the mean ± standard deviation (SD) of two independent experiments (n=2).

Time point	DEX release	Ph 6	Ph 7	Comparison
	24h LbL 0	9±4.2%	10±2.3%	Similar
	48h LbL 0	10±0.9%	11±1.9%	Similar
	72h LbL 0	21±2.2%	16±3.6%	Higher at pH 6
24 hours	2 W LbL 0	17±4.1%	7±2.9%	Higher at pH 6
	24h LbL 4	9±3.1%	15±0.8%	Higher at ph 7
	48h LbL 4	4±3.5%	13±2.1%	Higher at pH 7
	72h LbL 4	23±1.2%	9±1.5%	Higher at pH 6
	2 W LbL 4	16±1.5%	7±1.7%	Higher at pH 6
Time point	**DEX release**	**Ph 6**	**Ph 7**	**Comparison**
	24h LbL 0	27±%7.0	19±1.7	Higher at pH 6
	48h LbL 0	24±%2.5	12±2.0	Higher at pH 6
	72h LbL 0	39±%2.7	17±2.8	Higher at pH 6
48 hours	2 W LbL 0	30±2.9%	ns	Higher at pH 6
	24h LbL 4	24±3.1%	14±2.4	Higher at pH 6
	48h LbL 4	23±1.4%	7±5.0	Higher at pH 6
	72h LbL 4	21±5.1%	5±3.7	Higher at pH 6
	2 W LbL 4	8±2.6%	ns	Higher at pH 6
Time point	**DEX release**	**Ph 6**	**Ph 7**	**Comparison**
	24h LbL 0	42±2.0%	25±2.8	Higher at pH 6

72 hours	**48h LbL 0**	40±2.3%	20±3.0	**Higher at pH 6**
	72h LbL 0	27±15.1%	18±2.0	**Higher at pH 6**
	2 W LbL 0	ns	ns	**ns**
	24h LbL 4	41±3.8%	15±3.7	**Higher at pH 6**
	48h LbL 4	50±4.9%	21±6.2	**Higher at pH 6**
	72h LbL 4	18±7.3%	ns	**Higher at pH 6**
	2 W LbL 4	ns	ns	**ns**

Simultaneously, TNF-α production was investigated for LPS-activated macrophages treated with DEX release at pH=6 ((Table 17 and Figure 69).

ii) Effect of number of layers surrounding DEX layer (0 vs 4 layers)

When the effect of the type of LbL-functionalised particles (0 or 4 layers surrounding DEX layer) (ii) was investigated results (Table 16) showed that DEX released from LbL 0 particles caused a higher anti-inflammatory effect when compared to DEX released from LbL 4 particles. For NO production (Table 16) this behaviour was observed for most of the treatments at 48h and 72h. As for TNF-α production (Table 17 and Figure 69) results showed the same trend i.e. higher anti-inflammatory effect for DEX released from LbL 0 particles, but mostly for 24h and 48h LbL broths (Figure 69,Table 17).

Table 16. Comparison of the effect of DEX released from LbL functionalised-particles with 0 layer (LbL 0) or 4 layers (LbL 4) on NO decrease (%LPS control) at pH=6. Results were only presented for 24, 48h and 72h because at 18h NO decrease (%LPS) was not significant (ns). Data are the mean ± standard deviation (SD) of two independent experiments (n=2).

Time point	DEX release	LbL 0	LbL 4	Comparison
24 hours	24h LbL	9±4.2%	9±3.1%	comparable
	48h LbL	10±0.9%	4±3.5%	Higher for LBL 0
	72h LbL	21±2.2%	23±1.2%	comparable
	2 W LbL	17±4.1%	16±1.5%	comparable
Time point	**DEX release**	**LbL 0**	**LbL 4**	**Comparison**
48 hours	24h LbL	27±%7.0	24±3.1%	Higher for LBL 0
	48h LbL	24±%2.5	23±1.4%	comparable
	72h LbL	39±%2.7	21±5.1%	Higher for LBL 0
	2 W LbL	30±2.9%	8±2.6%	Higher for LBL 0
Time point	**DEX release**	**LbL 0**	**LbL 4**	**Comparison**
72 hours	24h LbL	42±2.0%	41±3.8%	Higher for LBL 0
	48h LbL	40±2.3%	50±4.9%	Higher for LBL 4*
	72h LbL	27±15.1%	18±7.3%	Higher for LBL 0
	2 W LbL	ns	ns	comparable

For example, at 48h, NO data showed that a 0.11-fold increase, 0.46-fold increase and 0.73-fold increase was respectively observed when comparing the ability to inhibit NO production of 24h, 72h and 2W broths from LbL 0 over the one observed for LbL 4 particles (*Table 16*).
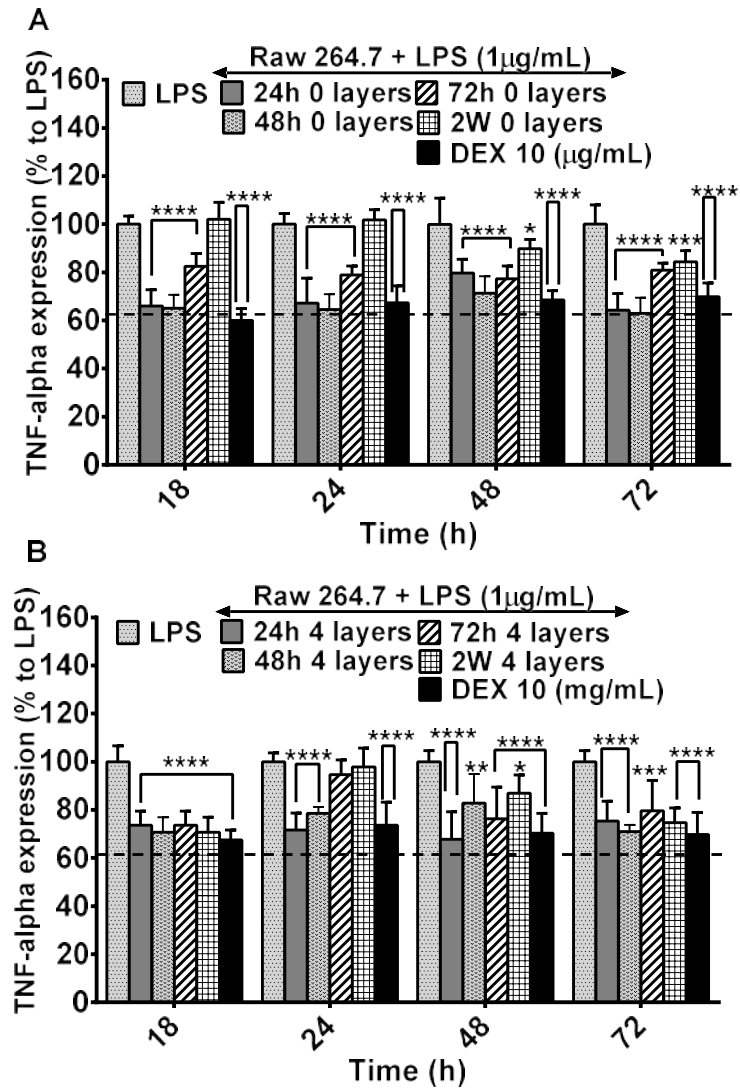
Figure 69. **The effect of DEX released from functionalised-TiO₂ particles (LbL route) on TNF-α production (TNF-α expression %to LPS control). LPS-activated RAW 264.7 macrophages were exposed to DEX released at pH=6 from LbL-*particles surrounded by (A) 0 layers (LbL 0) and (B) 4 layers (LbL 4)* during 18, 24, 48 and 72 hours. Broths used to treat the cells were collected at different time points to assess the effect of *DEX released after 24h (24h LbL 0 and LbL 4), 48h (48h LbL 0 and LbL 4), 72h (72h LbL 0 and LbL 4) and 2 weeks (2W LbL 0 and LbL 4)*. Culture supernatants were collected at 18, 24, 48 and 72h then analysed by ELISA for TNF-α. RAW 264.7 cells treated DEX (10 µg/mL) were utilized as positive control for anti-inflammatory effect/TNF-α inhibition. Data are the mean ± standard deviation (SD) of two independent experiments (n=2).**

Similarly, at 72h a 0.14-fold increase, 0.46-fold increase, 0.73-fold increase on the anti-inflammatory effect was respectively observed when comparing 24h, 72h and 2W broths collected from LbL 0 over the ones collected from LbL 4 particles. Likewise, TNF-α data showed the same trend but mostly for 24h and 48h LbL broths (*Figure 69*,*Table 17*), at 18h, 24h and 72h.As can be seen in Table 17, at 18h a decrease of 34% and 35% was observed for 24h and 48h LBL 0, whereas a decrease of 26% and 29% was respectively observed for 24h and 48h LBL 4 treatments. At 24h a decrease of 33% and 35% was observed for 24h and 48h LBL 0, whereas a decrease of 28% and 21% was respectively observed for 24h and 48h LBL 4 treatments.

Table 17. Comparison of the **effect of DEX released from LbL functionalised-particles with 0 layer (LbL 0) or 4 layers (LbL 4)** *on TNF-α decrease (%LPS control) at pH=6 for 18h, 24h, 48h and 72h.* **Data are the mean ± standard deviation (SD) of two independent experiments (n=2).**

Time point	DEX release	LbL 0	LbL 4	Comparison
18 hours	**24h LbL**	34±6.1%	26±5.3%	Higher for LBL 0
	48h LbL	35±5.0%	29±5.7%	Higher for LBL 0
	72h LbL	17±4.7%	26±5.3%	Higher for LBL 4
	2 W LbL	ns	39±5.7%	Higher for LBL 4
Time point	**DEX release**	**LbL 0**	**LbL 4**	**Comparison**
24 hours	**24h LbL**	33±9.4%	28±6.3%	Higher for LBL 0
	48h LbL	35±5.8%	21±2.3%	Higher for LBL 0
	72h LbL	21±3.4%	ns	Higher for LBL 0
	2 W LbL	ns	ns	ns
Time point	**DEX release**	**LbL 0**	**LbL 4**	**Comparison**
48 hours	**24h LbL**	20±5.2%	30±10.9%	Higher for LBL 4
	48h LbL	29±6.4%	17±11%?	Higher for LBL 0
	72h LbL	23±4.9%	24±12.0%	comparable
	2 W LbL	10±3.5%	13±6.9%	comparable
Time point	**DEX release**	**LbL 0**	**LbL 4**	**Comparison**
72 hours	**24h LbL**	36±6.4%	25±7.5%	Higher for LBL 0
	48h LbL	37±6.0%	29±2.6%	Higher for LBL 0
	72h LbL	19±2.5%	20±11.5%	Comparable
	2 W LbL	16±4.3%	25±5.5%	Higher for LBL 4*

Likewise, at 72h a decrease of 36% and 37% was observed for 24h and 48h LBL 0, whereas a decrease of 25% and 29% was respectively observed for 24h and 48h LBL 4 treatments. When comparing the anti-inflammatory effect of LbL 0 and LbL 4, for DEX released at 72h and 2W, a different inhibitory trend was observed for TNF- α production. Accordingly, for most of the time points results showed that the differences between DEX released from LbL 0 and LbL 4 particles were not so evident for 72h and 2W as the ones observed for DEX released at 24h and 48h. In fact, for DEX released at 72h and 2W a similar or non-significant decrease of TNF-α production was observed at 24h, 48h and 72h when comparing DEX released from LbL 0 and LbL 4. This is line with the drug release profile, where DEX released from LbL 0 or LbL 4 was almost identical for at 72h and 2W. Besides, for both NO and TNF-α production, when significant, the decrease induced by DEX released from LbL functionalised-particles was very closely matched the level of suppression observed for DEX (10 μg/mL) treatments

4. Discussion

4.1 DEX-loaded TiO$_2$ particles characterization

4.1.1 Average size and morphology

Overall, images obtained via transmission electron microscopy (TEM), revealed that for all synthetic routes tested (amino, mercapto and LbL), DEX-loaded functionalised TiO$_2$ particles maintained a spherical like-shape, which is characteristic from TiO$_2$ particles (Gao et al. 2004, Gouda 2012, Zhao et al. 2014). These results were also confirmed by SEM images, where no visible aggregation was detected.

Wang colleagues (2015) showed similar results during surface modification of porous TiO$_2$ particles where no significant morphological changes were observed after loading with folic acid and polyethylenimine (Wang et al. 2015a).

Furthermore, for amino and mercapto routes, TEM images showed an average size of 32nm for bare TiO$_2$ particles, and 32-45nm for functionalised ones. This increase in size could be attributed to DEX loading and surface functionalisation of TiO$_2$ particles. An increase of size after drug loading and surface functionalised of TiO$_2$-particles was previously reported by (Almalki et al. 2017) after functionalisation of TiO$_2$ particles with Polyethylene Glycol and Pentetic acid.

For LbL route, average size of 32nm was observed for amino-functionalised-TiO$_2$ particles, and 32-49 nm for LbL coated ones. Though this increase observed for LbL-coated particles size was not constant/gradual, since the particles with more layers (~39nm for ALG-DEX-CH-DEX-CH-ALG) showed a smaller average size than that of particles with less layers (~48nm CH-ALG). In other words, although new layers are added the average size did not show the expected significant increase, or if there is an increase it might be so small that TEM was not sensitive enough to detect it.

Altogether these results, lack of significant (p<0.05) morphological changes after TiO$_2$ particles functionalisation and increase of size after DEX loading, suggest the efficacy of synthetic routes applied to load DEX into TiO$_2$- particles, without damaging the particles structure

4.1.2 Zeta potential measurements

Amino and Mercapto route

The functionalization of particles surface is known for modifying the surface charge and the thickness of the double layer, therefore resulting in an alteration of the zeta potential (Z. Chen, Hsu, Battigelli, & Chang, 2006). In this context, zeta potential measurements are a key tool to characterize the functionalized TiO$_2$ particles, as it was observed for previous studies, that have utilized zeta potential measurements to assess the surface

functionalization of different particles (Y. Wang, Li, & Kong, 2013). Moreover surface properties are considered to affect the biological reactions around the titanium implants (Cai, *et al*., 2006), hence the zeta potential measurement of DEX-loaded particles obtained could be used to determine the potential biological behaviour (e.g. stability, cell affinity) of the model drug delivery system developed in future *in vitro* cell studies. Our results showed that an inverse correlation was observed between zeta potential of functionalized TiO_2- particles and pH for both mercapto (Figure 30) and amino route (Figure 22). These results can be explained based on the effect of the pH on the surface charge exhibited by the particles; particularly the influence of pH on the balance between protonated and unprotonated groups (Perni et al. 2018) present on the surface of TiO_2 particles. The pH dependence of the functionalised-TiO_2 particles (Figure 5) are consistent with that previous studies regarding TiO_2 functionalization (Cai *et al*., 2006), providing further confirmation of the presence of either the desired groups or DEX on the surface of the particles. For example, the positive surface charge observed after amino-functionalization of TiO_2 particles can be related to the amino groups (-NH_2) capability of accepting protons, becoming more positively charged i.e. NH_3^+ species (Z. Chen, *et al*., 2006). The decrease of surface charge (+20mV) observed under more alkaline conditions (pH>6), can be attributed to the deprotonation of the nitrogen groups, while at low pH these groups are highly protonated and thus a higher surface charge was observed (+40mV). In contrast, when compared to amino-functionalised TiO_2 particles lowest surface potentials were observed for TiO_2 particles-functionalised with succinic anhydride and pentanoic-acid, particularly for more alkaline pH values. A possible explanation for this character could be attributed to presence of carboxylic acid (–COOH) groups on surface of the particles, which exhibit a more negative character than NH_2- and SH-TiO_2 particles. Similar result was reported by Bergman *et al*., upon succinylation of amino-functionalized particles (Bergman *et al*., 2008). The same behavior i.e. more negative surface potential was observed after DEX loading, for both mercapto (Figure 30) and amino route (Figure 22). The higher negative zeta potential observed can be attributed to the presence of functional groups (-OH and -C=O) of DEX, suggesting the presence of the drug on the surface of the TiO_2 particles. Particularly, the fluorine group (9-Fluoro) has been described to affect the electron density of its "neighbors" i.e. functional groups (Yamazaki, Taguchi, & Ojima, 2009; Zahr, de Villiers, & Pishko, 2005). Therefore, in this specific case, the fluorine seems to be responsible for decreasing the pK_a value of hydroxyl moiety (11, 17, 21-trihydroxy) on DEX, thus resulting in a more negative zeta potential after DEX loading. Fratoddi and co-workers reported a similar result., where a negative zeta potential was observed after loading particles with DEX under alkaline conditions i.e. aqueous particles suspension (Fratoddi *et al*., 2012).

Moreover, a higher negative charge on the surface of conjugated Dex-loaded functionalised-TiO$_2$ particles was observed when compared to that of adsorbed ones, suggesting a higher loading of DEX. This result could indicate that EDC/Sulfo-NHS crosslinking agent utilized to conjugate DEX into functionalized TiO$_2$ particles have improved the reaction efficiency and consequently increased the DEX loading. This behavior can be explained based on the type of bond present between DEX and TiO$_2$ particles: regarding adsorbed particles the DEX is attached via Van der walls forces, which is a weaker and less stable bond than the covalent bond observed in conjugated particles. Therefore, the more stable bond present in conjugated-particles can easily result in higher amount of DEX on particles surface and consequently a more negative surface charge. Regarding LbL route the zeta potential measurements of the approaches tested (experiment 1,2, and 3) oscillate between 30 and 40 mV after CH adsorption, and around −20 to −30 mV after ALG adsorption (Figure 34,Figure 35). Typically, the surface charge density of polyelectrolytes, positive or negative, is respectively induced by the ionization of functional groups such as amine groups (CH) and carboxyl (ALG) (Lawrie et al. 2007). As for the constant alternated switching this is an indicative of the successful self-assembly of the polyelectrolytes CH and ALG (Caruso, et al., 1998; Wang, et al., 2008; Zhao, Mao, et al., 2006) on surface of amino-functionalised particles. These results are in line with Ye et al (2005) study that reported similar zeta potential values for the same CHI/ALG pair and template. Once more, the alternation of zeta potential after each new adsorption was not surprising, considering that this phenomenon is characteristic of the LbL assembly (Caruso, 2000; Suflet, et al., 2011). Additionally, it can be observed that after DEX layer deposition (anionic polyelectrolyte), the surface charge of particles is still positive. This lack of symmetric inversion in in zeta potential could be attributed to an incomplete coverage by DEX of the surface of particles. Indeed, previous studies reported the deposition of bioactive compounds without obtaining oppositely charged zeta potential values (Borkovec & Papastavrou, 2008, Hierrezuelo, et al., 2010). Moreover, for all graphs (Figure 34, Figure 35), it can be observed a typical zig−zag dependence, which is another evidence for the formation of consecutive layers and stability of the obtained multi-layered particles (Bazylińska, Skrzela, et al., 2012). Despite the lack of reversal in zeta potential signal, the value obtained after DEX addition was more negative when compared to the chitosan layers (+ 30-40 mV). Typically, this fact indicates that an electrostatic complex had been formed (Anal, et al., 2008), although with incomplete coverage of the particle surface. Therefore, it is possible to hint that the DEX layer was adsorbed, however it was not capable of forming layers dense enough to cover the charges from the preceding CH layer. This result is in line with that of Zhou et al. (2010) that reported a limited electrostatic interaction between bovine serum albumin

(BSA) and CH/ALG polyelectrolyte multilayers when CH was the outmost layer (Zhou, et al., 2010).

4.1.3. Thermogravimetric analysis (TGA)

Thermogravimetric analysis (TGA) was used to assess the presence or absence of organic components in the surface of TiO_2 particles, based on the observation of mass loss. Accordingly, a useful tool to confirm the attachment of organic functional groups (e.g. thiol, amine and carboxyl) or layers to TiO_2 particles surface, including the DEX loading. The thermogram of bare TiO_2 particles shows slight weight loss (<1.5%) suggesting a decreased presence of organic material on their surface, (Figure 25 and Figure 33). Moreover, it can be noted that TGA profile obtained was similar and in agreement to the one obtained by Batch el al group (Bach, *et al*., 2012). Bearing in mind that weigh loss in the second region (>200ºC) is primarily due to combustion of the organic matter, i.e., amine-silane or mercapto-silane, overall the TGA profiles obtained for DEX-loaded TiO_2 particles prepared by amino and mercapto routes, suggest the successful functionalisation of TiO_2 particles. As can be seen in the TGA profile of particles obtained via amino (Figure 25) and mercapto route (Figure 33) an increase of organic material (%) of approximately 3.1% and of 2.6% was respectively observed after APTES and MPTS-functionalization, thus confirming the successful attachment of amino and mercapto functional groups on the surface of TiO_2 particles. Moreover, being the molar mass of amine-silane, 209 g/mol, and mercapto-silane, 185 g/mol, it can be said that higher increase of organic material in NH_2-TiO_2 particles when compared to SH-TiO_2 particles is primarily the result of better functionalization by amine-silane than by mercapto-silane. Similar result was observed by Marjanovic and co-workers (2013), where FT–IR and TGA results showed a more effective functionalization of thermo-acid activated sepiolite by amine-silane than by mercapto-silane (Marjanovic et al. 2013).

Regarding DEX loading, conjugated particles presented a higher % of organic content on their surface when compared to adsorbed ones (Table 6, Table 8), particularly for the amino route where conjugated particles have 2% more of organic content on their surface when compared adsorbed ones. These results agree with zeta potential measurement.

When the LbL route was utilized, an increase of organic content (%) was observed after the addition of new layers (Figure 36, Figure 37). Although, since LbL route was being optimized i.e. number and type of layers, only for experiment 2 (Figure 37,Table 11), a gradual increase of organic content (%) after addition of each new layer was observed. Moreover, results showed that for approach utilized in experiment 2, particularly the increase of organic content (%) observed after each DEX layer deposition, together with

zeta potential measurements (i.e. high surface charge values after each layer deposition), strongly suggests that this approach could be the most suitable to obtain reproducible and stable LbL-DEX loaded particles. Therefore, the subsequent studies (e.g. drug release profile and biological studies) was assessed with LbL particles prepared by approach described in experiment 2.

4.1.4. Fourier Transformed infrared spectroscopy (FT-IR)

FT-IR spectroscopy has been used in previous studies to investigate the chemical groups present in a sample after surface modification. Therefore, in this study FT-IR was used to assess the chemical groups present on the surface of TiO_2 particles after each functionalization step. For amino and mercapto routes, results showed all particles showed similar peaks between 400 and 700 cm^{-1} (

I. Appendix, Figure 101,) which are characteristic of the model surface used in this study: the TiO_2 particles (Bagheri et al. 2013, Zhao et al. 2012). Apart from that, when analysing the spectrum of functionalised-TiO_2 particles new bands appeared, which could not be observed in the spectrum of bare-TiO_2 particles. For example, only for amino, mercapto and carboxyl functionalised TiO_2-particles (Figure 24), a new peak is observed at ~950cm^{-1} which is characteristic of Si-O chemical bonds (Chen & Yakovlev 2010). This reconfirms condensation reaction between methoxy groups of APTS/MPTS and the TiO_2 surface hydroxyl groups (OH). Since the residual (non-reacted) and physisorbed APTS has been removed by centrifugation in ethanol (toluene) solution, the mentioned peaks show that grafting of APTS on the TiO_2 particles has occurred successfully. Also, the broad band appearing at 3100–3600 cm^{-1} which is assigned to vibrations of hydroxyl groups (OH) on TiO_2 surface is less visible for particles functionalised with APTS/MPTS, which coincides with a decrease of hydroxyl groups due to the attachment of the amino/thiol functional groups on surface of TiO_2 particles (Sousa et al., 2012). As previously described in other studies (Cheng et al. 2006, Sabzi et al. 2009) the hydroxyl groups on the surface of the TiO_2 particles (Ti-OH) are reactive sites for the reaction with functional groups of silane (i.e. APTES and MPTES) compounds. As shown by the peaks around 1100 cm^{-1} which are characteristic from O-Si vibration. Particularly after APTS-functionalisation, new peaks can be observed at ~3000 cm^{-1}, ~1800 cm^{-1} and ~1360 cm^{-1}, which can be assigned to N-H and C-N bonds as reported in previous studies related to surface functionalisation with amino silane agents (Díez-Pascual & Díez-Vicente 2014, Lu et al. 2007, Wang et al. 2011, Zhao et al. 2012). For example, similar spectrum was observed by Sousa et al (2012) following functionalization of the silica nanotubes with APTES (Sousa et al. 2012). Likewise, similar peaks were reported by Bloemen and co-workers when investigating amino-functionalisation of iron oxide particles (Bloemen

et al. 2012). On the other hand, peaks/bands corresponding to thiol (SH) group could not be clearly observed (Figure 32) for particles functionalised with mercapto-silane (MPTES). This could be explained based on relative low content of thiol and poor sensitivity of IR to this functional group, as previous observed by Zhang and co-workers (Zhang et al. 2013). However the presence of bands at ~3000 and 2857 cm^{-1} which can be respectively assigned to the methyl (C–H vibration) of methoxy (OCH$_3$) and methylene (CH$_2$) groups (Marjanovic et al. 2013, Ukaji et al. 2007, Wang et al. 2011) were obvious, suggesting the new functional groups were successfully attached to the surface of TiO$_2$ particles (Marjanovic et al. 2013, Rostamian et al. 2011, Ukaji et al. 2007, Wang et al. 2011).

Regarding the FT-IR spectrum of functionalised-TiO$_2$ particles with succinic anhydride, new visible peaks which can be assigned to the carboxyl group where observed for amino route. For example, the presence of two new strong peaks between 1600-1800 cm^{-1}, which are characteristic of C=O stretching of carbonyl groups as reported in previous studies (Lee et al. 2006, Othman et al. 2012, Ramanathan et al. 2005, Siyamak et al. 2012). Likewise, when modifying TiO$_2$ particles with polyacrylic acid (PAA), Othman and co-workers (2012) observed similar peaks around 1690 cm^{-1} (Othman, et al. 2012), which provided evidence to prove that carboxyl acid (-COOH) group was present on the surface of the TiO$_2$ particles (Othman et al. 2012).Also, it worth to note that the peak at ~1360 cm^{-1} (C-N bond,(Wang et al. 2011) which was observed in spectra of amino-functionalised TiO$_2$ particles was absent for carboxyl-functionalised TiO$_2$ particles suggesting the successful surface modification of amine functionalised-TiO2 particles with carboxylic-acid (COOH). Furthermore, the two sharp peaks observed in the region of 1050-1160 cm^{-1} and 1185- 1277cm^{-1} for both carboxyl and DEX-loaded functionalised particles can be attributed to the symmetrical and asymmetrical stretching frequencies of the C-O ester groups.

These peaks were not as clear in the spectrum of functionalised particles obtained by mercapto route. As for DEX functionalisation, the FT-IR equipment was not sensitive enough to detect the characteristic peaks/bands (as observed in pure DEX, Figure 103), it was clear that different spectrum was observed for DEX-loaded particles. Such as the presence of strong band around 3100–3600 cm^{-1} which coincides with the increased presence the hydroxyl groups (O–H) due to the attachment of COOH functional and OH groups on surface of functionalised-TiO$_2$ particles. Also, for particles obtained by amino route, new band observed at ~1600-1800 cm^{-1}, respectively suggests the presence of C=O stretching of ester groups and of hydroxyl groups (OH) on TiO$_2$ surface. Similar peaks were observed by other studies, when analyzing the surface of DEX-loaded PLGA coatings (Zhang et al. 2015) and DEX-loaded onto layered double hydroxides (LDHs)

(Wang et al. 2015b). Furthermore, again for functionalised particles obtained by amino route, the two sharp peaks observed in the region of 1050-1160 cm^{-1} and 1185- 1277cm^{-1} for both carboxyl and DEX-loaded functionalised particles can be attributed to the symmetrical and asymmetrical stretching frequencies of the C-O ester groups, respectively, as previously reported (Everaerts et al. 2008). Therefore, the peaks at ~1075 and at ~1200 cm^{-1} that appear in the FT-IR spectrum of carboxyl and DEX-loaded TiO$_2$ particles clearly suggest the presence of either the desired groups (i.e. carboxyl, hydroxyl) or the DEX on the surface of functionalised TiO$_2$ particles.

As for DEX-loaded functionalised TiO$_2$ particles obtained by LbL route, FTIR results (Figure 38) showed that most of the peaks found in the spectra CH/ALG multilayer DEX-loaded functionalised TiO$_2$ particles after the addition of CH, ALG and DEX layers were very similar. Except for the band at ~1350 cm^{-1} which can be assigned to the C-N bond and was observed for amino functionalised particle, that was absent on the spectra of DEX-loaded CH/ALG functionalised-TiO$_2$ particles (Figure 38). Also, some new peaks were also observed when comparing the spectra of amino functionalised TiO$_2$ particles with the one of CH/ALG multilayer DEX-loaded functionalised TiO$_2$ particles; such as the strong peak observed at ~1650 cm^{-1} which belongs to the carbonyl group (C-O) stretching groups which are attributed to ALG and CH saccharide structure. Overall, these peaks match with the ones observed at spectrum of CH and ALG powders (Figure 104, Figure 105), and were in agreement with the ones reported for previous studies involving deposition of CH/ALG (Fernandes et al. 2011, Kulig et al. 2016, Lawrie et al. 2007, Li et al. 2008, MA Shafie, Attia Shafie 2013) onto drug-loaded particles.

The low sensitivity of FTIR to detect the addition of new layers (particularly DEX layer) could be explained based on their thickness. As shown by TEM results (Figure 39), after the addition of each new layer there is a minimal increase on the size (<10nm). of functionalised-TiO$_2$ particles, thus meaning that CH, ALG and DEX layers must be very thin (<10nm). This in agreement with previous studies (Morent et al. 2008) which have demonstrated the low sensitivity of FTIR to characterize surface modifications at nanometer level. A possible solution could be the utilization of a more surface sensitive technique such as X-ray photoelectron spectroscopy (XPS).

4.1.5. Drug loading (%) and encapsulation efficiency (%)

The drug loading (%) and encapsulation efficiency (%) were different when DEX was conjugated to functionalised-TiO$_2$ particles by electrostatic interaction (LbL route) or by covalent bonding (amino and mercapto routes). When assessing encapsulation efficiency, the DEX-loaded functionalised TiO$_2$-particles obtained by amino and mercapto (~68%) showed higher values than the ones observed for LbL route (~50%). Although the encapsulation efficiencies were higher for amino and mercapto routes, the total amount of DEX (mg) loaded per functionalised-particles (mg) was significantly higher for LbL route, as showed by drug loading calculations: ~40% (LbL route) and ~13% (amino/mercapto routes).

Moreover, for LbL route the number of CH/ALG layers surrounding DEX loaded-functionalised-TiO$_2$ particles has showed to significantly ($p < 0.05$) affect the drug content and encapsulation efficiency. Consequently, results (Table 13) showed that for sample 4 (DEX was surrounded by 4 CH/DEX/ALG layers), both encapsulation efficiency and drug loading were higher than for sample 0 (DEX was the outer layer). This difference was more evident for drug loading calculations (%), where an 0.37-fold increase of drug loading was observed for sample. This can be explained based on the number of DEX layers which are present in each sample: for sample 4 two layers of DEX were loaded into 250 mg of NH$_2$-functionalised particles whilst only one layer was loaded for sample 0. Therefore, a higher concentration of total DEX (~101mg) was loaded into the LbL particles sample 4, when compared to particles loaded with only one DEX layer (~67mg) (sample 0) onto 250mg of LbL-functionalised TiO$_2$ particles.

4.2. DEX release profile

The local delivery of glucocorticoids such as DEX, instead of systemic delivery, could be highly suitable for patients which undergo TJR surgery. Among others, the safe and effective deliver of the drug to the desired site of action by using drug-eluting implants would control the patient drug exposure over time, avoid the drug premature elimination, support the crossing of biological barriers, and minimize the side-effects caused by anti-inflammatory drug exposure elsewhere in the body (Lyndon et al. 2014, Zilberman et al. 2010). Also, and in terms of outcome for the patient, a post-operative dose of DEX would reduce the stress response and improve pain relief following surgery by modulating the acute phase response following hip and knee replacement (Allen et al. 2010, Backes et al. 2013, Salerno & Hermann 2006). Even though they have shown exceptional capabilities in terms of applicability and versatility, regarding orthopaedic field, most of the anti-inflammatory drug-eluting implants are still in early developing stages. Being one of the biggest challenges related to the drug release profile, critical parameters such as release time and rate, as well as dosage for optimal therapeutic concentration (Santos et al. 2014) are still being optimized. Due to this need, in our study we have investigated a novel anti-inflammatory drug-eluting implant model system: functionalised-TiO_2 particles loaded with DEX, prepared by different synthetic routes. This way we could assess the effect of linker between DEX and functionalised-TiO_2 particles on drug release kinetics e.g. release duration, rate, and concentration.

Based on previous studies (Bhardwaj et al. 2007, Urbanska et al. 2014, Wang et al. 2015b), we can assume that the DEX release profile will mainly depend on the structure and hydrolysis rate of the linker between DEX and functionalised-TiO_2 particles, which are strongly affected by the type of route i.e. amino, mercapto or LbL utilized on this study, and by the pH conditions of surrounding environment. Aiming to assess the effect of different environments, different pH buffers were employed to study the release of DEX from the functionalised-TiO_2 particles. PBS and acetate buffer were chosen to respectively mimic two distinct situations: physiological healthy conditions (pH~7.0), and inflammation represented by acid conditions (pH~6).

Overall, the release profiles obtained in this work present a good reproducibility, as shown by the relatively small deviations (5% total drug released) in independent experiments. Results from drug release studies have shown that release of DEX was in fact affected by type of synthetic route utilized to obtain functionalized-TiO_2 particles, as well as pH of the release environment/media (Figure 40, Figure 41). For instance, for amino and mercapto routes where DEX was covalently bounded to carboxyl-functionalised particles, drug was released within 24 hours. Furthermore, the highest concentrations of DEX were released under physiological conditions i.e. at pH=7 for both

amino (13.08 ±0.17 μg/mL) and mercapto (7.54±0.08 μg/mL) routes. This release profile can be explained based on the assumption that DEX is being released from functionalised-TiO_2 particles in a manner consistent with ester bond hydrolysis, increased degradation is observed when the pH increases, thus leading to the higher release of DEX at physiological pH than that at more acidic conditions. A similar drug release profile was observed by Nuttelman and co-workers (Nuttelman et al. 2006), when DEX was covalently attached to polyethylene glycol (PEG)-based hydrogel scaffold. In addition, results showed that independently of the pH conditions, it was evident that higher concentration of DEX was released when amino route was applied. When comparing DEX concentration released from amino-functionalised particles with that of mercapto-functionalised-particles, a ~3.5-fold and a ~1.85-fold increase was observed respectively at pH=6 and pH=7. This drug release profile is in agreement with TGA analysis which reveals that a higher % of organic content is observed after DEX attachment to amino-functionalised TiO_2 particles (6.37±0.83, Table 6) when compared to the ones obtained via mercapto route (4.79±0.37,Table 8). In this sense, since particles obtained via amino route have higher amount of DEX attached than the ones obtained via mercapto route, it makes sense that the concentration of drug released would be higher.

As for LbL route (experiment 2), DEX was attached to (amino)-functionalised TiO_2 particles, with subsequent deposition of CH and ALG layers, interactions between layers are mainly electrostatic. The most attractive feature of LbL technique is the possibility of obtaining a tuneable drug release (Wood et al. 2005) and consequent controlled host response (Macdonald et al. 2011), which ameliorates both the medical and financial burden of complications from implantation As for the polyelectrolytes pair, the advantages of CH and ALG have been previously highlighted in studies involving LbL coating of biomedical devices, including drug delivery (Hammond 2012, Tang et al. 2006). Besides being non-toxic and biocompatible polymers CH/ALG multilayers have a superior advantage of protecting DEX layer and proving a more controlled release (De Villiers et al. 2012, Rivera et al. 2015). Moreover, it is a convenient alternative for the commonly described biodegradable pair of polymers PLGA and PLA, since it does not involve the utilization of organic solvents and associated toxicological effects (Caetano et al. 2016). Nonetheless, no study of LbL assembly CH/ALG on functionalised TiO_2-particles with DEX as drug model has been reported. The drug release studies showed that DEX was released from functionalised-TiO_2 particles in a more controlled and prolonged manner (20 days release), when compared to that observed for mercapto and amino routes (24 hours). Consequently, allowing the possibility of obtaining a more prolonged and controlled release of DEX. These results are in line with previous studies

(Han et al. 2016, Jayant et al. 2009) that have demonstrated the efficacy of LbL coating in reducing the initial burst release, as well as prolonging the period of drug release (Buriuli & Verma 2017). Mainly because with LbL coating, the composition and number of layers surrounding the drug can be precisely tuned, hence allowing to modulate the release profile of drugs (Ariga et al. 2011, De Villiers et al. 2012, Wood et al. 2005). Moreover, the duration of DEX release from LbL-functionalised particles was higher than the one observed for other drug delivery systems reported in previous studies; such as 14 days release observed for N-(2- hydroxypropyl) methacrylamide copolymer (Wang et al. 2007), and the 15 days release observed for electro.spunned polycaprolactone nanofibers (Martins et al. 2010).

The release of DEX from LbL particles involves two processes: a) bulk media solution diffuse into the LbL particles to dissolve the DEX drug and b) the dissolved DEX molecules diffuse out of the LbL particles, through the surrounding layers (Pargaonkar et al. 2005). Since, different pH release media conditions are known to dissolve DEX in a different manner, and the diffusion of DEX proceeds through the layers (Pargaonkar et al. 2005), from the surface toward the core (functionalised-TiO_2-particles) different release profiles were observed. As can be seen in Figure 42 and Figure 43, in LbL route, overall DEX release profiles varied according to the (a) number of layers surrounding DEX layer, 0 layers (LbL 0) or 4 layers (LbL 4), and (b) the pH value of the release media (pH=6 vs pH=7). Accordingly, when comparing DEX released from LbL 0 and LbL 4, higher DEX concentrations were released from particles where DEX was the outer layer (LbL 0 and LbL 2). Whilst, when DEX layer was surrounded by CH/ALG layers (LbL 1, LbL3 and LbL 4) a more controlled release profile and smaller drug concentrations were released. In addition, a decrease of the initial burst release (24h) was observed for LbL particles surrounded by more CH/ALG layers. This trend was observed for both release media at pH=6 or pH=7. This could be attributed to the higher the number of CH/ALG layers surrounding DEX-loaded TiO_2 particles which results in a higher the diffusional path length that DEX has to traverse (Jayant & Srivastava 2007, Santos et al. 2018), as well as in a decrease of DEX exposure due to being in particles surface (outer layer).In this sense, our results agree with literature, several examples of enhancing the number of coating layers in LBL particles have shown to decrease both drug release concentration and initial burst release (Han et al. 2016, Jayant et al. 2009, Pargaonkar et al. 2005, Santos et al. 2018). Jayant and co-workers (2009) have reported a significant difference (p < 0.05) in the rate of DEX release when comparing uncoated and coated alginate microspheres. In this study the EDC/NHS-cross-linked (polyallylamine hydrochloride/ Poly (acrylic acid) coated-microspheres have shown to release only 29% (cumulative release) of DEX after 30 days, whereas for uncoated microspheres the

cumulative release of DEX was 100% after 22 days. Similar results were reported by Jayant and co-workers (2007), release studies showed that uncoated DEX-alginate microspheres demonstrate a cumulative release of 78% of initially encapsulated DEX as compared to one PSS/PAH bilayer coated microspheres, which demonstrate a cumulative release of 32% (Jayant & Srivastava 2007).

Apart from the effect of the number of layers, the pH value of the release media (pH=6 vs pH=7) also showed to affect DEX release from LbL-functionalised TiO_2 particles. The environmental conditions (i.e. pH of release media) on the quantity of DEX released can be extremely relevant for system application. In this context, the release profiles obtained in this study, could provide a good insight on the behaviour of this model system within the local where DEX will be released, the healthy (pH~7) and inflamed joints (pH~6) (De Nadai et al. 2013). Drug release studies performed in this study showed that independently of the number of layers (CH/ALG) surrounding DEX, a higher concentration of drug was released under more acidic conditions (pH<7) when compared to that released under physiological conditions (pH~7). This is agreement with previous studies (Feng et al. 2014, Han et al. 2016, Pargaonkar et al. 2005, Wang & Rempel 2013), where pH conditions have shown to affect the drug release profile of LbL-coated particles. This pH-dependent release can be explained based on behaviour (i.e. degree of ionization) of CH and ALG under different pH conditions. It is well known that in CH/ALG LbL systems, the ionic interactions between the carboxylate groups of ALG and the protonated amines of CH are a requirement for a stable assembly (Caetano et al. 2016, Lawrie et al. 2007). Previous studies have already reported this stability can be affected by pH, which cause variations degree of ionization of both CH and ALG (Santos et al. 2018, Shiratori & Rubner 2000). Mostly the pH variations affect the surface charge density, and hence alters the electrostatic interaction between CH/ALG layers. Since electrostatic interaction is the dominant driving force between CH/ALG layers and DEX, the differences observed in DEX release profile for different pH conditions can be explained based on the degree of ionization of CH and ALG polyelectrolytes (Feng et al. 2014, Han et al. 2016, Lawrie et al. 2007). Taking CH layer as an example, usually CH (pKa≈6.0-6.5) becomes cationic at more acidic conditions (pH=5.0-6.0), and as the pH becomes more acidic the more cationic CH become (more protonated amine group) (Silva et al. 2015). Although as reported by Chang et al. (2015) at neutral pH=7, CH becomes deprotonated, thus CH positive surface charge decreases or even becomes negative, and due to the formation of intramolecular hydrogen bond the CH molecules start to aggregate (Chang et al. 2015). This decrease of surface charge and molecules aggregation of chitosan could explain the sustained release of neutral conditions (pH~7.0). An example of these findings and a similar drug release trend to one observed

in our study was reported by Feng and co-workers that showed that release rate of anticancer drug, doxorubicin, from CH/ALG multilayer mesoporous silica nanoparticles was much higher at lower pH (pH<7) than that at physiological conditions (pH=7.4) (Feng et al. 2014).

Another probable explanation for higher DEX release under more acidic conditions can be based on ALG layer behaviour, more specifically on the degree of ionization of carboxyl groups. Typically, under more acidic conditions carboxyl groups are more prone to be deionized (Han et al. 2016)., thus diminishing the electrostatic interaction of ALG with the other layers (CH and DEX). Consequently, due to low electrostatic stability, layers surrounding DEX are more easily eroded than at under basic conditions.

Furthermore, the DEX release profile can also be explained based on higher solubility of DEX at more acidic conditions which leads to release of higher concentrations. As previously reported by Wang and co-workers the highest release of DEX occurred under the most acidic release conditions (pH<7.4). This study was reported that after 14 days, the following percentage of loaded DEX was released from the N-(2- hydroxypropyl) methacrylamide copolymer: 14%, 2.5% and 1%, respectively at pH=5.0, pH=6.0 and pH=7.4 (Wang et al. 2007). Similarly, Chung and colleagues showed a higher release of DEX at pH=7.4 (1.4 μg/mL) when compared to that of pH=6.8 (6.4 μg/mL) (Chung et al. 2015); when studying the ultrasensitive reactive oxygen species (ROS)-responsive hollow microsphere as anti-inflammatory drug delivery system. Also, Zolnik & Burgess (2007) reported that a faster release/kinetics of DEX from PLGA microspheres was observed at more acidic conditions (pH=2.4, 3.48/day) when compared to that at physiological conditions (pH=7.4, 2.13/day) (Zolnik & Burgess 2007).

Another example of the pH influence on drug release profile was observed for LbL 3 particles. More specifically the effect of pH conditions on the erosion of ALG layer, which was the outermost layer in LbL 3 particles (DEX+CH+DEX+ALG). As it was discussed above, the DEX release profile for all LbL-functionalised particles tested (LbL 0, LbL 1, LbL 2, LbL 3 and LbL 4) followed the same release trend, where the concentration of drug released from LbL particles has shown to decrease with the increasing number layers surrounding DEX. Accordingly, for LbL 0 and LbL 2 a higher concentration of DEX was released than for LbL 1, LbL 3 and LbL 4 particles. Furthermore, following the same logic the concentration of DEX released from LbL 3 was higher than the one released from LbL 4. Although at pH=7, a different behaviour was observed: DEX release profile obtained for LbL 3 particles was very similar to that of LbL 4 particles. Similar behaviour was reported by Han and co-workers, which have demonstrated that ALG layers were more easily eroded under acidic conditions (pH 6.0) than under weak basic conditions (pH 7.4) (Han et al. 2016). This resulted in weak interaction between ALG and DEX layer,

133

hence resulting in higher concentration of DEX released under more acidic conditions. On the other hand, at pH=7 DEX release was hindered by stronger interaction between DEX and ALG layer.

Moreover, it was observed that DEX concentration/release rate released from LbL particles decreased over the time. Being the highest concentrations of DEX released during the initial days (24h and 48h), whilst smaller concentrations were released at 1 and 2 weeks. Also, slightly higher concentrations of DEX were released at 72h, when comparing to the one release at 2W from both LbL 0 and LbL 4. This phenomenon can be related to the drug distribution across the LbL structure. The DEX encapsulated seems to have faced an extra physical barrier, resulting in a slowdown in the release rate; where the CH/ALG layers surrounding DEX act as a controllable barrier between the (amino)-functionalised TiO_2 particles and the release conditions (Li, P., et al., 2008). Haidar and co-workers (2008) have previously demonstrated that CH/ALG layers, provide a protective effect for shell degradation, thus delaying release of biological compounds.

The time-frame aspects of anti-inflammatory drug release that will modulate the foreign body response to implant are still not well understood. Although it is known that to obtain an efficiently modulation of inflammatory response, the release of drug should at least be controlled and continuous (Hickey, *et al*. 2002). Moreover, in terms of biological action, corticosteroids are known to bind to cytoplasmic glucocorticoid receptors, where at high-dose these drugs will increase the activation of anti-inflammatory genes, while at low concentrations a suppression of activated inflammatory genes will be observed (Dutra-Medeiros et al. 2014).

Taking into account that the inflammatory tissue response starts during the first seconds after device implantation (Figure 4), drug release profiles obtained for amino and mercapto route could be highly favourable to control initial acute inflammation (1-3 days) at the site of implantable devices (Hickey, Kreutzer, Burgess, & Moussy, 2002a). On the other hand, when LbL route was applied, a more prolonged (~20 days) and controlled release (CH/ALG layers-dependent) of DEX were observed, where overall a higher concentration of DEX was released from TiO_2 particles under more acidic pH value (pH=~6). All these characteristics suggest the potential of model system obtained by LbL route to avoid a prolonged acute inflammation, known as chronic inflammation. Moreover, a low burst release of DEX (<10 mg/mL), which can be controlled by CH/ALG layers, is important to prevent local toxic side effects out coming from a high concentration of anti-inflammatory drugs (Oray et al. 2016, Petit et al. 2014).

Overall, the release profiles obtained in this study for amino, mercapto and LbL routes show that that the model system developed here was able to protect DEX from the

surrounding environment, avoiding the immediate release. Particularly the one obtained by LbL route where DEX was released for prolonged period, and a controlled delivery of DEX at the implant site can be achieved by tailoring the number of CH/ALG layers around DEX. In addition, the highest concentrations of DEX were released under more acidic conditions, which is one of the pathological feature of inflamed joints (Wang et al. 2007). Due to these reasons, the release profile of DEX observed for TiO_2 particles obtained by LbL route, could be very suitable to achieve an adequate anti-inflammatory action after joint replacement surgery. Mainly because the high-dose of DEX released in an initial phase (1st week) could increase the activation of anti-inflammatory genes, whereas low concentration released at second phase (2-3weeks) would promote the suppression of activated inflammatory genes (Dugel et al. 2015, Dutra-Medeiros et al. 2014), and thus promote implant osteointegration. Moreover, it has been reported that extended hospital course (>3days) for patients undergoing orthopaedic surgery, (Bhusal et al. 2016, Qu et al. 2015) is caused by the inappropriate pain control. In this case, the controlled and extended release of DEX observed from LbL-functionalised particles could potentially improve the quality of life and compliance of patients by providing a better pain management in a post-surgery phase, thus minimizing the time spend in the hospital (Bhusal et al. 2016).

Another advantage of utilizing LbL route is that unlike amino and mercapto routes, no covalent binding is involved in the synthesis of DEX-loaded-functionalised TiO_2 particles, which allows DEX to remain intact (De Villiers et al. 2012). Therefore, the DEX released, which was detected by HPLC is not seen as a new chemical entity, which in terms of biological effect could show even better results due to "purity" of drug released. Moreover, being a deposition technique LbL route can be utilized to uniformly coat TJR implant surface, both extremely small features or larger surfaces(Macdonald et al. 2011). Altogether these results suggest LbL route as the most appropriated synthetic route to obtain a release profile to modulate the inflammatory response in TJR. However, as described in the following section, more studies (e.g. assessment of the anti-inflammatory effect and cellular viability) were needed to confirm these assumptions.

4.3. *Raw 264.7 cell* studies

From a cellular point of view, macrophages are the first immune cells to act towards invading organisms or tissue injury, and they play a key role in inflammatory response (Goodman et al. 2014, Hallab 2016, Nich et al. 2013). Hence, making them the in vivo targets for the anti-inflammatory drug-eluting implant model system here in develop. Therefore, cytotoxic and anti-inflammatory properties of DEX-loaded functionalised-TiO_2 particles were tested in a rapid and reproducible *in vitro* mouse macrophage-like cellular model, by utilizing murine RAW 264.7 cells. Previous studies utilizing Raw 264.7 cells have confirmed their ability to produce and release markers of inflammation (Chan et al. 2015, Hoareau et al. 2010, Joo et al. 2014). Therefore, these cells have proven a valuable tool for researchers conducting pharmacological research to identify novel anti-inflammatory drug candidates. Lipopolysaccharide (LPS) was utilized to activate the Raw 264.7 macrophages, resulting in the secretion of pro-inflammatory cytokines, including nitric oxide (NO) and tumour necrosis factor alpha (TNF-α) (Pinho et al. 2011, Sharma et al. 2007). The suppression of which was utilized to investigate anti-inflammatory effect of DEX released from functionalised-TiO_2 particles. Overall*, in vitro* studies showed that both DEX released from amino, mercapto and LbL-functionalised particles exerted an anti-inflammatory activity by decreasing NO and TNF-α production in LPS-activated macrophages. Although LbL particles showed a prolonged release of DEX which resulted in a more continued anti-inflammatory activity (at least 2 weeks) than that observed for amino and mercapto particles (24 hours). The utilization of DEX as an anti-inflammatory drug before and after joint replacement surgeries, mainly via oral administration, has been widely described (Backes et al. 2013, De Oliveira et al. 2011, Goodman et al. 2014). However, in this work, we elucidate for the first time the local anti-inflammatory and respective cytotoxic effects of DEX released from functionalised TiO_2 particles on LPS-activated murine macrophages.

4.3.1. Cellular viability

Cytotoxicity testing of implantable devices, such as TJR, is recommended by regulatory bodies (American Society for Testing and Materials, ASTM F2033-12) and is considered as one of the most fundamental tests for biocompatibility (Koschwanez & Reichert 2007, Schuh 2008, Values et al. 2005). Moreover, being important inflammatory modulators, NO and TNF-α can also be cytotoxic mediators (Kröncke et al. 2001, Sedger & McDermott 2014). For instance, when assessing biological activity naphthoquinones, Pinho and co-workers have reported that macrophages death would decrease the number of NO producing cells (Pinho et al. 2011), and thus providing erroneous results about anti-inflammatory efficacy. For this reason, preliminary cell viability studies were

performed as a complement to the anti-inflammatory activity assessment. Aiming to guarantee that the anti-inflammatory effect of DEX released from functionalised TiO_2-particles obtained by different synthetic routes will not be due to cell death/toxicity.

<u>Importance of preliminary viability studies</u>

Although sometimes preliminary studies can be repetitive and time consuming, they are often conducted to investigate whether crucial components of an experiment will be feasible, thus obtaining a more efficient study. In our study, the preliminary experiments were important to guarantee that concentrations and type of treatments (i.e. filtered or non-filtered) will not cause cell toxicity or misleading/false anti-inflammatory effect.

In a first stage preliminary studies were performed to investigate the toxicity of different concentrations of DEX alone and release buffers. Our results showed that the non-toxic effects of DEX occurred at lower doses (<20 µg/mg), at which increased cell growth and recovery from damage was observed even after 72h of exposure. However, at higher doses (60 and 100 µg/mL) and long-term exposure (72h), DEX has showed to be cytotoxic. Respectively a significant decrease on cellular viability of 50% was observed, when compared to control group. Similar results were reported by Wernecke at al. (2015), when assessing the dose and time dependence of DEX toxicity on chondrocytes (Wernecke et al. 2015). This study showed that low doses (2.5-50 µM) and short exposure times (<1 day) were correlated with maintenance of cell viability. On the other hand, for higher doses of DEX (>100 µM) and more prolonged culture times (72h), detrimental cellular effects were observed, such as decreased collagen levels, chondrotoxicity, and extracellular matrix breakdown.

As for preliminary studies concerning release buffers, results showed that when incubated with LPS most of the release buffers concentrations induced significant ($p<0.05$) decrease on cellular viability, except for the one where release buffer was diluted to 1:10 (10% concentration). This information was crucial when assessing the toxicity of DEX released from functionalised-TiO_2 particles, because treatments were diluted up to a concentration of 10% before being added to the Raw 264.7 cells. Moreover, when toxicity of DEX released from functionalised-TiO_2 particles was investigated, results obtained by MTT assay showed that the LPS-activated Raw 264.7 cells exposed to non-filtered samples presented significant ($p<0.05$) decrease on cellular viability. This decrease on cellular viability caused by non-filtered samples can be related to the presence of TiO_2 particles in the sample, which were removed when sample was filtered.

Together these results obtained from the preliminary studies were important to find out that samples should be filtered and diluted (1:10) before being added to Raw 264.7 cells,

otherwise the potential decrease of inflammatory markers (e.g. NO decrease) will be due to cell toxicity and not due to anti-inflammatory activity. Hence, the importance of performing preliminary studies before starting the main experiment was here in demonstrated.

<u>DEX released from functionalised-TiO$_2$ particles</u>

Results obtained from viability studies (MTT assay) indicated that DEX released from functionalised-TiO$_2$ particles obtained by amino/mercapto (Figure 51) and LbL (Figure 52) routes, did not caused appreciable cytotoxicity in LPS-activated RAW 264.7 cells; except at 72 hours, where a higher decrease (10-15%) on viability was observed. The decrease of cellular viability observed for DEX released from functionalised-TiO$_2$ particles is in line with that of DEX alone. This decrease could be explained based on DEX ability of inhibiting nuclear factor-kappa B (NF-Кβ). This transcription factor which plays a central role in inflammation, is also involved in several cellular processes (Brantley et al. 2001) such as cell proliferation and apoptosis. Thus NF-Кβ inhibitory ability of DEX could be hampering the cellular proliferation, and thus decreasing cellular viability of Raw 264.7 macrophages over longer period of exposure. Moreover, most of the studies involving DEX exposure to Raw 264.7 macrophages are performed for shorter periods of time such as 6,18 or 24 hours, suggesting that over incubation period of 72h exposure might be causing media toxicity which results in a decrease on cellular viability without any external stimulus. Similar results were reported by Wernecke at al. (2015), when assessing DEX toxicity on chondrocytes (Wernecke et al. 2015). This study showed that short exposure times (<1 day) were correlated with maintenance of chondrocytes viability. On the other hand, for more prolonged culture times (72h), DEX may have detrimental effects on cells, such as decreased collagen levels, chondrotoxicity, and extracellular matrix breakdown. It is also worth emphasizing that although significant (p<0.05), when compared to control group, this decrease on cellular viability cause by DEX released from functionalised-TiO$_2$ particles was not as significant (p<0.05) as the one induced on Raw macrophages treated with release buffer alone (~20%). In addition, results showed that cellular viability was never less than 80% relative to LPS control group. Because these are the same activated cells on which the anti-inflammatory activity is tested, this noncytotoxic behaviour suggests that the efficacy reported will be primarily due to the anti-inflammatory activity.

4.3.2 Optimization of *in vitro* inflammation system model

Exposure of macrophages to pathogens, such as bacterial LPS, initiates a signal transduction cascade that leads to secretion potent effector molecules, including increased production of pro-inflammatory cytokines such as TNF-α, and inflammatory mediators such as NO, the hallmarks of activated macrophages (Cho et al. 2008, Oh et al. 2012). In this context, the regulation of this signalling pathway is crucial for modulating the initial phases of the immune response to foreign pathogens. For that reason, *in vitro* models such as LPS-activated Raw 264.7 macrophages have been widely used for the screening of anti-inflammatory activity of different agents/compounds (Kim & Ha 2009, Pinho et al. 2011, Vairappan et al. 2013, Yang et al. 2014), and potential anti-inflammatory delivery systems (Bosnjakovic et al., 2011; Joo et al., 2014; S.-Y. Lee, et al., 2013; Terra et al., 2007; Yuan, Chen, Sun, Guan, & Xu, 2013), as evidenced by the abundance of scientific articles published over the last 10 years

In this study optimal experimental conditions, macrophages density and LPS concentration, were investigated to obtain a reliable and reproducible *in vitro* inflammation model. This is critical feature for any *in vitro* cell-based model when conducting biological research to identify novel drug delivery systems (Hughes et al. 2011, McKim 2010), which may or may not possess inherent cellular toxicological properties. Due to rapidity and simplicity, the measurement of NO production by Griess reagent was utilized as screening tool for this optimisation study. Although NO production by Griess reagent assay has been commonly utilized by the scientists, the optimization of experimental conditions to obtain a reliable *in vitro* inflammation model were still investigated in this study. In addition, the excessive production of NO has been considered to be toxic for macrophages (Mandrika et al. 2001). Hence the cellular viability of LPS-activated cells under different parameters (e.g. cell density and LPS concentration) was also investigated to complement the optimization of *in vitro* inflammation model. The importance of optimizing experimental conditions of inflammatory mediators production in LPS-activated macrophages have been described previous studies (Hosseini et al. 2014, Huang et al. 2012, Jacobs & Ignarro 2003). For instance, Huang and colleagues (2012) optimized the cell density, LPS concentration and duration of LPS stimulation to measure NO production in mouse peritoneal macrophages. A similar optimization study was performed by Tweedie et al. (2009) to measure TNF-α production in LPS-activated murine macrophages (Tweedie et al. 2009a).

In general, results showed that in fact NO production was affected by both cell density and LPS concentration. Similar results were reported by Hosseini and co-workers when optimising the conditions for evaluating NO production in microglia cell line (BV-2), NO

production followed a temporal pattern and showed to be cell-density and LPS-dose dependent (Hosseini et al. 2014). The optimal results, a quantifiable NO production at non-toxic levels, were obtained with combination of cell density of 2×10^4 cells/well and LPS concentration of 1 µg/mL.

Moreover, with optimised cell density (2×10^4 cells/well), NO and TNF-α production by LPS-stimulated Raw 264.7 cells showed to be dose-dependent and to increase over time (Figure 60). At 24h, LPS-stimulated cells showed to produce significant level of inflammatory NO and TNF-α proteins, respectively with an approximate 20 and ~74-fold increase when compared to control group. This is line with previous studies which have shown that LPS-activation of macrophages results in concentration-dependent and increased NO (Pinho et al. 2011, Wu et al. 2003) and TNF-α production (Tweedie et al. 2009b). Also, Chiou and co-workers (2000) showed a 16-fold increase in NO production of 24h-LPS-stimulated macrophages (1µg/mL) when compared to that of unstimulated ones. Similarly, an increased production TNF-α protein (112-fold increase) in LPS-activated macrophages was observed by Miller & hunt (1998) when compared to that of unstimulated cells only after 6 hours-exposure.

Furthermore, not only in LPS-stimulated cells the NO and TNF-α was increased (Figure 60), but also the majority of RAW 264.7 cells acquired dendritic morphology upon LPS stimulation (Figure 58). As observed by fluorescent microscopy, results showed that 24h, LPS-activated Raw 264.7 macrophages developed elaborate filopodia-like protrusions, like dendritic-cells type. These changes in macrophages cells morphology and size upon LPS exposition were also described by other authors (Lee et al. 2008, Saxena et al. 2003, van Helden et al. 2008); which have reported that when macrophages encounter stimuli like LPS, they undergo through morphological and phenotypic changes towards activated and polarized dendritic macrophages (M1 and M2 type) (Anderson et al. 2008, Mills & Ley 2014).

4.3.3 Anti-inflammatory activity

In general, implants, such as TJR, undergo tissue response after implantation into living tissues (Wu et al. 2015). During inflammatory process, cytokines such as NO and TNF-α are released, and thus they can be utilized for measuring the inflammatory reactions level after material implantation, including aseptic periprosthetic osteolysis (Bi et al. 2017, Boyce et al. 2005, Holt et al. 2007). There is a considerable body of evidence showing that there is an increased presence of TNF-α and NO in the fluid and inflamed periprosthetic membrane tissue obtained from loosened implants (Banaszkiewicz 2014a,b; Zhao et al. 2016). Because of its pivotal role in anti-inflammatory activity of macrophages, a significant effort has focused on developing therapeutic agents that regulate/decrease NO and TNF-α production.

<u>Preliminary studies</u>

Regarding NO production, preliminary studies showed that none of the tested compounds, DEX (Figure 61), release buffers (Figure 63, Figure 64), or DEX released from functionalised-TiO_2 particles (filtered samples) (Figure 65) induced changes in NO basal levels, when incubated without LPS. Meaning that release buffers and DEX released itself did not exert any effect i.e. inflammation or death on unstimulated-cells.

On the other hand, LPS-stimulated cells (control group) showed high and increasing levels of both NO and TNF-α during the study period of 72 hours. Although it should be noted that when LPS-activated Raw 264.7 cells were exposed to release buffers (Figure 63.B,Figure 64.B), results showed that among all concentrations tested only 10% did not cause a significant decrease ($p<0.05$) on the NO production, when compared to LPS control group. Although less pronounced, the same effect was observed for cellular viability (Figure 45). It is known that release buffers do not exert anti-inflammatory activity, therefore the cell death which was caused by high concentration of PBS leaded to an incorrect interpretation of NO inhibition. From these results, we could then conclude that NO decrease observed for release buffers with concentrations higher than 10%, was mainly caused by significant cell toxicity and not due to anti-inflammatory activity. For this reason, only treatments (filtered samples with 10% concentration) which did not cause a decrease on cellular viability with statistical meaning were considered to exert an anti-inflammatory effect. Together these results obtained for cells exposed to different concentrations of release buffers, have shown the importance of simultaneous assessing NO production and cellular viability.

Furthermore, when the effect of DEX alone (3.9–20 µg/mL) was assessed, a dose-dependent decrease of NO and TNF-α was observed, accordingly this effect was at its greatest when cells were exposed to 20 µg/mL of DEX. These observations are

consistent with earlier reports from other investigators who have shown that DEX significantly decreased levels inflammatory mediators such as TNF-a (Bouwmeester et al. 2004, Hermoso et al. 2004, Miller and Hunt 1998) and NO (Korhonen et al. 2002, Pinho et al. 2011) in LPS-activated macrophages. Miller & Hunt (1998) have showed a significant decrease of TNF-a concentrations of LPS-activated RAW 264.7 macrophages when exposed to DEX (Miller & Hunt 1998). For instance Yoon and co-workers (2010) have shown that DEX (20µM or 8 µg/mL) decreased LPS-induced production of TNF-in Raw 264.6 macrophages by ~40% (% to LPS control) (Yoon et al. 2010) after 24h exposure.

Model system: DEX-loaded-functionalised TiO$_2$ particles

As it was observed for DEX alone, DEX released from functionalised-TiO$_2$ particles obtained by amino, mercapto and LbL routes, decreased both NO and TNF-α production in LPS-activated macrophages. Together with results obtained from cellular viability studies (viability>80%), the anti-inflammatory efficacy of model system here in reported was confirmed excluding the hypothesis of a non-specific decline in protein synthesis due to drug-induced toxicity. Similar effect was observed in previous studies where the anti-inflammatory compounds tested have shown to simultaneous reduce LPS-induced nitrite accumulation and TNF-α secretion in RAW 264.7 macrophages (Chan et al. 2015, Joo et al. 2014, Kiemer et al. 2002). Moreover, when evidenced the anti-inflammatory efficacy of model system was very similar to the one observed for cells treated with positive control (DEX 3.9 and 10 µg/mL). Similar studies have reported the anti-inflammatory effect of DEX released from drug-eluting systems (Fratoddi et al. 2012, Luo et al. 2011, Ren et al. 2014, Vallejo-Heligon et al. 2016). Robinson and colleagues have shown that LPS activation of inflammatory cytokines expression was decreased through the presence of DEX (10µg/mL) released from amine-Functionalized Poly-p-xylene (Parylene A) surface, where a decrease of ~ 60% was observed on TNF-α expression when compared to LPS control group (Robinson et al. 2008).

However, when the anti-inflammatory effect of the synthetic routes applied was compared different anti-inflammatory effect/trend was observed: DEX released from functionalised-TiO$_2$ particles obtained by LbL route was more prolonged than that of amino and mercapto routes, 21 days instead of 24 hours. These results are in line with drug release studies which clearly showed that for particles obtained by LbL route DEX was released for longer periods (~21 days) than that of amino and mercapto routes (24h). Moreover, LbL showed to be a more controllable route, where the anti-inflammatory effect varied according to number of layers surrounding DEX. For example, under inflammatory conditions (pH<7), DEX released from LbL 0 was a more profound TNF-α

inhibitor than that of LbL 4, with highest inhibition observed at 72h of ~ 36% for the former (24h LbL 0) and 25% for the latter (24h LbL 4). Also, a stronger anti-inflammatory effect was observed for DEX released at 24h and 48h than that of 2 weeks. Once more, this anti-inflammatory effect is line with the drug release profile obtained for LbL functionalised-particles, where higher concentrations of DEX were released at earlier time points. Considering that acute inflammatory reaction occurs within 24–48 h (Jayant & Srivastava 2007), the demonstrated higher anti-inflammatory efficacy of DEX released at earlier time points will guarantee an effective modulation of acute phase. Moreover, although minor the anti-inflammatory effect observed for DEX released at 72h and 2W, is also important to guarantee that inflammation will be continuous modulated for at least 2 weeks. Consequently, the continuous and effective anti-inflammatory effect observed in this study, suggest that local release of DEX at the implantation site via the TiO_2 implant surface will be an approach to suppress the local chronic inflammatory response, and consequently avoid aseptic loosening.

Furthermore, it is important to highlight the biological relevance of this study, which simultaneous focuses on inhibition of different inflammatory mediators NO and TNF-α; and, also in contrast to most part of the studies reported in literature, the anti-inflammatory effect was assessed for longer period (i.e. 72h study instead of 18h/24h). Hence from a biological point of view, the results obtained in this study provide a more comprehensive and consistent information about the anti-inflammatory mechanism of the model system developed here Particularly the 3 days lasting anti-inflammatory efficacy reported in this study, suggests that our model system will modulate acute phase (~2-3 days) thus avoiding the unfavourable chronic phase. In addition, DEX released from functionalised-particle was added to the cells, just before LPS addition. This observation might be of special importance to elucidate the mechanisms of action of an anti-inflammatory eluting implant, particularly as a protective compound to avoid chronic inflammation. In this context it is interesting to learn that pre-treatment of macrophages with DEX attenuated LPS-cytokine-induced NO and TNF-α production.

Importance and potential application of model system

The results of the present work showed that DEX released may modulate the intensity of inflammatory processes by inhibiting the secretion of TNF-α and NO pro-inflammatory mediators. In terms of clinical application, this model system could be very useful to improve TJR outcome. Particularly after TJR surgery, where a prolonged and exacerbated inflammatory response can prolong surgical recovery and compromise implant outcome. The local anti-inflammatory effect exerted by DEX, as demonstrated by NO and TNF-α decrease, could promote a controlled inflammatory response i.e.

appropriate balance between pro-inflammatory and anti-inflammatory mediators (Bhusal et al. 2016). The need to modulate inflammation after TJR surgery is obvious, a prolonged (chronic) inflammatory response contributes to the pathogenesis of aseptic loosening, which is the most common indication for revision surgery. A body equilibrium around the implant, where appropriate conditions (i.e. bone formation over bone resorption) for bone growth are gathered, is a crucial factor to achieve osteointegration and long-term clinical function. There is strong evidence that TNF-α can promote bone resorption *in vitro* and *in vivo* in osteoblastic cell lines (Boyce et al. 2005, Holt et al. 2007, Lam et al. 2000, Lampiasi et al. 2016, Lin et al. 2014, Parameswaran & Patial 2010). Hence, being TNF-α a potent mediator of bone resorption (e.g. stimulates osteoclasts formation and differentiation), the TNF-α -inhibitory effect observed when LPS-activated cells were exposed to DEX, suggests that developed system would help to prevent periprosthetic osteolysis. Production of pro-inflammatory cytokines and mediators are crucial to resolve inflammation. Although, their overproduction often leads to less favourable outcomes such as chronic inflammation and tissue damage. Therefore, the NO and TNF-α inhibitory effect exerted DEX released from functionalised-TIO_2 particles on inflamed cells may serve as a potential strategy for modulating inflammation after TJR surgery.

Possible molecular mechanism to explain anti-inflammatory effect of DEX

Glucocorticoids, such as DEX, are indicated for the treatment of many inflammatory conditions; previous studies (Barnes 2006, Hermoso et al. 2004) have shown that clinically glucocorticoids exert their anti-inflammatory effect by binding to a glucocorticoid receptor (GR), which switches off multiple inflammatory pathways and genes and thus decrease the expression of pro-inflammatory cytokines. By directly affecting steroid-responsive gene transcription, DEX is known to suppress the production of pro-inflammatory mediators and cytokines such as NO and TNF-α. The mechanism by which DEX suppresses the macrophage function, has been reported to involve the suppression NF-Kβ, which is in part mediated by induction of IkBα gene transcription and subsequent increase in IkBα protein synthesis. Then newly synthesized IkBα protein inhibits NF-Kβ translocation to the nucleus by binding to its free form in the cytoplasm (Author et al. 1995, Beg & Baldwin As 1993), and hence resulting in a decrease in inflammatory proteins production; being all of this is triggered by DEX binding to GR expressed by macrophages (Crinelli et al. 2000).
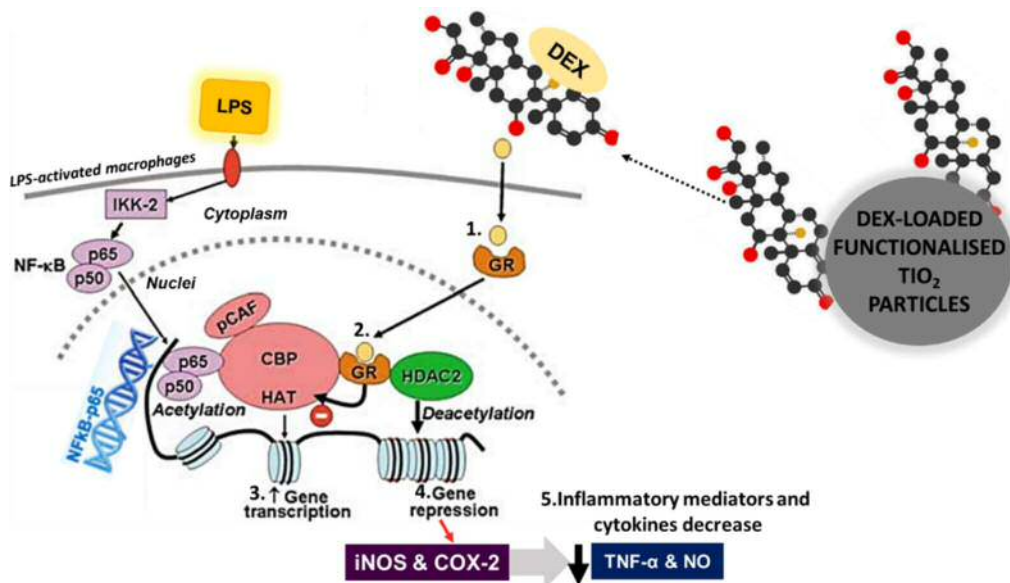
Figure 70. Schematic figure of possible signalling mechanisms of DEX released from functionalised-TiO₂ particles in inhibiting the LPS-induced inflammatory response.

Inflammatory genes are activated by LPS, resulting in activation of IKK2, which activates the transcription factor NF-Kβ. A dimer of p50 and p65 NF-κB proteins translocate to the nucleus and binds to specific κB recognition sites, as well as to co-activators, such as CBP or pCAF, which have intrinsic histone acetyltransferase (HAT) activity. This results in acetylation of core histone H4, resulting in increased expression of genes encoding multiple inflammatory proteins. Simultaneously, after activation by corticosteroids the GR translocate to the nucleus (1.) and bind to coactivators to inhibit HAT activity directly and recruiting HDAC2 (2.), which reverses histone acetylation leading in suppression of the transcription (3.) of these activated inflammatory gene and consequent repression (4.). (Abbreviations: CBP: cyclic binding protein; LPS: Lipopolysaccharide; IKK2: inhibitor of I-kB kinase-2, NF-Kβ: nuclear transcription factor Kβ; pCAF: p300-CBP associated factor; HAT: histone acetyltransferase; GR: glucorticoid receptor; HDAC2: histone deacetylase-2; DEX: dexamethasone).

In more detail, (Figure 70) after activation by DEX, GR translocate to the nucleus and bind to coactivators to inhibit histone acetyltransferase (HAT) activity and recruiting histone deacetylase-2 (HDAC2), which reverses histone acetylation, leading in suppression of the LPS-activated inflammatory genes. Alternatively DEX can also interact with DNA recognition sites to active transcription of anti-inflammatory genes (Barnes 2006, Vandevyver et al. 2013). When anti-inflammatory mechanism of DEX on LPS-activated macrophages was investigated by Jeon and colleagues, results indicated a dose-related inhibition of NF-κB/Rel and AP-1 (Jeon et al. 2000). Specifically, as measured by electrophoretic mobility shift assay (EMSA), DEX inhibited DNA binding of NF-κB/Rel and AP-1 proteins to their cognate DNA sites. Similarly, Yanamoto and

Gaynor (2001) have showed that DEX inhibition of both NO and TNF-α was due to the suppression of NF-κB activation (Yamamoto & Gaynor 2001).This signalling pathway (Figure 70) might explain our observation of a DEX reduction in TNF-α and NO in LPS-stimulated macrophages. Although further studies at transcription level are needed, the anti-inflammatory activity exerted by DEX released from functionalised-TiO$_2$ particles on the investigated inflammatory mediators seems to be mediated via a direct interaction of DEX with NO and TNF-α due to trans repression of the NF-κB signaling pathway.

.

5. Conclusion

Despite being one the most common complication of TJR, there is no approved therapy to avoid or treat aseptic loosening following wear-induced periprosthetic inflammation/osteolysis. Considerable research has been done to reduce wear debris release and their consequences, including modification on implants design and improvement of surgical techniques, although offering some promise none of these approaches have yet shown to inhibit or reverse particle-induced osteolysis in a human population with sufficiently powered, randomized, controlled trials. This leads to the conclusion that most part of the currently applied therapies, depend on the systemic administration of anti-inflammatory agents, meaning that their bioavailability at osteolytic lesions will mainly depend on the limited blood supply at bone-interface implant.

Therefore, localised release of anti-inflammatory drugs from implanted TJR could modulate the environment of this host cell/implant interface and related inflammatory events. Thus, overcoming the aseptic loosening and improve performance of these life-saving devices.

As a proof-of-concept, in this study different routes i.e. amino, mercapto and LbL, were applied to develop a drug delivery model system, that allows localized and tuneable delivery of anti-inflammatory drugs.

In general, results obtained from TGA analysis, SEM, TEM, FTIR and zeta potential measurements show that all routes applied to attach DEX to TiO_2 particles were successful. Moreover, since the primary hydroxyl group used to attach DEX to carboxyl-functionalized TiO_2 particles is present in most of the glucocorticoids, this chemistry would be applicable to conjugate other anti-inflammatory drugs. As for LbL, the only requirement is to tailor the solution of the anti-inflammatory drug, so it behaves as anionic polyelectrolyte, this can be easily achieved by adjusting the pH of the solution.

Overall results have also shown that depending on the synthetic route applied, the DEX-loaded-functionalised TiO_2 particles obtained present different features from size/morphology to drug release profiles. For example, when LBL route was utilized anti-inflammatory drug was released in higher concentration, and during a longer period (i.e. 3 weeks), when compared with DEX release profiles obtained for the mercapto and amino routes (24 hours). Hence, proving that different synthetic routes lead indeed to different release kinetics. Furthermore, in terms of clinical application, the results founded showed the possibility of tuning the pace and concentration of anti-inflammatory drug release through a different conjugation route.

Furthermore, *in vitro* studies using Raw 264.7 macrophages cell line indicated that DEX concentrations released from functionalised-TiO$_2$ particles obtained via amino, mercapto and LbL routes, presented anti-inflammatory activity. In other words, results from this study have shown that DEX decreased the production of two important inflammatory mediators: NO and TNF-α, without considerably adverse cellular effects; such providing vital information for the future medical applications (i.e. TJR) of the drug eluting model system proposed in this study. Although, based on previous clinical studies/evidence, it is known that in theory the functionalised-TiO$_2$ particles obtained by amino and mercapto routes, will not provide the release of DEX during the crucial time desirable to modulate inflammation i.e. period of 2 days to 2 weeks. On the other hand, when applied LbL technique, provided a prolonged anti-inflammatory effect (up to 2 weeks) when compared to amino and mercapto routes. In addition, by increasing the number of layers surrounding DEX it was possible to control the drug release rate and decrease the initial burst release; as well as to maintain the anti-inflammatory activity of DEX, as showed by Raw 264.7 macrophages studies.

Gathering such experimental biological evidence was critical; firstly, because most of the Raw 264.7 macrophages studies reported on literature were performed for periods of 18-24h. And, also because we could not find any study where Raw 264.7 macrophages had been exposed to PBS or acetate buffer media yet. Therefore, it is important to highpoint the importance of all preliminary experiments performed during this study to obtain reliable and reproducible data/results. Additionally, it is important to highlight the utility of the rapid and reproducible *in vitro* RAW 264.7 cell model, which allowed a good consistency in studying the anti-inflammatory role of DEX released from functionalised-TiO$_2$ particles. However, as most *in vitro* studies, RAW 264.7 cell model presents some limitations; parameters such as test sample concentrations, stability and/or potential transformation of test compounds, cell line specificity, duration of cell exposure to treatment samples, generation of artefacts by compounds in cell culture media, as well as other potential reactions should be considered when evaluating cell culture experimental results. Therefore, future animal studies should be designed to (i) investigate the potential of DEX loaded functionalised TiO$_2$ particles for the modulation of acute inflammatory phase, and (ii) completely understand the molecular pathways involved in the DEX-mediated anti-inflammatory response, particularly at transcriptional level.

Nonetheless, the innovative results of this study are very promising both in terms of 1) model system of anti-inflammatory drug eluting implant, where DEX was successfully attached to TiO_2-functionalised particles by all synthetic routes applied; and 2) biological studies, where as shown by our *in vitro* Raw 264.7 cell studies, the DEX released from TiO_2-functionalised particles apart from not being toxic for the cells, it also showed to exhibit an anti-inflammatory activity by attenuating the production of two critical inflammatory mediators, TNF-α and NO in LPS-stimulated macrophages. Particularly when LbL route was applied, suggesting that continuous release (at least 2 weeks) of DEX using LbL CH/ALG functionalised-TiO_2 surface would be able to control inflammation around the implant.

In terms of clinical application, the local delivery of DEX, which is attached to implant surface, can also overcome the several limitations of anti-inflammatory/osteolytic therapies such as lack of efficacy, systemic side-effects, and poor patient compliance. Moreover, the post-surgery period and the treatment regimen can be simpler because it requires fewer anti-inflammatory dosages and doctor visits than the traditional TJR surgery. Particularly, the local delivery of DEX, could prevent the main drawbacks of the conventional systemic delivery of anti-inflammatory drug, such as associated renal and liver complications. Therefore, the model system here in could be a potential approach for patients which undergo TJR, to avoid progressive osteolysis and/or to patients who need repeated revision surgery after joint replacement.

.

6. References

1. Aktan F. 2004. iNOS-mediated nitric oxide production and its regulation. Life Sciences. doi:10.1016/j.lfs.2003.10.042.

2. Allen KD, Adams SB, Setton L a. 2010. Evaluating intra-articular drug delivery for the treatment of osteoarthritis in a rat model. *Tissue Eng. Part B. Rev.* 16(1):81–92

3. Almalki M, Lai E, Li C. 2017. Polyethylene Glycol - Functionalized Titanium Dioxide Nanoparticles for Extended Release of Diethylenetriaminepentaacetic Acid into Lung Fluid to Enhance the Decorporation of Radioactive Actinides. *Nanosci. Nanomedicine Nanobiology J.* 1(1):1–6

4. Anderson J, Cramer S. 2015. *Host Response to Biomaterials*. Elsevier. Elsevier. doi:10.1016/B978-0-12-800196-7.00002-5.

5. Anderson J, Rodriguez A, Chang DT. 2008. Foreign body reaction to biomaterials. Seminars in Immunology.doi:10.1016/j.smim.2007.11.004

6. Anselmo AC, Mitragotri S. 2014. An overview of clinical and commercial impact of drug delivery systems. *J. Control. Release*. 190:15–28

7. Ariga K, McShane M, Lvov YM, Ji Q, Hill JP. 2011. Layer-by-layer assembly for drug delivery and related applications. *Expert Opin. Drug Deliv.* 8(5):633–44

8. Author G, Scheinman RI, Cogswell PC, Lofquist AK, Baldwin AS. 1995. Role of Transcriptional Activation of IκBα in Mediation of Immunosuppression by. *Source Sci. New Ser. J. Pet. Meteorit. D. E. Grady, J. Geophys. Res*. 270(85):283–86

9. Bach LG, Islam MR, Seo SY, Lim KT. 2013. A novel route for the synthesis of poly(2-hydroxyethyl methacrylate) grafted TiO 2 nanoparticles via surface thiol-lactam initiated radical polymerization. *J. Appl. Polym. Sci.* 127:261–69

10. Backes JR, Bentley JC, Politi JR, Chambers BT. 2013. Dexamethasone Reduces Length of Hospitalization and Improves Postoperative Pain and Nausea After Total Joint Arthroplasty: A Prospective, Randomized Controlled Trial. *J. Arthroplasty*. 28(8, Supplement):11–17

11. Bagheri S, Shameli K, Abd Sharifah Bee. H. 2013. Synthesis and characterization of anatase titanium dioxide nanoparticles using egg white solution via sol-gel method. *J. Chem.* 848205, 5 pp.

12. Bagherifard S. 2017. Mediating bone regeneration by means of drug eluting implants: From passive to smart strategies. *Mater. Sci. Eng. C*. 71:1241–52

13. Banaszkiewicz PA. 2014a. Production of cytokines around loosened cemented acetabular components: Analysis with immunohistochemical techniques and in

situ hybridization. In *Classic Papers in Orthopaedics*, pp. 89–91

14. Banaszkiewicz PA. 2014b. The synovial-like membrane at the bone-cement interface in loose total hip replacements and its proposed role in bone lysis. In *Classic Papers in Orthopaedics*, pp. 117–19

15. Banerjee I, Pangule RC, Kane RS. 2011. Antifouling coatings: Recent developments in the design of surfaces that prevent fouling by proteins, bacteria, and marine organisms

16. Barnes PJ. 2006. How corticosteroids control inflammation: Quintiles Prize Lecture 2005

17. Bartczak D, Kanaras AG. 2011. Preparation of peptide-functionalized gold nanoparticles using one pot EDC/Sulfo-NHS coupling. *Langmuir*. 27(16):10119–23

18. Baschant U, Culemann S, Tuckermann J. 2013. Molecular determinants of glucocorticoid actions in inflammatory joint diseases

19. Bastian O, Pillay J, Alblas J, Leenen L, Koenderman L, Blokhuis T. 2011. Systemic inflammation and fracture healing. *J. Leukoc. Biol.* 89(5):669–73

20. Bauer S, Schmuki P, von der Mark K, Park J. 2012. Engineering biocompatible implant surfaces. Part I: Materials and surfaces. *Prog. Mater. Sci.*

21. Bayliss LE, Culliford D, Monk AP, Glyn-Jones S, Prieto-Alhambra D, et al. 2017. The effect of patient age at intervention on risk of implant revision after total replacement of the hip or knee: a population-based cohort study. *Lancet*. 389(10077):1424–30

22. Beck RT, Illingworth KD, Saleh KJ. 2012. Review of periprosthetic osteolysis in total joint arthroplasty: An emphasis on host factors and future directions. *J. Orthop. Res.* 30(4):541–46

23. Bedke J, Stenzl A. 2010. Immunologic mechanisms in RCC and allogeneic renal transplant rejection

24. Beg AA, Baldwin As J r. 1993. The I kB proteins: multifunctional regulators of Rel/NF-kB transcription factors. *Genes Dev.* 7:2064–70

25. Bhandari M, Smith J, Miller LE, Block JE. 2012. Clinical and economic burden of revision knee arthroplasty. *Clin. Med. Insights Arthritis Musculoskelet. Disord.* 5:89–94

26. Bhardwaj U, Sura R, Papadimitrakopoulos F, Burgess DJ. 2007. Controlling acute inflammation with fast releasing dexamethasone-PLGA microsphere/pva hydrogel composites for implantable devices. *J. diabetes Sci. Technol.* 1(1):8–17

27. Bhusal P, Harrison J, Sharma M, Jones DS, Hill AG, Svirskis D. 2016. Controlled release drug delivery systems to improve post-operative pharmacotherapy

28. Bi X, Han L, Qu T, Mu Y, Guan P, et al. 2017. Anti-inflammatory effects, SAR, and action mechanism of monoterpenoids from radix paeoniae alba on LPS-stimulated RAW264.7 cells. *Molecules*. 22(5):

29. Bixler GD, Bhushan B. 2012. Biofouling: lessons from nature. *Philos. Trans. R. Soc. A Math. Phys. Eng. Sci.* 370(1967):2381–2417

30. Bloemen M, Brullot W, Luong TT, Geukens N, Gils A, Verbiest T. 2012. Improved functionalization of oleic acid-coated iron oxide nanoparticles for biomedical applications. *J. Nanoparticle Res.* 14(9):

31. Bogdan C. 2001. Nitric oxide and the immune response. *Nat. Immunol.* 2(10):907–16

32. Bosco R, Van Den Beucken J, Leeuwenburgh S, Jansen J. 2012. Surface Engineering for Bone Implants: A Trend from Passive to Active Surfaces. *Coatings*. 2(4):95–119

33. Bosnjakovic A, Mishra MK, Ren W, Kurtoglu YE, Shi T, et al. 2011. Poly(amidoamine) dendrimer-erythromycin conjugates for drug delivery to macrophages involved in periprosthetic inflammation. *Nanomedicine Nanotechnology, Biol. Med.* 7(3):284–94

34. Bouwmeester T, Bauch A, Ruffner H, Angrand P-O, Bergamini G, et al. 2004. A physical and functional map of the human TNF-alpha/NF-kappa B signal transduction pathway. *Nat. Cell Biol.* 6(2):97–105

35. Boyce BF, Li P, Yao Z, Zhang Q, Badell IR, et al. 2005. TNF-alpha and pathologic bone resorption. *Keio J. Med.* 54(3):127–31

36. Brantley DM, Chen CL, Muraoka RS, Bushdid PB, Bradberry JL, et al. 2001. Nuclear factor-kappaB (NF-kappaB) regulates proliferation and branching in mouse mammary epithelium. *Mol. Biol. Cell*. 12(5):1445–55

37. Bridges AW, García AJ. 2008. Anti-inflammatory polymeric coatings for implantable biomaterials and devices. *J. Diabetes Sci. Technol.* 2(6):984–94

38. Bryan NS, Grisham MB. 2007. Methods to detect nitric oxide and its metabolites in biological samples. *Free Radic. Biol. Med.* 43(5):645–57

39. Buckley CD. 2011. Why does chronic inflammation persist: An unexpected role for fibroblasts

40. Buriuli M, Verma D. 2017. Polyelectrolyte complexes (PECs) for biomedical applications. In *Advanced Structured Materials*, Vol. 66, pp. 45–93

41. Caetano LA, Almeida AJ, Gonçalves LMD. 2016. Effect of experimental parameters on alginate/chitosan microparticles for BCG encapsulation. *Mar. Drugs*. 14(5):

42. Caminade A-M, Turrin C-O. 2014. Dendrimers for drug delivery. *J. Mater. Chem.*

B. 2(26):4055

43. Cao H, Xu SY. 2008. EDC/NHS-crosslinked type II collagen-chondroitin sulfate scaffold: Characterization and in vitro evaluation. *J. Mater. Sci. Mater. Med.* 19(2):567–75

44. Chan PM, Tan YS, Chua KH, Sabaratnam V, Kuppusamy UR. 2015. Attenuation of Inflammatory Mediators (TNF-α and Nitric Oxide) and Up-Regulation of IL-10 by Wild and Domesticated Basidiocarps of Amauroderma rugosum (Blume & T. Nees) Torrend in LPS-Stimulated RAW264.7 Cells. *PLoS One*. 10(10):

45. Chang SH, Lin HTV, Wu GJ, Tsai GJ. 2015. pH Effects on solubility, zeta potential, and correlation between antibacterial activity and molecular weight of chitosan. *Carbohydr. Polym.* 134:74–81

46. Chen Q, Yakovlev NL. 2010. Adsorption and interaction of organosilanes on TiO2 nanoparticles. *Appl. Surf. Sci.* 257(5):1395–1400

47. Chen Y, Song S, Yan Z, Fenniri H, Webster TJ. 2011. Self-assembled rosette nanotubes encapsulate and slowly release dexamethasone. *Int. J. Nanomedicine*. 6:1035–44

48. Cheng Q, Li C, Pavlinek V, Saha P, Wang H. 2006. Surface-modified antibacterial TiO2/Ag+ nanoparticles: Preparation and properties. *Appl. Surf. Sci.* 252(12):4154–60

49. Cherian JJ, Jauregui JJ, Banerjee S, Pierce T, Mont MA. 2015. What Host Factors Affect Aseptic Loosening After THA and TKA?

50. Chiang ZC, Yu SH, Chao AC, Dong GC. 2012. Preparation and characterization of dexamethasone-immobilized chitosan scaffold. *J. Biosci. Bioeng.* 113(5):654–60

51. Cho H, Seon M, Lee Y, Kim J, Kim S, Park J. 2008. 3,3'-Diindolylmethane suppresses the inflammatory response to lipopolysaccharide in murine macrophages. *J Nutr*. 138(1):17–23

52. Chung MF, Chia WT, Wan WL, Lin YJ, Sung HW. 2015. Controlled Release of an Anti-inflammatory Drug Using an Ultrasensitive ROS-Responsive Gas-Generating Carrier for Localized Inflammation Inhibition. *J. Am. Chem. Soc.* 137(39):12462–65

53. Cobelli N, Scharf B, Hardin J, Santambrogio L, Crisi GM, et al. 2011. Mediators of the inflammatory response to joint replacement devices. *Nat. Rev. Rheumatol.* 20(10):S234–35

54. Cohly H, Stephens J, Markhov a, Angel M, Campbell W, et al. 2001. Cell culture conditions affect LPS inducibility of the inflammatory mediators in J774A.1 murine macrophages. *Immunol. Invest.* 30(1):1–15

55. Conde J, Dias JT, Grazu V, Moros M, Baptista P V., de la Fuente JM. 2014. Revisiting 30 years of biofunctionalization and surface chemistry of inorganic nanoparticles for nanomedicine. *Front. Chem.* 2:

56. Coutinho AE, Chapman KE. 2011. The anti-inflammatory and immunosuppressive effects of glucocorticoids, recent developments and mechanistic insights

57. Crinelli R, Antonelli a, Bianchi M, Gentilini L, Scaramucci S, Magnani M. 2000. Selective inhibition of NF-kB activation and TNF-alpha production in macrophages by red blood cell-mediated delivery of dexamethasone. *Blood Cells. Mol. Dis.* 26(3):211–22

58. Cummings NA, Nordby GL. 1966. Measurement of synovial fluid pH in normal and arthritic knees. *Arthritis Rheum.* 9(1):47–56

59. Dangas GD, Claessen BE, Caixeta A, Sanidas EA, Mintz GS, Mehran R. 2010. In-stent restenosis in the drug-eluting stent era

60. Das K, Bose S, Bandyopadhyay A. 2009. TiO2 nanotubes on Ti: Influence of nanoscale morphology on bone cell-materials interaction. *J. Biomed. Mater. Res. - Part A*. 90(1):225–37

61. Dattani R. 2007. Femoral osteolysis following total hip replacement

62. Dawes GJS, Fratila-Apachitei LE, Necula BS, Apachitei I, van Leeuwen JPTM, et al. 2011. Effects of Dexamethasone Loaded Plga Microspheres on Human Fetal Osteoblasts. *J. Biomater. Appl.*

63. De Jonge LT, Leeuwenburgh SCG, Wolke JGC, Jansen JA. 2008. Organic-inorganic surface modifications for titanium implant surfaces

64. De Nadai TR, De Nadai MN, Albuquerque AAS, De Carvalho MTM, Celotto AC, Evora PRB. 2013. Metabolic acidosis treatment as part of a strategy to curb inflammation

65. De Oliveira GS, Almeida MD, Benzon HT, McCarthy RJ. 2011. Perioperative single dose systemic dexamethasone for postoperative pain: a meta-analysis of randomized controlled trials. *Anesthesiology*. 115(3):575–88

66. De Oliveira GS Jr.; Almeida MD; Benzon HT;McCarthy RJ. 2011. Perioperative Single Dose Systemic Dexamethasone for. *Anesthesiology*. 115(3):575–88

67. De Villiers MM, Otto DP, Lvov YM. 2012. Application of Electrostatic Layer-by-Layer Nanocoating in Drug Delivery

68. Díez-Pascual AM, Díez-Vicente AL. 2014. Effect of TiO2 nanoparticles on the performance of polyphenylsulfone biomaterial for orthopaedic implants. *J. Mater. Chem. B*. 2(43):7502–14

69. Doadrio AL, Conde A, Arenas MA, Hernández-López JM, de Damborenea JJ, et

al. 2015. Use of anodized titanium alloy as drug carrier: Ibuprofen as model of drug releasing. *Int. J. Pharm.* 492(1–2):207–12

70. Dohan Ehrenfest DM, Coelho PG, Kang BS, Sul YT, Albrektsson T. 2010. Classification of osseointegrated implant surfaces: Materials, chemistry and topography

71. Dugel PU, Bandello F, Loewenstein A. 2015. Dexamethasone intravitreal implant in the treatment of diabetic macular edema. *Clin. Ophthalmol.* 9:1321–35

72. Dutra-Medeiros M, Alkabes M, Nucci P. 2014. Effectiveness of the Dexamethasone Intravitreal Implant for Treatment of Patients with Diabetic Macular Oedema. *Eur. Ophthalmic Rev.* 67–73

73. Elron-Gross I, Glucksam Y, Biton IE, Margalit R. 2009. A novel Diclofenac-carrier for local treatment of osteoarthritis applying live-animal MRI. *J. Control. Release*. 135(1):65–70

74. Erdemli Ö, Özen S, Keskin D, Usanmaz A, Batu ED, et al. 2014. In vitro evaluation of effects of sustained anti-TNF release from MPEG-PCL-MPEG and PCL microspheres on human rheumatoid arthritis synoviocytes. *J. Biomater. Appl.* 29(4):524–42

75. Evans CH, Kraus VB, Setton LA. 2014. Progress in intra-articular therapy. *Nat. Rev. Rheumatol.* 10(1):11–22

76. Everaerts F, Torrianni M, Hendriks M, Feijen J. 2008. Biomechanical properties of carbodiimide crosslinked collagen: Influence of the formation of ester crosslinks. *J. Biomed. Mater. Res. - Part A*. 85(2):547–55

77. Fan J, Myant C, Underwood R, Cann P. 2012. Synovial fluid lubrication of artificial joints: protein film formation and composition. *Faraday Discuss.* 156(0):69–85

78. Feng W, Nie W, He C, Zhou X, Chen L, et al. 2014. Effect of pH-responsive alginate/chitosan multilayers coating on delivery efficiency, cellular uptake and biodistribution of mesoporous silica nanoparticles based nanocarriers. *ACS Appl. Mater. Interfaces*. 6(11):8447–60

79. Fernandes LL, Resende CX, Tavares DS, Soares GA, Castro LO, Granjeiro JM. 2011. Cytocompatibility of chitosan and collagen-chitosan scaffolds for tissue engineering

80. Fratoddi I, Venditti I, Cametti C, Palocci C, Chronopoulou L, et al. 2012. Functional polymeric nanoparticles for dexamethasone loading and release. *Colloids Surfaces B Biointerfaces*. 93:59–66

81. Gallo J, Goodman SB, Konttinen YT, Wimmer MA, Holinka M. 2013. Osteolysis around total knee arthroplasty: A review of pathogenetic mechanisms

82. Ganesh M, Lee SG. 2013. Synthesis, characterization and drug release capability

of new cost effective mesoporous silica nano particle for ibuprofen drug delivery. *Int. J. Control Autom.* 6(5):207–16

83. Gao Y, Masuda Y, Seo W-S, Ohta H, Koumoto K. 2004. TiO2 nanoparticles prepared using an aqueous peroxotitanate solution. *Ceram. Int.* 30(7):1365–68

84. Getts DR, Terry RL, Getts MT, Deffrasnes C, Müller M, et al. 2014. Therapeutic inflammatory monocyte modulation using immune-modifying microparticles. *Sci. Transl. Med.* 6(219):

85. Gillies ER, Fréchet JMJ. 2005. Dendrimers and dendritic polymers in drug delivery

86. Ginebra MP, Canal C, Espanol M, Pastorino D, Montufar EB. 2012. Calcium phosphate cements as drug delivery materials

87. Gong D, Shi W, Yi S, Chen H, Groffen J, Heisterkamp N. 2012. TGFβ signaling plays a critical role in promoting alternative macrophage activation. *BMC Immunol.* 13:31

88. Goodman S. 2014. Bearing Surfaces for Joint Replacement: New Materials or New Problems. In *Metal-on-Metal Bearings: A Clinical Practicum*, Vol. 9781461489, eds. LC Jones, WO Haggard, AS Greenwald, pp. 13–20. New York, NY: Springer New York

89. Goodman SB, Gibon E, Pajarinen J, Lin T-HT-H, Keeney M, et al. 2014. Novel biological strategies for treatment of wear particle-induced periprosthetic osteolysis of orthopaedic implants for joint replacement. *J. R. Soc. Interface*. 11(93):20130962

90. Goodman SB, Ma T. 2010. Cellular chemotaxis induced by wear particles from joint replacements. *Biomaterials*. 31(19):5045–50

91. Goodman SB, Yao Z, Keeney M, Yang F. 2013. The future of biologic coatings for orthopaedic implants. *Biomaterials*. 34(13):3174–83

92. Goriainov V, Cook R, Latham JM, Dunlop DG, Oreffo ROC. 2014. Bone and metal: An orthopaedic perspective on osseointegration of metals

93. Gouda M. 2012. Augmentation of Multifunctional Properties of Cellulosic Cotton Fabric Using Titanium Dioxide Nanoparticles. *Adv. Nanoparticles*. 01(03):29–36

94. Gutowski CJ, Zmistowski BM, Clyde CT, Parvizi J. 2014. The economics of using prophylactic antibiotic-loaded bone cement in total knee replacement. *Bone Jt. J.* 96 B(1):65–69

95. Haak-Frendscho M, Wynn TA, Czuprynski CJ, Paulnock D. 1990. Transforming growth factor-beta 1 inhibits activation of macrophage cell line RAW 264.7 for cell killing. *Clin. Exp. Immunol.* 82(2):404–10

96. Hallab NJ. 2016. Biologic Responses to Orthopedic Implants: Innate and

Adaptive Immune Responses to Implant Debris. *Spine (Phila. Pa. 1976).* 41 Suppl 7:S30-1

97. Haller JA, Bandello F, Belfort R, Blumenkranz MS, Gillies M, et al. 2011. Dexamethasone intravitreal implant in patients with macular edema related to branch or central retinal vein occlusion: Twelve-month study results. *Ophthalmology*. 118(12):2453–60

98. Hammond PT. 2012. Building biomedical materials layer-by-layer. *Mater. Today*. 15(5):196–206

99. Han U, Seo Y, Hong J. 2016. Effect of pH on the structure and drug release profiles of layer-by- layer assembled films containing polyelectrolyte , micelles , and graphene oxide. *Sci. Rep.* 6(April):1–10

100.   Hausmann EHS, Hao SY, Pace JL, Parmely MJ. 1994. Transforming growth factor-beta 1 and gamma interferon provide opposing signals to lipopolysaccharide-activated mouse macrophages. *Infect. Immun.* 62(9):3625–32

101.   Hermanson GT. 2013. Functional Targets for Bioconjugation. In *Bioconjugate Techniques*, pp. 127–228

102.   Hermanson GT, Hermanson GT. 2013. Chapter 4 – Zero-Length Crosslinkers. In *Bioconjugate Techniques*, pp. 259–73

103.   Hermoso MA, Matsuguchi T, Smoak K, Cidlowski JA. 2004. Glucocorticoids and tumor necrosis factor alpha cooperatively regulate toll-like receptor 2 gene expression. *Mol. Cell. Biol.* 24(11):4743–56

104.   Hickey T, Kreutzer D, Burgess DJ, Moussy F. 2002a. In vivo evaluation of a dexamethasone/PLGA microsphere system designed to suppress the inflammatory tissue response to implantable medical devices. *J. Biomed. Mater. Res.* 61(2):180–87

105.   Hickey T, Kreutzer D, Burgess DJ, Moussy F. 2002b. Dexamethasone/PLGA microspheres for continuous delivery of an anti-inflammatory drug for implantable medical devices. *Biomaterials*. 23(7):1649–56

106.   Hickok NJ, Shapiro IM. 2012. Immobilized antibiotics to prevent orthopaedic implant infections

107.   Hoareau L, Bencharif K, Rondeau P, Murumalla R, Ravanan P, et al. 2010. Signaling pathways involved in LPS induced TNFalpha production in human adipocytes. *J. Inflamm. (Lond).* 7:1

108.   Holt G, Murnaghan C, Reilly J, Meek RMD, Features S. 2007. The biology of aseptic osteolysis. *Clin. Orthop. Relat. Res.* 460(460):240–52

109.   Holte K, Kehlet H. 2002. Perioperative single-dose glucocorticoid

administration: Pathophysiologic effects and clinical implications

110.   Hosseini NK, Jose S, Vidyadaran S, Nordin SA. 2014. Optimization of cell density and LPS concentration for the evaluation of nitric oxide production on BV-2 cells in a Griess assay. *Malaysian J. Med. Heal. Sci.* 10(2):1–8

111.   Huang L, Xia H, Lun Y, Yu C, Zhang Q, et al. 2012. Optimization of a lipopolysaccharide-stimulated nitric oxide production model in mouse peritoneal macrophages. *J. Neurosci. Methods.* 32(11):1646–50

112.   Huebner KD, Shrive NG, Frank CB. 2014. Dexamethasone inhibits inflammation and cartilage damage in a new model of post-traumatic osteoarthritis. *J. Orthop. Res.* 32(4):566–72

113.   Hughes JP, Rees S, Kalindjian SB, Philpott KL. 2011. Principles of early drug discovery. *Br. J. Pharmacol.* 162(6):1239–49

114.   Hughes SF, Hendricks BD, Edwards DR, Maclean KM, Bastawrous SS, Middleton JF. 2010. Total hip and knee replacement surgery results in changes in leukocyte and endothelial markers. *J. Inflamm.* 7:2

115.   Hunt LP, Ben-Shlomo Y, Clark EM, Dieppe P, Judge A, et al. 2014. 45-day mortality after 467779 knee replacements for osteoarthritis from the National Joint Registry for England and Wales: An observational study. *Lancet.* 384(9952):1429–36

116.   Iloki Assanga SB, Gil-Salido AA, Lewis Lujan LM, Rosas-Durazo A, Acosta-silva AL, et al. 2013. Cell growth curves for different cell lines and their relationship with biological activities. *Int. J. Biotechnol. Mol. Biol. Res.* 4(4):60–70

117.   Ingham E, Fisher J. 2005. The role of macrophages in osteolysis of total joint replacement

118.   Ion R, Vizireanu S, Stancu CE, Luculescu C, Cimpean A, Dinescu G. 2015. Surface plasma functionalization influences macrophage behavior on carbon nanowalls. *Mater. Sci. Eng. C.* 48:118–25

119.   Isowa N, Xavier a M, Dziak E, Opas M, McRitchie DI, et al. 1999. LPS-induced depolymerization of cytoskeleton and its role in TNF-alpha production by rat pneumocytes. *Am. J. Physiol.* 277(3 Pt 1):L606–15

120.   Issa K, Mont MA. 2013. Total hip replacement: Mortality and risks

121.   Italiani P, Boraschi D. 2014. From monocytes to M1/M2 macrophages: Phenotypical vs. functional differentiation

122.   Jacobs AT, Ignarro LJ. 2003. Cell density-enhanced expression of inducible nitric oxide synthase in murine macrophages mediated by interferon-β. *Nitric Oxide.* 8(4):222–30

123.   Jäger M, Zilkens C, Zanger K, Krauspe R. 2007. Significance of nano- and microtopography for cell-surface interactions in orthopaedic implants

124.   Jayant RD, McShane MJ, Srivastava R. 2009. Polyelectrolyte-coated alginate microspheres as drug delivery carriers for dexamethasone release. *Drug Deliv.* 16(6):331–40

125.   Jayant RD, Srivastava R. 2007. Dexamethasone release from uniform sized nanoengineered alginate microspheres. *J. Biomed. Nanotechnol.* 3(3):245–53

126.   Jebens EH, Monk-Jones ME. 1959. On the viscosity and pH of synovial fluid and the pH of blood. *J. Bone Joint Surg. Br.* 41–B(2):388–400

127.   Jeon YJ, Han SH, Lee YW, Lee M, Yang KH, Kim HM. 2000. Dexamethasone inhibits IL-1β gene expression in LPS-stimulated RAW 264.7 cells by blocking NF-κB/Rel and AP-1 activation. *Immunopharmacology.* 48(2):173–83

128.   Joo T, Sowndhararajan K, Hong S, Lee J, Park SY, et al. 2014. Inhibition of nitric oxide production in LPS-stimulated RAW 264.7 cells by stem bark of Ulmus pumila L. *Saudi J. Biol. Sci.* 21(5):427–35

129.   Kallala RF, Vanhegan IS, Ibrahim MS, Sarmah S, Haddad FS. 2015. Financial analysis of revision knee surgery based on NHS tariffs and hospital costs: does it pay to provide a revision service? *Bone Joint J.* 97–B(2):197–201

130.   Kawai M, Mödder UI, Khosla S, Rosen CJ. 2011. Emerging therapeutic opportunities for skeletal restoration

131.   Kawakami T, Kawamura K, Fujimori K, Koike A, Amano F. 2016. Influence of the culture medium on the production of nitric oxide and expression of inducible nitric oxide synthase by activated macrophages in vitro. *Biochem. Biophys. Reports.* 5:328–34

132.   Kiemer AK, Müller C, Vollmar AM. 2002. Inhibition of LPS-induced nitric oxide and TNF-α production by α-lipoic acid in rat Kupffer cells and in RAW 264.7 murine macrophages. *Immunol. Cell Biol.* 80(6):550–57

133.   Kim I-T, Ryu S, Shin J-S, Choi J-H, Park H-J, Lee K-T. 2012. Euscaphic acid isolated from roots of Rosa rugosa inhibits LPS-induced inflammatory responses via TLR4-mediated NF-kappaB inactivation in RAW 264.7 macrophages. *J. Cell. Biochem.* 113(6):1936–46

134.   Kim ID, Ha BJ. 2009. Paeoniflorin protects RAW 264.7 macrophages from LPS-induced cytotoxicity and genotoxicity. *Toxicol. Vitr.* 23(6):1014–19

135.   Koju N, Sikder P, Ren Y, Zhou H, Bhaduri SB. 2017. Biomimetic coating technology for orthopedic implants

136.   Konttinen YT, Takagi M, Mandelin J, Lassus J, Salo J, et al. 2001. Acid attack and cathepsin K in bone resorption around total hip replacement prosthesis. *J. Bone Miner. Res.* 16(10):1780–86

137.   Korhonen R, Lahti A, Hämäläinen M, Kankaanranta H, Moilanen E. 2002. Dexamethasone inhibits inducible nitric-oxide synthase expression and nitric oxide production by destabilizing mRNA in lipopolysaccharide-treated macrophages. *Mol. Pharmacol.* 62(3):698–704

138.   Koschwanez HE, Reichert WM. 2007. In vitro, in vivo and post explantation testing of glucose-detecting biosensors: Current methods and recommendations

139.   Kröncke KD, Fehsel K, Kolb-Bachofen V. 1997. Nitric oxide: cytotoxicity versus cytoprotection- how, why, when, and where? *Nitric Oxide*. 1(2):107–20

140.   Kröncke KD, Fehsel K, Suschek C, Kolb-Bachofen V. 2001. Inducible nitric oxide synthase-derived nitric oxide in gene regulation, cell death and cell survival. *Int. Immunopharmacol.* 1:1407–20

141.   Kulig D, Zimoch-Korzycka A, Jarmoluk A, Marycz K. 2016. Study on alginate-chitosan complex formed with different polymers ratio. *Polymers (Basel).* 8(5):

142.   Kurtz S, Ong K, Lau E, Mowat F, Halpern M. 2007. Projections of primary and revision hip and knee arthroplasty in the United States from 2005 to 2030. *J. Bone Joint Surg. Am.* 89(4):780–85

143.   Kurtz SM, Lau E, Ong K, Zhao K, Kelly M, Bozic KJ. 2009. Future young patient demand for primary and revision joint replacement: National projections from 2010 to 2030. *Clin. Orthop. Relat. Res.* 467(10):2606–12

144.   Labek G, Thaler M, Janda W, Agreiter M, Stockl B. 2011. Revision rates after total joint replacement: CUMULATIVE RESULTS FROM WORLDWIDE JOINT REGISTER DATASETS. *Bone Joint J.* 93–B(3):293–97

145.   Lai W-Y, Kao C-T, Hung C-J, Huang T-H, Shie M-Y. 2014. An evaluation of the inflammatory response of lipopolysaccharide-treated primary dental pulp cells with regard to calcium silicate-based cements. *Int. J. Oral Sci.* 6(2):94–98

146.   Lam J, Takeshita S, Barker JE, Kanagawa O, Ross FP, Teitelbaum SL. 2000. TNF-α induces osteoclastogenesis by direct stimulation of macrophages exposed to permissive levels of RANK ligand. *J. Clin. Invest.* 106(12):1481–88

147.   Lampiasi N, Russo R, Zito F. 2016. The Alternative Faces of Macrophage Generate Osteoclasts

148.   Landgraeber S, J??ger M, Jacobs JJ, Hallab NJ. 2014. The pathology of orthopedic implant failure is mediated by innate immune system cytokines

149.   Langlois J, Hamadouche M. 2011. New animal models of wear-particle osteolysis

150.   Lawrie G, Keen I, Drew B, Chandler-Temple A, Rintoul L, et al. 2007. Interactions between Alginate and Chitosan Biopolymers Characterized Using FTIR and XPS. *Biomacromolecules*. 8(8):2533–41

151.   Lee DK, Jang S, Kim MJ, Kim JH, Chung MJ, et al. 2008. Anti-proliferative effects of Bifidobacterium adolescentis SPM0212 extract on human colon cancer cell lines. *BMC Cancer*. 8:310

152.   Lee JW, Serna F, Nickels J, Schmidt CE. 2006. Carboxylic acid-functionalized conductive polypyrrole as a bioactive platform for cell adhesion. *Biomacromolecules*. 7(6):1692–95

153.   Lee K, Goodman SB. 2008. Current state and future of joint replacements in the hip and knee

154.   Lee SY, Kim HJ, Han JS. 2013. Anti-inflammatory effect of oyster shell extract in LPS-stimulated raw 264.7 cells. *Prev. Nutr. Food Sci.* 18(1):23–29

155.   Li G, Xie B, Pan C, Yang P, Ding H, Huang N. 2014. Facile conjugation of heparin onto titanium surfaces via dopamine inspired coatings for improving blood compatibility. *J. Wuhan Univ. Technol. Mater. Sci. Ed.* 29(4):832–40

156.   Li MD, Yang X. 2011. A retrospective on nuclear receptor regulation of inflammation: Lessons from GR and PPARs

157.   Li P, Dai Y-N, Zhang J-P, Wang A-Q, Wei Q, Ping L. 2008. Chitosan-Alginate Nanoparticles as a Novel Drug Delivery System for Nifedipine. *www.ijbs.org Int J Biomed Sci*. 4(3):

158.   Li Y-F, Rubert M, Yu Y, Besenbacher F, Chen M. 2015. Delivery of dexamethasone from electrospun PCL–PEO binary fibers and their effects on inflammation regulation. *RSC Adv.* 5(43):34166–72

159.   Lieder R, Darai M, Thor MB, Ng CH, Einarsson JM, et al. 2012. In vitro bioactivity of different degree of deacetylation chitosan, a potential coating material for titanium implants. *J. Biomed. Mater. Res. - Part A*. 100 A(12):3392–99

160.   Lin TH, Tamaki Y, Pajarinen J, Waters HA, Woo DK, et al. 2014. Chronic inflammation in biomaterial-induced periprosthetic osteolysis: NF-κB as a therapeutic target

161.   Linden J. 2012. Translational medicine: Longer life for artificial joints

162.   Longhofer LK, Chong A, Strong NM, Wooley PH, Yang S-Y. 2017. Specific material effects of wear-particle-induced inflammation and osteolysis at the bone–implant interface: A rat model. *J. Orthop. Transl.* 8:5–11

163.   Lopes PP, Silva MS, Fernandes MHV. 2013. Influence of ibuprofen addition on the properties of a bioactive bone cement. *J. Mater. Sci. Mater. Med.* 24(8):2067–76

164.   Losina E, Thornhill TS, Rome BN, Wright J, Katz JN. 2012. The dramatic increase in total knee replacement utilization rates in the United States cannot be fully explained by growth in population size and the obesity epidemic. *J. Bone Joint Surg. Am.* 94(3):201–7

165.   Lu Y, Pelton R, Brook MA. 2007. Biotinylation of TiO2 nanoparticles and their conjugation with streptavidin. *Langmuir*. 23(10):5630–37

166.   Lucke S, Hoene A, Walschus U, Kob A, Pissarek JW, Schlosser M. 2015. Acute and chronic local inflammatory reaction after implantation of different extracellular porcine dermis collagen matrices in rats. *Biomed Res. Int.* 2015:

167.   Lundberg JO, Weitzberg E, Gladwin MT. 2008. The nitrate-nitrite-nitric oxide pathway in physiology and therapeutics. *Nat. Rev. Drug Discov.* 7(2):156–67

168.   Luo X, Matranga C, Tan S, Alba N, Cui XT. 2011. Carbon nanotube nanoreservior for controlled release of anti-inflammatory dexamethasone. *Biomaterials*. 32(26):6316–23

169.   Lyndon JA, Boyd BJ, Birbilis N. 2014. Metallic implant drug/device combinations for controlled drug release in orthopaedic applications

170.   MA Shafie, Attia Shafie FHM. 2013. Formulation and Evaluation of Betamethasone Sodium Phosphate Loaded Nanoparticles for Ophthalmic Delivery. *J. Clin. Exp. Ophthalmol.* 4(2):1–11

171.   Ma W, Cheetham AG, Cui H. 2016. Building nanostructures with drugs

172.   Macdonald ML, Samuel RE, Shah NJ, Padera RF, Beben YM, Hammond PT. 2011. Tissue integration of growth factor-eluting layer-by-layer polyelectrolyte multilayer coated implants. *Biomaterials*. 32(5):1446–53

173.   MacInnes SJ, Gordon A, Wilkinson JM. 2012. Risk factors for aseptic loosening following total hip arthroplasty. *Recent Adv. Arthroplast.* 275–94

174.   MacMahon PJ, Eustace SJ, Kavanagh EC. 2009. Injectable Corticosteroid and Local Anesthetic Preparations: A Review for Radiologists. *Radiology*. 252(3):647–61

175.   Mandrika I, Muceniece R, Wikberg JE. 2001. Effects of melanocortin peptides on lipopolysaccharide/interferon-gamma-induced NF-kappaB DNA binding and nitric oxide production in macrophage-like RAW 264.7 cells:: Evidence for dual mechanisms of action. *Biochem. Pharmacol.* 61(5):613–21

176.   Marjanovic V, Lazarevic S, Jankovic-Castvan I, Jokic B, Bjelajac A, et al.

2013. Functionalization of thermo-acid activated sepiolite by amine-silane and mercapto-silane for chromium(VI) adsorption from aqueous solutions. *Hem. Ind.* 67(5):715–28

177.   Martins A, Duarte ARC, Faria S, Marques AP, Reis RL, Neves NM. 2010. Osteogenic induction of hBMSCs by electrospun scaffolds with dexamethasone release functionality. *Biomaterials*. 31(22):5875–85

178.   Masuzaki T, Ayukawa Y, Moriyama Y, Jinno Y, Atsuta I, et al. 2010. The effect of a single remote injection of statin-impregnated poly (lactic-co-glycolic acid) microspheres on osteogenesis around titanium implants in rat tibia. *Biomaterials*. 31(12):3327–34

179.   McKim JM. 2010. Building a Tiered Approach to In Vitro Predictive Toxicity Screening: A Focus on Assays with In Vivo Relevance. *Comb. Chem. High Throughput Screen.* 13(2):188–206

180.   Middleton CA, Pendegrass CJ, Gordon D, Jacob J, Blunn GW. 2007. Fibronectin silanized titanium alloy: A bioinductive and durable coating to enhance fibroblast attachment in vitro. *J. Biomed. Mater. Res. - Part A*. 83(4):1032–38

181.   Mihalko WM, Djenderedjian L, Cheema PS, Smith R. 2014. Effects of gelsolin on macrophage inflammatory responses to orthopaedic implant wear debris. *J. Long. Term. Eff. Med. Implants*. 24(1):57–63

182.   Miller L, Hunt JS. 1998. Regulation of TNF-alpha production in activated mouse macrophages by progesterone. *J. Immunol.* 160(10):5098–5104

183.   Mills CD, Ley K. 2014. M1 and M2 macrophages: The chicken and the egg of immunity

184.   Minagar S, Berndt CC, Wang J, Ivanova E, Wen C. 2012. A review of the application of anodization for the fabrication of nanotubes on metal implant surfaces. *Acta Biomater.* 8(8):2875–88

185.   Morent R, De Geyter N, Leys C, Gengembre L, Payen E. 2008. Comparison between XPS- And FTIR-analysis of plasma-treated polypropylene film surfaces. *Surf. Interface Anal.* 40(3–4):597–600

186.   Moskowitz JS, Blaisse MR, Samuel RE, Hsu HP, Harris MB, et al. 2010. The effectiveness of the controlled release of gentamicin from polyelectrolyte multilayers in the treatment of Staphylococcus aureus infection in a rabbit bone model. *Biomaterials*. 31(23):6019–30

187.   National Joint Registry. 2016. *National Joint Registry*. 12th Annual progress report National Joint Registry Reports. http://www.njrreports.org.uk/hips-all-procedures-activity/H03v2NJR

188.   National Joint Registry. 2017. 14th Annual Report-National Joint Registry for England, Wales, Northern Ireland and the Isle of Man

189.   Nich C, Takakubo Y, Pajarinen J, Ainola M, Salem A, et al. 2013. Macrophages-Key cells in the response to wear debris from joint replacements. *J. Biomed. Mater. Res. A*. 101(10):3033–45

190.   Nine M, Choudhury D, Hee A, Mootanah R, Osman N. 2014. Wear Debris Characterization and Corresponding Biological Response: Artificial Hip and Knee Joints. *Materials (Basel).* 7(2):980–1016

191.   Nuttelman CR, Tripodi MC, Anseth KS. 2006. Dexamethasone-functionalized gels induce osteogenic differentiation of encapsulated hMSCs. *J. Biomed. Mater. Res. - Part A*. 76(1):183–95

192.   Oh Y-CC, Cho W-KK, Oh JH, Im GY, Jeong YH, et al. 2012. Fermentation by Lactobacillus enhances anti-inflammatory effect of Oyaksungisan on LPS-stimulated RAW 264.7 mouse macrophage cells. *BMC Complement. Altern. Med.* 12(1):17

193.   Oida T, Weiner HL. 2010. Depletion of TGF-Beta from fetal bovine serum. *J. Immunol. Methods*. 362(1–2):195–98

194.   Oray M, Abusamra K, Ebrahimiadib N, Meese H, Foster CS. 2016. Long-term side effects of glucocorticoids. *Expert Opin. Drug Saf.* 338(1):14740338.2016.1140743

195.   Othman SH, Abdul Rashid S, Mohd Ghazi TI, Abdullah N. 2012. Dispersion and stabilization of photocatalytic TiO 2 nanoparticles in aqueous suspension for coatings applications. *J. Nanomater.* 2012:

196.   Papadimitriou S, Bikiaris D. 2009. Novel self-assembled core-shell nanoparticles based on crystalline amorphous moieties of aliphatic copolyesters for efficient controlled drug release. *J. Control. Release*. 138(2):177–84

197.   Parameswaran N, Patial S. 2010. Tumor necrosis factor-α signaling in macrophages. *Crit. Rev. Eukaryot. Gene Expr.* 20(2):87–103

198.   Pargaonkar N, Lvov YM, Li N, Steenekamp JH, De Villiers MM. 2005. Controlled release of dexamethasone from microcapsules produced by polyelectrolyte layer-by-layer nanoassembly. *Pharm. Res.* 22(5):826–35

199.   Pedersen BK, Febbraio MA. 2008. Muscle as an Endocrine Organ: Focus on Muscle-Derived Interleukin-6. *Physiol. Rev.* 88(4):1379–1406

200.   Pereira-da-silva MDA, Ferri FA. 2017. *1 - Scanning Electron Microscopy*

201.   Perni S, Martini-Gilching K, Prokopovich P. 2018. Controlling release kinetics of gentamicin from silica nano-carriers. *Colloids Surfaces A Physicochem. Eng. Asp.* 541:212–21

202.   Petit A, Sandker M, Müller B, Meyboom R, van Midwoud P, et al. 2014. Release behavior and intra-articular biocompatibility of celecoxib-loaded acetyl-capped PCLA-PEG-PCLA thermogels. *Biomaterials*. 35(27):7919–28

203.   Petruson K, Stalfors J, Jacobsson KE, Ny L, Petruson B. 2005. Nitric oxide production in the sphenoidal sinus by the inducible and constitutive isozymes of nitric oxide synthase. *Rhinology*. 43(1):18–23

204.   Pierson JL, Harris WH. 1994. Cemented revision for femoral osteolysis in cemented arthroplasties. Results in 29 hips after a mean 8.5-year follow-up. *J. Bone Joint Surg. Br.* 76(1):40–44

205.   Pinho BR, Sousa C, Valentão P, Andrade PB. 2011. Is nitric oxide decrease observed with naphthoquinones in LPS stimulated RAW 264.7 macrophages a beneficial property? *PLoS One*. 6(8):

206.   Pioletti DP. 2008. Using drug delivery systems to enhance joint replacement. In *Joint Replacement Technology*, pp. 397–406

207.   Popat KC, Eltgroth M, Desai TA. 2007. Drug eluting nanostructured coatings. *NSTI Nanotech 2007 Conf. St. Clara, Calif.*

208.   Porcheray F, Viaud S, Rimaniol AC, Léone C, Samah B, et al. 2005. Macrophage activation switching: An asset for the resolution of inflammation. *Clin. Exp. Immunol.* 142(3):481–89

209.   Pu H-L, Chiang W-L, Maiti B, Liao Z-X, Ho Y-C, et al. 2014. Nanoparticles with dual responses to oxidative stress and reduced pH for drug release and anti-inflammatory applications. *ACS Nano*. 8(2):1213–21

210.   Qu H, Bhattacharyya S, Ducheyne P. 2015. Silicon oxide based materials for controlled release in orthopedic procedures

211.   Rajamaki K, Nordstrom T, Nurmi K, Akerman KEO, Kovanen PT, et al. 2013. Extracellular acidosis is a novel danger signal alerting innate immunity via the NLRP3 inflammasome. *J. Biol. Chem.* 288(19):13410–19

212.   Rajpura A, Board T. 2013. Complications following total hip arthroplasty. In *Arthroplasty-Update*. InTech

213.   Ramanathan T, Liu H, Brinson LC. 2005. Functionalized SWNT/polymer nanocomposites for dramatic property improvement. *J. Polym. Sci. Part B Polym. Phys.* 43(17):2269–79

214.   Rao AJ, Gibon E, Ma T, Yao Z, Smith RL, Goodman SB. 2012. Revision joint replacement, wear particles, and macrophage polarization. *Acta Biomater.* 8(7):2815–23

215.   Ren K, Dusad A, Yuan F, Yuan H, Purdue PE, et al. 2014. Macromolecular prodrug of dexamethasone prevents particle-induced peri-

implant osteolysis with reduced systemic side effects. *J. Control. Release*. 175(1):1–9

216. Ren K, Dusad A, Zhang Y, Wang D. 2013. Therapeutic intervention for wear debris-induced aseptic implant loosening. *Acta Pharm. Sin. B*. 3(2):76–85

217. Ren K, Purdue PE, Burton L, Quan LD, Fehringer E V., et al. 2011a. Early detection and treatment of wear particle-induced inflammation and bone loss in a mouse calvarial osteolysis model using HPMA copolymer conjugates. *Mol. Pharm.* 8(4):1043–51

218. Ren PG, Irani A, Huang Z, Ma T, Biswal S, Goodman SB. 2011b. Continuous infusion of UHMWPE particles induces increased bone macrophages and osteolysis. *Clin. Orthop. Relat. Res.* 469(1):113–22

219. Revell PA. 2014. *Joint Replacement Technology*, Vol. 2. Elsevier

220. Ricciotti E, Fitzgerald GA. 2011. Prostaglandins and inflammation. *Arterioscler. Thromb. Vasc. Biol.* 31(5):986–1000

221. Rick Sumner D. 2013. Biological control of peri-implant bone remodeling and implant loosening (Sun Valley 2012). *IBMS Bonekey*. 10:

222. Rivera MC, Pinheiro AC, Bourbon AI, Cerqueira MA, Vicente AA. 2015. Hollow chitosan/alginate nanocapsules for bioactive compound delivery. *Int. J. Biol. Macromol.* 79:95–102

223. Robinson EM, Lam R, Pierstorff ED, Ho D. 2008. Localized therapeutic release via an amine-functionalized poly-p-xylene microfilm device. *J. Phys. Chem. B*. 112(37):11451–55

224. Rostamian R, Najafi M, Rafati AA. 2011. Synthesis and characterization of thiol-functionalized silica nano hollow sphere as a novel adsorbent for removal of poisonous heavy metal ions from water: Kinetics, isotherms and error analysis. *Chem. Eng. J.* 171(3):1004–11

225. Rozkydal Z, Janik P, Janicek P, Kunovsky R. 2007. Revision knee arthroplasty due to aseptic loosening. *Acta Chir. Orthop. Traumatol. Cech.* 74(1):5–13

226. Ryu JJ, Shrotriya P. 2013. Synergistic mechanisms of bio-tribocorrosion in medical implants. In *Bio-Tribocorrosion in Biomaterials and Medical Implants*, pp. 25–44

227. Saag KG, Furst DE, Greene JM. 2008. Major side effects of systemic glucocorticoids

228. Sabio G, Davis R. 2014. TNF-a and MAP kinase signalling pathways. *Semin. Immunol.* 26(3):237–45

229. Sabzi M, Mirabedini SM, Zohuriaan-Mehr J, Atai M. 2009. Surface

modification of TiO2 nano-particles with silane coupling agent and investigation of its effect on the properties of polyurethane composite coating. *Prog. Org. Coatings*. 65(2):222–28

230.   Salerno A, Hermann R. 2006. Efficacy and safety of steroid use for postoperative pain relief. Update and review of the medical literature. *J. Bone Joint Surg. Am.* 88(6):1361–72

231.   Santos A, Aw MS, Bariana M, Kumeria T, Wang Y, Losic D. 2014. Drug-releasing implants: current progress, challenges and perspectives. *J. Mater. Chem. B*. 2(37):6157–82

232.   Santos AC, Caldas M, Pattekari P, Fontes Ribeiro C, Ribeiro AJ, et al. 2018. Chapter 16 – Layer-by-Layer coated drug-core nanoparticles as versatile delivery platforms. *Des. Dev. New Nanocarriers*. 595–635

233.   Saxena RK, Vallyathan V, Lewis DM. 2003. Evidence for lipopolysaccharideinduced differentiation of RAW264.7 murine macrophage cell line into dendritic like cells. *J. Biosci.* 28(1):129–34

234.   Schäcke H, Döcke WD, Asadullah K. 2002. Mechanisms involved in the side effects of glucocorticoids. *Pharmacol. Ther.* 96(1):23–43

235.   Schroer WC, Berend KR, Lombardi A V., Barnes CL, Bolognesi MP, et al. 2013. Why are total knees failing today? Etiology of total knee revision in 2010 and 2011. *J. Arthroplasty*. 28(8 SUPPL):116–19

236.   Schuh JCL. 2008. Medical Device Regulations and Testing for Toxicologic Pathologists. *Toxicol. Pathol.* 36(1):63–69

237.   Sedger LM, McDermott MF. 2014. TNF and TNF-receptors: From mediators of cell death and inflammation to therapeutic giants - past, present and future

238.   Sharma JN, Al-Omran A, Parvathy SS. 2007. Role of nitric oxide in inflammatory diseases. *Inflammopharmacology*. 15(6):252–59

239.   Shiratori SS, Rubner MF. 2000. pH-dependent thickness behavior of sequentially adsorbed layers of weak polyelectrolytes. *Macromolecules*. 33(11):4213–19

240.   Sidney LE, Heathman TRJ, Britchford ER, Abed A, Rahman C V., Buttery LDK. 2015. Investigation of Localized Delivery of Diclofenac Sodium from Poly(D,L-Lactic Acid- *co* -Glycolic Acid)/Poly(Ethylene Glycol) Scaffolds Using an *In Vitro* Osteoblast Inflammation Model. *Tissue Eng. Part A*. 21(1–2):362–73

241.   Silva JM, Caridade SG, Costa RR, Alves NM, Groth T, et al. 2015. PH Responsiveness of Multilayered Films and Membranes Made of Polysaccharides. *Langmuir*. 31(41):11318–28

242.   Singh AK. 2016. Experimental Methodologies for the Characterization of Nanoparticles. In *Engineered Nanoparticles*, pp. 125–70

243.   Singhatanadgit W. 2009. Biological Responses to New Advanced Surface Modifications of Endosseous Medical Implants. *Bone Tissue Regen. Insights*. 2:1–11

244.   Siyamak S, Ibrahim NA, Abdolmohammadi S, Wan Yunus WMZ, Rahman MZAB. 2012. Effect of fiber esterification on fundamental properties of oil palm empty fruit bunch fiber/poly(butylene adipate-co-terephthalate) biocomposites. *Int. J. Mol. Sci.* 13(2):1327–46

245.   Slack SM, Horbett TA. 1995. The Vroman Effect. In *Proteins at Interfaces II: Fundamentals and Applications*, Vol. 602, pp. 112–28

246.   Smith C, Erasmus PJ, Myburgh KH. 2006. Endocrine and immune effects of dexamethasone in unilateral total knee replacement. *J. Int. Med. Res.* 34(6):603–11

247.   Sobieszczyk S, Klotzke R. 2011. Nanotubular titanium oxide layers for enhancement of bone-implant bonding and bioactivity. *Adv. Mater. Sci.* 11(1):17–26

248.   Solary E. 2012. When monocyte life hangs by a thread. *Blood*. 119(12):2699–2700

249.   Soromou LW, Zhang Z, Li R, Chen N, Guo W, et al. 2012. Regulation of inflammatory cytokines in lipopolysaccharide-stimulated RAW 264.7 murine macrophage by 7-O-methyl-naringenin. *Molecules*. 17(3):3574–85

250.   Sousa CT, Nunes C, Proença MP, Leitão DC, Lima JLFC, et al. 2012. PH sensitive silica nanotubes as rationally designed vehicles for NSAIDs delivery. *Colloids Surfaces B Biointerfaces*. 94:288–95

251.   Sun D, Zhuang X, Xiang X, Liu Y, Zhang S, et al. 2010. A novel nanoparticle drug delivery system: The anti-inflammatory activity of curcumin is enhanced when encapsulated in exosomes. *Mol. Ther.* 18(9):1606–14

252.   Sun J, Zhang X, Broderick M, Fein H. 2003. Measurement of Nitric Oxide Production in Biological Systems by Using Griess Reaction Assay. *Sensors*. 3(8):276–84

253.   Taha M, Chai F, Blanchemain N, Goube M, Martel B, Hildebrand HF. 2013. Validating the poly-cyclodextrins based local drug delivery system on plasma-sprayed hydroxyapatite coated orthopedic implant with toluidine blue O. *Mater. Sci. Eng. C*. 33(5):2639–47

254.   Takakubo Y, Berce A, Trebše R, Tamaki Y, Milošev I, et al. 2013. Wear and corrosion in the loosening of total joint replacements (TJRs). In *Bio-*

Tribocorrosion in Biomaterials and Medical Implants, pp. 74–110

255.   Takashiba S, Van Dyke TE, Amar S, Murayama Y, Soskolne AW, Shapira L. 1999. Differentiation of monocytes to macrophages primes cells for lipopolysaccharide stimulation via accumulation of cytoplasmic nuclear factor κB. *Infect. Immun.* 67(11):5573–78

256.   Talmo CT, Shanbhag AS, Rubash HE. 2006. Nonsurgical management of osteolysis: Challenges and opportunities. *Clin. Orthop. Relat. Res.*, pp. 254–64

257.   Talorete TPN, Bouaziz M, Sayadi S, Isoda H. 2006. Influence of medium type and serum on MTT reduction by flavonoids in the absence of cells. *Cytotechnology*. 52(3):189–98

258.   Tamaki Y, Sasaki K, Sasaki A, Takakubo Y, Hasegawa H, et al. 2008. Enhanced osteolytic potential of monocytes/macrophages derived from bone marrow after particle stimulation. *J. Biomed. Mater. Res. - Part B Appl. Biomater.* 84(1):191–204

259.   Tang Z, Wang Y, Podsiadlo P, Kotov NA. 2006. Biomedical applications of layer-by-layer assembly: From biomimetics to tissue engineering

260.   Tavakoli-Darestani R, Manafi-Rasi A, Kamrani-Rad A. 2014. Dexamethasone-loaded hydroxyapatite enhances bone regeneration in rat calvarial defects. *Mol. Biol. Rep.* 41(1):423–28

261.   Tejero R, Anitua E, Orive G. 2014. Toward the biomimetic implant surface: Biopolymers on titanium-based implants for bone regeneration

262.   Terra X, Valls J, Vitrac X, Mérrillon JM, Arola L, et al. 2007. Grape-seed procyanidins act as antiinflammatory agents in endotoxin-stimulated RAW 264.7 macrophages by inhibiting NFkB signaling pathway. *J. Agric. Food Chem.* 55(11):4357–65

263.   The NJR Editorial Board. 2016. 13th Annual Report-National Joint Registry for England, Wales, Northern Ireland and the Isle of Man

264.   Torrecillas R, Moya JS, Draz LA, Bartolomé JF, Fernández A, Lopez-esteban S. 2009. Nanotechnology in joint replacement

265.   Tweedie D, Luo W, Short RG, Brossi A, Holloway HW, et al. 2009a. A cellular model of inflammation for identifying TNF-α synthesis inhibitors. *J. Neurosci. Methods*. 183(2):182–87

266.   Tweedie D, Luo W, Short RG, Brossi A, Holloway HW, et al. 2009b. A cellular model of inflammation for identifying TNF-alpha synthesis inhibitors. *J. Neurosci. Methods*. 183(2):182–87

267.   Ukaji E, Furusawa T, Sato M, Suzuki N. 2007. The effect of surface

modification with silane coupling agent on suppressing the photo-catalytic activity of fine TiO2 particles as inorganic UV filter. *Appl. Surf. Sci.* 254(2):563–69

268.   Ulrich SD, Seyler TM, Bennett D, Delanois RE, Saleh KJ, et al. 2008. Total hip arthroplasties: What are the reasons for revision? *Int. Orthop.* 32(5):597–604

269.   Urbanska J, Karewicz A, Nowakowska M. 2014. Polymeric delivery systems for dexamethasone

270.   Vairappan C, Kamada T, Lee W-W, Jeon Y-J. 2013. Anti-inflammatory activity of halogenated secondary metabolites of Laurencia snackeyi (Weber-van Bosse) Masuda in LPS-stimulated RAW 264.7 macrophages. *J. Appl. Phycol.* 25(6):1805–13

271.   Vallejo-Heligon SG, Brown NL, Reichert WM, Klitzman B. 2016. Porous, Dexamethasone-loaded polyurethane coatings extend performance window of implantable glucose sensors in vivo. *Acta Biomater.* 30:106–15

272.   Vallés G, Pérez C, Boré A, Martín-Saavedra F, Saldaña L, Vilaboa N. 2013. Simvastatin prevents the induction of interleukin-6 gene expression by titanium particles in human osteoblastic cells. *Acta Biomater.* 9(1):4916–25

273.   Values T, Hip T, Materials P. 2005. Standard Specification for Total Hip Joint Prosthesis and Hip Endoprosthesis Bearing Surfaces Made of Metallic , Ceramic , and Polymeric. *Components.* (June):1–5

274.   van der Bruggen T, Nijenhuis S, van Raaij E, Verhoef J, Sweder van Asbeck B. 1999. Lipopolysaccharide-Induced Tumor Necrosis Factor Alpha Production by Human Monocytes Involves the Raf-1/MEK1-MEK2/ERK1-ERK2 Pathway. *Infect. Immun.* 67(8):3824–29

275.   van Helden SFG, van Leeuwen FN, Figdor CG. 2008. Human and murine model cell lines for dendritic cell biology evaluated. *Immunol. Lett.* 117(2):191–97

276.   Van Manen MD, Nace J, Mont M a. 2012. Management of primary knee osteoarthritis and indications for total knee arthroplasty for general practitioners. *J. Am. Osteopath. Assoc.* 112(11):709–15

277.   Vandevyver S, Dejager L, Tuckermann J, Libert C. 2013. New insights into the anti-inflammatory mechanisms of glucocorticoids: An emerging role for glucocorticoid-receptor-mediated transactivation

278.   von Knoch F, Marchie A, Malchau H. 2010. Total joint registries: a foundation for evidence-based arthroplasty. *Virtual Mentor.* 12(2):124–29

279.   von Wilmowsky C, Moest T, Nkenke E, Stelzle F, Schlegel KA ndreas. 2014. Implants in bone: part I. A current overview about tissue response, surface

modifications and future perspectives

280.   Vuk AŠ, Ješe R, Orel B, Dražič G. 2005. The effect of surface hydroxyl groups on the adsorption properties of nanocrystalline TiO2 films. *Int. J. Photoenergy*. 7(4):163–68

281.   Waldron NH, Jones CA, Gan TJ, Allen TK, Habib AS. 2013. Impact of perioperative dexamethasone on postoperative analgesia and side-effects: Systematic review and meta-analysis. *Br. J. Anaesth.* 110(2):191–200

282.   Wang D, Miller SC, Liu X-M, Anderson B, Wang XS, Goldring SR. 2007. Novel dexamethasone-HPMA copolymer conjugate and its potential application in treatment of rheumatoid arthritis. *Arthritis Res. Ther.* 9(1):R2

283.   Wang H, Rempel GL. 2013. PH-responsive polymer core-shell nanospheres for drug delivery. *J. Polym. Sci. Part A Polym. Chem.* 51(20):4440–50

284.   Wang S, Wen S, Shen M, Guo R, Cao X, et al. 2011. Aminopropyltriethoxysilane-mediated surface functionalization of hydroxyapatite nanoparticles: synthesis, characterization, and in vitro toxicity assay. *Int. J. Nanomedicine*. 6:3449–59

285.   Wang T, Jiang H, Wan L, Zhao Q, Jiang T, et al. 2015a. Potential application of functional porous TiO2 nanoparticles in light-controlled drug release and targeted drug delivery. *Acta Biomater.* 13:354–63

286.   Wang W-R, Li A, Mei W, Zhu R-R, Li K, et al. 2015b. Dexamethasone sodium phosphate intercalated layered double hydroxides and their therapeutic efficacy in a murine asthma model. *RSC Adv.* 5(30):23826–34

287.   Wang X, Chen D, Cao L, Li Y, Boyd BJ, Caruso RA. 2013. Mesoporous titanium zirconium oxide nanospheres with potential for drug delivery applications. *ACS Appl. Mater. Interfaces*. 5(21):10926–32

288.   Wernecke C, Braun HJ, Dragoo JL. 2015. The effect of intra-articular corticosteroids on articular cartilage: A systematic review. *Orthop. J. Sport. Med.* 3(5):1–7

289.   Wissink MJB, Beernink R, Pieper JS, Poot AA, Engbers GHM, et al. 2001. Immobilization of heparin to EDC/NHS-crosslinked collagen. Characterization and in vitro evaluation. *Biomaterials*. 22(2):151–63

290.   Wojdasiewicz P, Poniatowski ŁA, Szukiewicz D. 2014. The role of inflammatory and anti-inflammatory cytokines in the pathogenesis of osteoarthritis

291.   Wood KC, Boedicker JQ, Lynn DM, Hammond PT. 2005. Tunable drug release from hydrolytically degradable layer-by-layer thin films. *Langmuir*.

21(4):1603–9

292.   Wu C-H, Chen T-L, Chen T-G, Ho W-P, Chiu W-T, Chen R-M. 2003. Nitric oxide modulates pro- and anti-inflammatory cytokines in lipopolysaccharide-activated macrophages. *J. Trauma*. 55:540–45

293.   Wu D, Chen X, Chen T, Ding C, Wu W, Li J. 2015. Substrate-anchored and degradation-sensitive anti-inflammatory coatings for implant materials. *Sci. Rep.* 5:11105

294.   Wu EC, Andrew JS, Buyanin A, Kinsella JM, Sailor MJ. 2011. Suitability of porous silicon microparticles for the long-term delivery of redox-active therapeutics. *Chem. Commun.* 47(20):5699

295.   Wu P, Grainger DW. 2006. Drug/device combinations for local drug therapies and infection prophylaxis

296.   Wu S, Weng Z, Liu X, Yeung KWK, Chu PK. 2014. Functionalized TiO2 based nanomaterials for biomedical applications. *Adv. Funct. Mater.* 24(35):5464–81

297.   Yamamoto Y, Gaynor RB. 2001. Therapeutic potential of inhibition of the NF-kappaB pathway in the treatment of inflammation and cancer. *J. Clin. Invest.* 107(2):135–42

298.   Yang X, Kang M-C, Li Y, Kim E-A, Kang S-M, Jeon Y-J. 2014. Anti-inflammatory activity of questinol isolated from marine-derived fungus Eurotium amstelodami in lipopolysaccharide-stimulated RAW 264.7 macrophages. *J. Microbiol. Biotechnol.* 24(10):1346–53

299.   Yodyingyong S, Sae-Kung C, Panijpan B, Triampo W, Triampo D. 2011. Physicochemical properties of nanoparticles titania from alcohol burner calcination. *Bull. Chem. Soc. Ethiop.* 25(2):263–72

300.   Yoon W-J, Lee NH, Hyun C-G. 2010. Limonene Suppresses Lipopolysaccharide-Induced Production of Nitric Oxide, Prostaglandin E2, and Pro-inflammatory Cytokines in RAW 264.7 Macrophages. *J. Oleo Sci.* 59(8):415–21

301.   Yoshioka Y, Yamamuro a, Maeda S. 2003. Nitric oxide at a low concentration protects murine macrophage RAW264 cells against nitric oxide-induced death via cGMP signaling pathway. *Br. J. Pharmacol.* 139(1):28–34

302.   Yuan F, Chen J, Sun PP, Guan S, Xu J. 2013. Wedelolactone inhibits LPS-induced pro-inflammation via NF-kappaB Pathway in RAW 264.7 cells. *J. Biomed. Sci.* 20(1):84

303.   Zamora R, Vodovotz Y, Billiar TR. 2000. Inducible nitric oxide synthase and inflammatory diseases. *Mol. Med.* 6:347–73

304.   Zaveri TD, Lewis JS, Dolgova N V., Clare-Salzler MJ, Keselowsky BG. 2014. Integrin-directed modulation of macrophage responses to biomaterials. *Biomaterials*. 35(11):3504–15

305.   Zhang BGX, Myers DE, Wallace GG, Brandt M, Choong PFM. 2014a. Bioactive coatings for orthopaedic implants-recent trends in development of implant coatings

306.   Zhang J-M, An J. 2007. Cytokines, Inflammation and Pain. *Int Anesth. Clin.* 45(2):27–37

307.   Zhang J, Liu Y, Luo R, Chen S, Li X, et al. 2015. In vitro hemocompatibility and cytocompatibility of dexamethasone-eluting PLGA stent coatings. *Appl. Surf. Sci.* 328:154–62

308.   Zhang Z, Nix CA, Ercan UK, Gerstenhaber JA, Joshi SG, Zhong Y. 2014b. Calcium binding-mediated sustained release of minocycline from hydrophilic multilayer coatings targeting infection and inflammation. *PLoS One*. 9(1):

309.   Zhao AS, Zhou S, Wang Y, Chen J, Ye CR, Huang N. 2014. Molecular interaction of fibrinogen with thermally modified titanium dioxide nanoparticles. *RSC Adv.* 4(76):40428–34

310.   Zhao J, Milanova M, Warmoeskerken MMCG, Dutschk V. 2012. Surface modification of TiO2 nanoparticles with silane coupling agents. *Colloids Surfaces A Physicochem. Eng. Asp.* 413(September):273–79

311.   Zhao YP, Wei JL, Tian QY, Liu AT, Yi YS, et al. 2016. Progranulin suppresses titanium particle induced inflammatory osteolysis by targeting TNFalpha signaling. *Sci Rep*. 6(February):20909

312.   Zilberman M, Kraitzer A, Grinberg O, Elsner JJ. 2010. Drug-eluting medical implants

313.   Zolnik BS, Burgess DJ. 2007. Effect of acidic pH on PLGA microsphere degradation and release. *J. Control. Release*. 122(3):338–44

I. Appendix

A. Preliminary *in vitro* studies

Cell density optimization

Initially the aim of this study was to assess the behaviour of Raw macrophages 264.7 cell line upon exposure to dexamethasone-loaded functionalised TiO_2 particles for 7 days. To start these experiments, we decided to use the cell density reported in similar reports (Pinho et al. 2011), where a density of 1.5 x 10^4 cells/well was initially utilized for LPS-activated macrophages studies. The first preliminary cytotoxicity studies were performed for 7 days, although we noticed that after 5 days of culture the macrophages started overgrowing the well (Figure 71).
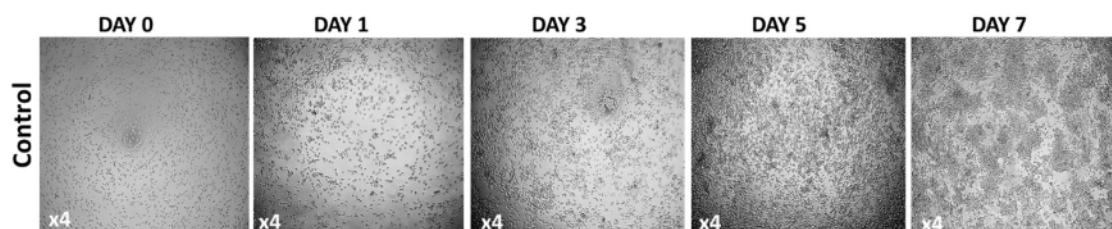
Figure 71. Raw 264.6 cells growth, with cell seeding density of 1.5 x 10^4 cells/well, was observed with inverted microscope for 7 days. All pictures have x4 magnification.

The MTT assay performed for 5 days, showed that this cell overgrowing was indeed causing a remarkable decrease of viability, when cells were exposed to dexamethasone and LPS combination or LPS alone (data not shown). Leading to the conclusion that the low cellular viability (<50%) observed was not caused by the treatments but due to the excess of cells inside the well (Figure 71). After performing preliminary cytotoxicity studies and observed the reduced cellular viability after 5 days of culture, we decided to study the cellular viability and nitric oxide production for only 3 days. This was a crucial parameter for our study, mainly because cytotoxicity has been related to NO production (Kröncke et al. 1997, Yoshioka et al. 2003). Therefore, the low cellular viability due to cell death observed could result in NO production, and lead to false results for the studies performed in LPS-activated cells.

Preliminary toxicity studies (RPMI media)

After optimizing the cell density (1.5×10^4 cells/well) and number of culture days (3 days), the cellular viability was then assessed when cells were exposed to DEX, and to the broths, collected from amino and mercapto routes (*Figure 72*).these results showed that only higher concentration of DEX ($>100 \mu$g/mL) significantly reduced cellular viability.
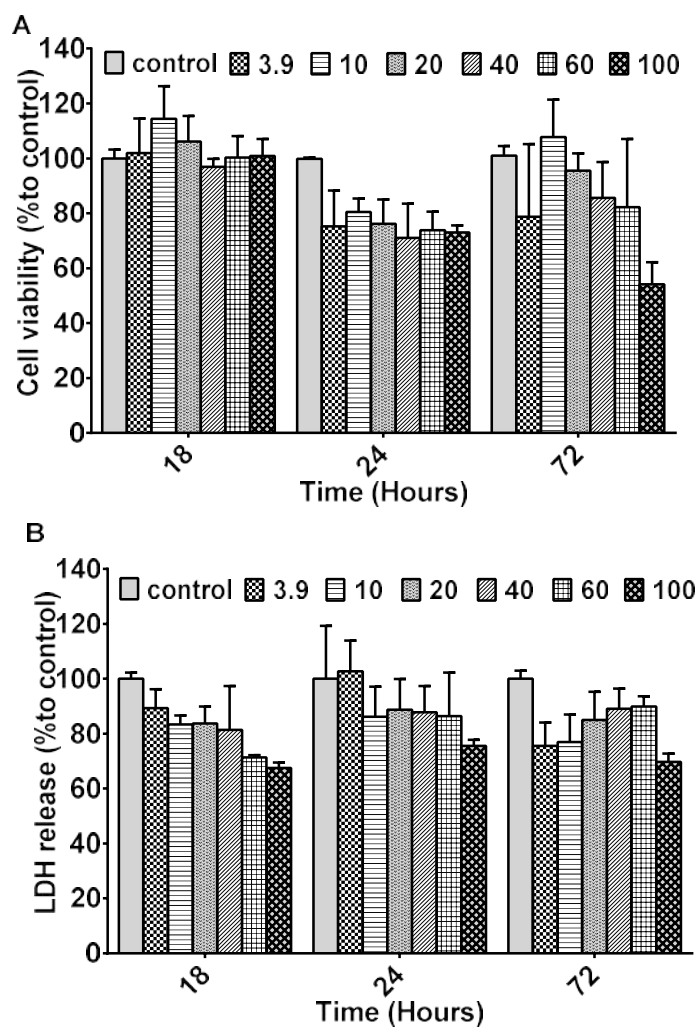
Figure 72. Effect of dexamethasone in cell viability. RAW 264.7 macrophages were exposed to range of concentrations between 3.9 and 100 µg/mL during 18h, 24h, and 72 hours. Cell viability was assessed by MTT (a) and LDH assay (b).
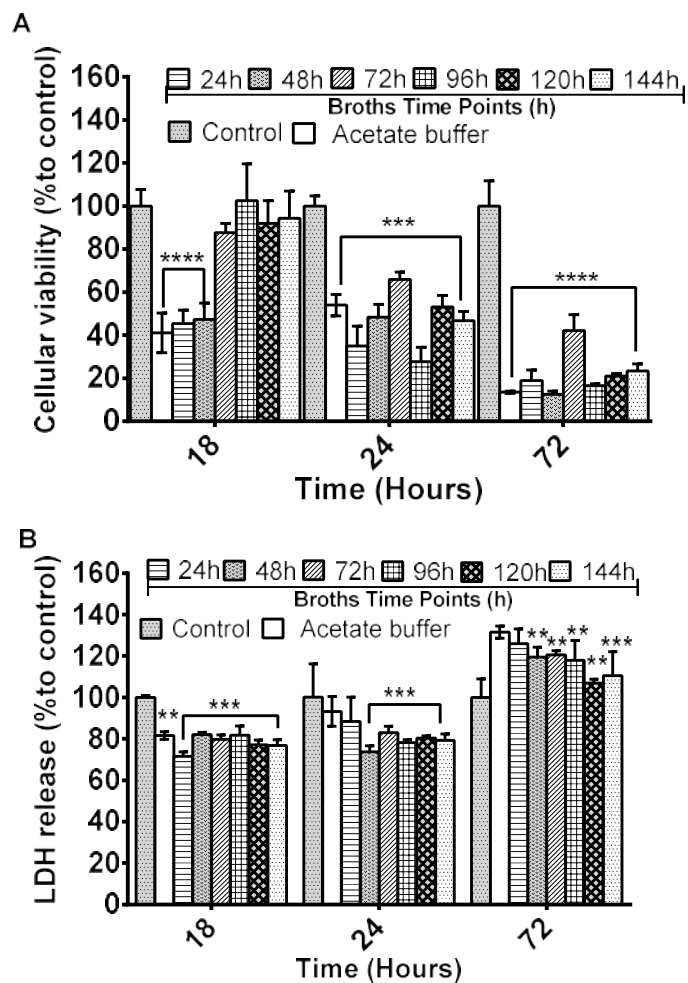
Figure 73. Effect of broths, collected different time points (24h-144h) from drug release studies (Amino Route) performed at pH 4, in cell viability. RAW 264.7 macrophages were exposed to broths during 18h, 1day, and 3 days. Cell viability was assessed by MTT (a) and LDH assay (b).
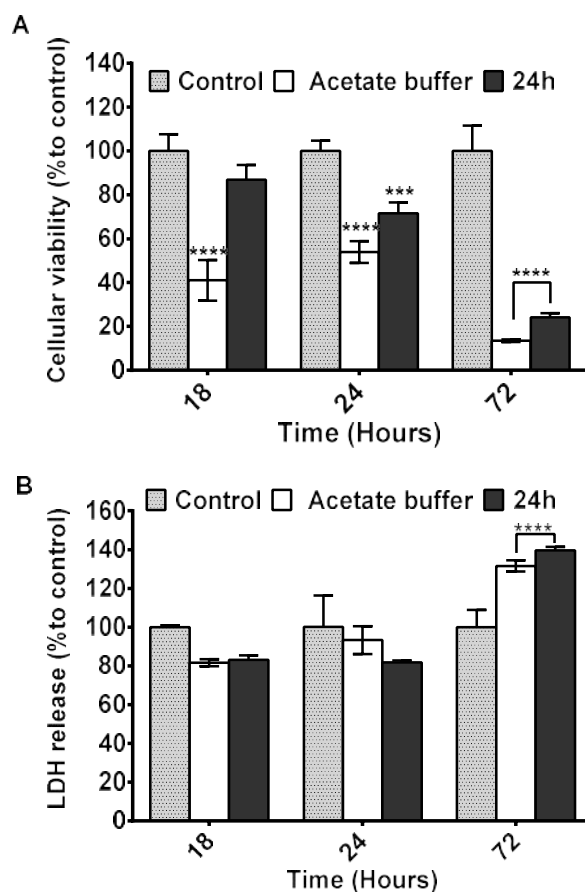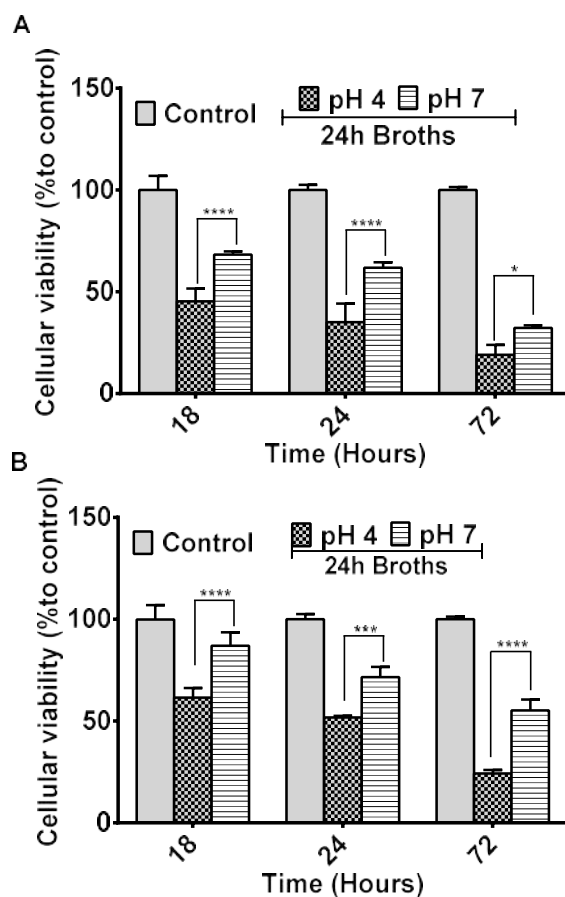
Figure 74. Effect of broths, collected at 24h time point, from drug release studies (Mercapto Route) performed at pH 4, in cell viability. RAW 264.7 macrophages were exposed to broths during 18h, 1day, and 3 days. Cell viability was assessed by MTT (a) and LDH assay (b).

When cells were exposed to broths collected from drug release studies performed at pH=4, results obtained (Amino Figure 73, and Mercapto Figure 74) show that for all broths tested the cellular viability was very low (<50% when compared to control), especially after 72h exposure. Moreover, broths obtained from the drug release studies of particles obtained via mercapto and amino route present very similar results, in other words all treatments collect from drug release studies performed at pH=4 cause a significant decrease (p<0.05) on cellular viability which was clearly time-dependent.
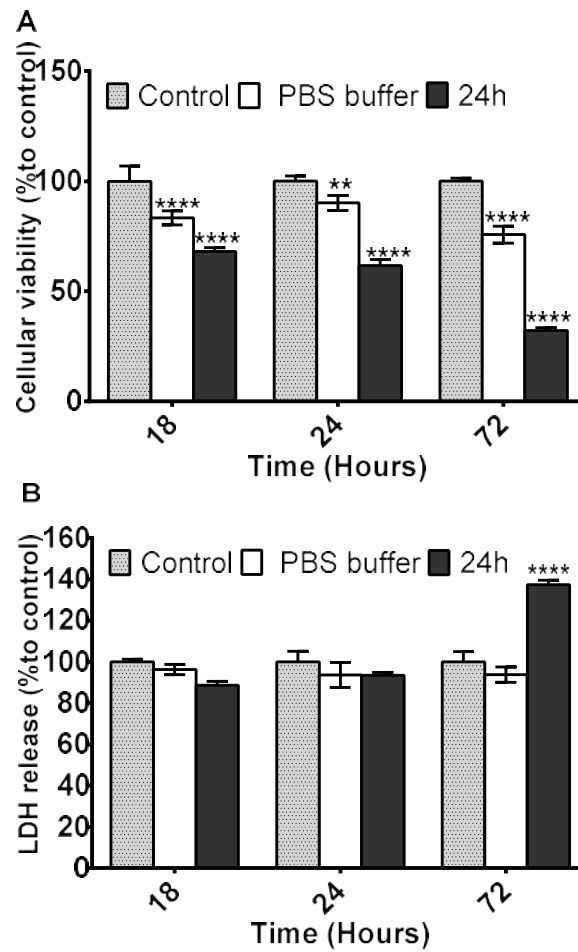
Figure 75. Effect of broths, collected at 24h time point) from drug release studies (Amino Route) performed at pH 7, in cell viability. RAW 264.7 macrophages were exposed to broths during 18h, 1 day, and 3 days. Cell viability was assessed by MTT (a) and LDH assay (b).

The cells exposed to broths collected from drug release studies performed at pH=7 (Amino Figure 75, and Mercapto Figure 76) still showed low cellular viability low (>60-70%) when compared to control, and was also time-dependent. Nonetheless the cellular viability when cells were exposed to broth collected at pH=7 was significantly higher (p<0.01) than the one observed for pH=4 (

Figure 77). For this reason, only broth collected at pH=6 and 7 were tested on the cells.
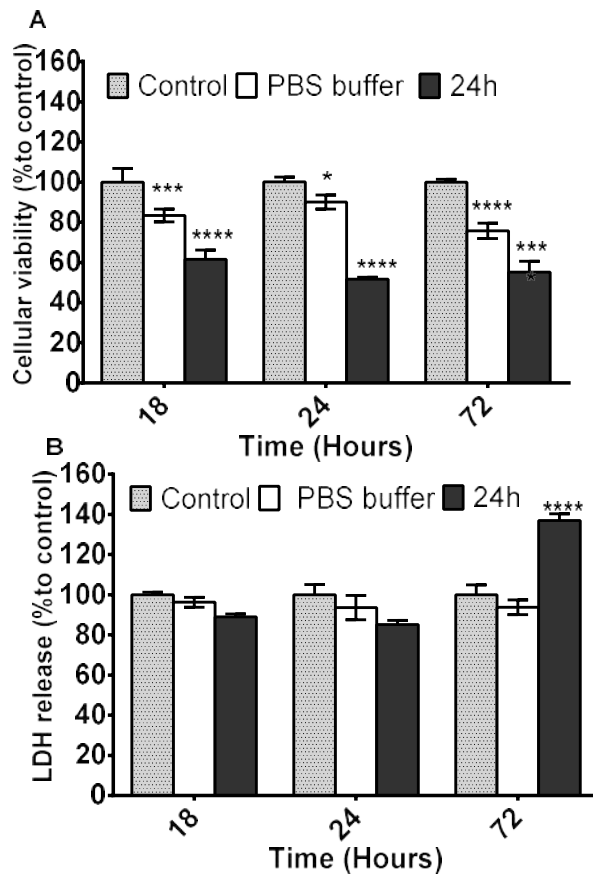
Figure 76. Effect of broths, collected at 24h time point, from drug release studies (Mercapto Route) performed at pH 7, in cell viability. RAW 264.7 macrophages were exposed to broths during 18h, 1day, and 3 days. Cell viability was assessed by MTT (a) and LDH assay (b).

Figure 77. Comparison of broths effect on cell viability, when collected from drug release studies performed at pH 4 and 7 for (A) amino and (B) mercapto routes. RAW 264.7 macrophages were exposed to 24h time point broths during 18, 24, and 72 hours. Cell viability was assessed by MTT assay.

Culture media change: From RPMI to DMEM Media

As a next step in this study, the NO production in LPS-activated cells was measured. Although initially we didn't get reproducible data, because RPMI 1640 medium (RPMI) has calcium nitrate in its composition (0.1g/L), which altered the levels of NO measured. This originated erratic results, where control cells (cells only exposed to media) showed higher NO production than LPS activated cells. Therefore, we decided to grow cells in DMEM media, which is known to have undetectable levels of nitrate. The nutrient content and concentrations, which vary in different culture media, are known to regulate physicochemical and physiological parameters of cells, such as growth (Iloki Assanga et al. 2013). Previous studies (Cohly et al. 2001, Kawakami et al. 2016) have shown that activation of various macrophages was influenced by culture medium. Particularly, Kawakami and co-workers (2016) showed that the NO production and iNOS expression in LPS-activated macrophages were remarkably different when different culture media,

F-12 and DMEM, were utilized. As previously reported (Talorete et al. 2006) the culture medium type has a significant effect on MTT reduction, particularly when it is used to measure cytotoxicity. For this reason, we decided to repeat all the cellular viability experiments, previously done with RPMI media for dexamethasone, with and without LPS.
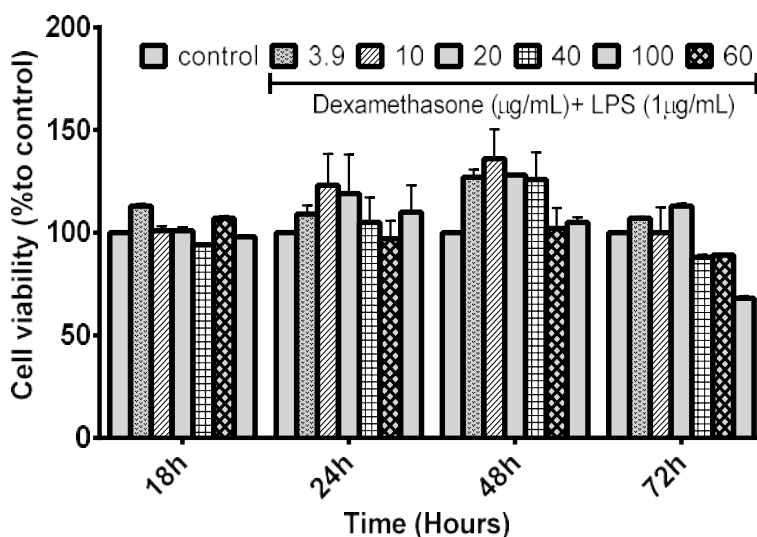
DEXAMETHASONE

Therefore, the cellular viability of DMEM-cultured Raw macrophages when exposed to DEX was assessed (Figure 78). Methylthiazolyl Tetrazolium (MTT) assay (Figure 78.a), and Lactase dehydrogenase assay (LDH release) (Figure 78.b) were used as indicators of cellular viability.
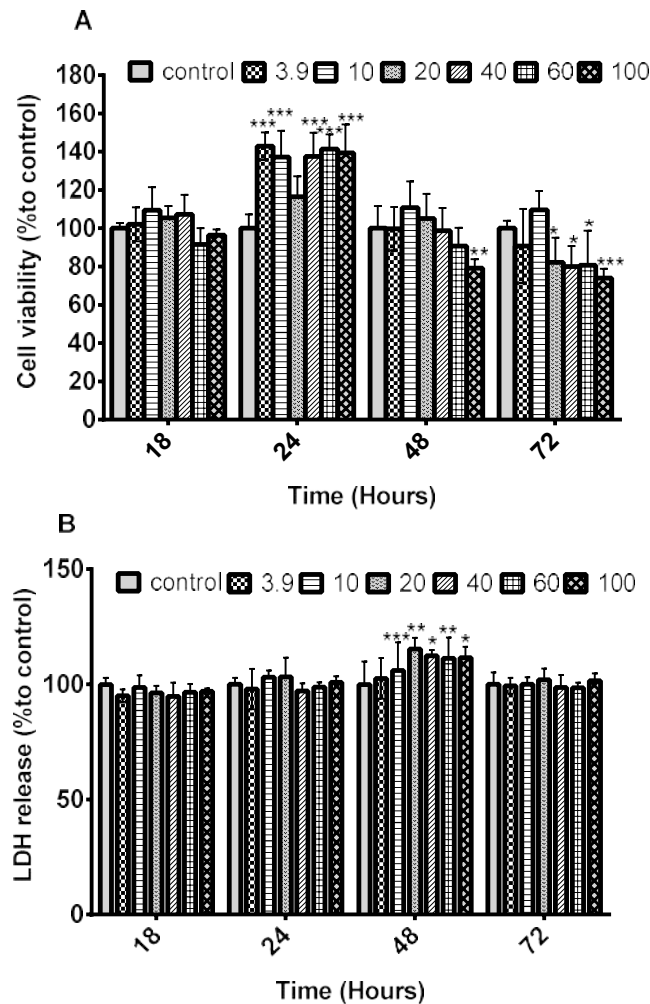

Figure 78. Effect of dexamethasone in cell viability. RAW 264.7 macrophages were exposed to range of concentrations between 3.9 and 100 µg/mL during 18h, 1day, 2 days and 3 days. Cell viability was assessed by MTT (a) and LDH assay (b).

Based on MTT assay, results show that exposure to dexamethasone concentrations up to 20 µg/mL during 72h exposure, did not show to considerable/significant (p>0.05) decrease the cellular viability of Raw 264.7 cells. The cellular viability observed for these concentrations was very close to values observed for the control.

On the other hand, higher concentrations of DEX, such as 40, 60 and 100 µg/mL, show to affect cellular viability in a significant way (p<0.05). Where the higher decrease on cellular viability, 20% when compared to the control, was observed after 72h, when cells were exposed to a dexamethasone concentration of 100 µg/mL. Moreover, after 24h exposure, macrophages show an increase on cell viability when compared to control (Figure 78.a). These differences in cell viability were not verified in the LDH assay (Figure 78.b). Results obtained with LDH assay, show that when exposed to all dexamethasone concentrations (3.9-100 µg/mL), macrophages release only release significant (p<0.05) amounts of LDH after 48h exposure. Therefore, as MTT assay allowed detecting more alterations on cellular viability than the measure of LDH release, the results presented herein for cell viability after treatments with broths and LPS were obtained by MTT assay. Regarding these differences observed for cell viability measured by MTT and LDH, the same results were reported by other authors (Pinho et al., 2011) where Raw 264.4 cells were exposed to DEX. Thus, showing that MTT assay is more sensitive in detecting alterations on cells survival than the measure of LDH release.

Figure 79. Effect of dexamethasone in cell viability of LPS-activated cells. RAW 264.7 macrophages were exposed to range of concentrations between 3.9 and 100 µg/mL and also to LPS (1µg/mL) during 18h, 1day, 2 days and 3 days. Cell viability was assessed by MTT assay.

NO production inhibition

By the second year of the PhD (August-October 2016), we had to discard the Raw 264.7 cells, because they stopped producing nitric oxide. Before discarding the cells, we tried to understand what was beyond the lack of NO production. Initially, the LPS activation experiment was repeated by starting to stimulate the cells with different concentrations of LPS to see how the cells reacted. Results obtained from this experiment (Figure 80). show that the amount of NO measured (μM/mL) was the same for LPS-activated cells (1 or 0.5μg/mL) or untreated cells (control) for all time points.
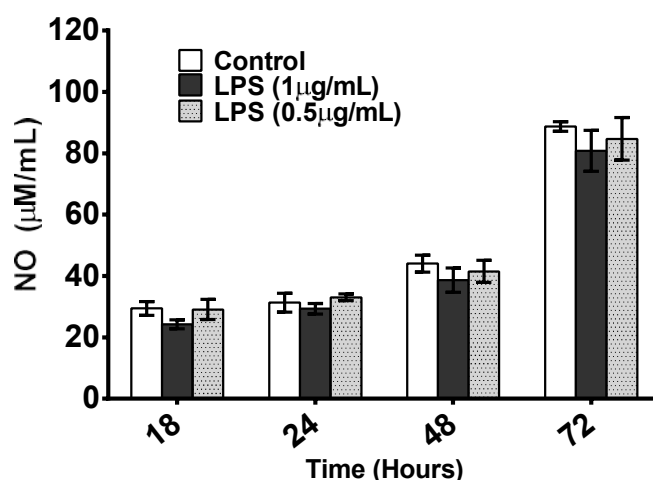
Figure 80. Nitric oxide (NO) production upon exposure to LPS during 18h, 24h, 48h and 72h.

Our next step was to measure the amount of NO on nitrite standard solutions (10 and 20 µM/mL), to assess if the Griess Reagent kit was still working (data not shown). We also tested the cells for mycoplasma (data not shown). The results obtained showed that both hypothesis was wrong, cells were not contaminated by neither mycoplasma or the Griess reagent was not working. As reported previously (Lai et al. 2014, Tweedie et al. 2009a) , we know that when exposed to LPS, macrophages (M0) undergo classical activation, where they differentiate into M1 macrophages. The classical activated M1 macrophages produce pro-inflammatory cytokines and also activate iNOS pathway, which is essential for generating NO molecule (Bogdan 2001, Kawakami et al. 2016). In contrast, when macrophages are exposed to anti-inflammatory stimulus, such as IL-4 or transforming growth factor β (TGF-β) (Gong et al. 2012, Oida & Weiner 2010), they undergo an alternative activation and become polarized into M2 macrophages. Being anti-inflammatory, these macrophages produce anti-inflammatory cytokines, which cause an increased expression of Arginase-1, an enzyme which competes with iNOS for a common limiting substrate L-arginine. So macrophage polarization states will depend on

the induction of iNOS (M1) or Arginase-1 (M2), which compete for the same L-arginine substrate (Mills & Ley 2014). Therefore, our hypothesis was that the batch of fetal bovine serum (FBS) had significant amounts of TGF-β (anti-inflammatory cytokine), which hindered the M1 polarization, and thus inhibited the macrophages ability to produce NO in response to LPS. This hypothesis is consistent with other studies (Haak-Frendscho et al. 1990, Hausmann et al. 1994), which also reported the inhibitory effect of TGF- β on iNOS mRNA expression/NO production by LPS-activated Raw 264.7 cells.

B. Complementary Images

HPLC calibration curve for DEX

To evaluate the concentration of DEX in the samples collected, a calibration curve of the HPLC detection of DEX was obtained (Figure 81). Briefly, a standard calibration curve was obtained by plotting the concentration (µg/mL) of standard DEX versus peak area (mAu). To prepare the standards, a stock solution of DEX (1mg/mL) was diluted to a range of concentration between 0.4 and 25 µg/mL. Results are presented as the average and standard deviation of three samples.
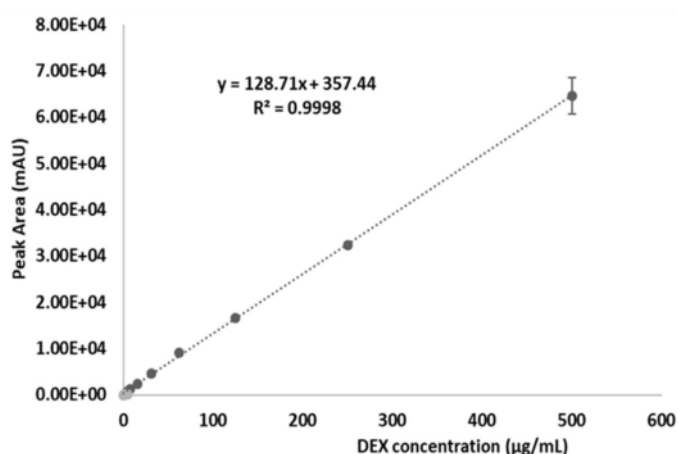
Figure 81. DEX standard calibration curve for different DEX concentrations (0-500 µg/mL)

Calibration curve for Nitric oxide (NO)

A standard calibration curve to quantify nitrite concentration on biological samples was generated using sodium nitrite ($NaNO_2$) as an external standard.
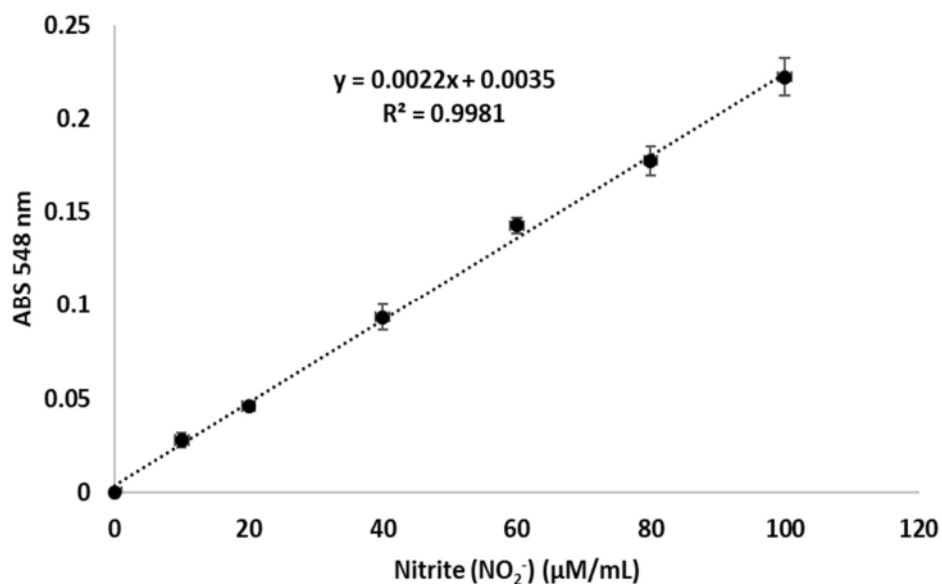
Figure 82 Standard curve for nitrite (NO_2^-) (colorimetric): mean of triplicates (+/-SD) with background readings subtracted.

## *Calibration curve for tumour necrosis factor alpha (TNF-α).*
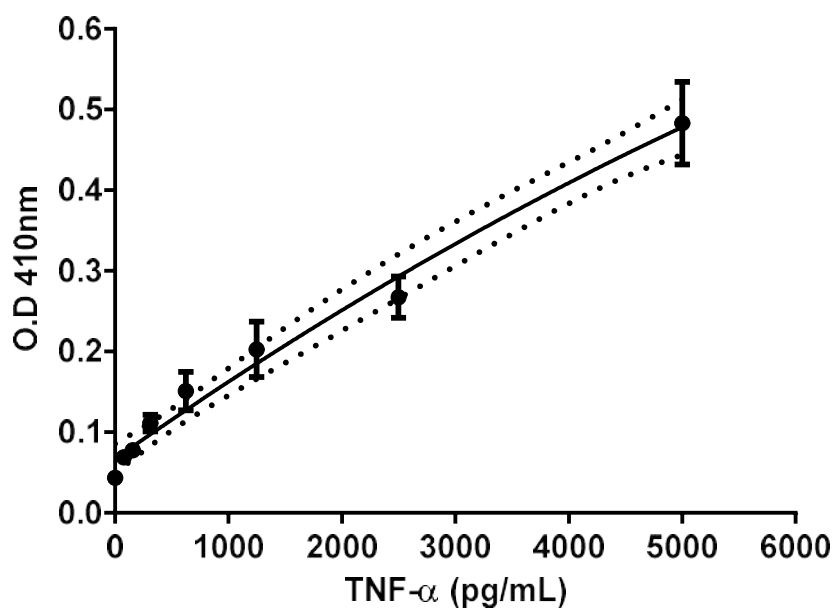
*Figure 83. Standard curve for murine tumour necrosis factor alpha (TNF-α).*

Raw 264.7 Cell Studies
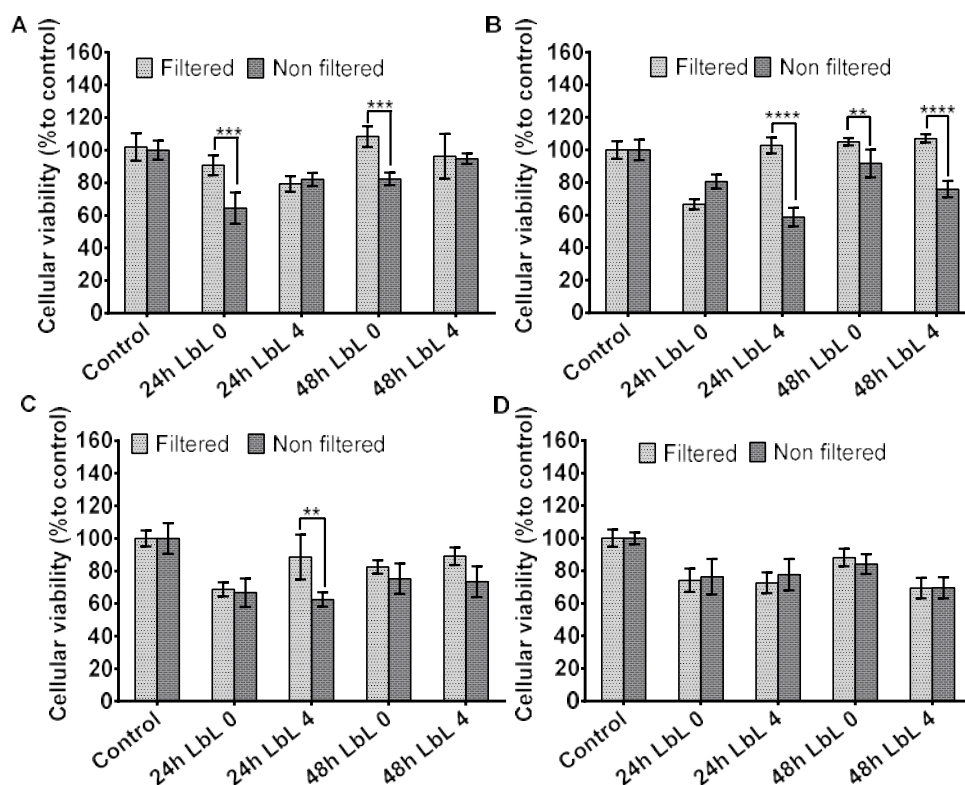
Figure 84. Effect of filtered and non-filtered broths, collected from drug release studies (LbL Route) performed at pH 6, in cell viability. RAW 264.7 macrophages were exposed to broths during (A) 18h, (B) 24h, (C) 48h and (D) 72 hours. Cell viability was assessed by MTT assay.
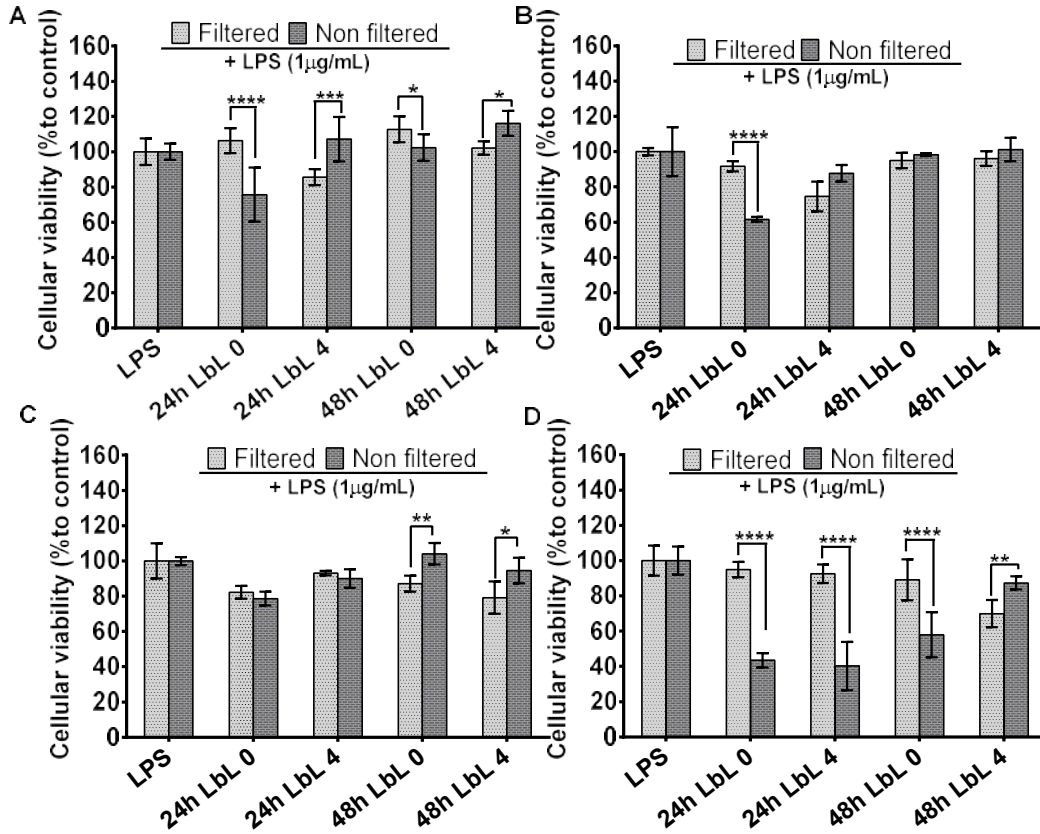
Figure 85. Effect of filtered and non-filtered broths, collected from drug release studies (LbL route) performed at pH 7, in cell viability. LPS-activated-RAW 264.7 macrophages were exposed to (A) 18h, (B) 24h, (C) 48h and (D) 72 hours. Cell viability was assessed by MTT assay.
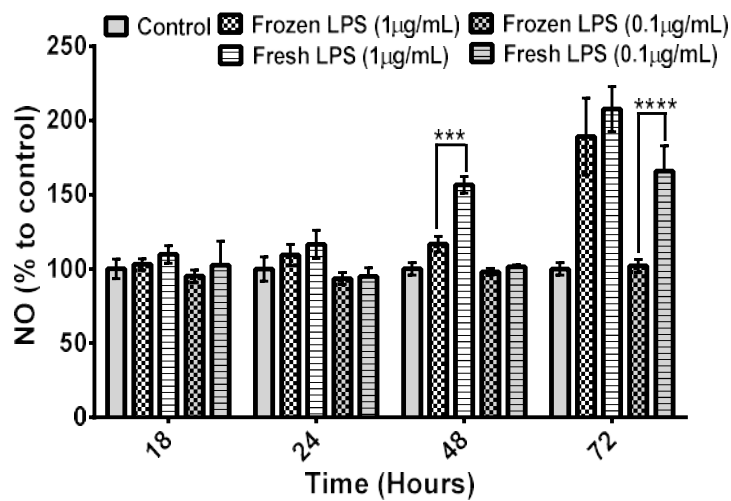
Figure 86. Nitric oxide (NO) production upon exposure to different LPS concentrations (0.1-1µg/mL range) prepared from fresh and frozen LPS stock solution during 18, 24, 48 and 72 hours.
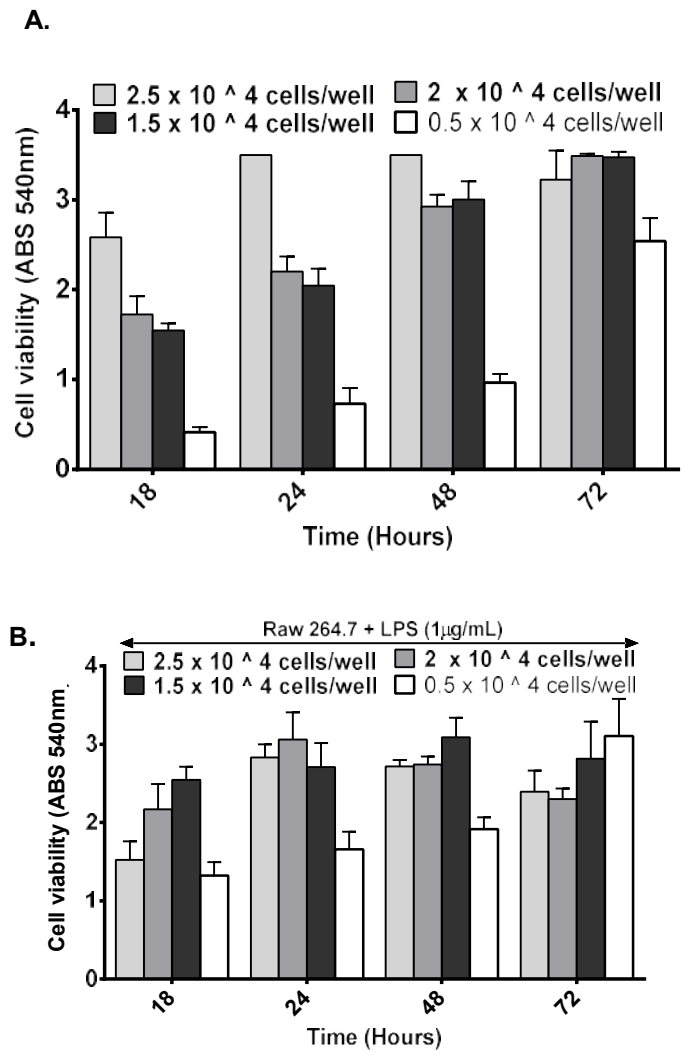
Figure 87. Cellular viability of Raw 264.7 macrophages without (A.) and with (B.) LPS (1µg/mL) during 18, 24, 48 and 72 hours-exposure was assessed by MTT assay, when different cell densities were utilized.
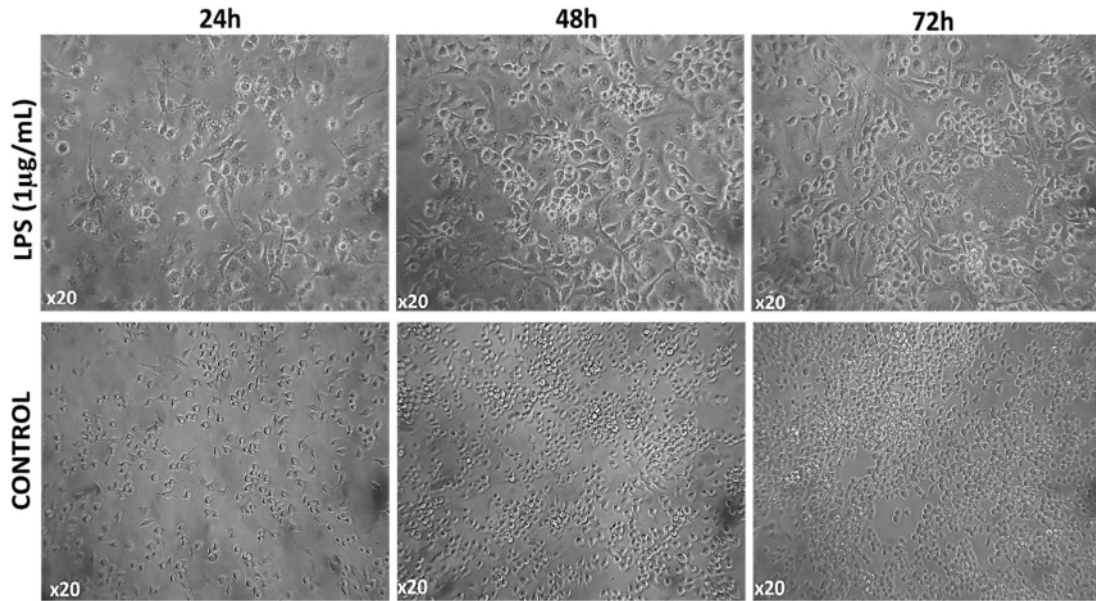
***Figure 88. Effect of LPS in Raw 264.7 cell viability was observed under inverted microscopy.***
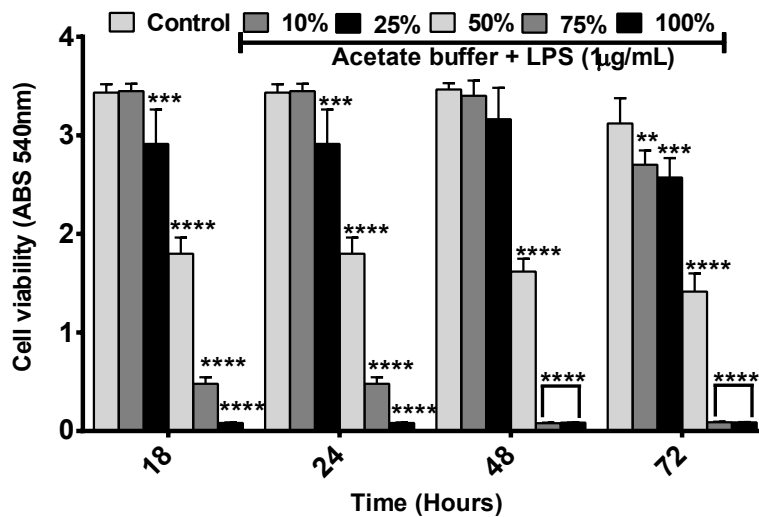
Figure 89. Effect of different concentrations of acetate, buffer utilized for drug release studies, with LPS in cell viability. RAW 264.7 macrophages were exposed to range of acetate buffer (pH=6) concentrations (10-100%) diluted in DMEM media, during 18, 24, 48 and 72 hours. Study done with 2 x10^4 cells /well + DMEM. Final graphs n=2
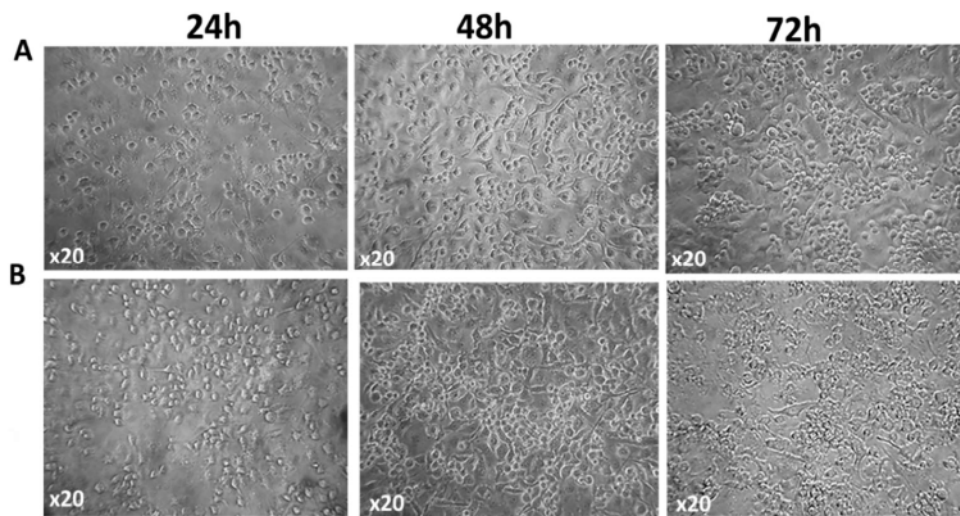
Figure 90. The effect of LPS (1 µg/mL) on the cellular viability of Raw 264.7 macrophages during 24, 48 and 72 hours-exposure was assessed by inverted microscopy, when different cell densities A (2x10^4 cells/well) and B (2.5x10^4 cells/well) were utilized.
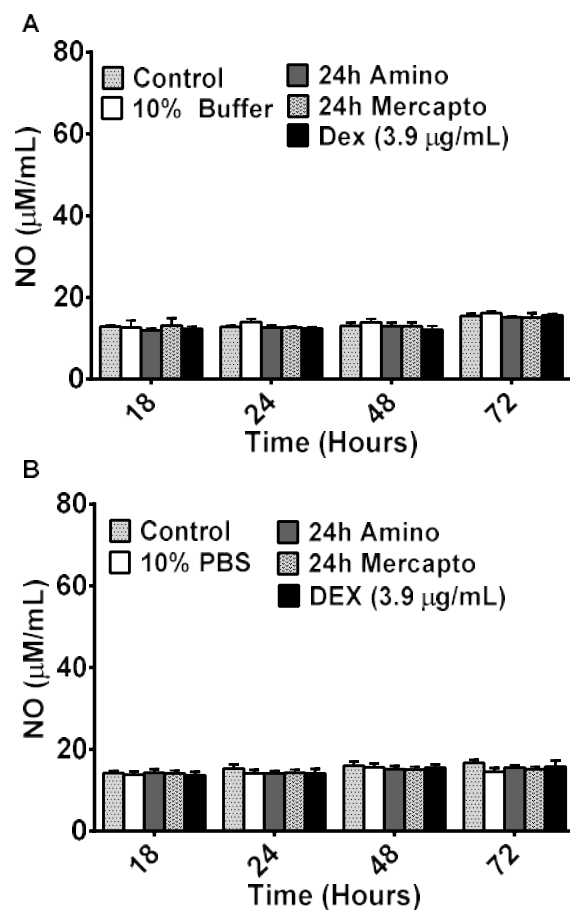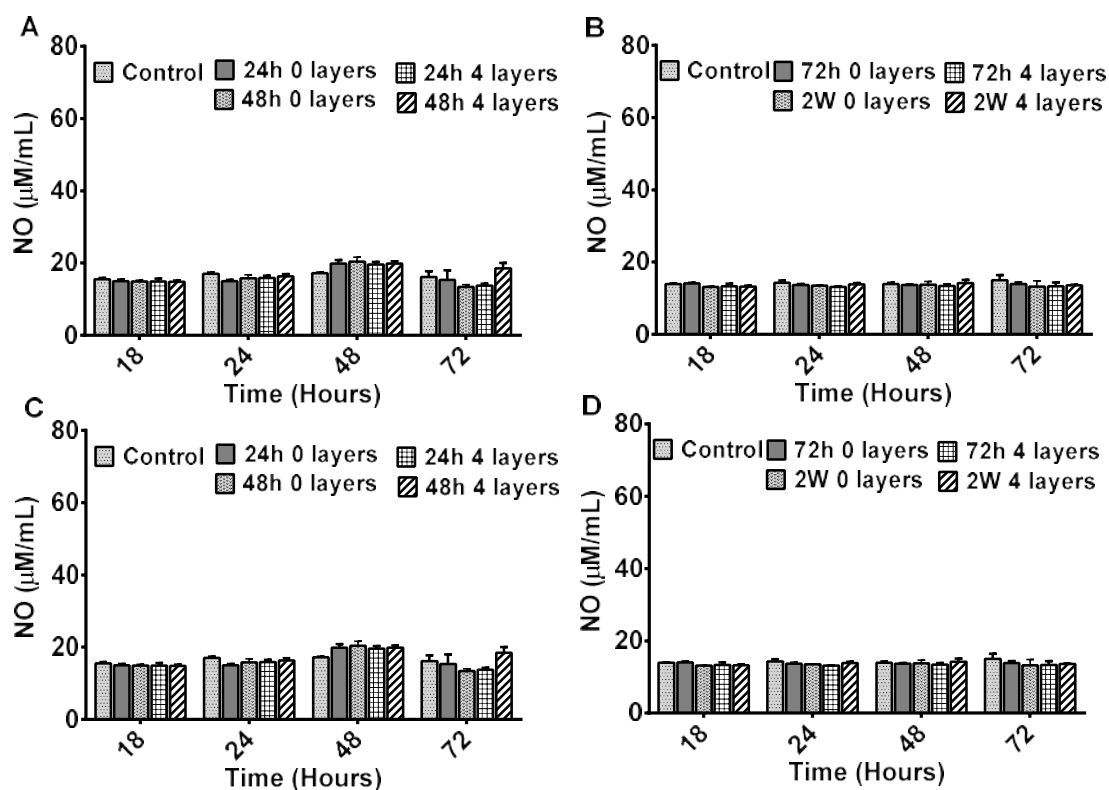
Figure 91. **Effect of DEX released from functionalised-TiO₂ particles (*amino and mercapto* route) *in NO production (µM/mL) in RAW 264.7 macrophages.* Cells were exposed to broths collected *at 24hours* from drug release *studies performed at pH=6 (A) and pH=7 (B)* during 18, 24, 48 and 72 hours.**
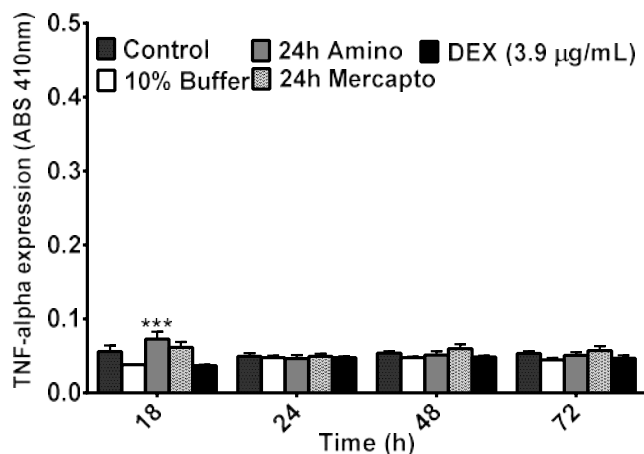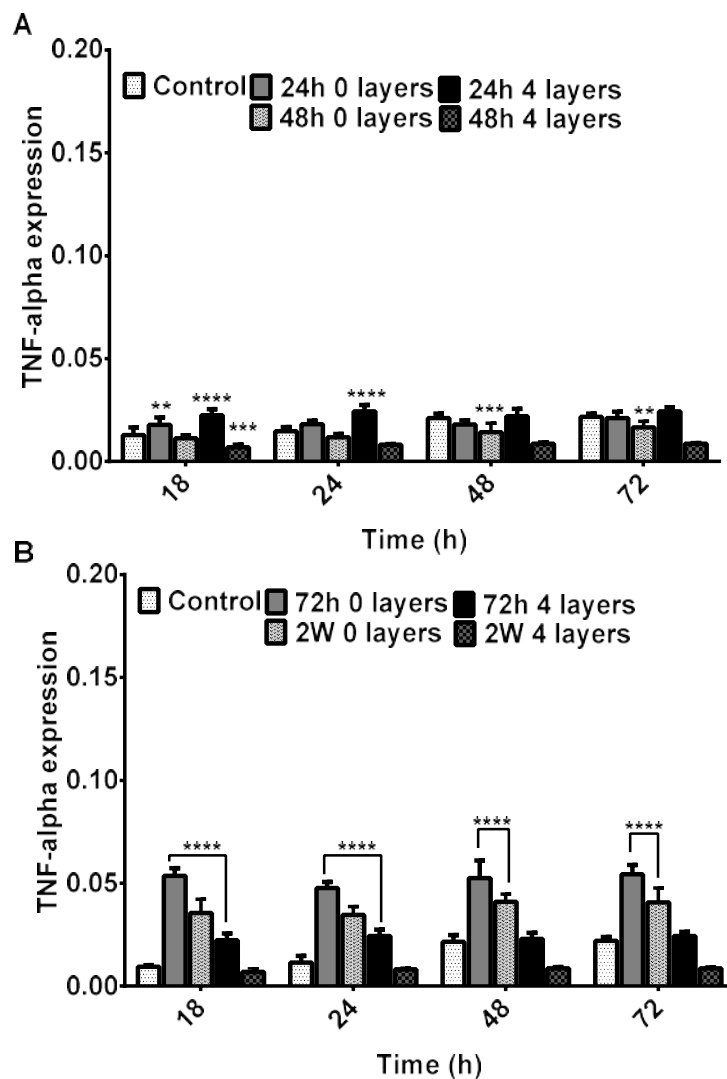
***Figure 92.* Effect of DEX released from functionalised-TiO₂ particles (*amino and mercapto* route) *in TNF-α production (pg/mL) in RAW 264.7 macrophages.* Cells were exposed to broths collected *at 24hours* from drug release *studies performed at pH=6* during 18, 24, 48 and 72 hours.**

***Figure 93.* Effect of DEX released from functionalised-TiO₂ particles (LbL route) *in nitric oxide (NO) production (µM/mL) in RAW 264.7 macrophages.* Cells were exposed to broths collected from drug release studies performed at pH=6 (A,B) and pH=7 (C,D), from *particles surrounded by 0 layers and 4 layers* during 18, 24, 48 and 72 hours. Broths used to treat the cells were collected at different time**

points to assess the effect of *DEX released after (A, C) 24h and 48h (24h 0 and 4 layers, 48h 0 and 4 layers), and 72h and 2W (72h 0 and 4 layers, 2 W 0 and 4 layers).*

Figure 94. **Effect of DEX released from functionalised-TiO$_2$ particles with 0 and 4 layers** *in TNF-α production (pg/mL) in RAW 264.7 macrophages.* **Cells were exposed to broths collected** *at 24h, 48h (A) or to 72h and 2 weeks (B)* **from drug release** *studies performed at pH=6* **during 18, 24, 48 and 72 hours.**
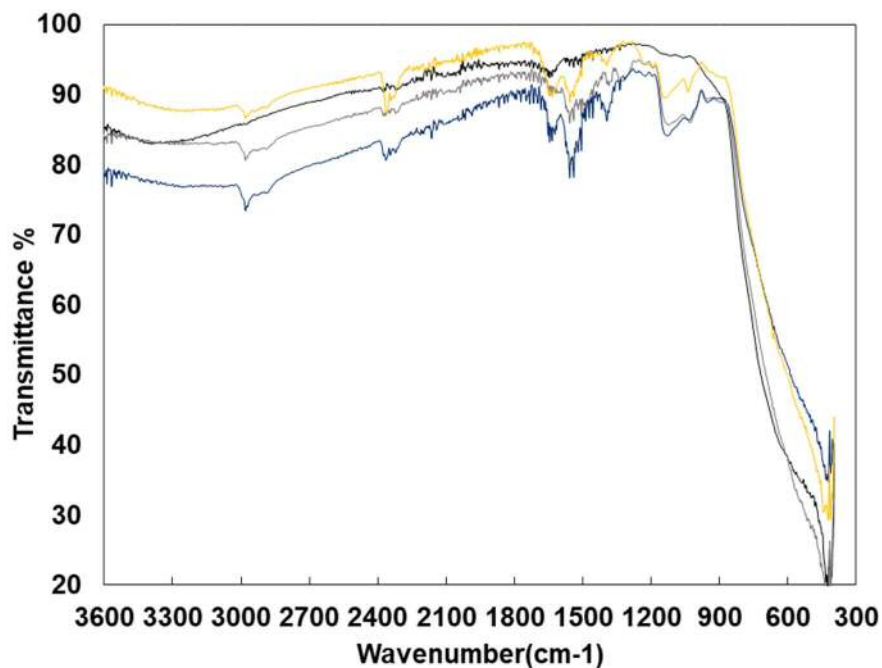
Figure 95. FT-IR spectra for different steps of TiO$_2$ nanoparticles functionalisation using amino route: bare-TiO$_2$ particles (---), amino-functionalised TiO$_2$ particles (---), carboxyl-functionalised TiO$_2$ particles (---), and DEX-loaded TiO$_2$ particles (---).
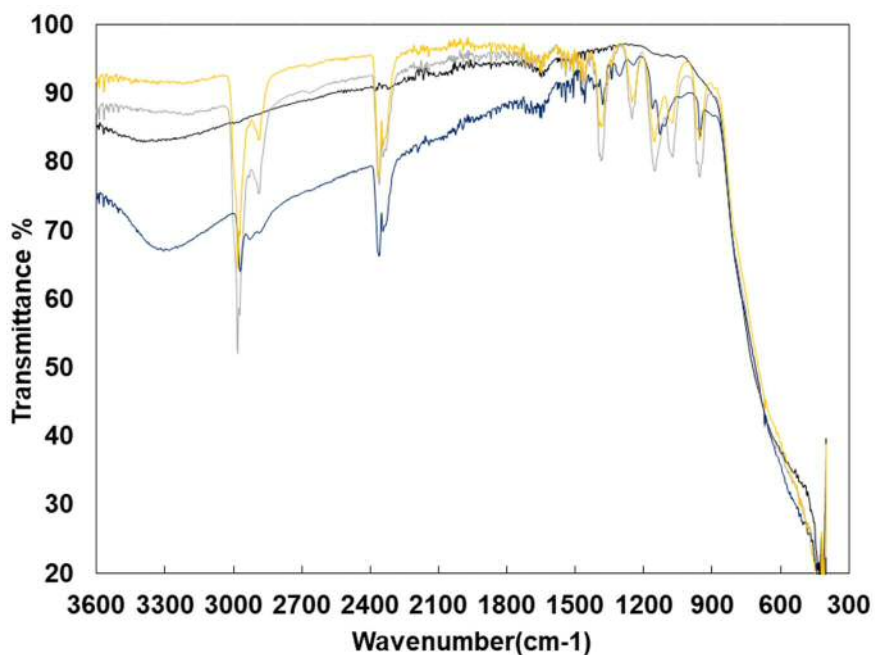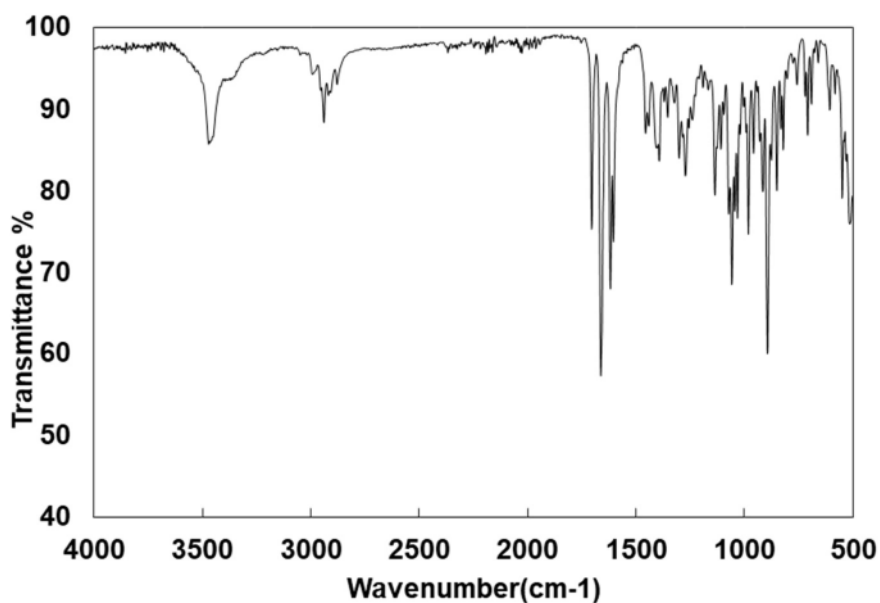

Figure 96. FT-IR spectra for different steps of TiO$_2$ nanoparticles functionalisation using mercapto route: bare-TiO$_2$ particles (---), mercapto-functionalised TiO$_2$ particles (---), carboxyl-functionalised TiO$_2$ particles (---), and DEX-loaded TiO$_2$ particles (---).

Figure 97. FT-IR spectra for pure Dexamethasone powder.

C. Particles Characterisation

Energy dispersive spectrometer (EDS)

Backscattered electron images in the scanning electron microscopy (SEM) display different compositional contrast that results from different atomic number elements and their distribution. On the other hand, the X-rays, which result from the electron beam interaction with the sample are simultaneous detected by an energy Dispersive detector which displays the signal as a spectrum of intensity versus X-ray energy, proving information on the chemical composition of the sample. Therefore, imaging by combined SEM/EDS allowed the analysis of the surface of functionalised-TiO_2 particles and in-depth information regarding chemical composition. Although EDS is not considered a surface analysis technique, it can be used in semi-quantitative mode to determine chemical composition of functionalised participles by peak-height ratio relative to a bare TiO_2 particles (Figure 98.). The EDS analyses for different functionalised particles obtained via amino and mercapto routes are respectively shown in Figure 99 and Figure 100
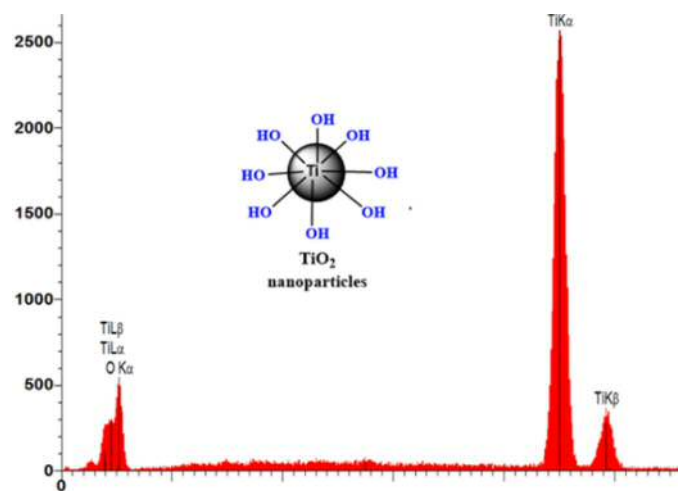
Figure 98. **Energy Dispersive X-ray spectroscopy (EDS) performed on the bare-TiO$_2$ particles.**

For amino route (Figure 99) after amino-functionalisation, the particles seem to be mainly composed of Si (Silicon), in contrast to the bare TiO$_2$ particles which mainly consist of Ti and O, i.e. titania. Silicon peak might suggest the presence of amino-silane (APTS) on the particles surface. As for carboxyl-functionalised particles, unexpectedly the Ti peak is higher, when compared to amino-functionalised particles, Regarding, DEX-loaded functionalised TiO$_2$ particles, the Si, Ti and O peaks are smaller when compared to carboxyl-functionalised particles, although the drug coating must be too thin for unambiguous detection by EDS. For mercapto route (Figure 100), after mercapto-functionalisation, new Si (Silicon) and S (Sulphur) peaks are observed, in contrast to the bare TiO$_2$ particles which mainly consist of Ti and O, i.e. titania. The sulphur and silicon peaks may indicate the presence of mercapto-silane on particles surface. Although, for carboxyl-particles no visible differences were observed when comparing them with mercapto-functionalised particles. On the other hand, dexamethasone-loaded TiO$_2$ particles, the S peak disappeared suggesting mercapto group (SH) was replaced by other groups. As all characterisation techniques, EDS has limitations in terms of analysis. It does not accurately detect the presence of light elements (Z<11), such as Nitrogen (for amino group), and fluorine (for DEX) are not identified even though they are present in the sample. The use of a more sensitive technique, such as XPS, could solve this problem.
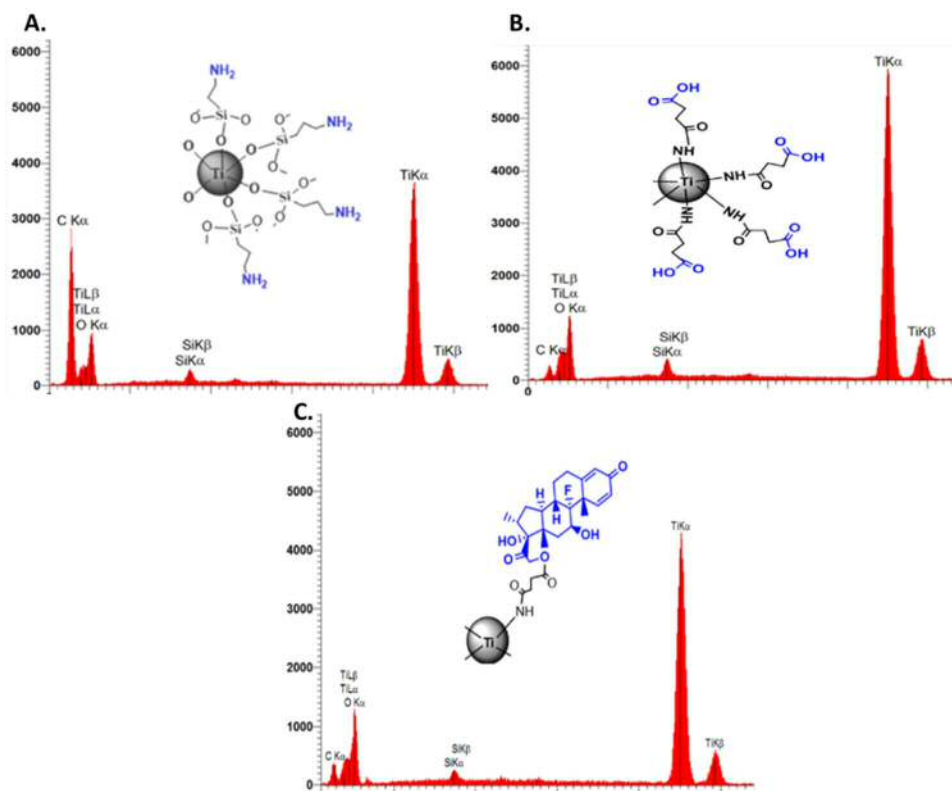
Figure 99. Energy Dispersive X-ray spectroscopy (EDS) (A) and Scanning Electron Microscopy (SEM) (B) performed on the functionalised-TiO₂ particles obtained by Amino route. From left to right, amino-TiO₂ and succinilated-TiO₂ particles, and Dex-loaded-TiO₂ conjugated particles.
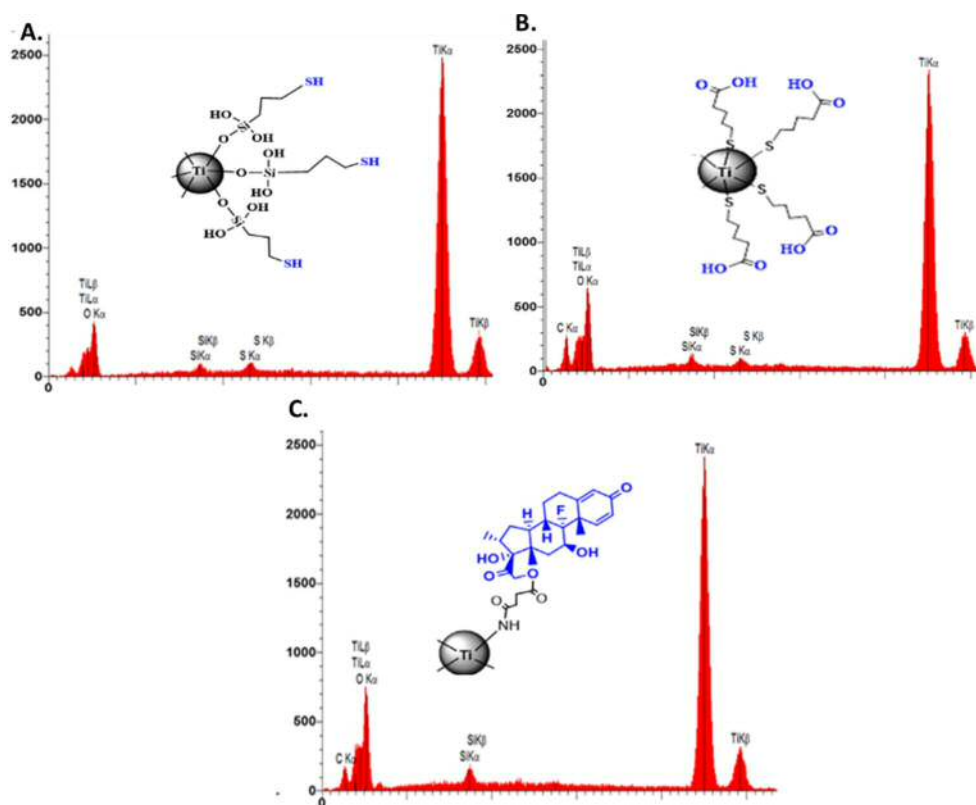
Figure 100. Energy Dispersive X-ray spectroscopy (EDS) (A) and Scanning Electron Microscopy (SEM) (B) performed on the functionalised-TiO$_2$ particles obtained by Mercapto route. From left to right, mercapto-TiO$_2$ and succinilated-TiO$_2$ particles, and Dex-loaded-TiO$_2$ conjugated particles.
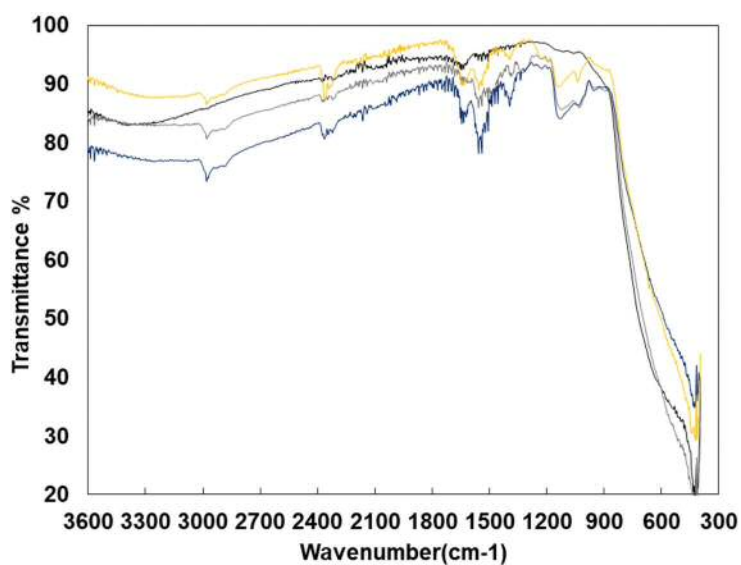
Fourier Transformed infra-red spectroscopy

Figure 101. FT-IR spectra for different steps of TiO₂ nanoparticles functionalisation using amino route: bare-TiO₂ particles (---), amino-functionalised TiO₂ particles (---), carboxyl-functionalised TiO₂ particles (---), and DEX-loaded TiO₂ particles (---).
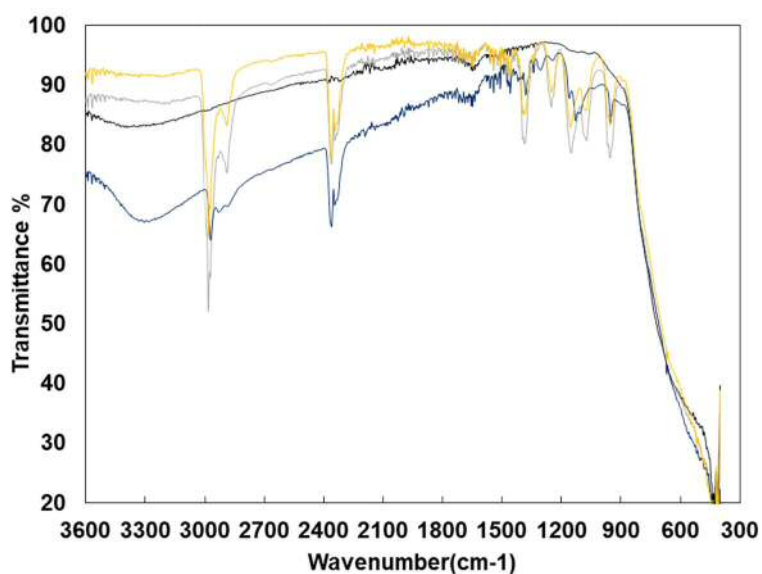

Figure 102. FT-IR spectra for different steps of TiO₂ nanoparticles functionalisation using mercapto route: bare-TiO₂ particles (---), mercapto-functionalised TiO₂ particles (---), carboxyl-functionalised TiO₂ particles (---), and DEX-loaded TiO₂ particles (---).
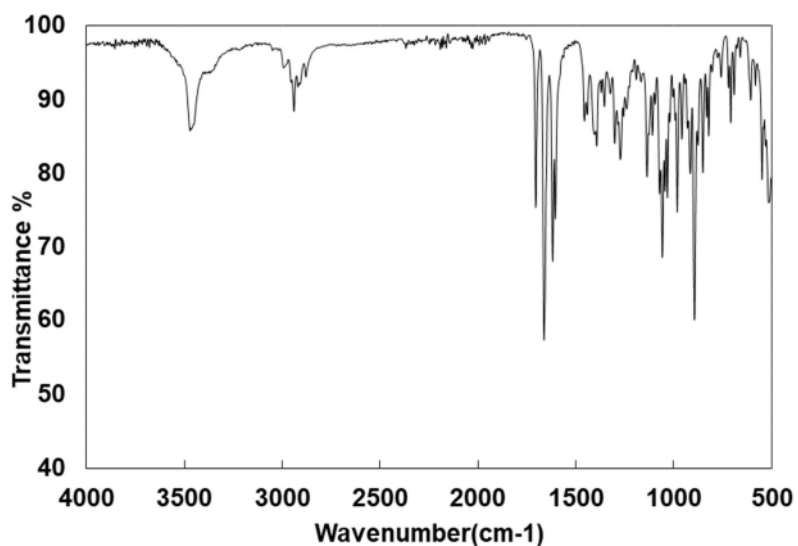
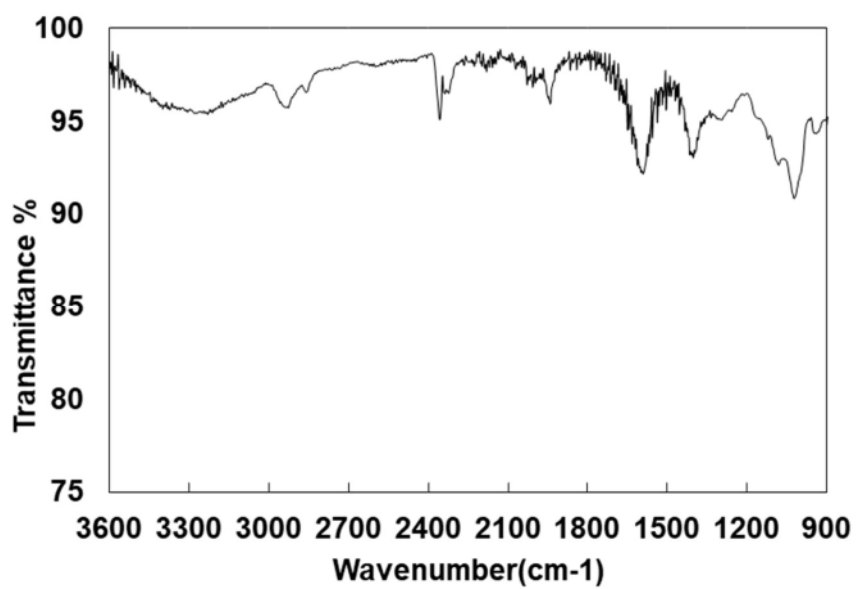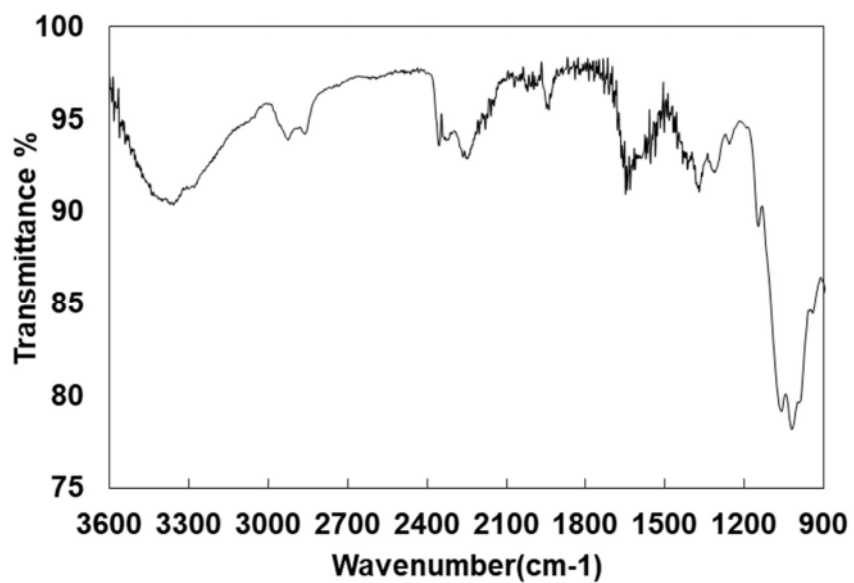**Figure 103. FT-IR spectra for pure Dexamethasone powder.**

Figure 104. FTIR spectra for pure (powder form) alginate (---).

Figure 105. FTIR spectra for pure (powder form) chitosan (---).

D. **Additional information**

Honor/Awards

- **April 2017:** "Dexamethasone-loaded TiO_2 nanoparticles to locally target wear-debris induced inflammation" was awarded with the best lecture at Postgraduate Research day, organized by the School of Pharmacy & Pharmaceutical Science, Cardiff University. (28th April)

- **December 2016:** Travel grant from British Council Researcher Links and Newton Fund was awarded to attend to Researcher Links Workshop: Healthcare Technologies for Aging Populations in Chengdu, China.

- **May 2016:** Sponsorship from Research & Engagement Committee of the School of Pharmacy & Pharmaceutical Science (Cardiff University) for attending to the 10th World Biomaterials Congress, Montréal, Canada 17th- 22th May.

- **April 2016:** "Dexamethasone-loaded TiO_2 nanoparticles to locally target wear-debris induced inflammation" was awarded with the best poster prize at Postgraduate Research day, organized by the School of Pharmacy & Pharmaceutical Science, Cardiff University. (6th April).

- **May 2015**: Sponsorship from Research & Engagement Committee of the School of Pharmacy & Pharmaceutical Science (Cardiff University) to purchase a Fourier transformed Infrared spectroscopy(FITR) for the PhD students of Pharmacy & Pharmaceutical Sciences School

Published work

To date I have published <u>1 paper, and co-authored one book chapter and two reviews:</u>

- "Hollow chitosan/alginate nanocapsules for bioactive compound delivery" in *International journal of biological macromolecules* (2015), Volume 76, pp 95-102.

- "Edible Bio-Based Nanostructures: Delivery, Absorption and Potential Toxicity" in Food Engineering Reviews (2015), Volume 7, Issue 4, pp 491-513.

- "Design of bio-nanosystems for functional compounds delivery" in Food Engineering Reviews (2014), Volume 6, Issue 1, pp 1–19

- "Flavouring and coating technologies for preservation and processing of foods" in Conventional and advanced food processing technologies (2013).

Poster and Oral Presentations

- *"Anti-inflammatory drug-eluting joint replacement: model system ".* Oral presentation at Researcher Links Workshop: Healthcare Technologies for Aging Populations in Chengdu, China (December 2016)
- "Dexamethasone-loaded TiO_2 nanoparticles to locally target wear-debris induced inflammation". Frontiers. Bioeng. Biotechnol. Conference Abstract: 10th World Biomaterials Congress (May 2016).

Teaching and Supervision

- **March 2015 - November 2016**: Teaching and Demonstrating by working as an assistant of lecturers of Pharmacy School and Cardiff Medical School (Health simulating center) in three different areas: Training (Blood pressure measurement, Inhalers utilization and technique, Basic Life support and Cardiopulmonary resuscitation (CPR), help with different courses such as Standard operation procedures and monograph preparation lecturers.
- **October 2014 – January 2014**: Co-supervisor of **Pharmacy graduate student** on final project "Preparation and characterization of Titanium-based nanoparticles loaded with anti-inflammatory drugs"

Networking and Collaboration evidence

- **March 2016 –Ongoing**: Committee member of Cardiff Institute of Tissue Engineering and Repair (CITER). CITER is an internationally recognized center of excellence in the field of tissue repair, regeneration and rehabilitation focusing on interdisciplinary research, education and clinical practice.
- **May 2016:** Volunteer organization member of 10th World Biomaterials Congress, Montreal, Canada 17-22th May. The skills and dedication of volunteers greatly contribute to the overall quality of the conference. This role was a great opportunity to meet, interact and network with a multicultural team of students from all over the world that share a common interest in Biomaterials.
- **December 2014- May 2015:** Organization member of Annual Speaking of Science Conference, 9th May 2015. This conference provides a valuable opportunity for postgraduates to give talks and posters across a wide range of subjects and disciplines. This forces them to simplify complex research ideas for a general audience and as a result the participating delegates discover the essence of research being undertaken across the scientific schools.

- **March 2014 – Ongoing:** <u>Post Graduate Staff Student Panel (SPSS) of Pharmacy and Pharmaceutical Sciences School</u>. The SSP responsibilities include helping with the induction event, welcome party and research day. We also discuss any issues that arise in the postgraduate community and make suggestions to enhance the post-graduated research experience.